THE EFFECT OF PLEATING DENSITY AND DUST TYPE ON PERFORMANCE OF ABSOLUTE FIBROUS FILTERS

By

Iyad Shareef Al-Attar

A Doctoral thesis submitted in partial fulfilment of the requirements for the award of Doctor Philosophy of Loughborough University.

July 2011

SUMMARY

The importance of clean air to the well-being of people and for the protection of industrial equipment has highlighted the critical role of air filter performance. The objective of this thesis is to study the filter performance characteristics namely; the pressure drop and the fractional efficiency of standard full scale (592x592x400 mm) mini-pleated HEPA absolute fibrous filters. Accurate filter performance prediction plays a significant role in estimating the lifetime of filters and reducing energy and maintenance operating costs. To ensure the appropriate filter selection has been made for a specific application, filter design must be further investigated to include pleat count and its corresponding surface area.

The investigations undertaken in this work were based on using standard SAE coarse and fine dust. This guaranteed that the results would be applicable globally irrespective of the geographical location or the field of application of the filtration technology. However, the performance of air filters used in gas turbine and HVAC applications tend to deviate from that predicted by laboratory results using standard air dust. This is especially true in regions known to have dust with characteristics deviating from that of standard dust, such as in Kuwait. Therefore, as part of this thesis, the Kuwaiti atmospheric dust has been characterized both chemically and physically in order to investigate the possible impact of these characteristics on the results of the filter performance. It transpired, however, that the characteristics of dust with extreme properties, represented in this case by Kuwaiti dust, fell between those of the characteristics of the two standard types of dust, namely, SAE coarse and fine dust. This finding, therefore, provides additional confidence in the generality of the results pertaining to the filter performance.

The work investigated the effects of ten different flow rates ranging from 500 to 5000 m^3/h with increment of 500 m^3/h. The four different pleating densities used to construct the filter were 28, 30, 32 and 34 pleats per 100mm. This experimental work was conducted while keeping other parameters such as filter media class unchanged. Pleating density may play a major role in achieving the optimum pressure drop and the required efficiency expected from such a filter. Such optimization was expected to

facilitate design alternatives supported by experimental results. A testing facility located in Limburg Germany at the EMW Filtertechnik GmbH was used for this testing. Two different particle size counters were used to cover a considerable particle size range. The results of the particle counter with size range of: 0.065 – 0.9 μm was used for the analysis since it covered the study of the Most Penetrating Particle Size (MPPS) with respect to the filter pleat density and face velocities. This experimental work involved testing ten industrial full scale HEPA filters, which were divided into three groups. The first two Groups (Group A and B), each consisted of four filters manufactured with different pleat densities of 28, 30, 32 and 34 pleat per 100 mm. The third Group C consisted of two filters; the first filter had horizontal pleat orientation while the second pleats were oriented vertically. Both filters in Group C had a pleat density of 28 pleat per 100 mm. Filters of Groups A and B were challenged with SAE coarse and fine dust, respectively. In the case of filters of Group C, only the initial pressure drop and efficiency measurements were conducted.

This experimental work has highlighted the underlying reasons behind the reduction in filter permeability due to the increase of face velocity and pleat density. The reasons which led to surface area losses of filtration media are due to one or combination of the following effects: pleat crowding, deflection of the entire pleated panel, pleat distortion at the corner of the pleat and/or filtration medium compression. The experimental data for fractional efficiency were fitted using a modified Lee and Liu [1982a] model. The proposed modified model was verified to show a good agreement with the experimental results. It is evident from entire array of experiments that as the particle size increases, the efficiency decreases until the MPPS is reached. Beyond the MPPS, the efficiency increases with increase of particle size. The MPPS shifts to a smaller particle size as the face velocity increases and the pleating density and orientation did not have a pronounced effect on the MPPS. The second part of this experimental work involved the dust loading process which showed a higher efficiency and pressure drop response of SAE fine dust when compared to SAE coarse dust. Increasing the mass of dust loads and flow rates have a significant effect on the filter efficiency while the effect of varying pleating density was negligible. Throughout this study, optimal pleat count which satisfies both initial and dust loaded pressure drop and efficiency requirements may not have necessarily existed. This experimental work has also suggested that a valid comparison of the pleat densities

should be based on the effective surface area which participates in the filtration action and not the total surface area the pleat density provides.

The work in this thesis has presented novel contribution in four aspects. Firstly, the full scale nature of the experiments resulted from using full scale standard industrial size HEPA filters constructed in V-shape banks cartridge in all the tests. Secondly, a novel explanation of when the surface area losses become a dominant factor in the filter permeability reduction. Thirdly, the discovery of the fact that increasing the pleating density could be counterproductive in terms of effective filtration surface area and filter permeability. Finally, the work has proposed new design alterations for maintaining effective surface areas. All design improvements are currently under review as they might require developmental work and investigation prior to any possible future implementation.

ACKNOWLEDGEMENT

I would like to extend my sincere appreciation to many great people from different countries that have helped and contributed to this thesis in one way or another:

From Loughborough University, I would like to express my special thanks to *Prof. Richard Wakeman* and *Dr. Steve Tarleton*, for their adroit guidance, continuous support, insight and inspiration. I dearly appreciate their phenomenal efforts in helping me comprehending the parameters of this thesis and for providing the appropriate environment to outperform. I would also like to thank Mr. Frank Page who has taught a great deal about scanning electron microscopy technology and assisted me in producing stunning and illustrative images to serve this thesis extremely well.

Across the English Channel to Germany, I would like to express my gratitude to *Mrs. Gerlinde Drache*, the Managing Director of EMW Filtertechnik for her generous support to this thesis. I highly acknowledge her immediate support to this research without hesitation and in making the entire air filtration testing facility in the laboratory at my disposal in the past four years. I also would like to thank *Mr. Kevin Drache* for granting me the opportunity to have full access to the manufacturing plant. His enormous cooperation and flexibility to accommodate the filter design requirements of this thesis have enormously helped me achieving great results. I also would like gratefully acknowledge *Mr. Jurgen Schwab* for his on-going full support of my thesis since the day it was born. My heartfelt thanks are extended to *Mr. Jorg Domach* who has shared a great deal of his experience in the air filtration testing facility and answered my questions without compliant. His contribution to the experimental work and setup has been tremendous. I also would like to thank *Mr. Norbert Fisher* for the informative exchange of technical discussion and his helping hand which has always been extended to support this research. I would also like to thank *Mrs. Kerstin Schwab, Mr. Markus Bartel, Ms. Rebecca Schenk* and the entire EMW team in Germany.

Across the Atlantic, to Toronto, Canada, I would like express my highest appreciation to the faculty of Applied Science and Engineering at University of Toronto for awarding me the *Thomas Hougg International* Scholarship. I specially would like to thank *Mrs. Pierina Filippone* for her international administrative support of my Award and for her continuous follow up of my entire PhD progress throughout the years.

To the Middle East, specifically in Kuwait, I would extend my sincere appreciation to my local supervisor *Dr. Adel Husain* whose outstanding assistance has always been forthcoming.

I greatly appreciate the support of my friends, Dr. *Mamdouh Refaat*, *Ayman Abu-Abed*, *Mujtaba Quadri, Eleanor Minuk, Julian Bonaparte* and *David Steadman* for their encouragement and support.

Last but not least, my heartfelt thanks to my *parents*, *brothers* and *sisters*; I would not have been able to earn this PhD without their exceptional support. My deepest appreciation is extended to my wife, *Hadeel*, for putting up with my absence from home without compliant. Her emotional support has proved invaluable in completing my PhD.

TABLE OF CONTENTS

NOMENCLATURE

Symbol	Description	Dimension
A	Area	m^2
A_c	Testing channel surface area	m^2
A_e	Effective surface area	m^2
A_L	Loss in surface area	m^2
A_{open}	Surface area of the opening of the filter	m^2
A_s	Surface area	m^2
A_u	Utilized filter surface area	m^2
B	Bed thickness of particles	m
C_1	Constant (Eq. 2.46)	
C_2	Constant (Eq. 2.46)	
C_c	Cunningham correction factor	
C_d	Correction constants (row 6 , Table 2.3)	
C_d'	Correction constants (row 5 , Table 2.3)	
$C_{n,d}$	Particle concentration downstream	cm^{-3}
$C_{n,u}$	Particle concentration upstream	cm^{-3}
C_r	Correction constants (row 5 , Table 2.3)	
D	Particle diffusion coefficient	
$D_{L,d}$	Dilution factor downstream	
$D_{L,u}$	Dilution factor upstream	
d_f	Fibre diameter	m
d_h	Test channel hydraulic diameter	m
d_p	Particle diameter	m
E	Total filter efficiency	%
F	Force	N
F_c	Compression force	N
F_d	Drag force	N
F_n	Normal force	N
F_s	Shear force	N
F^*	Fibre drag coefficient	N
g	Gravity	m/s^2
G	Filtration media grammage	g/m^2
h	Filtration medium thickness	m
h_c	Cake thickness	
H	Slope in equation (4.2)	
J	Coefficient in Equation (2.29)	
k	Boltzman's constant, $1.37x10^{-23}$	J/K
K_1	Filter constant depending on clean filter parameters (Equation 2.15)	
K_2	Filter constant depending on clean filter parameters (Equation 2.15)	
$K_{2\text{-}Stokes}$	Coefficient defined in Equation 2.18	
K_{KC}	Kozeny-Carman constant	
Kn	Knudsen number	
Kn_f	Knudsen number for fibre	
Kn_p	Knudsen number for particle	
Ku	Kuwabara hydrodynamic factor	
L	Pleat square length	m
L_f	Fibre length	m
L_x	Pleat width	m
L_y	Pleat length	m
M	Mass of collected particles	g
MMD	Mass median diameter	μm

N	Number of spheres per unit area (Eq. 2.16)	
N_d	Particle number downstream	
N_u	Particle number upstream	
P	Pressure	Pa
Pe	Peclet number	
P_o	Distributed load	Pa
P_t	Filter penetration	%
Q	Volumetric air flow rate	m^3/h
$Q_{s,d}$	Flow rate inside the sample nozzle downstream	m^3/h
$Q_{s,u}$	Flow rate inside the sample nozzle upstream	m^3/h
R	Interception parameter	
R_s	Resistance factor (Eq.2.19)	
Re	Reynolds number	
Re_D	Reynolds number for testing channel	
Re_f	Reynolds number for filter fibre	
Re_p	Reynolds number for particle	
S	Stopping distance	m
St	Stokes number	
T	Temperature	K
t_d	Sampling time in particle counter downstream	min
t_u	Sampling time in particle counter upstream	min
U	Air velocity	m/s
U_f	Velocity of air at the face of the filter	m/s
U_m	Media velocity	m/s
V_1	Testing channel velocity	m/s
V_2	Filter opening velocity	m/s
V_3	Filter media velocity	m/s
V_4	Stagnation velocity	m/s
V_5	Velocity at the edge of the pleat	m/s
Y	Distance between two limiting trajectories	m
Y_E	Young's modulus of elasticity (filtration media)	MPa
Z	Particle mobility	

Symbol	**Description**	**Dimension**
α	Filter's packing density	m^3/m^3
β_1	Diffusion coefficient	
β_2	Interception coefficient	
δ	Deflection of a pleat	μm
ΔP	Pressure drop	Pa
ΔP_c	Dust cake pressure drop	Pa
ΔP_D	Darcy pressure drop	Pa
ΔP_i	Initial pressure drop	Pa
ΔP_1	Pressure drop during the first dust feed	Pa
ΔP_2	Pressure drop during the second dust feed	Pa
ΔP_3	Pressure drop during the third dust feed	Pa
ΔP_4	Pressure drop during the fourth dust feed	Pa
ε	Filter porosity	
ε_c	Cake porosity	
η	Summation of the single fibre efficiencies	
η_D	Diffusion efficiency	
η_{DR}	Combined interception and diffusion efficiency term	
η_I	Inertial impaction efficiency	
η_R	Interception efficiency	
κ	Filter permeability	

$\kappa(M)$	Cake permeability as a function of mass collected	
λ	Gas mean free path	μm
μ	Air viscosity	Pa.s or kg.m/s
ξ	Correction factor for inhomogeneity	
π	Mathematical Constant (≈ 3.14159265)	
ρ	Density	kg/m^3
ρ_a	Density of air	kg/m^3
ρ_p	Density of particles	kg/m^3

ACRONYM

ASHRAE	American Society of Heating Ventilation and Refrigeration
DEHS	Diethyl Hexyl Sebacate
DIN	Deutsch International Norm
DOP	Dioctyl Phthalate
EDXS	Energy Dispersive X-rays Spectroscopy
HEPA	High Efficiency Particulate Arrestance
HVAC	Heating Ventilation and Air Conditioning
KISR	Kuwait Institute for Scientific Research
MPPS	Most Penetrating Particle Size
ULPA	Ultra Low Penetration Air

LIST OF FIGURES

Chapter One

Chapter Two

Chapter Three

Chapter Four

Chapter Five

CHAPTER ONE

Introduction

1.1 Statement of Objective

The objective of this research is to investigate experimentally the initial efficiency and dust loading of full scale *High Efficiency Particulate Air* (HEPA) filters and apply established equations to verify or otherwise their validity. The work in this thesis presents novel contribution through the full scale nature of the experiments resulted from using standard industrial size HEPA filters constructed in V-shaped banks in all the tests. Further, the filters were subjected to ten different flow rates with a range great enough to analyze the deviation from Darcy's (linear pressure drop). This work also experimentally investigates the effect of pleat density and orientation on the HEPA filter performance. Throughout this thesis, the phrase "filter performance" indicates two main performance characteristics namely; the pressures drop of the air filter and its efficiency. In studying these objectives it was envisaged that the filter panel design may require investigation and that literature claims of, for example, an optimum pleat density would be tested.

It was intended that the results should be in same way representative of the filtration of Kuwaiti atmospheric dust, but that these conditions are so extreme that they may not be achievable in testing an industrial scale filter in a laboratory setting. The Kuwait atmospheric dust was considered in this study as a benchmark for extreme climates. However, there are three key reasons which make the results of this thesis globally valuable:

1. The experimental investigation of full scale HEPA filters with standard dimensions.
2. The filters were loaded with international standard synthetic dusts namely; SAE fine and coarse dusts.
3. The dust concentration used in the dust feeding process for this experimental work was 70 mg/m^3 which conform to international standards [ASHRAE 52.2, 1999; DIN EN779, 2002].

1.2 Air Filtration Definition

Air filtration is the process of separating dispersed particles from a dispersing fluid by means of porous media [Pich, 1987]. Air filtration is a preventive measure to protect the human respiratory system as well as *Heating Ventilation and Air conditioning* (HVAC) equipment. Air filters are used to remove aerosol particles from air at different efficiencies with the least possible resistance. The filter's overall efficiency and pressure drop are the main performance characteristics considered in this study.

1.3 The Importance of This Study

Air filters constitute an important part of providing clean air to a building and maintaining the rated energy efficiencies of air conditioning equipment. In clean room applications such as hospitals, air conditioning systems are run throughout the year and involve extensive use of pleated HEPA filters with 100% fresh air. Aerodynamic and efficient pleated HEPA filters are highly desired due to excessive and escalating energy costs worldwide. This study will examine the possibility of introducing pleated HEPA filters with lower pressure drop which would have a significant impact on the performance of HVAC equipment and gas turbines performances.

In Kuwait climate for example, 75-80% of the power generated is consumed by air conditioning units [Ministry of Electricity and Water, 2000]. This requires an annual cooling capacity of seven months and reported an average electrical peak load in July to be 114% higher than that in January [Statistics Department and Information Centre, 1998]. Therefore, aerodynamic HEPA filters which would provide any conservation of energy by lowering the pressure drop directly enhance power generation and reduce fuel consumption. Efficient HEPA filters with aerodynamic designs would be of a great global interest.

In Sahara desert such as the Arabian Peninsula and specifically Kuwait, sand storms are frequent and dreadful [Al-Sanad *et al*] as shown in Figure 1.1. Dust storms increase the particle concentration in the air and affect the dust loading of the air filters in the air handing units. Evaluated dust concentration can cause bridging of particle to form dendrites on the surface of the fibrous final filters used and impair them from acting as depth filters.

[a] Clear skies day [b] Sand storm day

[Images taken of the same view during current study May 2005]

Figure 1.1: Illustration of the effect of sand storms on visibility.

1.4 Pleated Filters

This research focuses on the performance of standard full scale absolute filters specifically HEPA V-bank filters as shown in Figure 1.2. The HEPA filters are disposal rigid filter cartridges with an extended surface area by means of several small pleats. This dry type filter has a specified minimum efficiency against dioctyl phthalate (DOP) or Diethyl hexyl sebacate (DEHS) or sodium chloride. HEPA and ULPA, *Ultra Low Penetrating Air* filters are rated at MPPS [Tarleton and Wakeman, 2008]. Pleated filters provide additional filter media to reduce the air velocity through the filter media. This enables the filter to increase the collection efficiency for a given pressure drop as well as reducing energy consumption [Chimack *et al*, 2000]. Due to their high surface area, pleated filters are also appropriate to use in the return air duct when re-circulating air in building.

Figure 1.2 Pleated HEPA air filter tested in this study [EMW Filtertechnik].

This thesis is concerned with the performance of full scale HEPA filters constructed in V-shaped banks. The testing involves the initial and dust loaded pressure drop and efficiency measurements using international synthetic dusts. This experimental investigation considers several parameters which affect the HEPA filter performance such as dust type, flow rate, filter surface area losses, pleat density and orientation.

Chapter Two of this thesis offers a literature review on the pressure drop and overall removal efficiency. It starts by presenting the most frequently discussed pressure drop models of air filter as they are loaded with aerosol. The single fibre efficiency for each collection mechanism as well as overall efficiency will also be discussed. The final section of this review deals with absolute pleated fibrous filters and the parameters influencing their performance. Chapter Three presents the air filtration testing facility used in this experimental work which is located in Germany, the experimental procedures and the associated equipment used to complete the testing. Chapter Four presents the results and analysis of the experimental work and finally Chapter Five discusses the overall conclusions and future recommendations for further research and investigation.

CHAPTER TWO

LITERATURE REVIEW

In this chapter, a review of the previous literature is presented to highlight the research conducted in earlier years. A special attention is directed toward the efficiency models and their suitability to be used in the curve-fitting techniques in Chapter 4 to present a modified equation to better predict the overall efficiency of the full scale pleated V-shaped absolute filters.

2.1 Flow Through Fibrous Medium

To solve a problem in the aerosol filtration a good description of the flow fields around the fibre inside the filter is required. The calculation of the velocity field around a single fibre is based on the Navier-Stokes equation with a low Reynolds approximation due to Oseen [Devienne, 1958]. The literature offers wide range of different flow models to describe the flow fields using Potential flow and Lamb flow [Davies, 1973]. However, these models do not consider the effect of the neighbouring fibre. This effect was first taken into account by Kuwabara [1959] and Happel [1959]. Both of these theories differ from the isolated fibre models since they consider the fibre in finite space or "cell"; each cell corresponds to a fibre described by a cylinder surrounded by the fluid and can be considered as an independent entity as shown in Figure 2.1. The cell model was published by Kuwabara [1959] and Happel [1959] to describe the flow field of a fluid through banks of parallel fibres. The Kuwabara model was later applied by Kirsch and Fuchs [1963, 1968] to study the pressure drop through a filter. Fuchs and Stechkina [1963, 1966] applied the Kuwabara model to the theoretical description of the diffusion mechanism.

The cell theory is considered the simplest quantitative approach where the problem is reduced to finding the air flow around a single fibre and that is typical for every fibre. The flow pattern within the cell is related to its diameter. The cell diameter determined by the proximity of neighbouring fibres is related to the packing density of the filter [Harrop and Stenhouse, 1969]. The greatest strength of the cell theory is its simplicity which made it the basis of many simple numerical calculations of filter

properties. However, Brown [1997] stated that a rigorous theory of pressure drop and particle capture would require that the flow problem to be solved for each fibre then the results will be averaged. In the cell theory, the fibres are averaged and then flow equation is solved. Although it is much easier approach, it is less satisfactory. The cell theory neither accounts for interstitial regions of the filter nor the irregular structure of the filtration media. In a filter media, the filter fibres are not all perpendicular to the flow direction which also influences the packing density since it is affected by the fibre position.

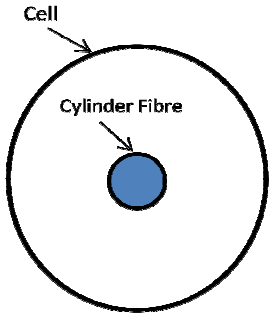

Figure 2.1: Cell model considers a fibre in a finite space.

The motion of a continuous fluid is considered to obey the Navier-Stokes equation and is solved by describing the flow field with appropriate boundary conditions.

$$\frac{\mu}{\rho}\nabla^2 U - \frac{1}{\rho}\nabla p = (U \cdot \nabla)U \tag{2.1}$$

where μ is the air viscosity, U the velocity of air flow through the medium and ρ the air density. The right hand side of equation (2.1) is the velocity gradient and the left hand side is the pressure drop and viscous terms.

Stokes solved the Navier-Stokes equations based on the assumption that inertial forces are negligible compared with viscous forces acting at any point in the fluid surrounding a spherical particle [Hinds, 1998]. When inertia is neglected, the equation is simplified to:

$$\frac{\mu}{\rho}\nabla^2 U - \frac{1}{\rho}\nabla p = 0 \tag{2.2}$$

or

$$\nabla p = \frac{\mu}{\rho}\nabla^2 U \tag{2.3}$$

To apply these equations, the gas passed around a fibre must be treated as a continuous medium [Devienne, 1958]. This can be assumed when the Knudsen

number for fibres or particles is in the range of $Kn<10^{-3}$. The Knudsen number for fibres is given by

$$Kn_f = \frac{2\lambda}{d_f} \tag{2.4}$$

where λ is the gas mean free path and d_f is the fibre diameter. Given that the value of λ is 0.0653 μm [Fuchs, 1964], this condition is fulfilled for fibres with a diameter of 65.3 μm and larger. However, Scurrah [1999] mentioned that the slip condition will occur for fibres of diameters of 2 μm or less.

Another important assumption of Stoke's law is that the relative velocity of the gas right at the surface of the sphere is zero. Particles close in size to the mean free path of the gas will settle faster than predicted by Stokes law because there is "slip" at the surface of the particle [Hinds, 1998]. The Knudsen number for particles is given by:

$$Kn_p = \frac{2\lambda}{d_p} \tag{2.5}$$

where d_p is the particle diameter. The Cunningham correction factor, C_c, was introduced by Cunningham [Cunningham, 1910] to account for the slip condition. The Cunningham factor is always greater than one and defined as:

$$C_c = 1 + \frac{2.52\lambda}{d_p} \tag{2.6}$$

The Cunningham correction factor is used in the calculation of the diffusion coefficient to compute Peclet number appearing the single fibre efficiency for diffusion. There are two cases where the Stokes flow may not be a good approximation. The first one when considering coarse filters where the Reynolds number is too high. The second case is when filters under examination have very fine fibres which mean the molecular nature of air is significant and must be taken into account [Brown, 1993a]. The Stokes flow, as described by equation (2.3) is steady state and highly dependent on the filter medium structure, which in the case of fibrous filters is neither completely ordered nor totally random [Brown, 1993a].

2.2 Initial Pressure Drop Models

The flow through an air filter is considered to be low speed, incompressible, Newtonian and is governed by Darcy's Law:

$$\Delta P_D = \frac{\mu U h}{\kappa} \tag{2.7}$$

where κ is the permeability of a porous substance and h is filter medium thickness. Permeability is a basic quantity which in the continuum region is a descriptive constant for each porous substance [Matteson and Orr, 1987]. Most of the pressure drop relations are based on Darcy's Law which states that the pressure drop across an air filter is proportional to the air flow through it. The pressure drop across the filter is a function of drag force F_d acting on a unit length of a filter fibre and the fibre length per unit filter area L_f. The fibre length per unit area of a filter is a function of the filter structure. The pressure drop expression becomes:

$$\Delta P = F_d L_f \tag{2.8}$$

The drag force, F_d , is proportional to the fibre drag parameter, F^*, μ *and* U_o [Liu *et al*,1986].

$$F_d = F^* \mu U_o \tag{2.9}$$

The fibre drag coefficient is a function of packing density α which is defined as the ratio of the fibre volume to total volume in a fibrous filter unit [Filtration Dictionary, 2008]. Then fibre drag parameter then becomes:

$$F^* = \frac{4\alpha}{Ku} \tag{2.10}$$

According to the Kuwabara theory for flow around a cylinder in a fibrous filter, Ku is the Kuwabara hydrodynamic factor, which is dimensionless and defined as:

$$Ku = -\frac{1}{2}\ln\alpha + \alpha - \frac{1}{4}\alpha^2 - \frac{3}{4} \tag{2.11}$$

Where α is the filter packing density defined as the ratio of fibre volume to the total volume in a fibrous filter unit [Tarleton and Wakeman, 2008]. The pressure drop expression becomes:

$$\Delta P = F^* \mu U L_f \tag{2.12}$$

Substituting for L_f, the pressure drop becomes:

$$\Delta P = F^* \frac{4\mu\alpha Uh}{\pi d_f^2} \tag{2.13}$$

Various models of the dimensionless drag coefficient suggested by several authors are listed in Table 2.1. The associated pressure drop models using the drag force listed in Table 2.1 along with Darcy's Law were compared with experimental results of this study in Section 4.2.4.

Author	Expression of F^*
Davies (1952)	$F^* = 16\pi\alpha_f^{0.5}(1 + 56\alpha_f^3)$ For $0.006 < \alpha_f < 0.3$ $F^* = 16\pi\alpha_f^{0.5}$ For $\alpha_f < 0.006$
Happel (1959)	$F^* = 8\pi\left(\frac{1}{-ln\alpha_f - \left(\frac{1-\alpha_f^2}{1+\alpha_f^2}\right)}\right)$
Kuwabara (1959)	$F^* = 8\pi\left(\frac{1}{-ln\alpha_f + 2\alpha_f - 0.5\alpha_f^2 - \frac{3}{2}}\right)$
Stechkina and Fuchs(1963)	$F^* = 8\pi\left(\frac{1}{-ln\alpha_f - \frac{3}{2}}\right)$

Table 2.1: Various models of drag force coefficient suggested by several authors.

The filtration behaviour of the clean air filters is well-established and especially reviewed by Davies [1973, 1983], Kirsch and Stechkina [1977], and Brown [1993b]. The model developed by Davies [1952, 1973] to deal with clean filters was used under the assumption that dust particles settle uniformly on each fibre. Such settlement increases the fibre diameter and the packing density.

The expressions of Happel [1959], Kuwabara [1959] and Fuchs and Stechkina [1963] were established from theoretical calculations for a viscous flow perpendicular to an array of parallel cylinders. However, the pressure drop predicted by these models is different from the experimental measurements of Davies [1952]. A possible explanation is that real filters do not have a regular geometry, as assumed in the

theoretical model. The empirical model proposed by Davies [1952], which has been tested for a large amount of experimental data, is the most frequently used. Thomas *et al* [1999, 2001] predicted that pressure drops by all theories are higher than the ones observed experimentally in fibrous filters. He also reasoned the over prediction to be due to the non-uniformity of fibrous structure. Such non-uniformity can also influence the dust cake formation and its structure due to the dynamic re-arrangement of particles [Dittler *et al*, 1998].

The models in Table 2.1 over predict the pressure drop due to the irregular structure of the filter media. Inhomogeneity in filtration media creates non-uniformity in the gas flow and affects the filtration behaviour of the filter. Several authors [Kirsch and Stechkina, 1978; Lee and Liu, 1982a, 1982b] accounted for this irregularity by introducing the inhomogeneity factor ξ. The values of this factor were determined experimentally and were found to be from 1.13 to 1.7. Kirsch *et al* [1971, 1973, 1978, 1985] developed the fan model to refine Happel and Kuwabara models. Although, their models showed some improvements, the inhomogeneity factor was still required.

The inhomogeneity factors mentioned in the previous paragraph are specific to the filtration media used in these studies. It is important to note though that the filter tested in this study are pleated mediums constructed in a V-shaped cartridge. Therefore, the above mentioned inhomogeneity factors may not be appropriate for this study.

2.3 Pressure Drop of Clogged Filter

When an air filter starts to collect dust particle either within its depth and/or at its surface, the description of the filtration performance becomes more complex to describe. Dust particles form a so-called dust cake as they deposit on the filter medium and this layer of dust acts as an additional layer of filtration. Dust cakes can be formed by a combination of two primary mechanisms, which are bridging and complete blocking. Bridging takes place when particles smaller than the pore sizes in the filter medium form a cake, this occurs when the particles are at a higher concentration than the feed [Wakeman and Tarleton, 1999]. On the other hand, complete blocking is a sieving process that occurs when particles are larger than the

pore sizes. Figure 2.2 illustrates dendrites which is an example of dust cake agglomerates.

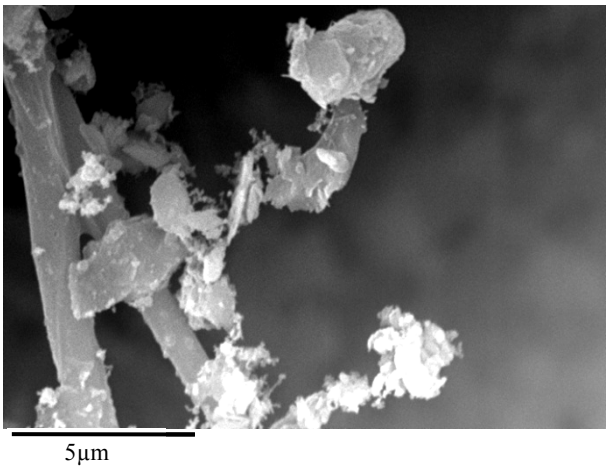

Figure 2.2: Scanning electron micrograph of dendrite formation.

The fragile nature of dust cake and its thickness variability with time makes the filtration analysis more complex. Therefore, knowledge of dust cake properties such as cake porosity and permeability is imperative to better predict the filtration performance [Schmidt, 1997a]. When gas flows through a filter, dust cake forms on its surface, and generates an aerodynamic drag. Such drag increases the mechanical compression on the layers closer to the filter surface which in turn reduces their thickness and permeability [Neiva and Goldstein, 2003].

Several authors presented their models to describe the pressure drop of dust loaded filters. Some models started with basic principle and developed models that describe mass loading as a function of pressure drop, while other models presented a correlation type model where a group of experiments is conducted to predict the mass loading as a function of pressure drop by means of an equation. Davies [1973] and Walsh [1996] described the morphology particle of deposit from dendrites qualitatively. However, in Walsh [1996] study, the filtration medium characteristics were not fully reported except the packing density. He associated the pressure drop response to the penetration of the filter to predict the clogging point by means of the departure point of the pressure curve from linearity. Although Payatakes [1977] was the first to develop theoretical models for particle dendrites growth and their effect on penetration and pressure drop, he did not compare his model with experimental results

as microscopic details were required and are difficult to compare experimentally. Kanaoka [1990] on the other hand conducted experiments on flat filter mats and proposed a technique to predict the pressure drop of a dust loaded filter based on the drag theory. He associated the applicability of his proposed technique to the condition that the effective fibre diameter and the drag coefficient of a dust loaded fibre are given as a function of accumulated volume of captured particles. He also highlighted that his model's accuracy would have improved if the filter structure was very well defined.

The above mentioned authors considered that depth deposition changes the internal structure of the fibrous material. While Kanaoka [1990] considered that particle deposition increases the fibre diameter during the stationary filtration stage, Bergman *et al* [1979] assumed that the filter may be considered as a medium where two sorts of fibres during the deposit of particles. The first sort is composed of initial fibres, and the second is the collected particles forming dendrites. This approach is equivalent to adding the pressure drop of a clean filter ΔP_i and the pressure drop of collected particles ΔP_c:

$$\Delta P = \Delta P_i + \Delta P_c \tag{2.14}$$

This model assumes there is no interference between the loaded particles and the filter medium. It also assumes that both the filter and cake are rigid, porous beds, superimposed on one another, and that the flow through them is laminar [Novick *et al*, 1998]. The approach considers that the two pressure drops are independent. However, in practice, interference exists between the collected particles and the fibres which influence the respective air flow patterns. It follows that each component of ΔP being described by Darcy's law is as follows:

$$\Delta P = K_1 U + \frac{K_2 U M}{A} \tag{2.15}$$

where $\Delta P_i = K_1 U$ and $\Delta P_c = K_2 U M / A$. K_1 and K_2 are unknown in this model since the velocity can be calculated from the total volumetric gas flow rate and the total surface area available for the filtration. K_1 depends solely on the properties of the individual filter, and can easily be measured for a particular filter from the slope of ΔP versus velocity curve. K_2 can be modelled by considering the pressure drop across the filter for a cake comprising isolated spheres with a porosity ε approaching 1; K_2 can be determined using Stokes law:

$$\Delta P_c = \frac{3\pi\mu U_m d_p N}{C_c} \tag{2.16}$$

where U_m is the filter medium velocity and N is the number of spheres per unit area. The mass of particles collected, M:

$$M = \frac{\pi N \rho d_p^3}{6} \tag{2.17}$$

yields:

$$K_{2-stokes} = \frac{18\mu}{\rho d_p^2 C_c} \tag{2.18}$$

This equation is valid for spherical aerosol particles. It is also based on the assumption that particles are of a uniform distribution far apart from one another so that the gas flows around a particle is not affected by a neighbouring particle. In practice, the particles touch one another and the gas stream lines around one particle are affected by neighbouring particles. This causes a pressure drop increase to be greater than that expected from Stokes law. Therefore, a resistance factor, R_s, is introduced to account for the difference.

$$K_2 = R_s K_{2-stokes} \tag{2.19}$$

The resistance factor, R_s, is always greater than 1, increasing as the porosity decreases and approaching 1 as the porosity increases. Different researchers have developed alternative methods of defining the resistance factor [Carmen, 1956; Wakeman, 1986]. Kozeny and Carmen [Carmen, 1956] assumed that gas flows through capillaries with a surface area equal to that of the particles making up the cake. The capillary volume is set equal to the cake void volume, and R_s can be expressed as:

$$R_s = 2K_{KC}\frac{(1-\varepsilon_c)}{\varepsilon_c^3} \tag{2.20}$$

Where K_{KC} is the Kozeny-Carman constant and is equal to 4.8 for spherical particles and 5 for non-spherical particles.

Penicot *et al* [1999] estimated the cake porosity based on the cake thickness and the particle density. They also introduced another approach to evaluating the cake porosity by considering the rise of pressure drop after being loaded with dust. This estimate was made with the calculation of the slope of the linear part of the pressure drop curves. It was assumed that the pressure drop of the cake could be compared

with the filter media thickness, packing density of the particles and the particle size that corresponds to the fibre diameter. By such comparison, and according to Davies' law [1952] and the slope value for a given set of operating conditions, the cake porosity could be estimated. Schmidt and Löffler [1990] found that the porosity of dust cake layer decreased with increasing pressure loss.

The determination of filter medium parameters such as cake porosity is not very easy to obtain but important to describe pressure drop response. Novick *et al* [1992] introduced a model that describes the pressure drop response without having to obtain cake porosity. They achieved this by means of collecting data of the mass loaded filters as a function of aerosol particle size, density and shape and then correlating the data to an equation that can be applied to wide variety of aerosol filter system design. This approach is useful in predicting the relationship between ΔP and aerosol mass loading for untested filter systems. They performed experiments on different material based on variety of particle shape and their density characteristics, namely, sodium chloride, ammonium chloride and aluminium oxide. The flow rate through the HEPA filter used was held constant during the tests. Figure 2.3 illustrates the particle size and mass loading for each plot as a function of pressure drop. It can be seen that the mass loading increases as the mass median diameter (MMD) of the aerosol is increased for a given pressure drop [Novick and Klassen, 1998]

Image Omitted

Figure 2.3: Typical HEPA filter loading response to NaCl aerosols [Novick *et al*, 1992].

Bergman [1979] showed that a set of loading curves for a single material with different particle diameters could be normalized to one curve by plotting the mass collected as a function of the increase in pressure divided by the particle diameter. Novick *et al* [1992] considered the presence of the dust cake. Nevertheless, their approach required knowing the dust packing density which is hard to obtain even experimentally. They considered the rise in pressure drop as the pressure drop of dust cake when compared with the clean filter resistance. They found that such simple normalization is insufficient when considering particles of various densities. They suggested that the slope of each line was determined for a given data set of pressure change as a function of mass loading. This value is then set equal to the specific resistance, K_2, times the gas filtration velocity, U, as in the Equation (2.14). Each K_2 value obtained from a graph of the mass loading as a function of ΔP was plotted as a function of the inverse particle diameter as show in Figure 2.4. Mass Median Diameter (MMD) was chosen for the particle diameter of the distribution since it represents the mass loading on the filter and it can be easily measured. The following equation was introduced as a result of the curve fitting to the data when combined with ΔP_o of the clean filter.

$$\Delta P = \Delta P_o + \left[\frac{0.963}{MMD} - 1.64\times10^5\right]\frac{UM}{A_s} \qquad (2.21)$$

Image omitted

Figure 2.4: Specific resistance K_2 as a function of particle diameter for different materials. [Novick *et al*, 1992].

Equation 2.22 can be re-arranged to show that difference in pressure drop as:

$$\Delta P - \Delta P_o = \left[\frac{0.963}{MMD} - 1.64\times10^{5}\right]\frac{UM}{A_s} \tag{2.22}$$

Where number is the bracket is the slope of the pressure drop response represented by the total value of the bracket in equation (2.23). In Section 4.4, linear regression techniques will be applied to equation 2.23 to curve fit the experimental data. To check the variation of slope relative to the dust type and mass loading, each dust loaded pressure drop response will be curve-fitted separately.

Another model which considered filter clogging was introduced by Rabei *et al* [2010a, 2010b] for pleated filters is:

$$\Delta P = \mu\left[\frac{h}{\kappa(M)} + \frac{h_c}{\kappa_c}\right]U_m \tag{2.23}$$

Where h_c and $\kappa(M)$ are defined as cake thickness, cake permeability as a function of mass collected and cake permeability respectively. The appropriateness of this model to be used for the analysis of the current study is discussed in Section 2.10

Several researchers considered the performance of filters during dust loading [Davies, 1973; Karadimos and Ocone 2003; Walsh, 1995; 1996; 1998]. Some studied the clogging of fibrous filters [Kanaoka and Hiragi, 1990; Payatakes and Gradon 1980; Japuntich *et al*, 1994; 1997, Payatakes and Okuyama, 1982; Payatakes and Tien, 1976] studied the pressure drop response and the filtration efficiency for loaded fibrous filters and observed the growth of dendrites experimentally. Kanaoka and Hiragi [1990] proposed a technique to predict the pressure drop of dust-loaded filter based on drag theory. It was observed that the outward growth rate of agglomerates depends upon the collection mechanism and is fastest for the case of diffusion, moderate for interception and slowest for inertial capture. However, the validity of this technique is based on the effective fibre diameter and the drag coefficient of a dust loaded fibre is given as a function of accumulated volume of captured particles.

The pore diameter of the filter medium plays an important role in the aerosol separation process. Japuntich *et al* [1994] loaded filters of different pore diameters with stearic acid having 1.16 or 2.20 µm monodisperse particle sizes in order to

examine filter pressure drop response. As illustrated in Figure 2.5, it was found that the filter medium with the smallest pore diameter have the greatest pressure drop. They also compared the pressure drops for the above particle sizes and the same mass loading but using a filter medium with a 26.2 µm pore diameter. It was found that the pressure drop at 1.16 µm and 2.20 µm were 14 and 18 mmH_2O, respectively. When they increased the mass loading to 20 g/m^2, the respective pressure drops increased to 79 and 29 mmH_2O. The results reveal that a smaller particle size causes a greater increase in pressure drops during loading because of their surface area addition which consequently increases the drag force in the filter matrix. The effect of different dust types is examined in this study by loading SAE coarse and fine dust into Group A and B filters respectively to assess filter performance.

Image omitted

Figure 2.5: Pressure drop versus mass challenge (g m^{-2}) 1.16 µm aerodynamic loading of flat filters of different pore diameters. [Japuntich *et al*, 1994].

The Kozeny-Carman equation relates the permeability to porosity and specific surface. It generally works well for incompressible materials over narrow porosity ranges. However, it cannot be used for the compressible cakes or non-spherical particles, and fails when the porosity is greater than 0.7. It therefore has limited validity for fibrous filters, although for fully clogged filters Japuntich *et al* [1994] showed that the pressure drop across the filter increases in accordance with the Kozeny-Carman equation.

Filter clogging by particles of different sizes was studied by several authors [Davies, 1970; Japuntich, *et al*, 1994; Thomas *et al*, 2001, Frising et al, 2005]. Understanding filter clogging enables gas turbine engineers and HVAC designers to determine the lifetime and the pressure drop where filter replacement should take place. The filter structure may be changed internally if particles deposit within the media, or externally if deposited on its surface to form a new layer of dust. Such change in structure affects the pressure drop response of the filter which also depends on air velocity. As far as particle size is concerned, finer particles caused higher pressure drop and are considered more clogging than larger particles [Snyder and Pring, 1955; Pich, 1966; Stenhouse *et al*, 1992; Japuntich, *et al*, 1994].

ASHRAE Standard defines the filter clogging as the mass accumulation of a polydispersed dust at the arbitrary upper limit pressure drop for an air filter [ASHRAE, 1999]. The ASHRAE definition of clogging point does not predict when the dust cake forms on filter medium [Japuntich, *et al*, 1994, 1996] and therefore, they defined filter clogging for fibrous filters as the upper transition point, where the curve becomes linear again. It can also be defined as the change of regime from depth to surface filtration. Figure 2.6 shows actual pressure drop versus mass challenge curve for a depth loading filter. In the initial stage, the curve is linear, this linearity signifies that particles are depositing within the fibrous structure, and then a departure from linearity suggests filter cake formation. The pressure drop curve becomes linear again from the cake formation point. Similar observations have been made by other authors [Pich, 1966; Gupta *et al*, 1993; Novick *et al*, 1992]. Clearly, delaying the dust cake formation by extending the depth filtration part extends the life time of the filter. Japuntich *et al.* [1996] attempted to enhance the efficiency of a fibrous filter by increasing its depth using successive layers. Their study have emphasized that to obtain useful combinations of filter life and efficiency, the depth of the filter cake has to be considered as a function of pore diameter.

Image omitted

Figure 2.6: Pressure drop versus mass challenge per filter face area with point of filter cake formation [Japuntich *et al*, 1994].

Karadimos and Ocone [2003] numerically simulated the effect of the fluid flow recalculation of complete aerosol particle deposition up to the clogging point of fibrous filters. This was done by solving both the flow of the carrier gas and the flow of the particles past the fibre. Their numerical study suggests that the efficiency increased with aerosol loading. However, a slower single fibre efficiency increase was observed with time which they attributed that particles and gas. However, the study did not consider the pressure drop change of the filter.

Tangent to loading curve

Mass Challenge g/m^2

The literature scope whether it is theoretical and experimental was limited to the study of flat filters and small scale pleated panel HEPA filters and the filter properties were not always fully reported. Further, the studies which conducted experimental work on HEPA filters used a maximum of 300x300mm pleated panel HEPA filter and not a full scale V-shaped like cartridge with higher surface area with a dimension of 592x592 mm which is the scope of this study.

2.4 Single Fibre Efficiency

Efficiency is considered the other most important performance parameter to be examined after considering the pressure drop of the filter. The overall efficiency of a filter is based on the combination of the dominant collection mechanisms. Therefore,

the particle size is of paramount importance in determining the overall filter efficiency. The single fibre efficiency for each mechanism will be introduced individually in the subsequent sections.

2.4.1 Single Fibre Efficiency due to Impaction (η_I)

The impaction mechanism occurs when a particle follows the gas streamlines but comes in contact with the fibre as illustrated in Figure 2.7. The impaction mechanism depends on the particle size, density of the dust, depth of the filter and the velocity of the air flow. Impact disposition of particles on a fibre depends on both Stokes number and Reynolds number [Kirsch and Stechkina, 1977; Payatakes and Gradoń, 1980; Ogorodnikov and Budyka, 1993; Ilias and Douglas, 1989]. The Stokes number, *St,* is defined as the ratio of the stopping distance, *S*, to the fibre diameter:

$$St = \frac{S}{d_f} = \frac{\rho_p d_p^2 C_c U_o}{18 \mu d_f} \tag{2.24}$$

The Reynolds number determines the region of the flow field in the filter. For Re < 1, Yeh and Liu [1974a] derived an equation (2.29) for the single-fibre efficiency due to inertial mechanisms. They calculated the flow field according to Kuwabara [1959] in which the influence of neighbouring fibres is taken into account. Therefore a hydrodynamic factor, *Ku*, is introduced which only depends on the packing density or solidity, ε (Kuwabara, 1959). The single fibre efficiency due to the inertial impaction mechanism is given by Yeh and Liu [1974a] as;

$$\eta_I = \frac{St(J)}{2Ku^2} \tag{2.25}$$

where $J = \left(29.6 - 28\alpha^{0.62}\right)R^2 - 27.5R^{2.8}$ for R<0.4 [Hinds, 1998]. The inertial impaction single fibre efficiency then becomes:

$$\eta_I = \frac{St}{2(Ku)^2}\left[\left(29.6 - 28\alpha^{0.62}\right)R^2 - 27.5R^{2.8}\right] \tag{2.26}$$

It is important to note that inertial deposition of particles does not depend on *Re* at its low values, but is determined by the filter packing density [Kirsch and Stechkina, 1977].

Image omitted

Figure 2.7: Illustration of the impaction mechanism [Adapted from: Donovan, 1985].

Most of the previous inertial deposition calculations from different models [Payatakes and Gradoń, 1980; Ogorodnikov and Budyka, 1993; Ilias and Douglas, 1989] were obtained from experiments were done on real filters by describing the flow field near a fibre The structure non uniformity tends to complicate the assessment of the inertial mechanism. The effect of such non-uniformity has greater influence on the impaction mechanism than on the diffusion and interception mechanisms [Ogorodnikov and Budyka, 1993].

Although inertial impaction is one of most important mechanisms in the process of air filtration, it will not be considered in the analyses of this study since the particle size considered in this study is sub 1 μm. Further, Section 2.5 will discuss the underlying reasons behind ruling out the impaction mechanism from the analysis using previous studies from the literature.

2.4.2 Single Fibre Efficiency due to Interception (η_R)

Interception mechanism occurs when a particle is attached to the fibre surface because of its diameter as illustrated in Figure 2.8. When examining Stokes number, it is evident that if particle density, the air fluid velocity or the fibre diameter is increased so that the Stokes number is infinite, the particle will have enough inertia to travel in a straight line. The limiting trajectory for this case is:

$$Y = \frac{d_f + d_p}{2} \tag{2.27}$$

On the other hand, if the Stokes number is zero, this signifies that the particle has no inertia due to a low density, low velocity, and/or small diameter. Therefore, the particle would follow the fluid streamline which is basically an interception collection. For collection to occur in this manner, the fluid streamline on which the aerosol particle begins its trajectory passes the fibre at less than $d_p/2$ from the fibre surface.

Image omitted

Figure 2.8: Illustration of the interception mechanism [Adapted from: Donovan, 1985].

Several studies have shown the relative independence of the interception mechanism of the gas velocity [Brown and Wake, 1991; Lee and Mukund, 2001; Jaroszczjk *et al*, 2002]. This independence can be contrasted to flow dependent characteristics of diffusion and impaction [Lee and Mukund, 2001]. Dorman [1964] stated that interception mechanism is independent of the gas velocity, except in so far as the flow pattern changes with velocity. Jaroszczjk *et al* [2002] on the other hand highlighted the role of particle size and its velocity in the filtration processes and suggested that it may be determined experimentally by using actual filter media with careful selection of test sample and contaminants. In this study, the particle size and velocity effects on fractional efficiency are examined in Section 4.3.2.

The single fibre efficiency due to interception, η_R depends on the dimensionless parameter R, defined by:

$$R = \frac{d_p}{d_f} \tag{2.28}$$

The single fibre collision efficiency caused by interception mechanism, η_R, is in the range Re < 1, given by [Lee and Liu, 1982a; Lee and Ramamurthi, 1993]:

$$\eta_R = \left(\frac{1-\alpha}{ku}\right)\frac{R^2}{1+R} \tag{2.29}$$

Clearly, the interception efficiency will be greater when the interception parameter, R is higher. Liu & Rubow [1986] defined the single fibre interception efficiency, η_R, as:

$$\eta_R = \frac{1}{\xi}\left(\frac{1-\alpha}{Kn_f}\right)\left(\frac{R^2}{1+R}\right) \tag{2.30}$$

where ξ is the dimensionless correction factor used to account for inhomogeneity. Yeh and Liu [1974a] have determined experimentally that the value of ξ is approximately 1.6 for polyester filters. The same value provides acceptable agreement with empirical data for glass fibre filters.

2.4.3 Single Fibre Efficiency due to Diffusion (η_D)

For particles of 1 µm and smaller, complex interactions between Brownian diffusion and inertial effects results in the so-called; Most Penetrating Particle Size (MPPS). The MPPS is defined as the particle size at which the filter efficiency is the lowest at a given flow rate [NAFA, 2001]. MPPS is only significant when dealing with *absolute* filters such as HEPA and ULPA filters. The diffusion mechanism is illustrated in Figure 2.9.

Image omitted

Figure 2.9: Illustration of the diffusion mechanism [Adapted from: Donovan, 1985].

Prediction of MPPS is of vital importance because the corresponding minimum efficiency can become one of the dominant considerations in the design and operation of air filters. 0.3 μm particle size was originally referred to as the MPPS. However, the development of the laser photometer dust particle counter has provided evidence that the MPPS is less than 0.3 μm and depends not only on the filter medium, but also on the velocity of air passing through it [NAFA, 2001]. According to theoretical predictions, MPPS is shifts to smaller particle size when air velocity increases. The effect of air velocity, pleat density and orientation on the MPPS is examined discussed in Section 4.5 of this study.

For particles smaller than the MPPS, Brownian movement is significant and the diffusion mechanism is dominant [Brown 1993b, Davies 1973]. The Peclet number, *Pe,* which characterizes the intensity of diffusion deposition, would therefore be an important parameter. An increase in the Peclet number decreases the single fibre diffusion efficiency. Kirsch and Fuchs [1968] found that the fibre efficiency due to diffusion for fibrous filters at $Kn = 0$ does not depend on the packing density in a large range of α and is a function of Peclet number only. The Peclet number is defined as:

$$Pe = \frac{Ud_f}{D} \tag{2.31}$$

where D is the diffusion coefficient.

Emi *et al* [1982] obtained numerical solutions of the velocity field around a transverse cylinder for a wide range of Reynolds numbers and fibre volume fractions of a filter. The convective diffusion equation, with the numerical solutions of velocity profiles, was solved in the range of Peclet numbers $1–10^4$. The efficiency of a fibre calculated at Re = 1 is in good agreement with Stechkina's analytical expression for creeping flow, and at large Reynolds numbers approaches Natanson's potential flow expression. Davies [1973] presented the single fibre efficiency due to the diffusion effect as:

$$\eta_D = 2R\mathrm{Pe}^{-\frac{2}{3}} \tag{2.32}$$

Lee and Lui [1982a] presented their diffusion single fibre efficiency by using the Kuwabara cell model as follows:

$$\eta_D = 2.6\left(\frac{1-\alpha}{ku}\right)^{\frac{1}{3}} \mathrm{Pe}^{-\frac{2}{3}} \tag{2.33}$$

They also claimed equation 2.39 is applicable for wide range of conditions such as high packing density α that by including the factor (1- α) in theoretical expression.

2.5 Overall Filtration Efficiency

The overall efficiency of a filter, E, is a function of the single fibre efficiency, η [Hinds, 1998]. Filtration efficiency in general is a function of particle size, particle shape, filtration velocity and frequently particle charge which makes the comprehensive evaluation of air filter efficiency a difficult task [Letourneau *et al*, 1990; Penciot *et al*, 1999]. In addition, caution must be exercised when assessing the overall efficiency by considering the results of the combined effect of all collection mechanisms. The overall efficiency of a filter, E and filter penetration P_t is given by [Lee and Lui, 1982a; Hinds, 1998]:

$$P_t = 1 - E = \exp\left(\frac{-4\alpha\eta h}{\mu d_f}\right) \tag{2.34}$$

where η is the summation of the single fibre efficiencies for each mechanism and defined as:

$$\eta = 1 - (1-\eta_D)(1-\eta_R)(1-\eta_I)(1-\eta_{DR}) \tag{2.35}$$

As discussed earlier, the single fibre efficiencies due to different transport mechanisms can be calculated provided the flow field around the filter fibre, usually characterised by the Reynolds number. Nguyen and Beeckmans [1975] conducted an experimental study on the single fibre efficiencies of fibrous filters as they are loaded with monodispersed aerosol particles in the size range of 0.95-1.75 µm at various face velocities. Figure 2.10 illustrates that the filter has the lowest efficiency at the 0.95 µm particle size at the same face velocity. They used a commercial fibrous filter with fairly uniform fibres of 24.4 µm, a packing density of 1.09% and thickness of 1.35 cm.

Image omitted

Figure 2.10: Experimental single fibre efficiencies vs. face velocities for the fibrous filter used. Solid lines calculated by proposed correlation for each particles diameter [Nguyen *et al* 1975].

The filter efficiency is highly affected by air the velocity. Figure 2.11 illustrates velocity variation effect on filter efficiency for different particle sizes and for a packing density of 0.05, 1 mm filter medium thickness and 2 μm fibre diameter. Clearly, increasing the velocity will reduce single fibre efficiency due to diffusion and the impact efficiency rises [Hinds, 1998]. The aerosol penetration through fibrous filters was measured [Kirsch, 1972; Kirsch and Lahtin, 1975]. They evaluated the combined diffusion and interception efficiency considering the fibre polydispersity. They found that the maximum penetration occurs with lower particle sizes with rising flow velocity. Clearly, the air velocity is of a critical importance to the filtration process since it influences the filters behaviour. Therefore, face velocity variations are also another important aspect of this study and its effect on filter permeability, pressure drop and fractional efficiency is presented in Section 4.2.

Image omitted

Figure 2.11: Filter efficiency versus particle size for face velocities of 0.01 and 0.1 m/s [Hinds, 1998].

Kaufmann [1963] was uncertain how the overall filtration efficiency could be evaluated as result of all collection mechanisms. He combined curves for two mechanisms and calculated the combined penetration as a product of each penetration due to each individual mechanism. Davies [1973] disagreed with Kaufmann's approach even though it was a great advance at the time; his disagreement was incorrectly based upon ideal flow. Further, if the filter used has a fibre diameter of 20 μm and air velocity through it is 15 cm/s, then Reynolds number becomes 0.2. This indicates that the flow around the fibre at such low Reynolds number is viscous and the inertia of air is insignificant. In viscous flow, the presence of the fibre affects the flow pattern at upstream distances of many radii. The flow opens out gradually to pass the fibre. In ideal flow the inertia of the air prevents this from happening until only one or two radii upstream, spreading of flow to pass the fibre is rapid [Davies 1973]. Figure 2.12 shows the single fibre efficiency for each collection mechanism as well as the overall efficiency.

Image omitted

Figure 2.12: Overall efficiency and single fibre efficiency for each collection mechanism [Hinds, 1998].

In gas filtration, it is common to assume that each mechanism acts independently of any others. When evaluating the overall efficiency of a filter, the mechanisms considered are diffusion, interception and inertial impaction since they are the most important as indicated by Davis [1973]. Several studies [Ramarao *et al* ,1994; Lee and Lui, 1982a; Hinds, 1998] approached the problem of assessing the overall efficiency when more than one collection mechanism is dominant. This was done by assuming that the sum of the single fibre efficiencies is the addition of the individual mechanisms. Yeh and Liu [1974a] considered diffusion, interception and impaction simultaneously and solved for the filtration efficiency numerically to yield:

$$\eta = \eta_D + \eta_R + \eta_I \tag{2.36}$$

Dawson [1969] also proposed the expression for single fibre efficiency under the combined effect of Brownian diffusion, interception and impaction. However, knowing the particle size distribution challenging the filter will enable the appropriate assessment of the filter. This can be done by initially determining which mechanism or mechanisms is/are dominant in the filtration process. Stechkina *et al* [1969] considered the diffusion and interception mechanisms are the dominant mechanisms

when considering the MPPS and used an individual expression for each mechanism and then added a third term to consider their combined effect:

$$\eta = \eta_D + \eta_R + \eta_{DR} \tag{2.37}$$

where η_{DR} is the single fibre efficiency under the combined effect of diffusion and interception. Lee and Liu [1982a] also considered that for particle size range of 0.1 and 0.3 μm, impaction mechanism may not be important. The practice of simple addition of the individual filtration mechanisms is based on the assumption that only one mechanism is dominant while the contributions of the other mechanisms are not significant. Lee and Liu [1982a] suggested that this assumption is adequate based on the fact that as the particle size increases, the efficiency due to diffusion decreases whilst the interception mechanism becomes increasingly prominent. Lee and Lui [1982a] assumed that neither incorporating the impaction mechanism nor the combined effect of diffusion and interceptions in the analysis have provided a significant enhancement to the efficiency results. Lee and Lui [1982a] justified their assumption based on the comparison they conducted between Yeh and Liu [1974a] and Stechkina *et al* [1969] illustrated in Figure 2.13 which shows a satisfactory agreement with their theoretical results for Pe ≤ 30,000 and Re ≤ 0.2. Therefore, they expressed the total single fibre efficiency as:

$$\eta = \eta_D + \eta_R \tag{2.38}$$

Although adding individual separate efficiencies seem basic, it has given reasonable results for combined efficiencies without having to consider the impaction mechanism or a combined term for interception and diffusion. Based on these assumptions, Lee and Liu [1982a] presented the sum of the single fibre efficiency as:

$$\eta = 2.6\left(\frac{1-\alpha}{Ku}\right)^{\frac{1}{3}} Pe^{-\frac{2}{3}} + \left(\frac{1-\alpha}{Ku}\right)\left(\frac{R^2}{1+R}\right) \tag{2.39}$$

Image omitted

Figure 2.13: Comparison between Equation (2.46) and theories of Stechkina *et al* [1969] and Yeh and Liu [1974a], [Lee and Liu, 1982a].

Lee and Liu [1982a] followed the method of the Friedlander [1958] and Spielman and Goren [1968] by multiplying both sides of the Equation (2.39) by $Pe\ \frac{R}{\sqrt{1+R}}$. They verified their assumptions by plotting their results to compare with Yeh and Liu [1974a] and found that their assumption is safe and can be used for practical application as shown in Figure 2.14. The Lee and Liu [1982a] comparison showed that the differences between the two efficiencies are negligible. In addition, the Reynolds and Peclet numbers of this experimental study is well below the limits, namely, Pe ≤ 30,000 and Re ≤ 0.2. Further, the Lee and Liu model [1982a,1982b] takes into account the flow interference effects of neighbouring fibres which provides better representation of the actual flow profile in the filter. Therefore, Equation 2.39 will be the starting point of the initial fractional analysis for this study in Section 4.4.

Image omitted

Figure 2.14: Comparison between Lee and Liu [1982a] model and Yeh and Liu [1974a], [Lee and Liu, 1982a].

Several authors have proposed a semi-empirical correlation of Lee and Liu [1982] applies to a continuous-flow regime [Lee and Liu, 1982; Liu and Rubow, 1990; Payet *et al,* 1992], i.e. for the case when the fibre diameter is much larger than the mean free path of gas molecules (λ). In this case, the fibre Knudsen number can be neglected. However, this approach may not be correct when examining filter media with a small fibre diameter [Brown, 1993b]. For example, higher classes HEPA filters such as H12, H13 and H14 usually have greater number of submicron fibres, in which case the flow around the fibre must consider the effects of the slip flow especially when Knudsen number is more than 10^{-3}.

Liu and Rubow [1990] corrected Lee and Liu model by considering the slip flow, however, the efficiency was more than unity. It was later modified by Payet [1991] who introduced a correction factor (Peclet number) to bring the efficiency to less than unity at low Peclet number. Experimental results by Payet *et al* [1992] reported a good agreement with this model for a particle size range of 0.08-0.4μm.
The model of Payet is given by:

$$\eta = 1.6\left(\frac{1-\alpha}{Ku}\right)^{\frac{1}{3}} Pe^{\frac{-2}{3}} C_1 C_2 + 0.6\left(\frac{1-\alpha}{Ku}\right)\left(1+\frac{Kn}{N}\right)\left(\frac{N^2}{1+N}\right) \tag{2.40}$$

the constants are:

$$C_1 = 1 + 0.388 Ku\left(\frac{(1-\alpha)Pe}{Ku}\right)^{\frac{1}{3}} \tag{2.41}$$

and

$$C_2 = \frac{1}{1+1.6\left(\frac{(1-\alpha_f)}{Ku}\right)Pe^{\frac{-2}{3}} C_1} \tag{2.42}$$

Several studies investigated the capture of charged dust particles by electrets. [Brown *et al;*1994a, 1994b]. Other authors such as Kirsch and Stechkina [1977] measured the penetration of uncharged monodispersed particles with radii of 0.9 to 2.9 µm through model filters consisting of grids made from wires of diameter 8.9 and 25 µm. They evaluated the collection efficiency due to inertia and interception of particles, and experimental results have shown a good agreement with the theoretically predicted values of particle penetration for all values of interception parameter and Stokes number. However, experimental results were lower than the theoretical ones with large grid number at high velocity due to insufficient particle mixing. The study of Brown and Wake [1999] described the behaviour of air filters in terms of the layer efficiency and the mass of deposited aerosol per unit volume which resulted in a doubling of the layer efficiency. Their study has also shown that the aerosol penetration decreases approximately exponentially with time as dust loading increases. This effect will be investigated in this study as filter Groups A and B will were loaded with two different dust types, namely, SAE fine and coarse which will also allow to the study the effect of particle size and its distribution on pressure drop and fractional efficiency of the filter.

Table 2.3 lists different efficiency models for diffusion and interception mechanisms for different authors.

Efficiency Models

	Author	(Diffusion)	Interception	Remarks
1	Stechkina &Fuchs (1966)	$\eta_D = 2.9Ku^{-1/3}Pe^{-\frac{2}{3}}+0.62Pe^{-1}$	$\eta_R = \frac{1}{2\,Ku}[2(1+R)Ln(1+R)-(1+R)+(1+R)^{-1}]$	Kuwabara Flow $Ku = -\frac{1}{2}\ln\alpha - 0.75 + \alpha - \frac{1}{4}\alpha^2$ Second term of equation is negligible when Pe >100
2	Davies (1973)	$\eta_D = 1.5Pe^{-\frac{2}{3}}$		$Pe = \left(\frac{d_f U}{D}\right)$
3	Lee & Liu (1982a)	$\eta_D = 2.6(\frac{1-\alpha}{Ku})^{1/3}Pe^{-\frac{2}{3}}$	$\eta_R = \left(\frac{1-\alpha}{Ku}\right)\left(\frac{R^2}{1+R}\right)$	Kuwabara Flow
4	Lee & Liu (1982b)	$\eta_D = 1.6(\frac{1-\alpha}{Ku})^{1/3}Pe^{-\frac{2}{3}}$	$\eta_R = 0.6\left(\frac{1-\alpha}{Ku}\right)\left(\frac{R^2}{1+R}\right)$	Kuwabara Flow
5	Liu & Rubow (1990)	$\eta_D = 1.6(\frac{1-\alpha}{Ku})^{1/3}Pe^{-\frac{2}{3}}C_d$	$\eta_R = 0.6\left(\frac{1-\alpha}{Ku}\right)\left(\frac{R^2}{1+R}\right)C_r$	Kuwabara Flow $C_d = 1 + 0.388\,Kn_f\left(\frac{(1-\alpha)Pe}{Ku}\right)^{\frac{1}{3}}$ $C_r = 1 + 1.996\frac{Kn_f}{R}$
6	Payet *et al*. (1991)	$\eta_D = 1.6(\frac{1-\alpha}{Ku})^{1/3}Pe\,C_d{}^{-\frac{2}{3}}C_d'^{-\frac{2}{3}}$	$\eta_R = 0.6\left(\frac{1-\alpha}{Ku}\right)\left(\frac{R^2}{1+R}\right)C_r$	Kuwabara Flow $C_d' = \frac{1}{1+1.6(\frac{1-\alpha}{Ku})^{1/3}Pe^{-\frac{2}{3}}C_d}$
7	Gougeon *et al*. (1996)	$\eta_D = \frac{1.6(\frac{1-\alpha}{Ku})^{1/3}Pe^{-\frac{2}{3}}C_d}{1+1.6(\frac{1-\alpha}{Ku})^{1/3}Pe^{-\frac{2}{3}}C_d}$	$\eta_R = 0.6\left(\frac{1-\alpha}{Ku}\right)\left(\frac{R^2}{1+R}\right)C_r$	Kuwabara Flow
8	Lee & Ramamurthi (1993)	-	$\eta_R = \frac{(1-\alpha)R^2}{Ku\,(1+R)}$	$Ku = -\frac{1}{2}\ln\alpha - \frac{3}{4} + \alpha - \frac{\alpha^2}{4}$
9	Kirsch and Fuchs (1968)	$\eta_D = 2Pe^{-\frac{2}{3}}$	-	Based on the experimental measurements, coefficient 2 is empirically determined
10	Pich (1966)	$\eta_D = \frac{2.86}{Ku^{\frac{1}{3}}Pe^{\frac{2}{3}}}\left(1+\frac{0.388KnPe^{\frac{1}{3}}}{Ku^{\frac{1}{3}}}\right)$	-	

Table 2.3: Efficiency models for diffusion and interception mechanisms for different authors.

2.6 Dust Cake Compression

Compression of dust cake occurs when the compression force is greater than the resisting force to the deformation or collapse of dendrites [Stöcklmayer et al, 1998]. Dust layer is compressed by the drag force acting on the particles. Consequently, porosity and permeability may decrease due to such compressive stresses caused by the cumulative aerodynamic drag force acting on the cake particles [Neiva and Goldstein, 2003].

Several methods were developed to investigate the compression behaviour of dust cakes. [Höflinger *et al*, 1994] introduced the first simulation model where maximum adhesion force and friction angle of particle particles were used as simulation parameters to calculate the resistance force on the compression of dust cake through drag force. Dust cake compression possibility was determined by comparing the magnitude of the compression force with that of resistance force on compression. While their work was the first to deal with the dust cake compression of monodisperse particles, they did not account for the particle size effect on the dust cake compression. Jeon and Jung [2004] considered such effect of particle size on pressure drop response by loading particles of 7.5 and 15 μm in diameter at the same mass density. They found that, as illustrated in Figure 2.15, the total pressure drop through the dust cake composed of 7.5 μm particles is much higher than that of 15 μm particles. It is clear from this study and other studies [Aguiar and Coury, 1996; Endo *et al*, 1998] that smaller particles tend to result in larger pressure drop through the dust cake.

Image omitted

Figure 2.15: Effect of particle size on the increase of pressure drop with the increase in real density [Jeon and Jung, 2004].

Several studies have been conducted to describe the trends of dust cake formation [Schimdt, 1997a;1997b, Schmidt and Löffler, 1990; Schmidt and Pilz, 1996]. Most of these studies have focused on dust porosity and mass, the particle size and shape and the operation condition such as face velocity. Endo *et al* [1998] performed real time pressure drop measurement and examined the dust cake height under fixed parameters such as particle size distribution, particle shape and flow rate. He was able to develop an analytical expression to correlate the above-mentioned physical properties to the height and porosity of the cake, and the flow rate and pressure drop.

When particles start to collect other particles, dust cake properties play a vital role in evaluating the filter's performance in the surface filtration stage. Cake porosity and thickness are two very imperative parameters that can only be predicted experimentally [Penicot *et al*, 1999; Morris and Allen, 1996]

To determine if the dust cake compression occurs, it is important to establish the forces associated with compression behaviour of the dust cake. The normal force is defined as the force acting on the particle along the centreline connecting the two centres of particles. The shear force is defined as the force required moving the particle in an upper layer along the perimeter of the contacting particle in the lower layer. On the other hand, friction force plays a role in preventing the particle from moving [Höflinger, 1994; Stöcklmayer and Höflinger, 1998].

Adhesion forces such as van der Waals forces, electrostatic mechanisms and surface tension forces play the role of keeping particle in contact with filter fibre when deposited. In many studies, only van der Waals forces are considered when operating under the assumptions that particles are not electrically charged and the humidity effect is negligible and therefore, no rise in surface tension occurs between particles due to condensed water.

For dust cake compression to occur, the compression force must be larger than the resisting force to the deformation or collapse of dendrites. Figure 2.16 shows the compression force, F_c, acting on the dust particle. Such force can be divided into normal, F_n, and shear force, F_s.

Image omitted

Figure 2.16: Forces acting on a dust cake particle [Stöcklmayer and Höflinger, 1998].

2.7 Filtration Media Characteristics

The characteristics of filtration medium will be addressed in this section. These characteristics include fibre diameter and the associated size distribution. These parameters are characterized in this study and reported in Section 4.1.1. The effects of these characteristics on the filtration will be discussed using the available literature.

Several authors have attempted to study the effect of fibre size on the filtration performance. Kirsch *et al* [1974] were the first to address the problem of two fibre size filtration media. They studied the pressure drop, flow field and diffusional deposition of aerosols in the simplest model of polydisperse fibrous filter consisting of rows of parallel cylinders with different radii arranged perpendicular to the flow direction at low Reynolds numbers. Their study has shown that the pressure drop and diffusional particle deposition can be calculated from the mean cylinder radius even when the radii differ several times.

Lisowski *et al* [2001] measured the performance of textile fibre filter materials with monodisperse aerosol and standard ASHRAE dust which is polydispersed [ASHRAE 51.1, 1992]. The monodispersed aerosol ranged from 1.5 to 9 µm. Pressure drop and efficiency measurement shows the closest agreement between the 7 µm monodispersed aerosol and ASHRAE dust which has a mass-mean diameter of 7.7 µm They also found that smaller particles penetrated the filtration medium greater than larger particles.

The orientation of the fibre relative to the direction of the airflow influences the pressure drop and the removal efficiency. A filter made of fibres parallel to the airflow would have only one half of the resistance of a filter having similar fibres arranged perpendicular to the airflow [Langmuir 1942; Davies 1952]. The expression for the pressure drop is given by [Kuwabara, 1959]:

$$\Delta P = \frac{2\alpha h \mu U_o}{Ku\left(d_f\right)^2} \tag{2.43}$$

Brown [1984] developed a theory for the capture of particles by fibre parallel to the airflow direction. His theoretical development shows that a 5% penetration can be achieved by a system of parallel fibre filter of only one third of the thickness and about one-sixth of the resistance of an equally efficient perpendicular fibre filter.

2.8 Aerosol Characteristics

The characteristics of aerosols that most affect the performance for an air filter includes particle size, particle shape, mass, concentration and electrical properties. The most important of these is the particle size [ASHRAE, 2000].

2.8.1 Particle Size

Particle size is considered to be a fundamental parameter for characterising the behaviour of aerosol. In fact, all properties of aerosol depend on particle size while some depend strongly on it [Reist, 1984; Hinds, 1998]. A particle is generally imagined to be spherical and its diameter is usually used to describe its size. Unfortunately, there are several ways of defining particle size particularly for those of irregular shapes. Table 2.4 lists common particle diameters definitions used in the literature. As particle size and its distribution highly influences the filtration behaviour of air filters, both of these parameters are measured for Kuwaiti atmospheric dust and compared with other synthetic dusts. The objective of the comparison to investigate the effects of particle size distribution on the pressure drop and fractional efficiency of full scale HEPA filters.

Table Omitted

Table 2.4: Particle diameter definitions [Reist, 1984; Hinds, 1998].

2.9 Flow Through Pleated Media

Pleated filters are commonly used in various applications related to gas turbines, space and nuclear industries and clean room applications. The critical nature of these applications requires specific filtration performance. Therefore, accurate prediction of the pleated filters performance is of a paramount importance in order to make appropriate filter selection by achieving an optimized filter design. The main design feature under examination in this study is the pleating density.

Pleating the filter medium provides larger surface area in a given space, which decreases the air medium velocity. As far as the filter efficiency is concerned, slower medium velocity translates into a longer aerosol's residence time inside the filtration medium which increases the probability of the particle-fibre contact. As a result, this leads to an enhancement of diffusional capture efficiency leading to increased particle loading capacity per unit area when compared with a flat sheet medium. Pleating filtration media also enables an increase in the collection efficiency for a given pressure drop, provides higher dust holding capacity and reduces energy consumption [Chimack and Sellers, 2000]. In terms of structural integrity, pleated medium panels are more stable than a flat sheet of the same medium, which is inclined to deform and eventually rupture.

According to Darcy's Law, there exists a linear relationship between pressure drop response and flow rate, which also signifies that the permeability of the filtration medium does not change and the pressure drop should vary linearly with the filtration velocity. Therefore, an intuitive attempt to lower pressure drop would be to lower the

medium velocity by increasing the surface area. Therefore, the pressure drop of the filter is expected to continue to decrease as the pleating density increases. However, when excessive number of pleats or overpleating is introduced, the pressure drop also increases as a result of the increased fluid viscous drag in the pleat spacing. Therefore, the higher the pleating density, the higher the pressure drops. Clearly, there are two competing contributions to the overall pressure drop. This problem was considered by several authors [Raber, 1982; Yu and Goulding, 1992; Chen *et al;* 1995; Lücke and Fissan, 1996; Fabbro *et al*, 2000; 2002], however, all these studies used lower face velocities than the ones used in this study. Therefore, the pleating density will be varied in this study and will be subject to various face velocities matching the ones it encounters during real industrial operations.

The pressure drop through the pleat is generated by the alterations in cross-sectional area as the air flows into and out of the pleat [Brown, 1993b; Chen *et al*, 1995]. The total pressure drop across the pleated filter is a result of the pressure drop across the filter media, flow contraction in the upstream region, viscous drag between the fluid and porous surface on both the upstream and downstream channels, and flow expansion in the downstream region.

Unlike the extensive literature covering the clean and dust loaded flat filters, the literature dealing with pleat design, pleat density and other optimization parameters is limited and the results do not follow any simple theoretical patterns [Brown, 1993b]. The problem of fluid flow through a panel pleated filter media was investigated by Pui *et al* [1994] and Chen and Pui [1996]. Yu and Goulding [1992] published an approximate solution of the problem based on analytical considerations. The ideal number of pleats may vary with the material used and the conditions of the filtration [Brown, 1993b]. Chen *et al* [1995] suggested that there is an optimal pleat count defined where the pressure drop is lowest. However, in their study no consideration was given to the efficiency requirement. The existence of the optimal pleat count will be discussed in association with the efficiency requirement in Section 4.4.4.

Few models have been proposed to calculate the efficiency and the pressure drop of filters under steady flow conditions. Lucke and Fissan [1996] developed models that relate the filtration performances of a plane medium to the pleated medium but did not

extend their study to examine filter cartridges constructed in V-shape like the HEPA ones considered in this study. It is important to note that filter cartridges provide larger filtration area in a confined space by means of compact stable pleated panels which extends the life time of filter and reduces maintenance costs.

The upstream and downstream flow domains of a filter pleat are governed by the incompressible Navier-Stokes and continuity equations. Through the porous filtration media, Darcy's equation can be used for modelling, assuming the media is porous. The validity of this equation is based on the assumptions that the fluid is homogeneous, and that there is no interaction between the fluid and the media. Further, it is assumed that the flow rate is kept relatively low and the pleat geometry is rigid. The pressure drop increases at small pleat count due to reduced surface area and increased media face velocity, and at large pleat count due increased viscous drag in the pleat spacing. Rabei *et al* [2010a] suggested that there exists a two pleat counts, one where the filter capacity is maximized and another defined the optimal pleat count where the pressure drop is a minimum. At this pleat count or density, the viscous drag and the media resistance are at their minimum.

Chen *et al* [1995] developed a numerical finite element model to optimize the pleating density of filter materials with different permeabilities. Their results show that for a given pleat height and specific filter medium, the optimal pleat count increases as the filter media permeability decreases. Figure 2.17 illustrates minimum pressure drop for the HEPA filter for different pleat counts. As the pleat height increases, the optimal number of pleats required to achieve the minimum pressure drop for such case is reduced.

Image omitted

Figure 2.17: Initial pressure drops as function of pleat count and height for HEPA filter material [Chen *et al*, 1995].

Prior to the work of Chen *et al* [1995], Yu and Goulding [1992] conducted a similar study without considering the pressure drops due to flow contraction, developing flow and flow expansion. Figure 2.18 shows that at low pleat count; the pressure drop predicted by Chen *et al* [1995] numerical model is higher than Yu and Goulding's. This difference was expected by Chen *et al* [1995] since his model included other pressure drops which were neglected by Yu and Goulding [1992].

Image omitted

Figure 2.18: Comparison of Chen's model and model of Yu and Gouling (1992) for mini-pleated filters with two different pleat heights [Chen *et al*, 1995].

Several studies have subjected HEPA filters to variable velocities and measured their penetration [Sinclair, 1976; Leibold and Wilhelm; 1991, Vendel *et al*; 1990, 1992a, 1992b, Payet *et al*; 1992, Mouret *et al*, 2009]. Sinclair [1976] study has shown that the efficiency of the HEPA filters tested was much greater for the particle diameter range from 100 down to 1 nm than for 0.3 DOP. He also showed that the efficiency of the HEPA filters decreased with increasing velocity from 5 to 70 cm/s as would be expected from diffusion theory. The work of Chen *et al* [1995] considered panel pleated filters with relatively small flow rates and the pleating densities considered had a highest of 40 pleats per 100 mm. They only considered in their numerical study three velocities of 25, 100, 250 fpm (127, 510, 1270 mm/s) compared to 10 different velocities used in this study. The pleating densities considered in this study vary from 28 to 34 pleats per 100 with an increment of 2 pleats per 100 mm. Further, this study experimentally investigated the effect ten different flow rates and their corresponding face velocities to study their effect on the pleating density, pressure drop and filtration medium permeability.

Golan and Parekh [1985] considered mathematical modelling of several hydrodynamic phenomena of fluid flow for semi-dense pleated structures in cartridge filters. The pleat was assumed to be composed of a membrane sandwiched between two supportive layers, one upstream and one downstream, of different permeability values. Four different cases of semi-dense pleated configurations were considered: constant and pressure-dependent downstream layer permeability with time-variant and time-dependent membrane permeability. The relationship between pleat physical properties, fluid flow rate, pressure drop and overall efficiency was evaluated, and they considered an ‘optimal’ or effective membrane area of a pleated cartridge to be a product of the actual area multiplied by pleat efficiency. Longer pleats and a thinner downstream supportive layer were claimed to increase the actual area, but there may be an adverse effect on efficiency primarily because of lower downstream layer permeability.

Few studies considered the clogging of pleated filter [Benmachou *et al*, 2003; Rabei *et al*, 2010a]. Benmachou *et al* [2005] developed a clogging model considering that the main capture mechanism is sieving. In the current study, the dominant mechanisms are interception and mechanism since HEPA filter are experimentally

investigaged. On the other hand, Rabei *et al* [2010a] presented a clogging model of pleated filters by combining a semi-analytical model of the flow in pleated filter and an empirical model of a planar filter applied locally along the pleated channels. Their model took into account the formation dust cake of variable thickness at the porous wall of the pleated filter entrance channels. Their study considered two optimal pleat densities, one considering the maximum filter capacity and another due to a minimum pressure drop. It was found in their study that the former pleat count is greater. In their experimental study, a single and low flow rate of 389 m^3/h was used with small scale filter with face dimensions of 89 by 220 mm. The pleating density used was limited to 8 and 12 pleats per 100 mm. Their dust loading experiments were done using Arizona dust.

The study of Rabei *et al* [2010a] used low filtration velocities lower than the ones considered in the present work. On the other hand, Rabei *et al* [2010b] considered higher filtration velocities of a maximum of 1.5 m/s using a filtration medium of a 15-30 µm fibre range. Although the Reynolds number was between 1.3 and 3 for both fibre diameters respectively, the authors still used Darcy's Law reasoning that to the fact that the deviation from linearity at such Reynolds number is not significant and the main contribution to the overall pressure drop is not due to the porous medium but to pressure loss in the pores channels. Although the Rabei *et al* [2010b] work is good representation for the study of filter clogging, the study used small filter elements with a low surface of nearly 0.02 m^2, permeability and filter medium thickness of 2.28 $x10^{-10}$ m^2 and 2.85 mm respectively. It is apparent that the filtration medium properties, filtration velocities, the filter design and the pleating densities are different from the ones used in the current study.

Wakeman and Harris [1993] developed a methodology for modelling pleated cartridges, in order to predict magnitude and direction of fluid and particle velocities, the pressure distribution, permeability of the filter cake or a measure of particle deposition. If cake starts building during filtration, the volume of the flow region upstream of the pleat will change, posing extra complexity to the problem. It was assumed that there was no formation of cake, which is the practical case when filtering low concentrations of smaller particles. The model was specific to 'star' pleat configurations, which were considered to have symmetry in the radial direction,

therefore requiring only half of the pleat to be modelled. The free flow was modelled by the unsteady state Navier–Stokes equation and the pressure drop in the porous region was calculated by the Darcy equation, and the governing equations were solved using a classical finite difference scheme. The number of particles trapped in the porous medium was related to the magnitude of flow through the medium and its history at a particular point. The flow was radial in free flow region upstream of and far from the filter medium, and flow deviated as it approached the pleat surface in order to pass through the porous structure. A smaller amount of fluid flows through about 50% of the pleat face with most of the flow through the area between the inner tip of a pleat and centre of the pleat face before the stage of solids deposition.

The pressure differential developed over a pleat was primarily dependent on the porous medium permeability in the initial stages of filtration (before deposition of particles). After the solids start to deposit, the pressure loss is a function of the overall permeability (which decreases with time) of the medium and the deposited solids. The work pointed to a need to develop a three-dimensional model to generate a better representation of the cartridge filter. The need to use depth filtration equations as well as the classical Darcy equation to account for internal deposition of solids was also recognized.

Wakeman *et al* [2005] developed a simulation code that can model fluid hydrodynamics in permeable media and pleated filter cartridges and used it to evaluate the performance and design of pleated cartridge filter elements. They analysed the effects of medium compression, pleat deformation and pleat crowding. A permeability model that interprets medium compression effects and which is based on data obtained from flat sheets of the filter material used in the fabrication of filter cartridges is incorporated into the main model. During pleating, bending and creasing of the medium deforms it and leads to a loss of permeability and/or effective filtering area. Authors reasoned the deviations from Darcy's law due to the combined effects of medium compression, pleat crowding and pleat deformation which leads to reduction in filtration area. Although the study of Wakeman *et al* [2005] focused on the filtration of hydraulic fluids used in aeronautical applications, the approaches taken were generic and should be applicable to a range of designs of cartridge filters developed for many different applications [Hanspal *et al*, 2005].

The pleat geometry influences the pressure drop of the filter as presented by Caesar and Schroth [2002]. They compared the pressure drop response of a rectangular and V-shaped pleat. As shown in Figure 2.19, the filter with a V-shaped pleat had a lower pressure drop when compared with the rectangular pleat filter. They considered that the flow through a V-shaped pleat filter is ideal particularly when large pleat depths and small pleat count distance are involved. While their study results favoured the V-shape, their study did not involve any dust loading or the effect on the pleat shape on permeability. The pleat shape is not considered is this study as the main subject is pleat density and orientation.

Image omitted

Figure 2.19: Comparison of the total pressure drop in dependence on the pleat distance for V-shaped and rectangular pleat geometries [Caesar and Schroth, 2002].

2.11 Summary

The literature offers a wide range of studies on the performance of clean filters. Several authors have studied loading filters with monodisperse and polydispersed aerosols. Most of these studies considered flat fibrous filter medium and the filtration performance was examined. Other literature have considered penetration of pleated HEPA filters both clean and loaded with solid particles, liquids droplets and a mixture of both. The literature scope whether it is theoretical or experimental was limited to the study of flat filters and small scale pleated panel HEPA filters and the filter properties were not always fully reported. Although some studies were done on pleated filtration media, the literature available on pleated panels of HEPA filters is rather limited and is mainly based on numerical approaches used for performance analysis and considered small scale pleated panel filters.

It is evident from the literature review that the filtration process is complex and varies with several parameters. The assessment of air filter performance is influenced by several parameters such as face velocity, filter medium properties, filter design, aerosol characteristics, ambient conditions and dust types and their loading conditions. The complexity of air filter performance evaluation lies in the simultaneous variations of all these parameters. Various assumptions were made in the literature in order to simplify the evaluation process of air filters. However, this evaluation can be viewed as a performance indication rather than exact filter behaviour. Furthermore, there are some parameters are time-dependent such as mass loading, dust cake thickness, the overall fibre shape, the filter porosity which leads to variation to the filter medium geometry due to particle deposition.

The novel contribution of this study begins with the full scale experiments and HEPA filter constructed in a V-shape bank cartridge. The HEPA filters used were of standard dimensions and not a flat sheet media or small scale panel filter considered previously in the literature. This experimental work also investigated the effect of varying flow rate on the filter performance by measuring the pressure drop and fractional efficiency for ten different flow rates. The range of the flow rates used in the testing is great enough to analyze the deviation from Darcy's Law (linear pressure drop). Through the novel flow rate variations examined in this study, the underlying reasons of surface area losses of filtration media which led to permeability reduction are highlighted. In addition, the pleat density and orientation on the initial pressure drop, fractional efficiency and associated MPPS of HEPA filters are also examined. The filters were subject to different synthetic dusts (SAE fine and coarse) loaded at standard dust concentration to study their effect on the performance of pleated full scale V-shaped HEPA filter cartridges. This study also presents novel explanation in investigating the counterproductive effect of increasing pleat density in terms of effective filtration surface area and filter permeability. Chapter Three introduces the experimental facility used to conduct the planned experiments and Chapter Four provides the relevant analysis of experimental results and introduces a modified model to predict the pressure drop and efficiency. Finally, Chapter Five presents the new design alterations for maintaining effective surface areas suggested in this study.

CHAPTER THREE

EXPERIMENTAL FACILITY AND PROCEDURES

This experimental work involved the testing of ten glass fibre pleated cartridges of HEPA Class H10 filters according to DIN EN 1822 Standard [1998]. The first eight filters were manufactured by EMW Filtertechnik in Germany with pleating densities varying from 28 to 34 pleats per 100 mm, giving a range of surface areas. For the remaining two filters, the pleating density and the filter class remained the same but with a change in the pleat orientation relative to the air flow. The pressure drop measurements for the flat sheet media used in manufacturing of the tested filters were also measured.

The eight manufactured filters were divided into two groups, A and B. Both Groups underwent similar testing procedures with the exception that Group A was challenged with SAE coarse dust while Group B was challenged with SAE fine dust. For initial fractional efficiency measurements, all ten filters were challenged with DEHS. The remaining two filters with vertical and horizontal pleat orientations were not dust loaded. The layout of the cartridge type filter used in this study is shown in Figure 3.1; it has face dimensions of 592 x 592 mm with a depth of 400 mm. The filter cartridge has four V-shape banks which contains eight pleated media panels. The complete dimensions are shown in Appendix C.

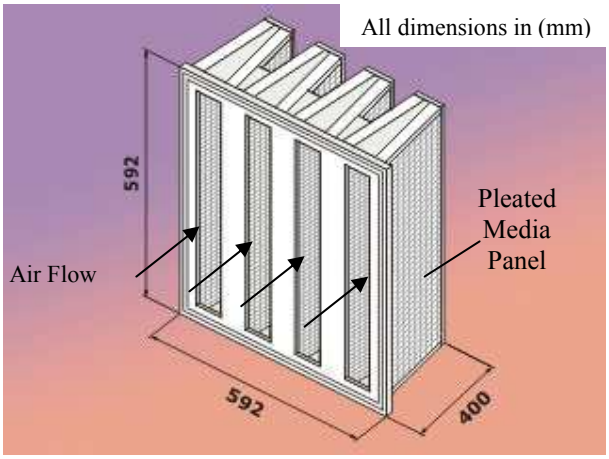

Figure 3.1: Pleated filter with the V shape design type filter 31 m^2 under study [EMW Filtertechnik].

This chapter covers the testing facility, the experimental procedures and the associated equipment used to complete the testing such as the dust feeder, particle counter and aerosol generator. It also lists the experimental procedures for all ten filters used in this research for both DEHS for initial fractional efficiency and SAE synthetic dusts loading.

3.1 Experimental Test Facility

The facility used for this experimental work which is shown in Figure 3.2, is located at EMW Filtertechnik in Limburg Germany. This facility, with the schematic diagram is shown in Figure 3.3, was built to the standard required by DIN EN 1822 [1998] which consists of several square duct sections with 610 mm × 610 mm nominal inner dimensions, except for the section where the filter is installed. This section has nominal inner dimensions between 616 mm and 622 mm. The length of this duct section is 1.1 times the length of the filter, with a length of one metre.

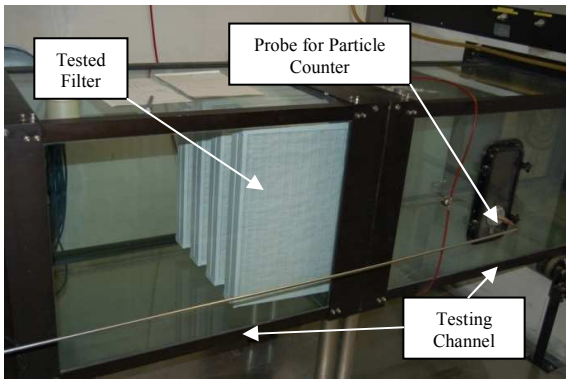

Figure 3.2: EMW testing facility located in Germany.

The HEPA filter is placed upstream from where the aerosol is dispersed and mixed to create a uniform particle concentration in the air that is to be fed to the filter. The air then goes through upstream section that consists of the mixing orifice in the centre of which the dust feeder discharge nozzle is located. Downstream of the dust feeder is a perforated plate intended to achieve a uniform dust distribution. In the last section of duct, the upstream aerosol sampling head is installed as shown in Figure 3.3.

The pressure drop across the test filter was measured using static pressure taps located before and after the test filter. In order to avoid turbulence, the mixing orifice and the perforated plate were removed during the initial pressure drop measurements. In

addition, to avoid systematic error, these parts were also removed during initial efficiency measurements.

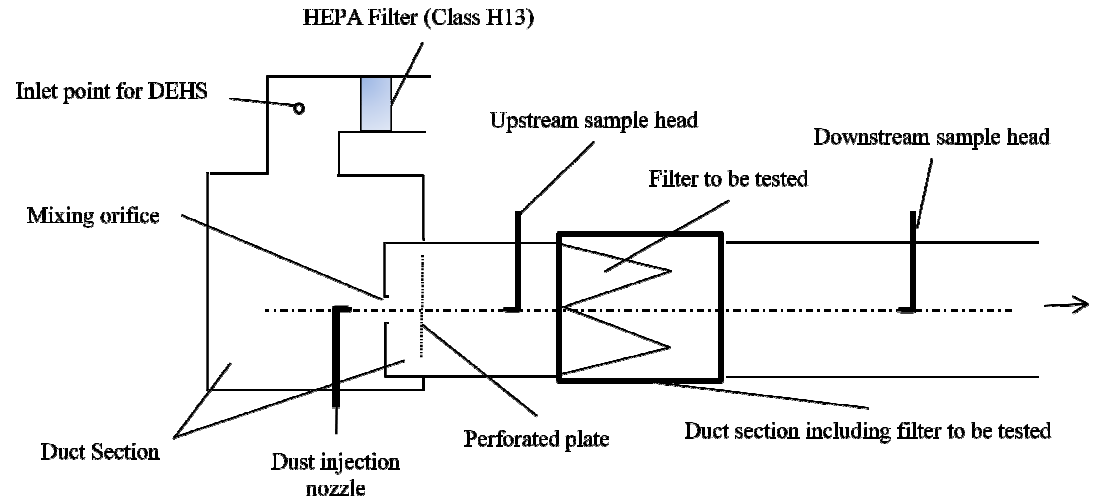

Figure 3.3: Schematic diagram of the testing facility built according to DIN 1822 [1998].

The dimensions of the duct are shown in Figure 3.4. The duct material is electrically conductive and electrically grounded, has a smooth interior finish and is sufficiently rigid to maintain its shape at the operating pressure. The whole test duct is made of transparent glass to enable the observation of the filter and other equipment. There are access doors to facilitate monitoring of test progress as shown in Figure 3.5.

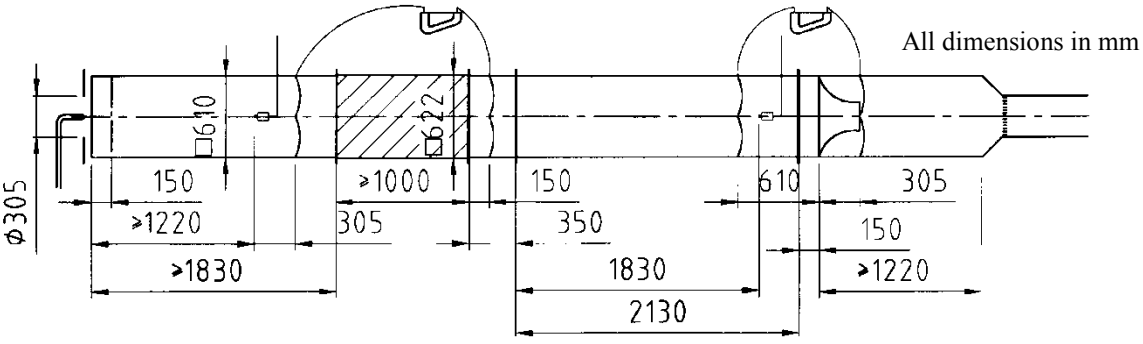

Figure 3.4: Dimensions of the testing facility built according to DIN 1822 [DIN 1822, 1998].

Figure 3.5: Access door and nozzles for efficiency measurement.

3.2 Dust Dispenser

The dust dispenser used in this experimental work was a PALAS, model BEG-1000. Dust to be dispersed is loaded into the powder reservoir with a belt feed unit as well as an ejector as shown in Figure 3.6. The bulk material that is to be dispensed is continuously fed from the powder reservoir (shown in Figure 3.79) to the conveyer belt of the feed unit and then taken from the belt by means of constantly rotating brush. The particles are sucked from the brush to the head of the ejector where they are dispersed by a high velocity gas flow. The dust concentration used in the dust feeding process for this experimental work was 70 mg/m^3 which conform to international standards [ASHRAE 52.2, 1999; DIN EN779, 2002]. At this concentration, 245 g can be fed per hour.

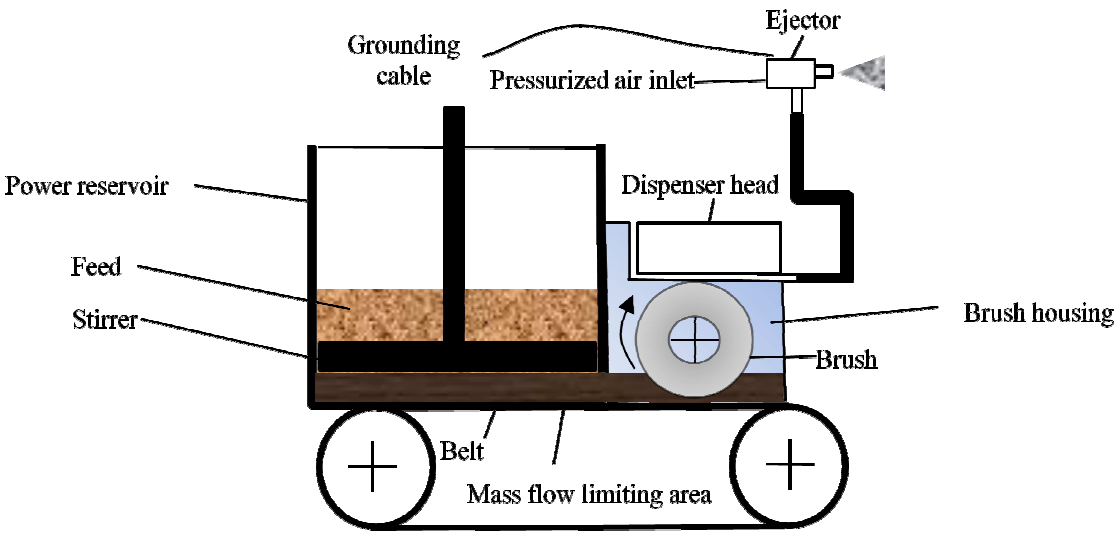

Figure 3.6: The operating principle of the Palas BEG-100 dust feeder [Palas Manual].

Figure 3.7: The powder reservoir towards the end of dust feeding.

The introduction of the dust to the airstream is by means of a nozzle as shown in Figures 3.7. The feed nozzle is placed so that it is perpendicular to the plane of front of the testing facility as shown in Figure 3.8.

Figure 3.8: The feeding nozzle of Palas BEG-100 dust feeder.

Figure 3.9: The feeding nozzle direction of the Palas BEG-100 dust feeder relative to the testing facility.

3.3 Aerosol Generation

The aerosol used in the experimental work was DEHS (DiEthylHexylSebacate). The test aerosol DEHS was produced by a Laskin nozzle which is widely used in performance testing of HEPA and ULPA filters. The DEHS properties are listed in Table 3.1.

DEHS Properties	
Density	912 kg/m^3
Melting point	225 K
Flash point	> 473 K
Vapour pressure	1.9 µPa at 273 K
Refractive index	1.450 at 600 nm
Dynamic viscosity	0.022 to 0.024 kg/m.s
CAS number	122-62-3

Table 3.1: The properties of DEHS used in this study.

The aerosol generator used in the experiments is shown in Figure 3.10 and consists of a small container with DEHS liquid and a Laskin nozzle. The aerosol is generated by feeding compressed particle-free air through the Laskin nozzle. The atomised droplets are then directly introduced into the test rig. The pressure and air flow to the nozzle are varied according to the test flow and the required aerosol concentration. For a test flow of 0.944 m^3/s the pressure is about 17 kPa, corresponding to an air flow of about 0.39 dm^3/s (1.4 m^3/h) through the nozzle.

Figure 3.10: The PALAS aerosol generator used in the generation of DEHS.

3.4 Palas Particle Counter PCS-2000

The particle counting and sizing was initially done using of Palas Particle Counter sizer PCS-2000 shown in Figure 3.11. This particle counter sizer measures the light scattered by single particles that cross a constantly illuminated measuring volume. The height of the resulting scattered light impulse can be interpreted in terms of particle size while the number of pulses per unit of time is proportional to the particle number concentration. Since the size range of this counter is 0.19-10 µm it cannot detect the expected MPPS range; hence the initial efficiency measurements obtained by this particle counter were not analyzed and are listed in Appendix E. However, the dust- loaded efficiencies were measured using this counter because it can handle a flow rate 3500 m^3/h and the measurements are listed in Appendix K for both filter groups.

Figure 3.11: The PALAS Particle Counter PCS-2000.

3.5 HS-LAS Particle Counter PMS Model 32 Channels

The particle counter used in the fractional efficiency measurement was an HS-LAS Particle Counter PMS Model 32Ch. This high sensitivity laser aerosol spectrometer probe has 32 channels capable of sizing particles over a size range from 0.065 – 0.9 µm, which enables detection of the MPPS.

The HS-LAS 32 channels operate on the principle that the light scattered by a particle with an active laser cavity is a direct function of its size. Particles produce pulses of radiant energy during transit through the laser beam. These light pulses are sensed by detectors and sized with a 32 channels pulse height analyzer. Particles are aerodynamically focused to a sample stream diameter one-fifth as large as the laser

beam (approximately 200 μm in diameter). The central 200 μm of the laser beam is a region with less than 15% intensity variation. This gives the HS-LAS 32 channels means of resolving particles at high concentration with greatly improved accuracy. The particle size range of HS-LAS facilitates study of the effect of pleating density and face velocity on the MPPS and the corresponding minimum efficiency. The optical system diagram is shown in Figure 3.12. The entire data for all filters are listed in Appendix D.

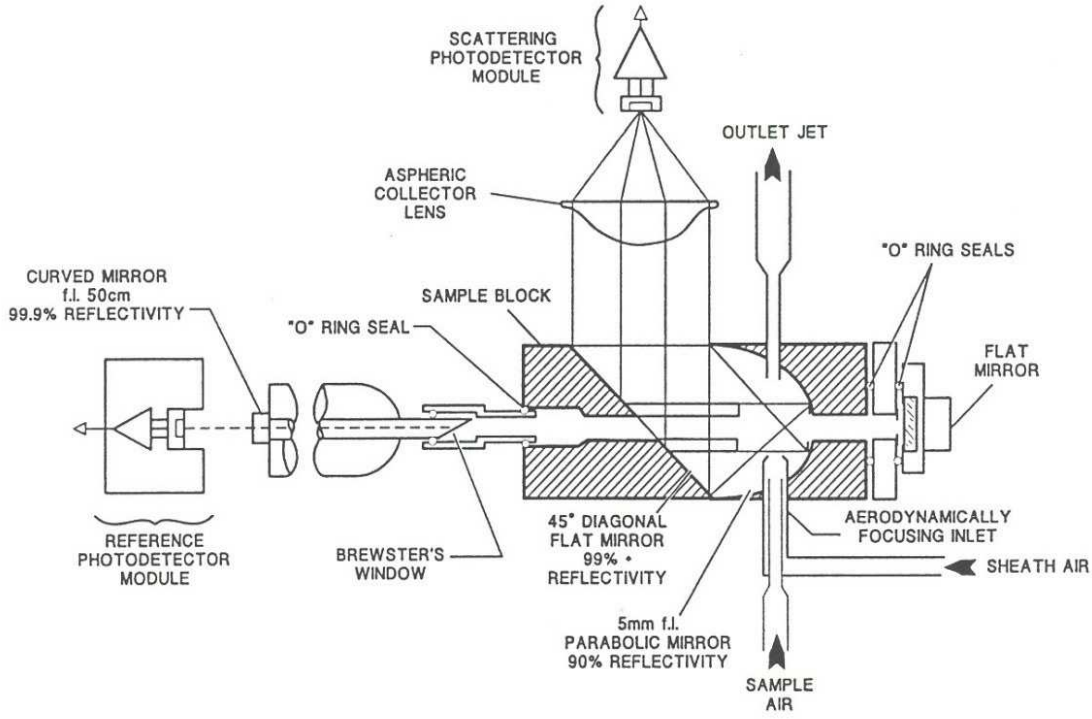

Figure 3.12: The optical system diagram of PMS HS-LAS Particle Counter [PMS HS-Catalogue].

The final data listed in Appendices D, E and K are calculated by obtaining upstream (N_u) and downstream (N_d) particle concentration from the particle counter. The concentrations are then multiplied by the dilution factors used upstream ($D_{L,u}$) and downstream ($D_{L,d}$) respectively. The recommended upstream and downstream by manufacturer for HEPA filter testing are 10000 and 100 respectively. The final efficiency data is first calculated by equation 3.1:

$$E = 1 - P_t = 1 - \frac{C_{n,d}}{C_{n,u}} \tag{3.1}$$

where $C_{n,d}$ and $C_{n,u}$ are the number concentrations downstream and upstream respectively and defined as :

$$C_{n,u} = \frac{(N_u)(D_{L,u})}{(Q_{s,u})(t_u)} \tag{3.2}$$

and

$$C_{n,d} = \frac{(N_d)(D_{L,d})}{(Q_{s,d})(t_d)} \tag{3.3}$$

Where $Q_{s,u}$ and $Q_{s,d}$ are the flow rate inside the sampling nozzle upstream and downstream respectively and is equal to 1 cm^3/min. Sampling time of one minute was used for both upstream (t_u) and downstream (t_d) times respectively.

3.6 Young's Modulus of Elasticity for Filter Media.

The Young's modulus of elasticity was measured in the Kuwait Institute of Scientific Research (KISR) laboratory. This measurement was conducted using a universal testing machine (Testometric FS 150), shown in Figure 3.13. The machine used is a computerized multi-functional hydraulic machine for the determination of different mechanical properties of building materials such as tensile, compression, flexure, compression and adhesion strengths. Three readings were taken to ensure reproducibility of the results and are listed in Table 3.2.

The three samples used for the measurement had a length of 100 mm and a width of 25mm. The thickness of the filtration media was measured to be 0.31 mm which differs from the measured thickness from the SEM. The reduction in thickness is due to flexibility of glass fibre material which gave a different thickness reading when compressed by the machine holder. The test speed used was 5 mm/min and the measurements were conducted by means of cross head movement using a load cell of 5000 N and without a use of extensimeter. The measurements and machine settings are summarized in Appendix N.

	Young's Modulus (N/mm^2)
Min	231
Mean	248
Median	241
Max	271
Standard Deviation	21
Variance	42

Table 3.2: The Young's modulus of elasticity of filtration media used in this study.

Figure 3.13: The universal testing machine used to measure the filter medium Young's modulus of elasticity (Testometric FS 150) at K.I.S.R. in Kuwait.

3.7 Energy Dispersive X-ray Spectroscopy (EDXS)

Energy dispersive X-ray spectroscopy is an analytical procedure used for chemical characterization. The dust sample was prepared by mounting it rigidly on a specimen stub. To prevent electrostatic charge accumulation at the surface during electron irradiation, the upper surface of dust is coated with very thin layer of gold due to its electrical conductivity. A scanning electron microscopic image is imported to the elemental analysis software connected to the SEM where the spectrum of interest is selected for analysis as shown in Figure 3.14. The software provides the elemental content output as shown in Figure 3.15. The spectroscopy technique starts by shooting an electron beam to energize the electrons in dust. Chemical characterization is conducted by virtue of interactions between electromagnetic radiation and analyzing X-rays emitted by the excited electrons of the dust in response to being struck with charged particles. Fundamentally, the chemical characterization is due mainly to the principle that each element has a unique atomic structure allowing each element to be identified distinctively through their characteristic energies. These X-rays are collected to allow for the chemical characterization of the dust sample [Spurny K. R. 1999].

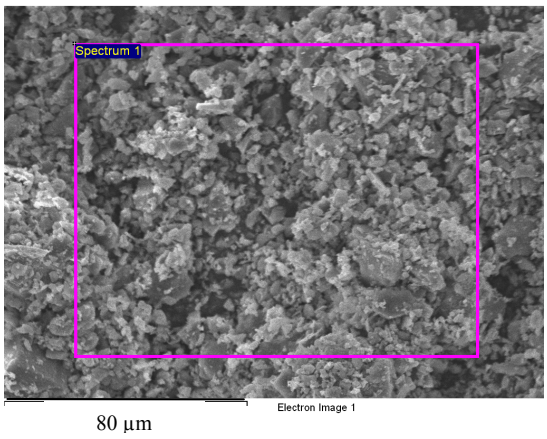

Figure 3.14: Sample of the selected spectrum used for chemical characterization of SAE fine dust.

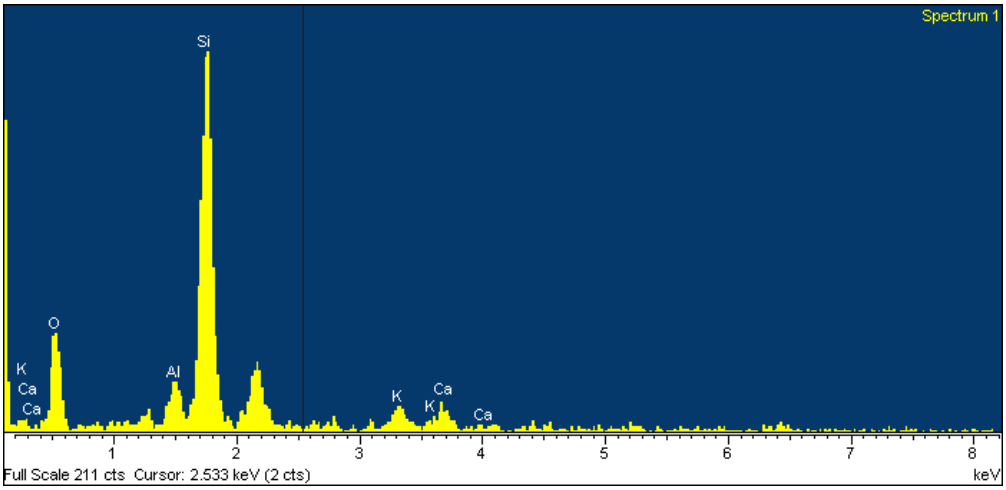

Figure 3.15: Sample of X-ray spectra of SAE fine dust.

3.8 Particle Size Distribution Measurements

Dust sizing was done using a Malven Mastersizer 2000 which using an optical unit to capture the actual scattering pattern (presentation) from a field of particles. The sizing is done through two distinct procedures. The first procedure is the measurement which involves capturing the scattering pattern from a sample which is the function of the optical unit. The detector within the optical unit is made of several individual detectors. Each detector will collect the light scattering from a particular range of angles. The Mastersizer then takes over 2000 snap shots (sweeps) of the scattering pattern and averages the results. Once the measurement is complete the raw data contained in the measurement are then analyzed by Malvern software. Prior to sample measurement, a background measurement is made that measures the scattering pattern with no sample since it could be contaminated with impurities within the water, on the windows, lenses and/or electrical noise. After adding the sample, the Mastersizer

determines the correct concentration of the sample by measuring the amount of laser light that been lost by passing it through the sample - this is referred to as obscuration and is given as a percentage.

***The measurement procedure**:*

1- Select the appropriate lens based on the size distribution expected (lense 300RF).
2- Align the optics of the Mastersizer so that the laser hits the centre of the detector.
3- Document the measurement.
4- Measure the background by measuring the scattering pattern with no sample.
5- Add the sample which consists of water and 7 grams of the dust to be sized.
6- Measure the scattering pattern.
7- Choose the "Polydisperse" model.
8- Choose the appropriate presentation by choosing the refractive index of the dust (1.5295) and the refractive index of the water (1.3300).
9- Select Standard-Wet (3OHD). This presentation assumes that particle is suspended in water.
10- Analyse the measurement.

3.9 Experimental Rig Verification

To verify that the experimental setup produces reproducible and reliable data, the air filtration testing facility has undergone a verification procedure. This procedure included three repeated measurements of the pressure drop for each flow rate of the ten different flow rates starting 500 m^3/h and ending at 5000 m^3/h. Further, the fractional efficiency verification employed three different flow rates 1000, 2000 and 3000 m^3/h. The characteristics of the filter used in this procedure are similar to the ones used in the research with a surface area of 23.5 m^2. The verification procedure conducted included pressure drop and fractional efficiency measurements:

1. Install the filter and close tightly the duct section and ensure it is leakage free.
2. Turn on the fan.
3. Measure and record the pressure drop starting at 500 to 5000 m^3/h.
4. Turn off the fan.

5. Wait for few minutes, then turn on again and repeat steps 2 to 4.
6. Turn off the fan.

The verifications of the pressure drop response and fractional efficiency are shown in Figures 3.16 and 3.17 respectively. It can be concluded that the facility produces reproducible pressure drop and fractional efficiency measurements and the testing procedures are safe to be conducted.

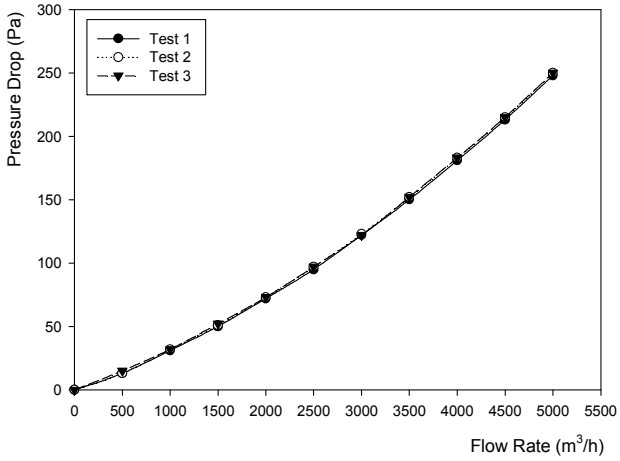

Figure 3.16: Pressure drop response verification of the testing facility (three readings).

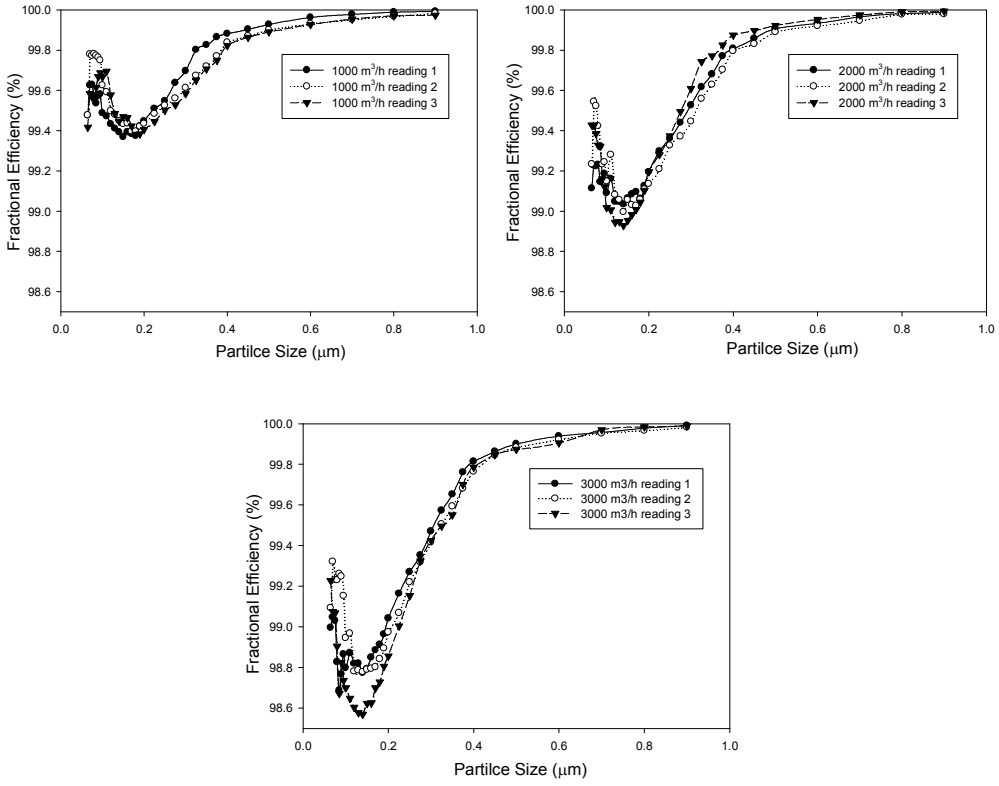

Figure 3.17: Fractional efficiency verification of the testing facility (three readings).

3.10 Experimental Procedure

The test facility provided pressure drop and particle size efficiency measurements. The filter groups (A) and (B) were loaded with AC coarse and AC fine test dust respectively. The experimental procedures started with Group A, followed by Group (B). The initial pressure drop and initial fractional efficiency was measured using DEHS for the filters with horizontal and vertical pleats with no dust loading. Complete experimental matrix is shown in Appendix B.

The efficiency measurement versus flow rate was performed with the PMS HS-LAS particle counter with a size range of 0.065 – 0.9 μm. The flow rate was varied from 500 m^3/h to 5000 m^3/h in increments of 500 m^3/h. The steps involved in the experimental procedures are listed below.

Initial Pressure Drop Measurement:

1. Record pleating density of each filter and the corresponding surface area before testing.
2. Label each filter.
3. Install the filter in the testing rig.
4. Turn on the fan.
5. Set the flow rate to 500 m^3/h.
6. Wait few minutes and monitor the pressure difference gauge until the reading is stable.
7. Record the pressure drop measurement when the reading is stable.
8. Increase the flow rate by 500 m^3/h and repeat step 7.
9. Repeat step 8 until 5000 m^3/h is reached.
10. Make sure all ten readings of pressure drop measurements are obtained and recorded.
11. Install the next filter and repeat steps 1-10.

Initial Fractional Efficiency Measurement:

1. Connect the PMS HS-LAS particle counter.
2. Set the flow rate to 500 m^3/h.
3. Feed DEHS through the mixing orifice of the testing rig.
4. Measure the fractional efficiency.

5. Increase the flow rate by 500 m^3/h and repeat step 14.
6. Repeat step 5 until a flow rate of 3000 m^3/h is reached.
7. Ensure that six fractional efficiency measurements are obtained and recorded.
8. Repeat steps 1-7 using Palas Particle Counter PCS-2000**.**

Dust Loaded Pressure Drop and Fractional Efficiency Measurements:

1. Install the dust feeder.
2. Load dust feeder with 250 g of AC coarse test dust.
3. Set the flow rate to 3500 m^3/h.
4. Starting the dust feeding process to the filter.
5. Record pressure drop every 5 minutes.
6. Once the dust feeding process of 250 g is completed, install the particle counter and set the flow rate to 500 m^3/h.
7. Measure the fractional efficiency of the partially loaded filter, using DEHS.
8. Increase flow rate by 500 m^3/h and repeat the fractional efficiency measurement until a flow rate of 3500 m^3/h is attained.
9. Ensure that seven fractional efficiency measurements are completed and recorded.
10. Calculate mass fed versus time.
11. Load the dust feeder with another 250 g.
12. Repeat steps 3-11 until 1000 g of dust has been fed. This completes the test run for one filter.
13. Turn off the fan, clean the test facility and remove the dust-loaded filter.
14. Install a clean one with the different pleating density.
15. Repeat steps 1-13 for the remaining filters in Group (A) for different pleating densities.
16. Repeat steps 1-14 for Filter Group B for each pleating density using AC fine dust.

3.11 Summary

The air filtration testing facility was prepared for testing and verified to give reproducible data. All ten filters were manufactured with variable pleating densities and the initial pressure drop and efficiency measurements were conducted using Palas Particle Counter PCS-2000 and HS-LAS PMS particle counters. Since the former does not cover the MPPS, the data produced were not used for initial efficiency measurements. The eight filters split into two groups were challenged with AC fine and AC course dusts and pressure drop and efficiency measurement were also conducted. The particle counter PCS-2000 was used to conduct the dust loaded efficiency measurements since it can accommodate higher flow rates such 3500 m^3/h which HS-LAS PMS particle counter cannot handle. The data produced thus far will be analyzed in Chapter Four to study the effects of air face velocity, pleat density and pleat orientation on the filter's permeability, initial and dust loaded pressure drop response, initial and dust loaded fractional efficiencies of full scale HEPA V-bank cartridge minipleat filters.

CHAPTER FOUR

Results and Discussion

In this Chapter, the experimental results are addressed and discussed appropriately. This Chapter also describes the particle size distribution of the atmospheric and synthetic dusts used in the dust loading processes. In addition, filter medium and pleated panel properties in this experimental work. Appropriate models available in the literature are used to predict the initial and dust loaded pressure drops as well as initial fractional efficiency of the full scale V shaped filter cartridges with various pleating densities and face velocities.

4.1 Filter Properties

HEPA filters are made from fibrous material. Glass fibre filtration media was selected for all experiments in this work. This type of medium is extensively used in Kuwait as it exhibits better resistance to high temperatures and has smaller fibre size compared to synthetic media. Glass fibre media are highly porous with a low resistance to air flow. The filter's performance is affected by several variables such as filter medium thickness, permeability, packing density, fibre diameter as well as structure and design of the filter cartridge. Furthermore, operating conditions such as filtration velocity and temperature also affect the filter's performance, in addition to the characteristics of the aerosol such as particle size distribution, particle shape and density.

4.1.1 Filter Media Characteristics

The glass fibre media used in this testing is of Class H10 according to DIN Standard 1822 [1998]. The fibre diameter was measured using scanning electron microscope images, examples are shown in Figure 4.1. The smallest and largest measured fibre diameter for the three HEPA media samples are listed in Table 4.1. The packing density and porosity calculation is shown in details in Appendix J. Microscopic examination reveals that as the filter class of the filter medium increases, the fibre diameter range

decreases. Figure 4.2 show the fibre size distribution of the filtration medium used in the work.

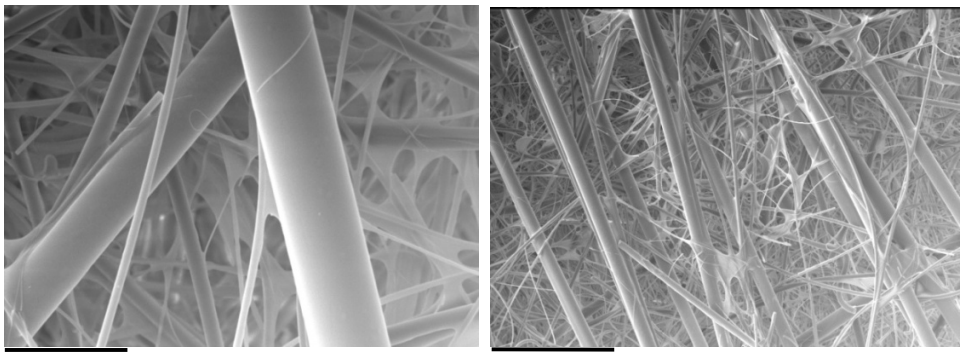

Figure 4.1: Scanning electron microscopic images used for fibre diameter measurement of HEPA filter medium class H10 according to DIN 1822[1998].

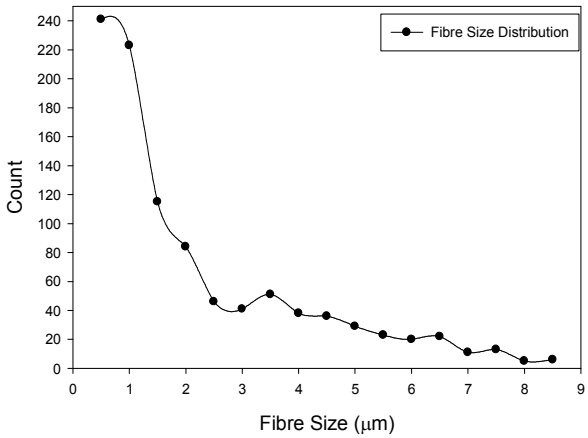

Figure 4.2: Fibre diameter distribution of the HEPA filtration medium class H10 used in the experimental work.

HEPA (H10) [DIN 1822, 1998]	
Fibre Diameter Range	0.5-8.5 µm
Average Fibre Diameter	2.1 µm
Media Thickness	500 µm
Packing Density	0.06
Porosity	94%
Fibre Shape	Circular

Table 4.1: Fibre diameter range and media thickness for different HEPA filter material.

Different samples of fibrous filters have been examined by scanning electron microscope to determine whether the filter medium consists of mainly circular fibres or non-circular ones. All used filters samples examined from Kuwait had a circular shape. The filtration medium used in this experimental work also has circular shaped fibres, as illustrated in Figure 4.3.

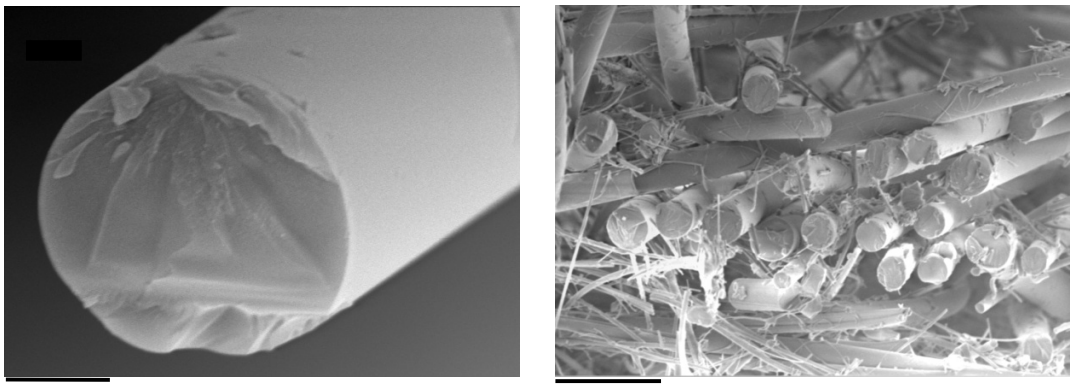

(a) (b)

a) 4µm circular fibrous fibre b) Fibres with circular cross-section

Figure 4.3: Scanning electron micrograph of cross-section of fibrous fibre used in this study.

4.1.2 Observations of Manufacturing Defects

Different manufacturing observations have been highlighted during the scanning electron microscope examinations. Figure 4.4 shows unblown media and possible excessive use of adhesive, particularly in high efficiency media. All of the above manufacturing defects may influence the filtration performance. In Figure 4.5 illustrate the excessive use of adhesive seen in higher filter class such as H13 and H14 [DIN EN 1822, 1998] which reduces permeability. It was noticed that adhesive is excessively used in absolute filter media where fibres have diameters smaller than 2 µm to add mechanical stability. Some other manufacturers add larger fibres to gain similar mechanical stability.

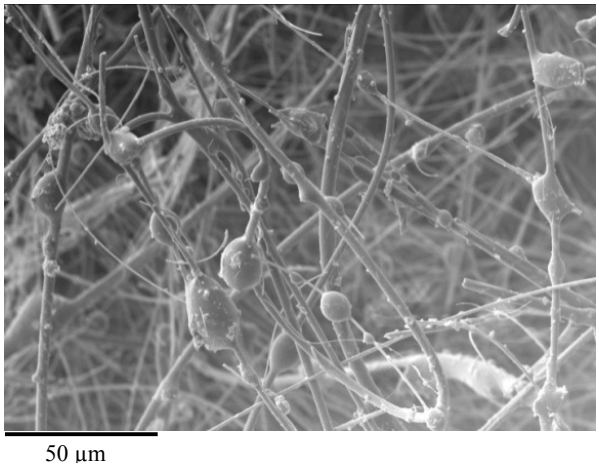

Figure 4.4: Unblown filtration media.

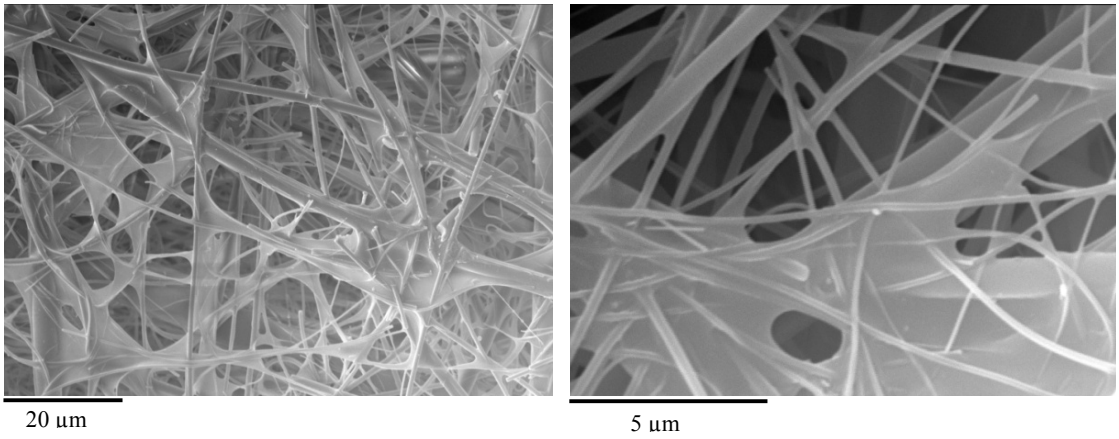

Figure 4.5: Samples of excessive adhesive use in the filtration medium.

4.1.3 Pore Size Distribution Measurement

Sizing circular cross-section pores is quantitatively expressible in terms of diameter. However, for irregular cross-sections, there is no convenient and quantitative way to measure pore size. The pore size distributions for three different classes of HEPA filter media were measured using a PMI Porometer. At the bubble point pressure, the first air bubble starts coming through the largest pore of the filtration medium indicating its pore size. The bubble point diameters for different classes of HEPA filter are tabulated in Table 4.2. As the efficiency increases from HEPA 10 to HEPA 14, the largest pore diameter decreases. The smaller the mean flow pore diameter, defined as the pore

diameter through which half of the flow passes, the greater the efficiency of the filter. The pore size distribution is illustrated in Figure 4.6.

	HEPA [H10]	**HEPA [H12]**	**HEPA [H14]**
Largest pore diameter (µm)	20.1	7.6	5.9
Mean flow pore diameter (µm)	5.4	2.1	1.75

Table 4.2: Pore characteristics for different HEPA filter material.

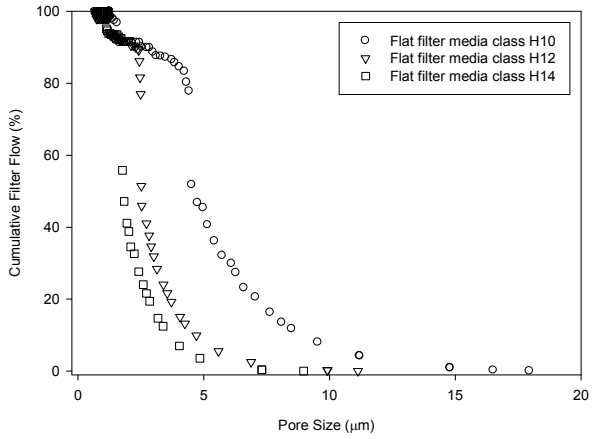

Figure 4.6: Pore size distribution for HEPA filter medium of Class H10, H12 and H14 according to DIN 1822 [1998].

Flow has a tendency of seeking the largest pores through fibrous filters. When the filter is loaded with dust, the characteristics of the filter change due to both internal and surface deposition of dust particles. Dust deposition occurs by straining or impact, or by inertia or diffusion, which effectively reduces the pore diameter.

The difficulty in the manufacturing process lies in the arrangement of the fibres so that a homogeneous medium is produced. Due to the polydisperse fibre diameters and different fibre length, it is very difficult to arrange the fibre in a random but comparable manner all over the filter medium. In addition, substantial variations in sheet thickness make the filter media heterogeneous. A view of a HEPA filter medium cross section is shown Figure 4.7. As highlighted in Chapter 2, the heterogeneity in the filter media caused by

local fluctuation of the structure leads to local fluctuation of the permeability in a filter medium. These different permeabilities lead to fluctuations of the local flow velocity.

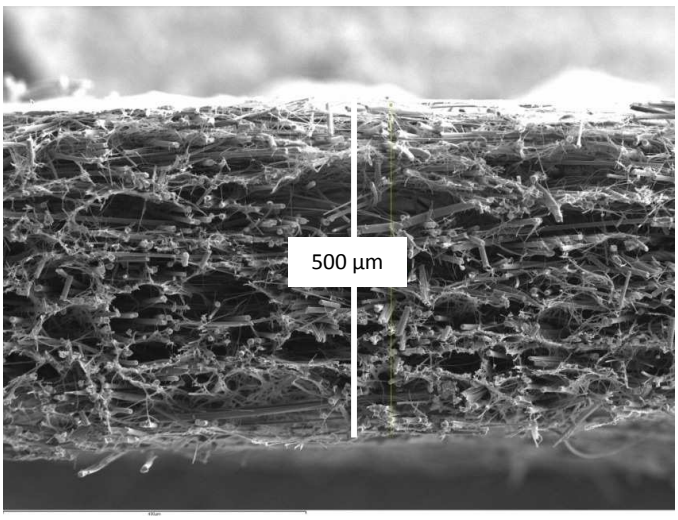

Figure 4.7: Scanning electron micrograph of a HEPA filter cross-section.

4.1.4 Pleated Module Properties

Pleating the filter medium provides larger surface area in a given space, which increases particle loading capacity per unit area when compared with a flat sheet medium. Furthermore, pleated medium panels are more stable than a flat sheet of the same medium, which is inclined to deform and eventually rupture. Another major advantage of increasing the surface area is to decrease the air velocity on the medium. Such decrease in the medium velocity translates into increasing the residence time of aerosol inside the filtration medium and consequently, increases the probability of the particle-fibre contact and leads to an enhancement of diffusional capture efficiency. However, an excessive number of pleats or overpleating in a given area in an air filter cartridge may also lead to failure by rupturing or cracking the filtration medium. Consequently, the pleating density, defined as the number of pleats per unit length in the filter cartridge has to be optimized to provide the desired efficiency at the least possible pressure drop. Four different pleating densities were chosen for that purpose in this work to better understand their filtration performance.

4.1.4.1 Description of Manufactured Filters

Eight filters were manufactured by EMW Filtertechnik with pleating densities varying from 28 to 34 pleats per 100 mm. The pleating densities were varied by an increment of 2 pleats per 100 mm. Table 4.3 lists all filters used for testing with their corresponding surface areas. The manufactured filters were divided into two groups, termed A and B. Both Groups underwent similar testing procedures with the exception that Group A was challenged with SAE coarse dust while Group B was challenged with SAE fine dust.

The air enters the filter media through four openings. Each opening has a height of 522 mm and width of 65 mm. The air leaves the cassette after it has passed through eight panels of pleated filter medium. The face of the filter is shown in Figure 4.8 after installation in the test rig. The pleating densities and calculation of their corresponding surface areas are showed in Table 4.3. However, it is important that casting material is required to bond the filtration pleated media to the plastic housing to eliminate leakage. The process of adding such casting material is not always controlled and is responsible for the surface area differences noted between Filter 28A and 28B as well as 34A and 34B. A sample calculation of the total surface for each filter under examination is shown below:

$$Total\ Surface\ of\ \ Pleated\ Filter$$
$$= 2 \times (No.of\ Pleats) \times (Pleat\ Depth) \times (Panel\ Width) \times (No.of\ Panels)$$

FILTER	PLEAT DENSITY (PLEATS/100 mm)	SURFACE AREA (m^2)
28A	28	23.9
28B	28	24.6
30A	30	26.6
30B	30	26.6
32A	32	27.3
32B	32	27.3
34A	34	28.8
34B	34	28.9

Table 4.3: The filters tested with their corresponding surface areas.

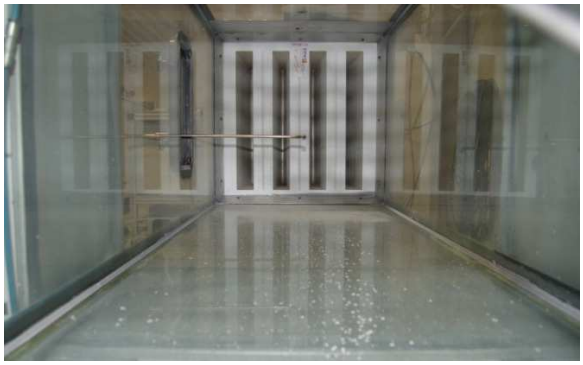

Figure 4.8: Pleated filter with the V shape design during in the test rig.

Inside the filter, the media is pleated to provide extended surface area by means of varying the pleat density in a given length as shown in Figure 4.9. In a 592 x 592 mm cassette with a depth of 400 mm, a surface area of 24 to 29 m^2 can be achieved. The filter contains eight panels each has a height of 522 mm and total width of 380 mm. The maximum operating temperature may reach up to 80°C. The polystyrene housing is equipped with a leakage-free casting provided by endless foam all around the filter's frame. Figure 4.10 highlight the definition of pleat density, pleat height and pleat depth as they will be used in this study.

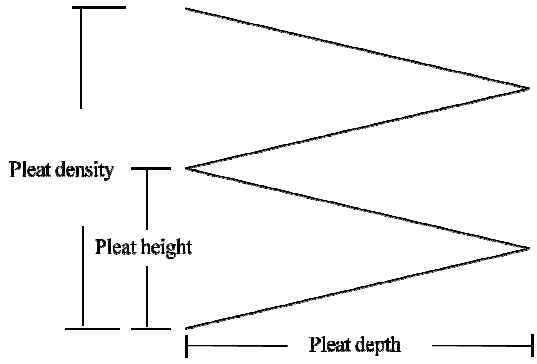

Figure 4.9: Extending the surface area is provided by means of varying pleat density and lowering pleat height.

4.2 Clean Gas Permeation

The passage of the clean gas through the filtration was assessed and the pressure drop and efficiency were measured. No dust loading took place at this stage.

4.2.1 Reynolds Number and Flow Regime

Reynolds number is used to verify the flow regime in the testing tunnel and through the filter medium. A Reynolds number check for the filter medium using the fibre diameter at the flow rates of 500 and 5000 m^3/h gives respectively:

$$\mathrm{Re}_{f500} = \frac{\rho U_{500} d_f}{\Delta P} = \frac{(1.177)(5.64\times10^{-3})(2.1\times10^{-6})}{1.85\times10^{-5}} = 7.54\times10^{-3}$$

$$\mathrm{Re}_{f5000} = \frac{\rho U_{5000} d_f}{\Delta P} = \frac{(1.177)(56.4\times10^{-3})(2.1\times10^{-6})}{1.85\times10^{-5}} = 75.4\times10^{-3}$$

Therefore, the flow inside the filter medium is laminar since Re < 0.2.

The Reynolds number in the rig's rectangular duct with a hydraulic diameter, h_d = 610 mm, at flow rates of 500 and 5000 m^3/h gives respectively:

$$\mathrm{Re}_{D500} = \frac{\rho U_{500} d_h}{\Delta P} = \frac{(1.177)(0.373)(0.61)}{1.85\times10^{-5}} = 14{,}476$$

$$\mathrm{Re}_{D5000} = \frac{\rho U_{5000} d_h}{\Delta P} = \frac{(1.177)(3.73)(0.61)}{1.85\times10^{-5}} = 144{,}760$$

Therefore, the flow inside the duct is turbulent since Re > 4000

4.2.2 Filter Permeability

The flow inside the filter medium is laminar and therefore, permeability, κ, can be obtained by means of Darcy's equation. Darcy's Law states that the pressure drop across an air filter is proportional to the air flow through it. The flow through an air filter is considered to be low speed, incompressible, Newtonian and is governed by Darcy's Law:

$$\kappa = \frac{\mu U h}{\Delta P} \tag{4.1}$$

where κ is the permeability of the filter medium, μ the air viscosity, and U the air velocity. h is the medium thickness which was measured by means of scanning electron microscope images to be 500 μm, the pressure drop was measured from the set of experiments conducted using the test tunnel.

The initial pressure drop of eight filters was measured for different flow rates ranging from 500 to 5000 m^3/h with an increment of a 500 m^3/h. The pressure drop readings of filter series A are listed in Table 4.4. The pressure drop response of the four filters of Group (A) is shown in Figure 4.10.

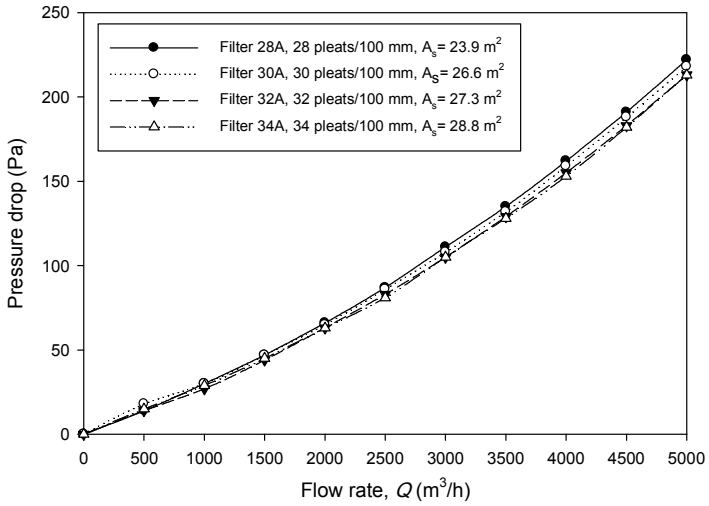

Figure 4.10: Initial pressure drop versus flow rates for Group ~~(~~A~~)~~ filters.

A sample permeability calculation is shown below of the lower and upper flow rates used in the experimental work, 500 and 5000 m^3/h respectively:

$$\kappa_{500} = \frac{\mu U h}{\Delta P} = \frac{(1.85\times10^{-5})(5.64\times10^{-3})(5\times10^{-4})}{17} = 3.07\times10^{-12}\ \text{m}^2$$

$$\kappa_{5000} = \frac{\mu U h}{\Delta P} = \frac{(1.85\times10^{-5})(56.4\times10^{-3})(5\times10^{-4})}{218} = 2.40\times10^{-12}\ \text{m}^2$$

Table 4.4 list the permeabilities for all corresponding pressure drops and face velocities using Darcy's equation. It can be seen that as the flow rate and therefore the face velocity increases, the permeability decreases as shown in Figure 4.12. Table 4.4 also shows that as the pleat density increases, permeability is reduced. However, for both filter groups A and B, permeability seems to have remained the same as the pleating density increased

from 30 pleat/100 mm to 32 pleats/100 mm. Figure 4.11 shows that the permeability of filter 30B and 32B have the same permeability for different face velocities. However, filter 30A exhibited higher pressure drop response than 28A and 28B with surface areas 23.9 and 24.6 m^2 respectively and consequently, its permeability reduced. As the pleating density continued to increase from 26.6 to 27.3 m^2 for filters 30B to 32B respectively, the latter filter exhibited lower pressure drop and higher permeability. This could be an early sign of going through the optimal pleat count (at least from pressure drop standpoint).

Filter	**28A, A_S = 23.9 m^2**			**30A, A_S = 26.6 m^2**			**32A, A_S = 27.3 m^2**			**34A, A_S = 28.8 m^2**		
Q (m^3/h)	ΔP (Pa)	U_f (mm/s)	κ x10^{-12} (m^2)	ΔP (Pa)	U_f (mm/s)	κ x10^{-12} (m^2)	ΔP (Pa)	U_f (mm/s)	κ x10^{-12} (m^2)	ΔP (Pa)	U_f (mm/s)	κ x10^{-12} (m^2)
500	14	5.78	3.82	18	5.22	2.68	14	5.08	3.36	15	4.82	2.97
1000	30	11.57	3.57	30	10.44	3.22	27	10.17	3.48	29	9.64	3.07
1500	47	17.36	3.42	47	15.65	3.08	44	15.25	3.21	45	14.45	2.97
2000	66	23.12	3.24	65	20.86	2.97	63	20.34	2.99	63	19.27	2.83
2500	87	28.90	3.08	86	26.08	2.81	83	25.42	2.83	81	24.09	2.75
3000	111	34.68	2.89	108	31.30	2.68	105	30.50	2.69	105	28.91	2.55
3500	135	40.46	2.78	132	36.52	2.56	129	35.59	2.55	128	33.72	2.44
4000	162	46.24	2.64	159	41.74	2.43	155	40.67	2.43	153	38.54	2.33
4500	191	52.02	2.52	188	46.96	2.31	183	45.75	2.31	182	43.36	2.20
5000	222	57.80	2.41	218	52.20	2.21	213	50.84	2.21	213	48.18	2.09
Filter	**28B, A_s = 24.6 m^2**			**30B, A_s = 26.6 m^2**			**32B, A_s = 27.3 m^2**			**34B, A_s = 28.9 m^2**		
Q (m^3/h)	ΔP (Pa)	U_f (mm/s)	κ x10^{-12} (m^2)	ΔP (Pa)	U_f (mm/s)	κ x10^{-12} (m^2)	ΔP (Pa)	U_f (mm/s)	κ x10^{-12} (m^2)	ΔP (Pa)	U_f (mm/s)	κ x10^{-12} (m^2)
500	17	5.65	3.07	15	5.23	3.22	15	5.09	3.14	15	4.80	2.96
1000	30	11.29	3.48	30	10.46	3.22	29	10.19	3.25	29	9.61	3.06
1500	47	16.94	3.33	48	15.69	3.02	45	15.29	3.14	47	14.41	2.84
2000	66	22.59	3.17	66	20.92	2.93	63	20.38	2.99	63	19.21	2.82
2500	86	28.23	3.04	87	26.15	2.81	84	25.48	2.81	84	24.01	2.64
3000	108	33.88	2.90	111	31.38	2.61	107	30.57	2.64	107	28.82	2.49
3500	134	39.52	2.73	136.5	36.61	2.47	131	35.67	2.52	131	33.62	2.37
4000	161	45.17	2.60	165	41.83	2.35	158	40.76	2.39	159	38.42	2.24
4500	188	50.81	2.50	193.5	47.06	2.24	186	45.86	2.28	186	43.22	2.15
5000	218	56.46	2.40	226.6	52.30	2.13	216	50.95	2.18	218	48.03	2.04

Table 4.4: Initial pressure drop vs. face velocities and permeabilities for different pleating densities.

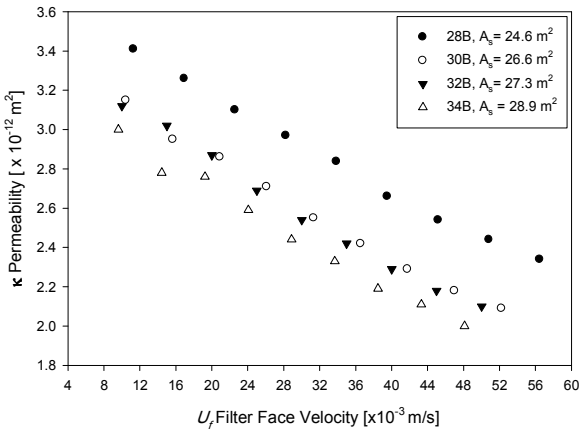

(Fibre glass medium, Medium thickness h =500 μm, f_d= 2.1 μm**)**

Figure 4.11: Permeability versus face velocities for filters of Group B.

4.2.3 Deviation from Darcy's Law

The Darcy pressure drop model will be further examined to compare with the experimental work. The Darcy model gives a linear relationship between pressure drop response and flow rate, which also signifies that the permeability of the filtration medium does not change. However, the experimental results exhibit a non-linear one which means the filter's permeability is changing as the flow rate varies, even though flow inside the medium is laminar. All permeabilties were computed for different flow rates in the Section 4.2.1. Given this change of permeability, it is important to understand the underlying reasons for the permeability reduction.

The permeability change is due to losses in surface area in the filtration medium or to compression of the medium. To evaluate the filter's utilized surface area, A_u, the Darcy pressure drop should be obtained by fitting a linear relationship to the first four points in Figure 4.10 taking into account Darcy's law. It assumes that there was no surface area losses occur during operation and the filter permeability remained unchanged. For example at a flow rate of 5000 m^3/h, the pressure drop is 222 Pa for Filter 28A as shown in Table 4.4. However, if the permeability were to remain unchanged, the Darcy linear pressure response would be 150 Pa. Therefore, for Filter 28A, at a flow rate of 5000 m^3/h gives the applied force by the flow rate, F as:

$$F = \Delta PA = (150\,\text{Pa})(24\,\text{m}^2) = 3600\ \text{N}$$

For the flow rate of 5000 m^3/h, the experimental pressure drop is 222 Pa, hence:

$$A_u = \frac{(3600\ \text{N})}{(222\ \text{Pa})} = 16.2\ \text{m}^2$$

The lost or unused surface area of the filter, A_L, is equal to:

$$A_L = A_s - A_u = 24 - 16.2 = 7.8\ \text{m}^2$$

This indicates that air flow did not get access to a filter area equivalent to 7.8 m^2. The Darcy model gives a linear variation of pressure drop with flow rate where there is no compression of the filtration medium thickness. For a pleat through which fluid flow obeys Darcy equation, the losses of media surface due to pleat crowding and/or expansion of pleats as well as media distortion at the corner of the pleat would have more influence on the filter surface area losses. Figure 4.12 illustrates the loss in the tested filters' surface areas versus their pleating densities. It can be seen that as the pleating density increases, not all of such surface area is utilized, and the higher the pleat density, the greater the losses in the surface area of the pleated filter. However, Filter 28A and has minimum surface area losses compared to the other filters in the same group.

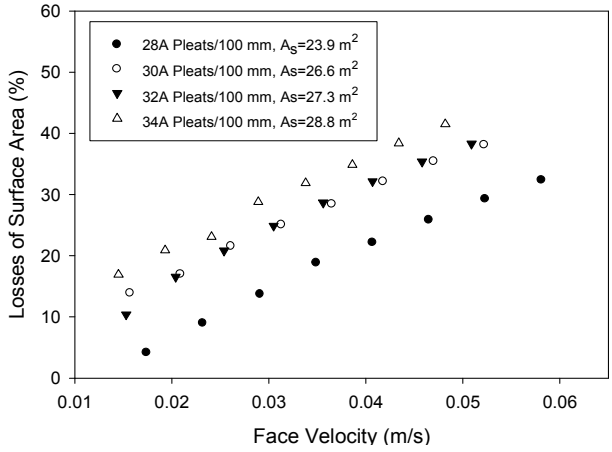

Figure 4.12: The losses of surface area of the different pleating densities filters at different face velocities.

It is evident from Figure 4.12 that while higher pleating densities provide additional surface area, the losses of surface area also increases as the face velocity increases, which in turn means the air stream not accessing all of the surface area provided. Figure 4.12 also shows that losses are similar in the 30 and 32 pleating densities. Examining Table 4.4, Filters 32A and 32B have lower pressure drop than 30A and 30B respectively. Filters with 32 pleats per 100 mm would be better from a pressure drop point of view and they have similar surface area losses compared to the 30 pleats per 100 mm filters. However, the comparison to determine the optimal pleat count is not complete until both filter's efficiency curves are examined both on the initial and dust loaded efficiency counts. This is simply to check that while filter 30 has less surface area and has similar surface area losses when compared with 32 pleats per 100 filters. The area losses are not due entirely to one factor and there is no apparent optimal pleat density for a given rate. The data show the area of the filter media is fully utilized at 500 m^3/h and underutilized at higher flow rates.

The area losses tend to increase with the increase of flow rate and with the increase of pleating density. The area loss due to the flow rate points to deformation of pleat structure and/or the panel itself. The increase of loss of pleating density suggests that the filter is overpleated and may be possible to obtain equally as good filtration using a lower number of pleats. For a fixed pleating density and a given flow rate, there exist a minimum pressure drop that meets the efficiency requirement of the standards.

Figure 4.13 illustrates that the losses of filter medium, which in turn means that air flow does not get access to such surface area, and as a result this part of the filtration medium does not participate in the filtration process but at the same time it plays a role in increasing the resistance of the filter. Figure 4.143 also shows the higher the pleating density the greater the losses in the surfaces area of the filter. However, to reduce the pleating density is not a valid solution as it may compromise both the overall efficiency of the filter and mechanical/structural stability of the pleated panel.

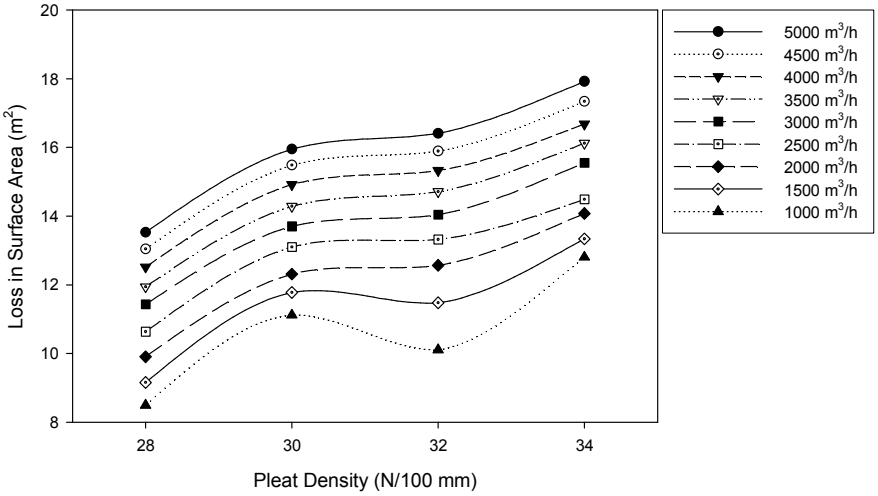

Figure 4.13: Losses of filter's surface area of Group B versus pleating density compared to Darcy equation.

This is an important aspect of the design of the filter because it would also reflect on the manufacturing cost. Introducing additional media that cannot be accessed by the air flow may not provide significant enhancement to the efficiency, but to the contrary, increases the resistance of the filter due to permeability reduction, defeats the intended purpose to the filtration process. At a flow rate of 5000 m^3/h, the Darcy pressure drop is 150 Pa for Filter 28A and the face velocity can be worked out using the linear pressure drop to be:

$$U = \frac{\kappa \Delta P}{\mu h} = \frac{(2.41\times10^{-12})(150)}{(1.85\times10^{-5})(5\times10^{-4})} = 0.039\text{m/s}$$

Consequently, the required surface area required to keep the permeability unchanged is:

$$A = \frac{Q}{U} = \frac{5000}{(0.039)(3600)} = 35.5\,\text{m}^2$$

The actual surface area is 23.9 m^2 and therefore for a flow rate of 5000 m^3/h an additional 11.6 m^2 is required. In the above calculation, it was assumed that when 11.6 m^2 are added to the surface area, all of it will be utilized and no losses will occur which

is not the case. Further, in practice, adding such an additional surface area is not feasible and therefore, design alterations have to be considered to make an effective use of existing surface area provided by the pleating density.

Increasing the air flow rate increases the face velocity which reduces the filter's permeability as illustrated earlier in Figure 4.12. Table 4.5 lists the percentage of the surface area losses with increase of pleating density and flow rate. As the flow rate is increased, the permeability is reduced for a given filter due to combination of the following reasons:

For a pleat through which fluid flow obeys Darcy equation, the losses of media surface area due to one or combination of the following reasons:

- Pleat crowding, a geometric effect caused by excessive number of pleats in the pleated panel in the same space. The filtration medium surface area losses occur by having too many pleats next to each other. Clearly, as the pleat density increases, the surface area losses increase.

- The face velocity increase will distort the pleats and consequently they will come in contact with one another resulting in surface area loss.

- Deflection of the entire pleated panel causing permeability reduction or by viscous or shear at the corner of the pleat would have more influence on the filter surface area losses. In the absence of the sufficient support on the back side of the pleated panels, the deflection is more pronounced.

- Pleat distortion at the corner of the pleat caused by delamination of the fibres layers from the filtration medium. Clearly, the higher the number of pleats, the greater this effect has on permeability reduction of the filtration medium. This effect also increases as face velocities increase.

- Filtration medium compression and therefore, the medium thickness will reduce resulting in a higher pressure drop. It can also result from medium folding which leads to tension in the outer region of the pleated medium and compression at the inner region. Medium compression could also be due to the drag force exerted by flowing fluid on the surfaces of the particles or fibres forming the medium. Therefore, the medium compression increases as the shear stress acting on the fibre surfaces increases causing the pressure drop to rise. The contribution of this effect to the overall increase in pressure drop is verified in Section 4.5.

Pleat Density	**28A**	**30A**	**32A**	**34A**
Total A_s (m^2)	**23.9**	**26.6**	**27.3**	**28.8**
Q (m^3/h)	A_{Loss} (%)	A_{Loss} (%)	A_{Loss} (%)	A_{Loss}(%)
500	0	0	0	0
1000	0	10.1	2.6	14.07
1500	4.2	13.9	10.4	17.0
2000	9.0	17.0	16.5	20.9
2500	13.7	21.6	20.8	23.1
3000	18.8	25.1	24.9	28.8
3500	22.1	28.5	28.7	31.9
4000	25.9	32.1	32.2	34.9
4500	29.3	35.4	35.4	38.4
5000	32.4	38.1	38.3	41.5

Table 4.5: Surface area losses versus different flow rates for different pleating densities.

Increasing the air flow rate increases the face velocity which reduces the filter's permeability. As the flow rate is increased, the permeability is reduced for a given filter due to combination of the following reasons: Increasing the pleating density in the same given space leads to pleat crowding and consequently losses of surface area that the air flow cannot get access to. The face velocities increase will distort the pleats and consequently they will come in contact with on another resulting in surface area loss. The filtration medium will also experience compression and therefore, the medium thickness will reduce resulting in higher pressure drop as well.

Previous studies have highlighted the optimal pleat count. Chen *et al* [1995] developed a numerical finite element model to optimize the design of the pleats of filter materials with different permeabilities. Their results show that for a given pleat height, the optimal pleat density increases as the filter media permeability decreases. Currently, most filter manufacturers have the same pleat density for all filter classes. This may signify ineffective use of the media since less pleat density is needed with lower filter classes. On the other hand, optimal pleat density has also to be considered from an efficiency point of view. For example, a pleat count might be optimal from a pressure drop standpoint but it may not be able to achieve the desired efficiency. Therefore, optimal pleat density should be addressed in conjunction with efficiency.

Another reason which may have contributed to permeability reduction is geometrical deformation occurring at the corner of the pleat as revealed by the scanning electron microscopic images of Figure 4.14. The higher the number of pleats, the more geometrical deformation is expected to take place. Therefore, additional permeability reduction is expected in higher pleating densities such 32 and 34 pleats/100 mm. It is also apparent in all pleating densities for all flow rates. An additional deformation or buckling is expected to take place in the overall pleated panel which would also lead to loss of surface area and reduction in permeability. This sort of bulking could also lead to the fracture of the pleated panel during operation.

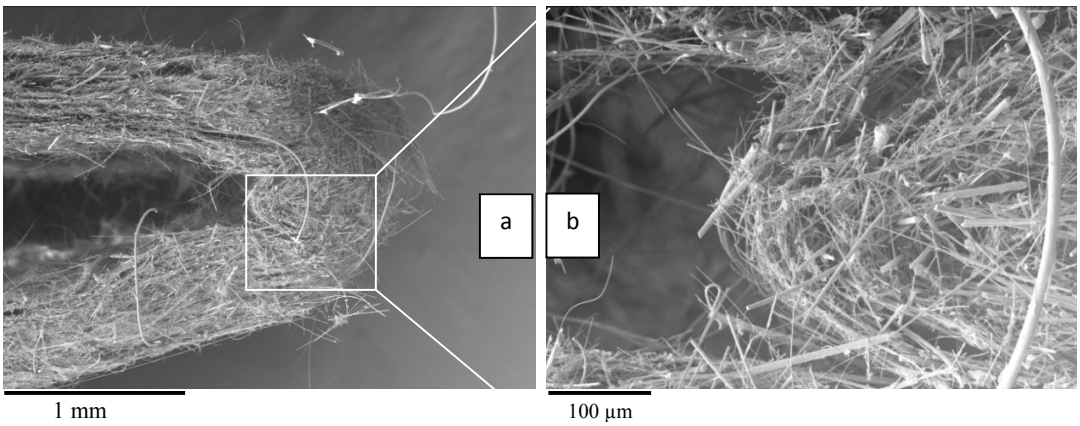

[a] Compression at the inner bend of a single pleat of the glass fibre media used.

[b] Compressed zone of the pleat.

Figure 4.14: Geometrical alteration of a mini-pleat corner of a fibrous filter media.

Examining closely the design of the filter and the arrangement of the pleats and their densities as shown in Figure 4.15, when the flow rate is increased, the media starts to deform and permeability tends to reduce. Pleats will come in contact together and a loss in surface area will take place. This also indicates that the pleating density may be excessive given the allowed space in the filter housing.

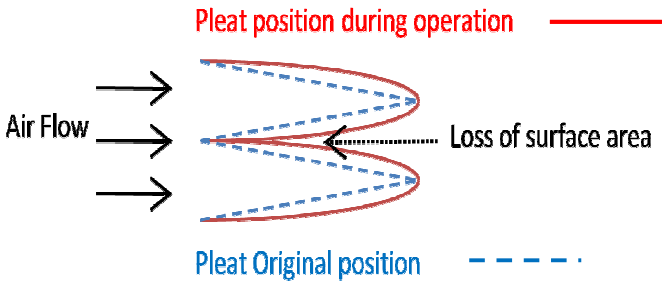

Figure 4.15: Illustration of expansion of the filter and loss of the surface area.

4.2.4 Experimental Pressure Drop Validation

The pressure drop data obtained experimentally have been compared against theoretical models as illustrated in Figure 4.16. It is evident that experimental data of all tested filters deviate from linearity which is common feature of all listed theoretical models. Such deviation is reasoned to the surface area losses discussed in Section 4.2.3 and several authors as related this deviation to the irregular geometry or imhomogenity of fibrous media and introduced different value for it. It is evident that none of the models used fit the experimental data. Further, it is important to note that these models were presented to describe a flat sheet filter and a full scale pleated filter. Further, the filter used in this study was a V-shaped as shown previously in Figure 4.9. The entire comparisons for rest of the filter are shown in Appendix I.

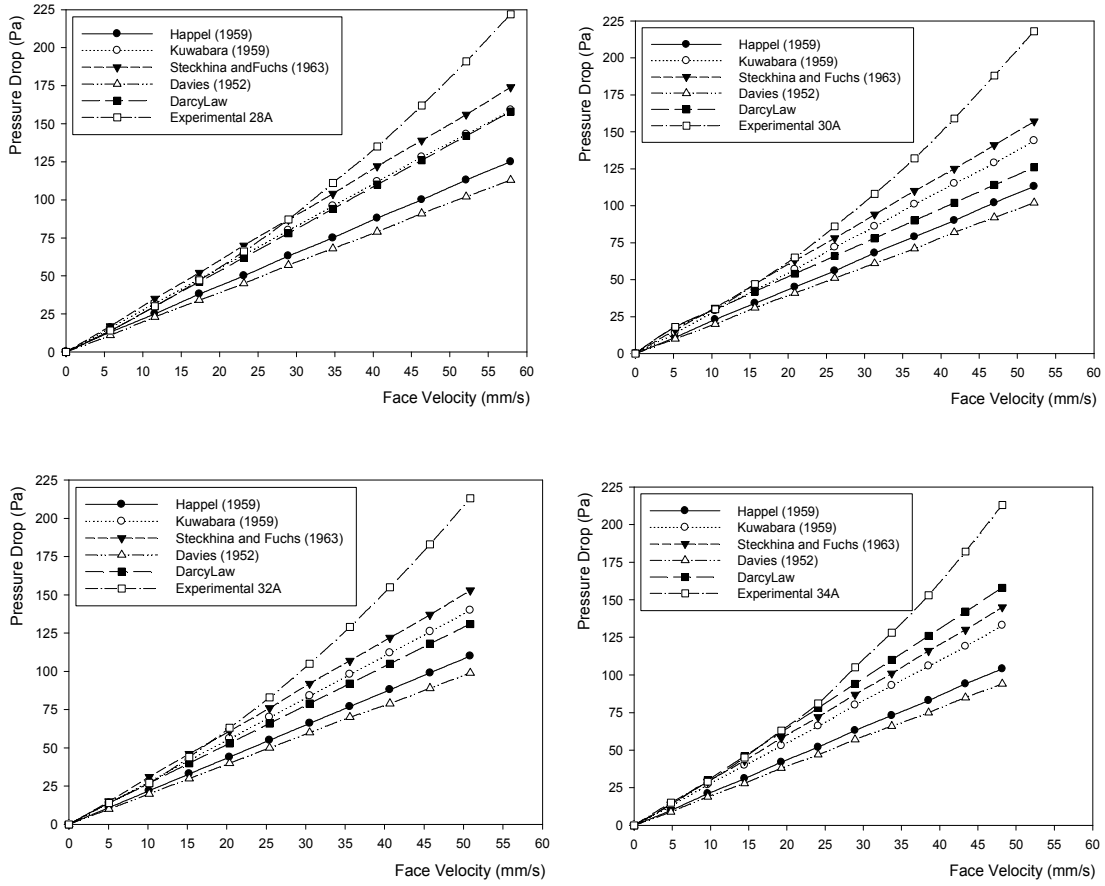

Figure 4.16: Validation of experimental pressure drop for filter group A.

4.2.5 Pleat Deflection Analysis by Representation of a Plate with Distributed Load

An important aspect associated with permeability reduction is the losses of filter medium surface area. To further examine such losses, it is essential to verify if the neighbouring pleats are touching one another. This can be investigated by modelling the pleat as a simply supported plate as shown in Figure 4.17 with dimensions $L_x = L_y$. The front view of the pleat used in this analysis along with the distance between two pleats is shown a scanning electron micrograph in Figure 4.18.

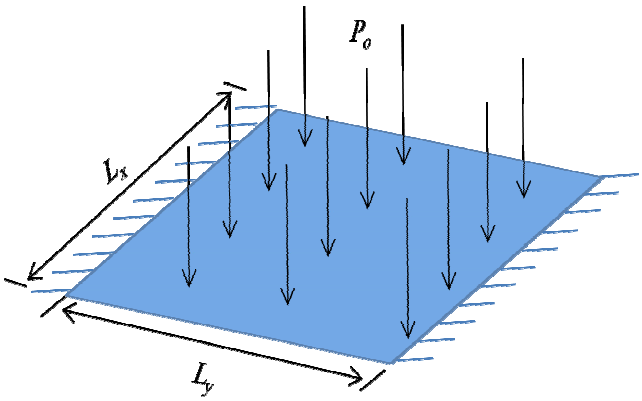

Figure 4.17: Representation of the pleat by means of a simply supported plate.

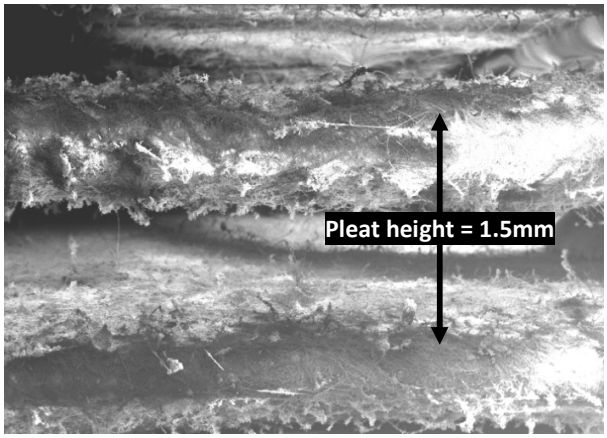

Figure 4.18: SEM of a front view of a few pleats of the pleated panel filter used in the testing.

Representation of the pleat as a simply supported plate is assumed since a plate is characterized by the fact that its thickness it relatively small compared to the dimensions in the plane of middle surface. The representation is shown in Figure 4.19 will facilitate the calculation of the deflection of each pleat and therefore, the total deflection could be compared with distance measured by the scanning electron microscope image. If the combined deflection is greater than 1.5 mm, that means the pleats are touching one another.

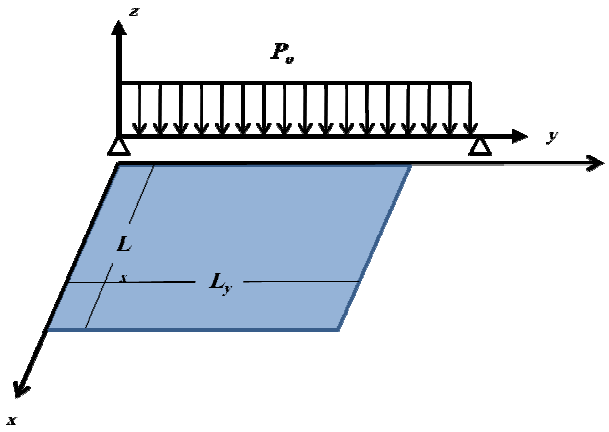

Figure 4.19: Isometric view of few pleats of pleated panel filter used in the testing.

The equation used for the deflection calculation for both filter group A and B is shown below [Ugural and Fenster, 2003]:

$$\delta_{\max} = 0.0454 P_o \frac{L^4}{Y_E h^3} \tag{4.1}$$

where Y_E is Modulus of Elasticity is measured to be equal to 248 (N/mm^2) for the fibre glass material used in this study with values tabulated in Table 3.2. Further, since the pleat has a square dimensions, therefore $L_x = L_y = L$, where $L = 28$ mm.

Similar types of calculation are shown for all other flow rates to illustrate the deflection expected in Table 4.6. It can also be noticed that as the flow rate increases the deflection of the pleat increases. On the other hand, as the pleating density increases, the pleat deflection decreases. For example, filter 32A and 34B exhibit the least pleat deflection versus flow rate, if both filter achieve the same efficiency, filter 32A would be a better selection since it requires less surface area. Figure 4.20 shows the deflections of the experimental data of filter 28A which highlights non-linear variation with flow rate. Appendix H illustrates all predicted pleat deflections for the tested filters.

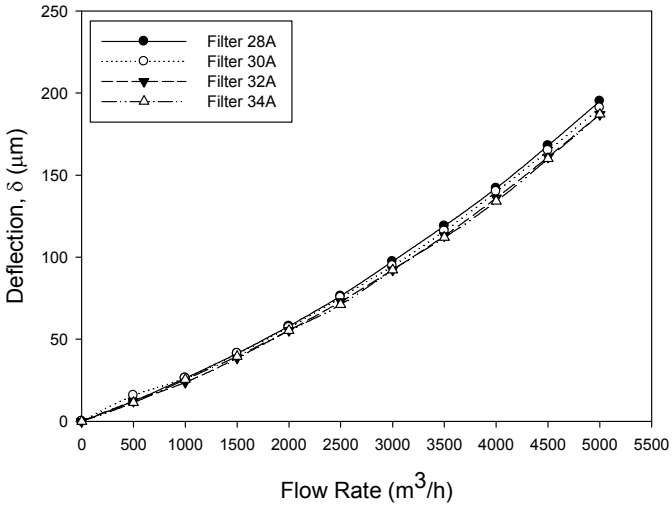

Figure 4.20: The comparison between deflections versus flow rate for different pleating densities for filter Group (A).

FILTER	**Deflection δ (μm)**			
Q (m^3/h)	**28A**	**30A**	**32A**	**34A**
500	12.3	15.8	12.3	11.4
1000	26.3	26.3	23.7	25.5
1500	41.3	41.3	38.6	39.5
2000	58.0	57.1	55.3	55.3
2500	76.4	75.5	72.9	71.1
3000	97.4	94.8	92.2	92.2
3500	119.0	116	113.0	112.0
4000	142.0	140	136.0	134.0
4500	168.0	165	161.0	160.0
5000	195.0	191	187.0	187.0

Table 4.6: Estimated pleat deflections using Equation (4.1) using the Young's modulus value.

In this analysis two assumptions were made:

1- All air flow pressure applied to the pleat and the pleat is solid sheet of fibres only. In fact, the pleat is porous and pressure exists in the air phase. Some of the pressure will be transported to the fibre by drag at the fibre surfaces.

2- Deflections are minimum because that the modulus of elasticity is for glass fibre sheet only. While in fact, the glass sheet in made of air and glass fibre, and air constitutes larger part of the media.

To get a better feel of what is deflection in the pleat, a modulus of elasticity of 50% of the value measured for the fibre glass material considering that 50% of the air pressure causes the deflection of the fibre network, The area loss due to deflection of the pleat is small and limited to the creasing/bend of the pleat.

The deflections estimated by the simply supported plate theory are listed in Table 4.7 using 50% of the Young's modulus of elasticity value obtained experimentally. It is clear that as the flow rate increases, the deflection increases. The largest distance between two pleats is in the front and it is equal 1.5 mm. For high flow rates such as 4500 m^3/h the total deflection is equal to 336 μm x 2 = 672 μm which amounts to 90% of the total opening between two pleats. However, inside the pleat, the opening of the pleat decreases in the direction of the air flow that means the pleats will touch one another. It can also be noticed that as the pleating density increases, the deflection decreases which could be due to the greater rigidity the extra pleats would give to the entire pleated panel. The comparison between the deflections using the measured modulus of elasticity and 50% of the value of it are shown in Figure 4.21.

FILTER	**Deflection δ (μm)**			
Q (m^3/h)	**28A**	**30A**	**32A**	**34A**
500	24.6	31.6	24.6	22.8
1000	52.6	52.6	47.4	51
1500	82.6	82.6	77.2	79
2000	116	114.2	110.6	110.6
2500	152.8	151	145.8	142.2
3000	194.8	189.6	184.4	184.4
3500	238	232	226	224
4000	284	280	272	268
4500	336	330	322	320
5000	390	382	374	374

Table 4.7: Estimated pleat deflections using Equation (4.1) using 50% of the Young's modulus value.

The filtration media moduli of elasticity measurements were done using a 5000 N load cell where the applied load did not exceed 18 N. Therefore, further investigation is

recommended using a smaller load cell (for example 100 N) and an external extensimeter to improve the accuracy of the results.

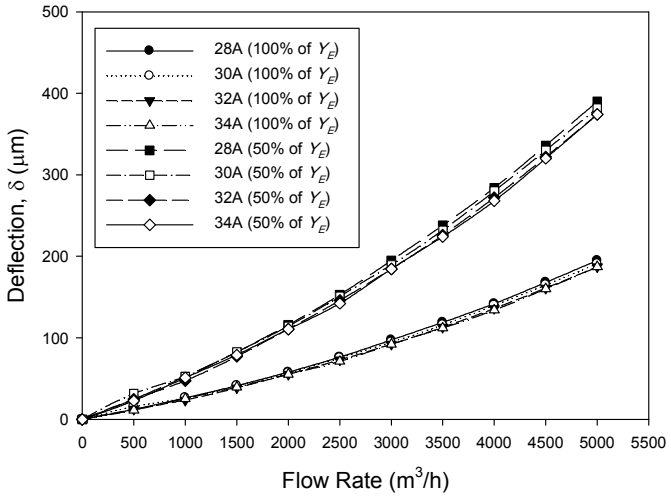

Figure 4.21: Deflection comparison between using Equation (4.1) using 100% and 50% of the filtration media Young's modulus value.

4.2.6 The variation of Velocities during Testing

The air velocity varies in the testing tunnel and through the filter. For a flow rate of 5000 m^3/h for example, the velocity at point (1) on Figure 4.23 is equal to the flow rate divided by the testing cross section, A_c,:

$$U_1 = \frac{Q}{A_c} = \frac{5000}{(0.61 \times 0.61)(3600)} = 3.73 \text{m/s}$$

However, at point (2) the air experience a reduction in surface area and the effective area becomes the area of the four openings of the filter. Therefore, the air velocity at point (2) increases to:

$$U_2 = \frac{Q}{4A_{open}} = \frac{5000}{4(0.522 \times 0.067)(3600)} = 9.93 \text{m/s}$$

The air velocity continues to increase as air flows deeper onto the "V" cross section. On the other hand, as the air approaches the surface area of the filter medium, equal to 24 m^2 for filter (28A), the velocity experience substantial reduction to become:

$$U_3 = \frac{5000}{(24)(3600)} = 0.58\,\text{m/s}$$

Eventually, at point (4) is stagnation and velocity is zero. Figure 4.22 illustrates the variations of the air velocities through different points in the testing. However, in the "V" shaped part of the filter the velocity would increase at the cross section reduces and then suddenly slows down due to the surface area of the filter to 0.058 m/s.

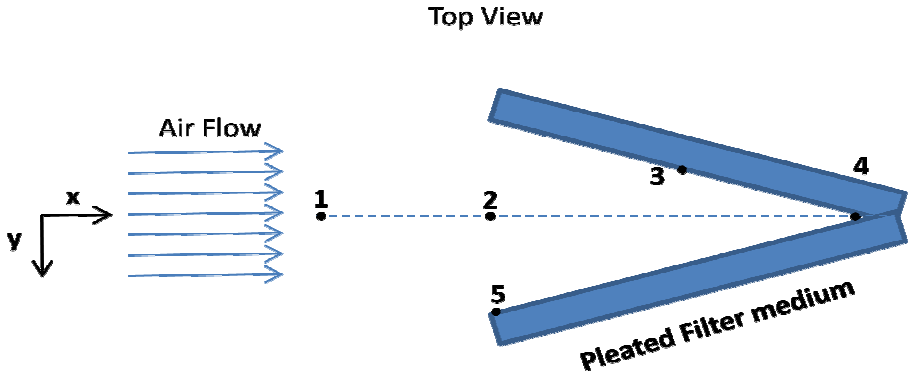

Figure 4.22: The position of different velocities experienced within the pleat.

This variation of the air velocity gives a rise to a variation in gas flows over the panel upstream faces. Assuming the air pressure is constant over 1-2-4, and is the same as at 3, then the air flow rates vary along 4-5 due to lateral flows of air into the upstream voids between the pleats. The cumulative force on the panel face leads to deformation of the panel when it is insufficiently supported.

4.2.7 Practical Implication during Dust Loading

It was observed that a whole pleated panel buckles at flow rates of 3500 m^3/h and higher which will also cause the pleats to come together. This leads to pleat geometrical deformation and eventually the whole pleated panel may fracture. An example of a filter which has fractured in Kuwait is shown in Figure 4.23.

Figure 4.23: A fractured pleated media panel of minipleat filter used in an HVAC application in Kuwait.

A sample of the same filters used for this experimental work was used to obtain SEM images of the dust loading conditions. Figure 4.24 show SEM examination of a used minipleat sample in a filter used in air handling unit in Kuwait. This filter has reached its final pressure drop (600 Pa) which is recommended by the manufacturer. Dust cake formation is apparent but no evidence of surface deposition has occurred before or after the full utilization of the depth filter. The filter fibres can barely be seen due to the dust loading.

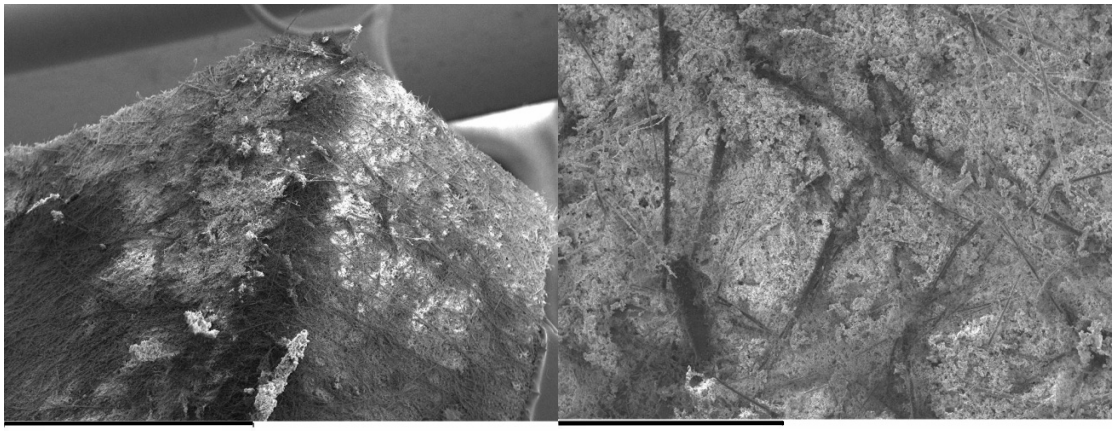

4 mm 300 µm

[a] Formation of dust cake on the surface of filter pleat. [**b**] Top view of the surface loaded with atmospheric dust.

Figure 4.24: SEMs of sample of dust surface deposition on a fine filter pleat used in HVAC application in Kuwait.

4.3 Filtration of Air

The process of air filtration is a complex process which is influence by several factors pertaining to the dust physical and chemical characteristics. To better understand and evaluate the filtration process and influential parameters affecting the filtration performance of air filters, an in-depth analysis of the dust must be conducted.

4.3.1 Dust Characterization

Kuwait and synthetic dust was characterized physically and chemically to better learn about their behaviour in the filtration process. The physical and chemical characteristics of synthetic dust were examined to choose one that represents the Kuwaiti atmospheric dust. The three dusts chosen are commonly used dusts worldwide by filtration industries specifically in Kuwait and the Gulf area to provide test reports by which filter selection is made.

4.3.1.1 Chemical Characterization – EDXS

The three synthetic dusts chosen for the characterization process are; ASHRAE, SAE fine and SAE coarse have been analyzed using *Energy Dispersive X-ray Spectroscopy* (EDXS) to determine their chemical composition.

The analysis shows that the Kuwaiti atmospheric dust is mainly silica and also contains aluminium, calcium, iron and some traces of potassium and magnetism. The silica content is the Kuwaiti dust is higher of that is ASHRAE dust and lower than SAE coarse and fine dust. Unlike ASHRAE and SAE coarse dust, the Kuwait atmospheric dust does not contain carbon. SAE fine dust contains aluminium, calcium and traces of potassium. The analysis of the ASHRAE dust does not show any presence of aluminium, calcium and traces of potassium which are found in the Kuwaiti dust. SAE fine and coarse on the other hand, contain aluminium, calcium and traces of potassium. Furthermore, ASHRAE dust contains cotton lint as shown in Figure 4.25 which is absent in the Kuwait dust.

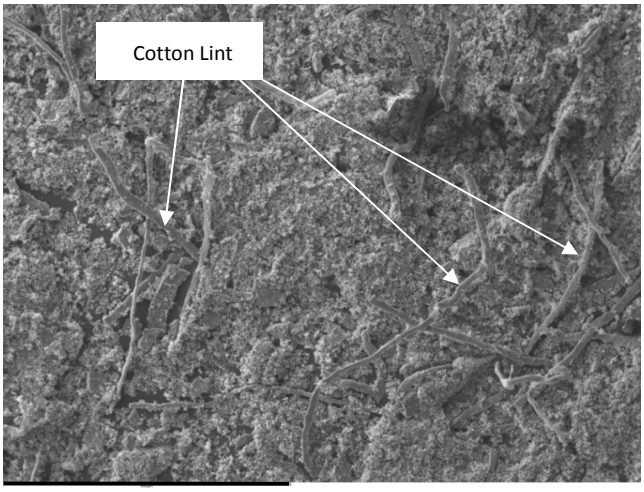

Figure 4.25: The existence of cotton lint in the ASHRAE dust.

While it is difficult to decide on the most representative dust using EDXS analysis, the SAE fine dust seems to be the closest to the Kuwaiti atmospheric dust from a chemical composition stand point. Clearly, no one dust of the selected dusts is fully representative of the Kuwaiti dust. Table 4.8 lists the chemical composition of samples of the Kuwait atmospheric dust, ASHRAE dust, SAE fine and SAE coarse dusts.

Element	Kuwait atmospheric	ASHRAE	SAE fine	SAE coarse
O	42.25	23.30	49.80	45.37
C	-	55.88	-	19.70
Mg	3.62	-	-	-
Al	7.75	-	4.31	-
Si	**29.18**	**20.82**	**38.80**	**34.93**
Ca	9.39	-	3.02	-
Fe	7.80	-	-	-
K	-	-	4.07	-
Totals	100.00	100	100	100

Table 4.8 The chemical composition of Kuwait atmospheric dust.

4.3.1.2 Particle Size Distribution

While it is hard to obtain a commercially produced dust that fits the physical and chemical characterization of the Kuwait atmospheric dust, the particle size analysis comparison can be conducted using the particle size distribution of the Kuwaiti samples obtained. Ten samples of Kuwaiti atmospheric dust were obtained from Kuwait Scientific Research Center (KISR). The dust samples were then sized to obtain the particle size distribution using a Malvern Master sizer. Each sample was inserted into an ultrasonic

bath for one minute to ensure that the dust was dispersed. A 300RF lens was used which provides a size range between 0.05 and 880 μm. Since the Kuwait atmospheric dust was found from EDXS analysis to be mainly silica, therefore, a refractive index of 1.5 was used. The same refractive index was used for the synthetic dusts. Figure 4.26 shows the particle size distribution comparison between Kuwaiti atmospheric dust and the commercial synthetic dusts selected for the analysis.

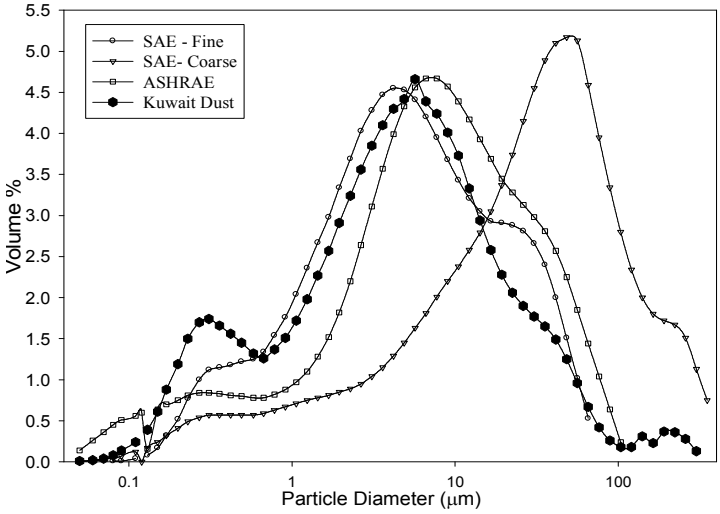

Figure 4.26: Particle Size distribution comparison between Kuwaiti Atmospheric Dust (sample 1) and commercially available dusts.

Sizing measurements revealed the dust size distribution of ASHRAE dust was dissimilar to the all of ten Kuwait dust samples as shown in Table 4.8. The size distribution of SAE coarse dust was also different from the Kuwaiti particle size distribution. This signified that each dust has different settling velocities, which increase rapidly with particle size and density. The particle size distribution of the SAE fine seems to be the closest to the Kuwaiti atmospheric dust.

Table 4.9 lists the measured value of the mean diameters, volume mean diameters and surface area mean diameters of synthetic dusts in addition to the Kuwaiti one. The obtained specific surface area mean diameter of ASHRAE and SAE coarse dust particles by Malvern Master Sizer are 1.84 and 1.75 μm respectively. Both measurements are lower than the surface area mean diameter of the Kuwait dust which has a range of 3.22 to 5.74 μm. The drag force is affected by the surface area of the particle which in turn

means the drag force created by ASHRAE dust particle is lower than the Kuwait one. The mean surface area of SAE fine dust particles is 3.73 µm/g which falls into the Kuwait atmospheric dust range of specific surface area mean diameter.

	Mean Particle Size (µm)	**Volume Mean Diameter (µm)**	**Surface Area Mean Diameter (µm/g)**	**Specific Surface Area (m^2/g)**
KWT 1	5.03	14.14	1.34	4.47
KWT 2	5.11	25.85	1.21	4.94
KWT 3	4.94	27.63	1.04	5.74
KWT 4	8,54	35.52	1.31	4.58
KWT 5	6.94	21.44	1.54	3.54
KWT 6	13.24	31.09	1.69	3.22
KWT 7	6.43	34.20	1.16	4.71
KWT 8	6.26	18.15	1.35	4.43
KWT 9	6.36	26.86	1.45	4.13
KWT 10	7.32	26.86	1.53	3.93
ASHRAE	5.63 - 8.00	51.15	3.27	1.84
SAE Fine	10.24	36.23	1.61	3.73
SAE Coarse	33.18	57.18	3.41	1.75

Table 4.9: Various experimental relevant diameters and properties of the Kuwaiti and Synthetic dusts under study.

4.3.1.3 Kuwaiti and Test Dusts

Prior to loading the filters under test with solid aerosol, it is imperative to characterize physically and chemically the commercially available dusts. Such characterization facilitated a comparison with the Kuwaiti atmospheric dust. Three types of synthetic dusts were selected for physical characterization namely; ASHRAE, SAE 726 coarse, and SAE 726 fine. Since most of the filters used in Kuwait are evaluated by means of ASHRAE dust was also included in the analysis in order to assess its appropriateness for filter performance via its similarities in physical and chemical characteristics to Kuwaiti atmospheric dust.

ASHRAE synthetic dust is composed by weight of 72% standardized SAE 726 fine dust (Arizona Road Dust), 23% powdered carbon, and 5% cotton linters. Standardized air cleaner test dust is classified from dust gathered in a desert area in Arizona. It is predominantly silica and has a mass mean diameter of approximately 7.7 µm, a geometric standard deviation of approximately 3.6 µm, and density of approximately 2.7 g/cm³.

The powdered carbon is carbon black in powder form, with ASTM D3765 CTAB surface of 27± 3 m^2/g, ASTM D2414 DBP adsorption of 0.68± 0.7 cm^2/g, and ASTM D3265 tint strength of 43 ± 4. The SAE 726 fine test dust is composed of mineral dust predominantly silica with other oxides present. It has a specific gravity 2.6 – 2.7 g/cm^3 [ASHRAE, 1999]. On other hand, SAE 726 coarse dust is a naturally occurring mineral sand predominantly SiO_2 with other oxides present. It has a mass mean diameter of approximately 7.7 µm, a geometric standard deviation of approximately 3.6 µm, and density between 2.6 and 2.7 g/cm^3.

4.3.1.4 Reasons for Dust Selection

The particle shape of the Kuwaiti atmospheric dust along with ASHRAE Synthetic, SAE 726 coarse, and SAE 726 fine dusts was examined using a scanning electron microscope. Figure 4.27 show that SAE coarse and fine dusts as well as the Kuwait atmospheric dust are mainly nonspherical particles. As discussed in Chapter Two, the drag force varies with the particle shape which in turn affects the aerodynamic behaviour. A spherical particle has higher velocity than an irregular particle with the same weight [Dorman 1974]. The aerodynamic behaviour of particles affects the filtration performance of air filters. Therefore, the angular velocity of irregular dust particles should be considered, and a modified equation of motion for spherical particles may be used to describe the non-spherical particle dynamics with more accuracy.

The true densities of all dusts were measured using a pycnometer. From a true density standpoint, all synthetic dusts have different densities when compared to the Kuwait atmospheric one. The true density of Kuwaiti atmospheric dust is higher than ASHRAE dust and lowers than both SAE fine and coarse dusts. True densities of all dusts are listed in Table 4.10.

The SAE fine and SAE coarse will be chosen for the dust loading processes since they represent a fine and coarse particle size distributions, in other words, they act as a lower and upper limit from a size distribution point of view respectively. It also happens that the Kuwaiti dust fell between the two size distributions.

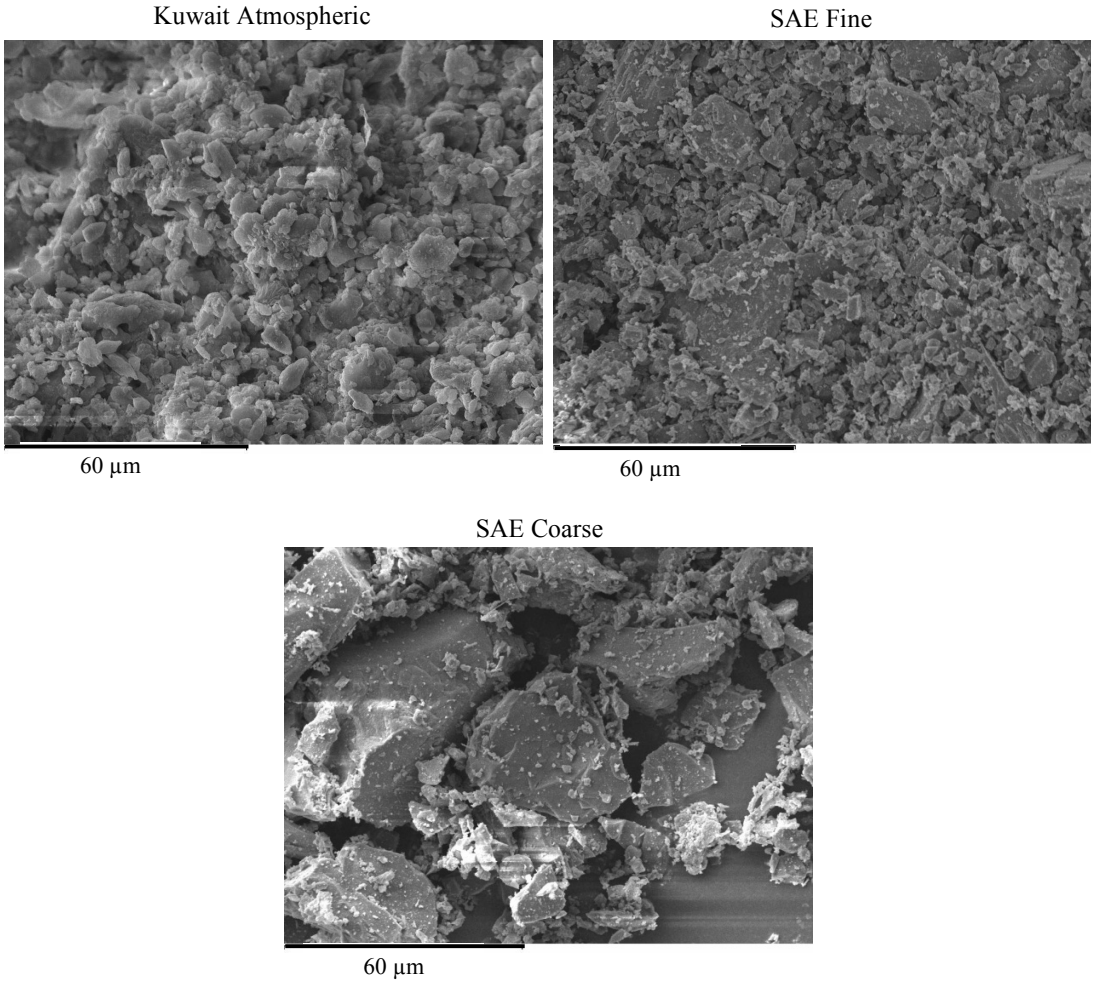

Figure 4.27: Scanning electron microscopic comparison showing images of Kuwaiti atmospheric, SAE fine and coarse dust.

Dust	Mean Measured Density (g/cm³)	Standard deviation of the three samples (g/cm³)
ASHRAE 52/76	2.22	0.042
SAE 726 Coarse	2.59	0.061
SAE 726 Fine	2.61	0.068
Kuwait Atmospheric	2.45	0.074

Table 4.10: True density measurement for Kuwaiti and Synthetic dust under study.

For the scope of this experimental work, the filter series A was be challenged by SAE fine while the series B filters was challenged by SAE coarse dust. Scanning electron microscope images of the same scale are shown of both dusts in Figures 4.31 and 4.32 for comparison purposes. It is evident that the SAE fine contains finer particle when compared to the SAE coarse dust. Dust particles of both dusts seem to have similar shape.

4.3.1.5 Particulate Matter in Kuwait Atmosphere

Several filter samples from different locations in Kuwait were examined using a scanning electron microscope to identify common air contaminants existing in the Kuwaiti atmosphere. Figure 4.28 shows SEM examination which revealed pollen grains deposition on the surface of the filter media. Pollen grains discharged by weeds, grasses and trees are capable of causing hay fever [Jacobson and Morris, 1977]. Most pollen grains are hygroscopic and, therefore, vary in mass with humidity [ASHRAE, 2001]. A pollen count of 10 to 25 may make hay fever sufferers experience the first symptoms [ASHRAE, 2001]. The pollen grain found in the SEM examination of the filter media used in Kuwait ranged in size between 10-60 μm.

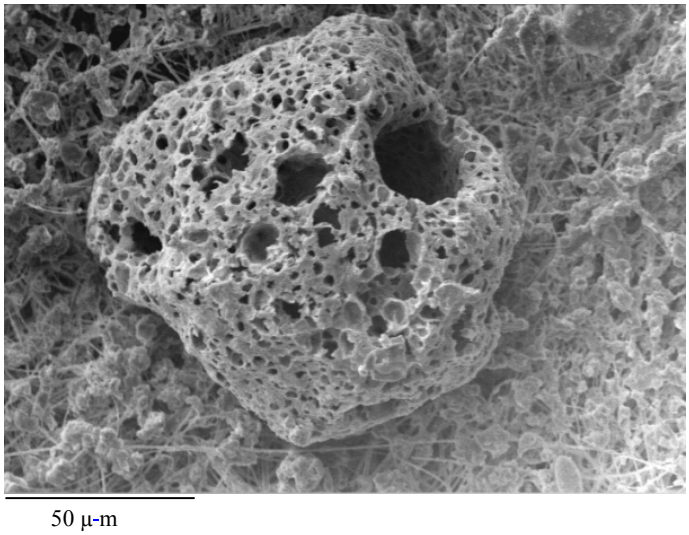

Figure 4.28: SEM examination of air filters used in air conditioning units in Kuwait.

4.3.2 Initial Efficiency Measurement Using DEHS

The initial efficiencies were measured for all filters at each flow rate using the PMT LPS particle counter which analyzed in the size range of 0.065-0.900 μm. The flow rates varied from 500 m^3/h up to 3000 m^3/h, with 500 m^3/h increments. This sort of measurement is of critical importance since it determines the MPPS for each flow rate and therefore, the filter class can be determined. Appendix G lists the initial efficiency measurement for the corresponding flow rates for each filter.

4.3.2.1 Effect of Gas Velocity and Pleat Density on MPPS

The variations of flow rate from 500 to 3000 m^3/h have facilitated the investigation of gas velocity on the filter performance. In this section, the filter efficiency is considered and MPPS variations are examined. The filter efficiency decreases as particle size increases until the MPPS is reached. Beyond the MPPS, the efficiency increases with the increase of particle size as shown in Figure 4.29. It also shows for the particle size range 0.065 - 0.9 µm the efficiency generally decreases with the increase of gas velocity. This signifies that the diffusion mechanism is dominant and interception effect is relatively independent of the gas velocity variations which are in agreement with previously studies.

Examining the efficiency curve for 3000 m^3/h, it is evident that the fluctuations of efficiencies are higher than lower flow rates and its corresponding MPPS. Increasing the gas velocity shortens the particle residence time inside the filtration medium. Consequently, it reduces the possibility for a particle to fibre contact and therefore the efficiency is lowered. It can also be noticed the MPPS shifts towards a smaller particle size. However, the measured initial fractional efficiency and its corresponding MPPS fluctuated for flow rates of 2000-3000 m^3/h due to particles bounce and/or detachment after they had been attached to the fibre surface. When the velocity is increased, the particle can re-entrain itself into the air stream and therefore lower the overall efficiency. In fact, this was evident as at flow rate of 2500 and 3000 m^3/h, the H10 filter class requirement of an efficiency of 85% @MPPS was not satisfied. On the other hand, the same filter was able to achieve such requirement for filter classification of H10 for flow rates of 1000-2000 m^3/h. Furthermore, for the flow rate of 500 m^3/h, the same filter could in fact be classified as H11. All filter classifications are reference to Standard DIN 1822 [1998].

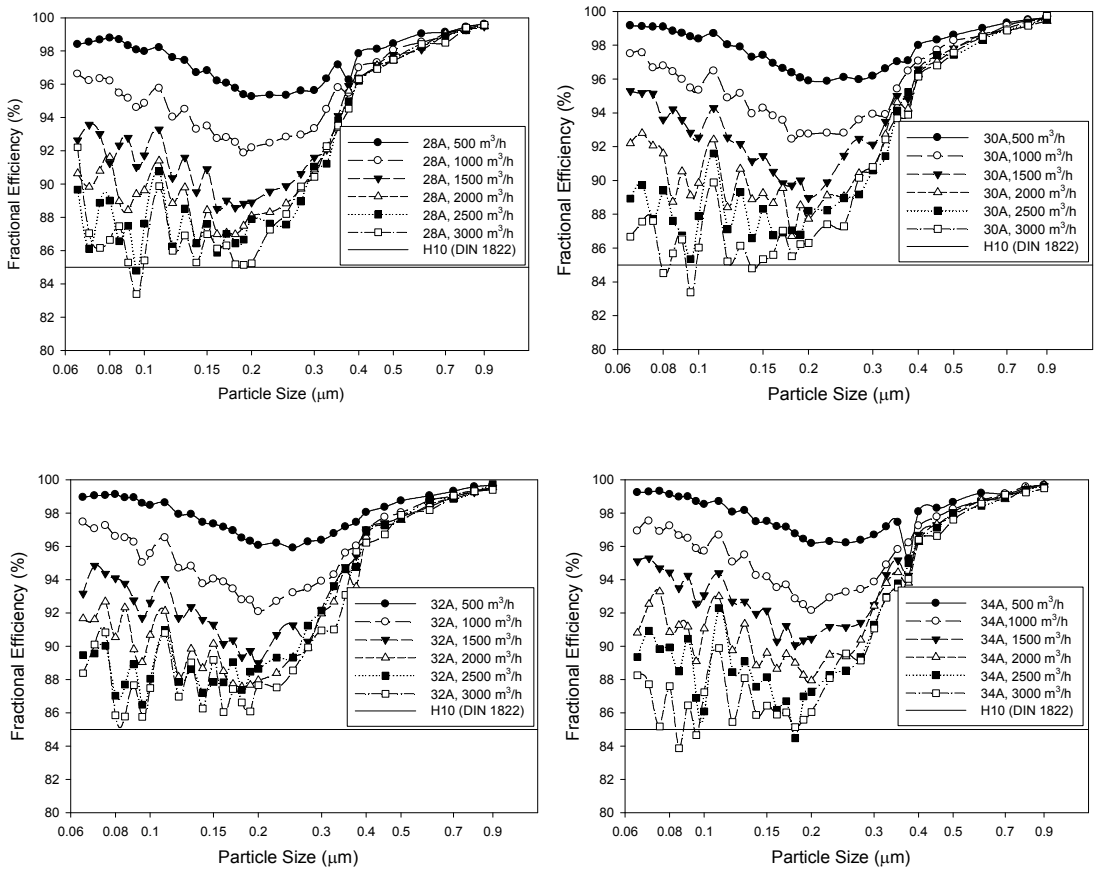

Figure 4.29: Initial efficiency [DIN 1822, 1998] vs. particle size for different flow rates (Group A).

The effects of flow rate and pleat density on the MPPS and its corresponding efficiency are listed in Table 4.11. From a pleat density standpoint, the MPPS increased slightly or remained the same as the pleating density increased. Figures 4.30 and 4.31 illustrate the effect of the filter face velocity on the MPPS for different pleating densities for Filter series A and B respectively. It can be noticed that the MPPS decreases with the increase of filter's face velocity for all pleating densities a given surface area and filter medium. In terms of minimum corresponding efficiency, it decreased as the face velocity increased for all pleating densities. Figures 4.30 and 4.31 are nominally the same but have a small variation caused by the minor differences in surface area during manufacturing as discussed in Section 4.1.4.1.

Flow rate m^3/h	28A MPPS (µm)	28A E%	30A MPPS (µm)	30A E%	32A MPPS (µm)	32A E%	34A MPPS (µm)	34A E%
500	0.200	95.27	0.225	95.87	0.250	95.90	0.375	95.24
1000	0.190	91.87	0.180	92.45	0.200	92.08	0.200	92.14
1500	0.160	88.51	0.200	88.97	0.200	88.99	0.180	90.06
2000	0.140	86.39	0.180	86.71	0.180	87.55	0.200	87.93
2500	0.095	84.79	0.095	85.35	0.095	86.48	0.180	84.47
3000	0.095	83.38	0.095	83.38	0.095	85.74	0.085	83.87
	28B MPPS (µm)	**28B E%**	**30B MPPS (µm)**	**30B E%**	**32B MPPS (µm)**	**32B E%**	**34B MPPS (µm)**	**34B E%**
500	0.225	95.32	0.225	95.79	0.200	96.24	0.225	95.81
1000	0.180	91.61	0.190	92.04	0.250	91.89	0.200	91.69
1500	0.180	88.50	0.190	89.17	0.180	89.01	0.180	89.21
2000	0.180	85.41	0.180	86.84	0.160	87.24	0.170	88.21
2500	0.090	85.80	0.180	82.83	0.180	86.07	0.180	84.30
3000	0.085	80.53	0.095	81.68	0.180	85.55	0.180	84.91

Table 4.11: Initial efficiency for Filter 28A and 28 B according to DIN 1822 vs. air flow rate.

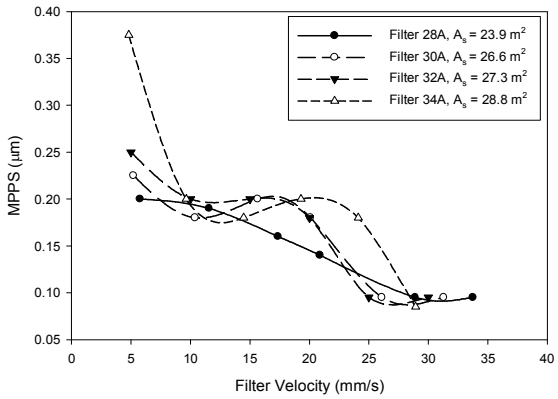

Figure 4.30: Most penetrating particle size vs. filter's face velocity for (Group A).

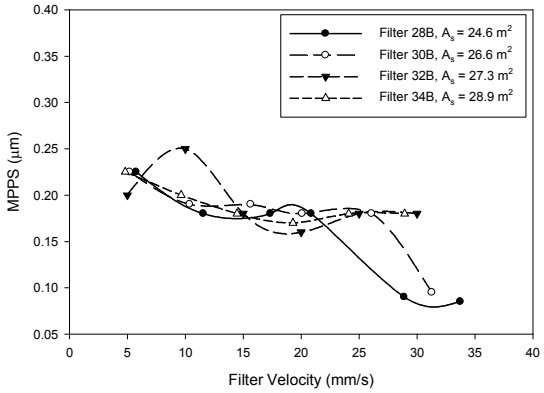

Figure 4.31: Most penetrating particle size MPPS vs. filter's face velocity (Group B).

To investigate further the effect of flow rate and the corresponding filter face velocities, the 3000 m^3/h efficiency curves were plotted in one graph for comparison purposes as shown in Figure 4.32. This choice of flow rate comparison was made for two reasons; first, efficiency curves and their curve fitting results show that there are several points that do not fit the curve compared to other flow rates. The second reason is that at this flow rate the filter classification requirement of H10 is not achieved. The plots show that there is no significant effect of the pleat density on the efficiency curves at 3000 m^3/h. Figure 4.33 shows that only 32A has satisfied the filter class requirement of HEPA H10 according to the DIN 1822 Standard. This is also illustrated from a face velocity stand point in Figure 4.33 which shows that filter 32A is only filter that satisfied the H10 threshold limit by DIN 1822 Standard while other filters failed to do so for face velocities beyond 22 mm/s.

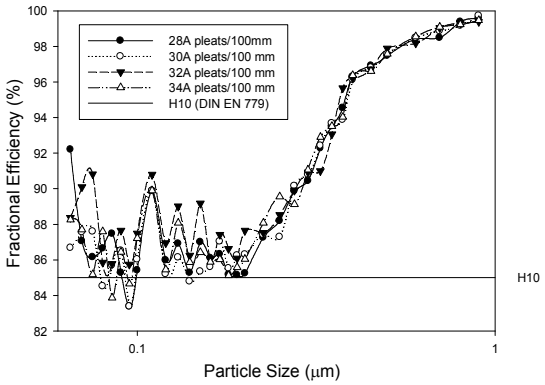

Figure 4.32: Initial efficiency vs. particle size for flow rate of 3000m^3/h (A filters).

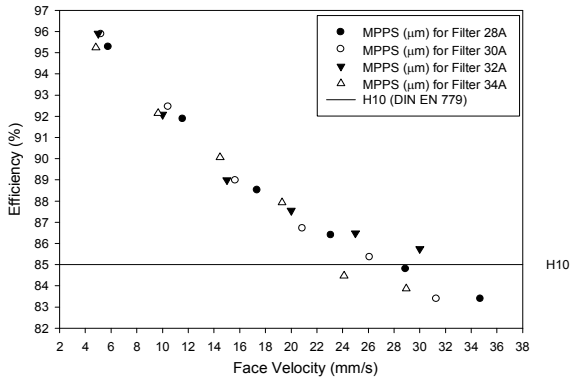

Figure 4.33: Initial efficiency vs. different face velocities for different pleating densities (A filters).

4.3.3 Filter Efficiency Using Test Dusts

Description of initial filter behaviour constitutes a small part of the filter's life time. While the study of clean filter performance is important, it does not predict the behaviour of the same filter during dust loading. When particle deposition begins to take place within the filtration medium, the filter's inner mechanical structure changes causing the overall efficiency and pressure drop to increase. Eventually, particles will collect other particles leading to dendrite formation which would finally lead to dust cake formation. To better understand dust loaded filter performance, group A and B were loaded with SAE coarse and SAE fine dust respectively. Fractional efficiencies were measured after each dust feed every 500 m^3/h increment and starting at 500 m^3/h. On the other hand, the pressure drop responses were measured every five minutes at a single flow rate of 3500 m^3/h.

4.3.3.1 Effect of Pleat Density on Pressure Rise

A filter with 28 pleats per 100 mm was loaded with AC coarse dust. The 1000 g of dust was loaded in four increments each of 250 g. The pressure rise was always linear with time. The 1000 g was mainly deposited within the depth of the filter without a significant dust cake formation. Figure 4.34 shows the pressure drop response for different pleating densities for Filter group A after each dust loading stage.

.

As dust starts to be fed into the filter by means of a dust feeder, dust settlement into the depth of the filtration medium around the fibre and the rise in pressure drop is negligible. This is called the stationary filtration stage and it is represented by a linear response as shown in Figure 4.34. Filter 34A has the lowest pressure drop and a linear response which could be that the 1000 grams of dust were not enough to make the filter depart from the stationary depth filtration to non-stationary filtration and finally to the dust cake formation. Furthermore, Filter 34A has the highest losses in the surface area and filter 38A has the least losses in the surface area. However, Filter 28A satisfies the efficiency requirement and its pressure drop response is acceptable and still a linear response. In other words, the 1000 g also did not form dust cake on the surface on the filter surface.

This indicates that Filter 28A is more economical from cost point of view as well as from efficiency and pressure drop standpoints.

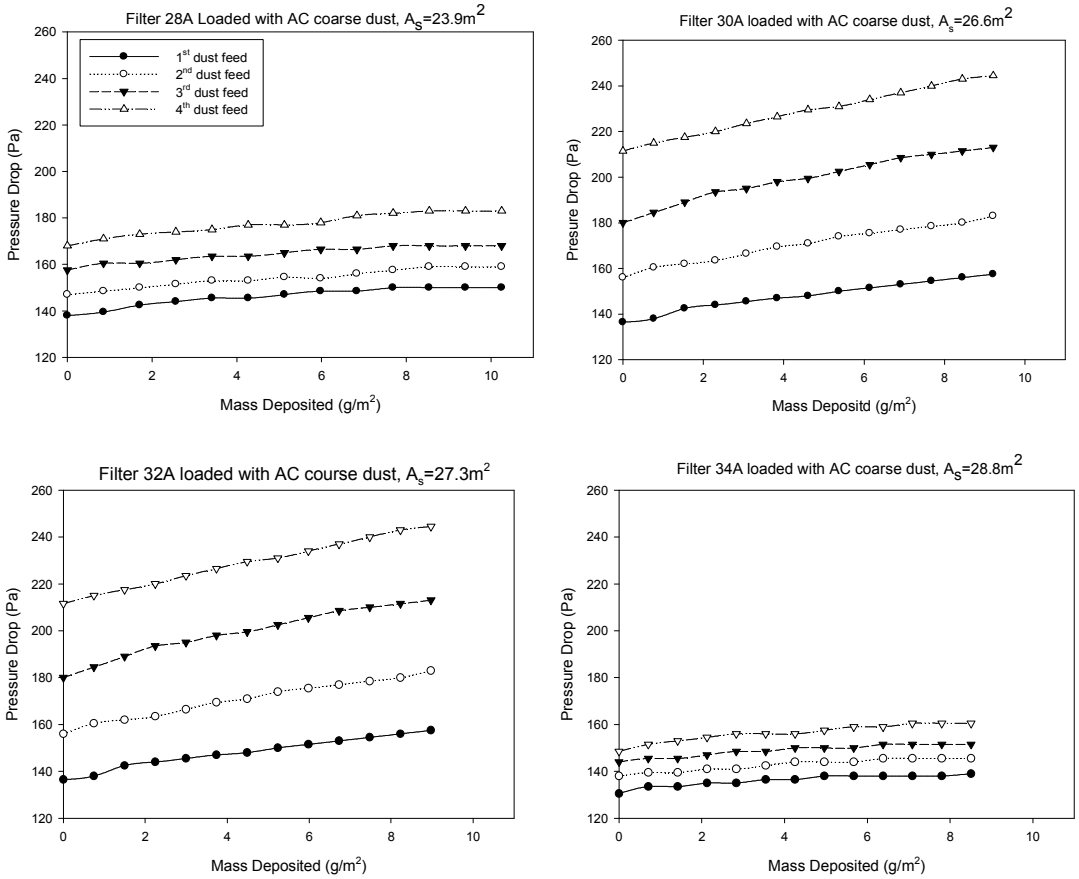

Figure 4.34: Behaviour of the time-dependent particle deposition in different pleating density filters (Group A) at flow rate of 3500m^3/h.

While the dust feeding was completed in 60-70 min, it was noticed towards the end of the dust feeding stage that a very small portion of dust in the reservoir was not going through to the conveyer belt and therefore it was unfed as shown in Figure 4.35. This caused the pressure drop response to level off after 55-70 minutes of feeding. The reliability of dust feeding data may only be considered for the first 45 minutes of feed. In the beginning of the feed, the weight of the whole dust 250 g ensured the transport of dust onto the conveyer belt, but when there was a small layer left in the dust reservoir toward the end of the feeding (as shown in Figure 4.35), it was insufficient to transport the final dust

onto the conveyer. Figure 4.36 shows the pleats after the fourth dust feed and the dust settlement at the hot melt of a pleat.

Figure 4.35: The unused/unfed dust in the powder reservoir towards the end of each dust feeding process.

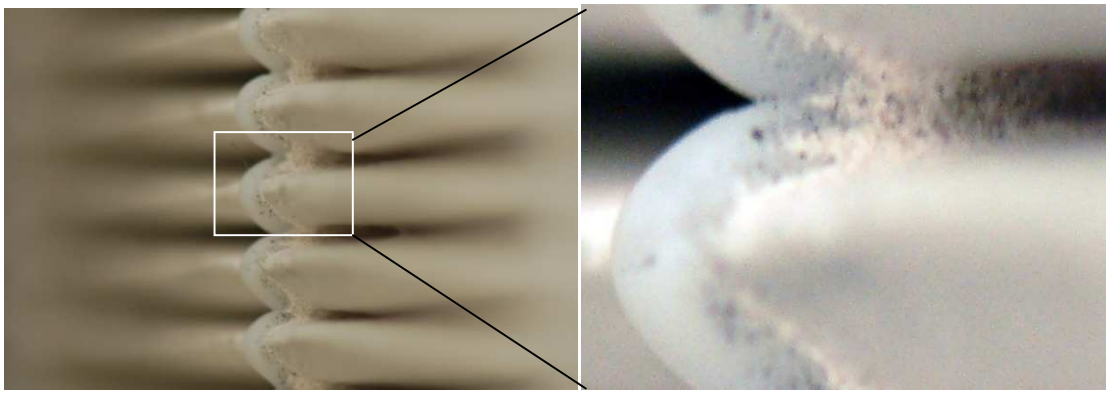

Figure 4.36: Images of the hot melt separating the pleats and a close up of the dust collected around it.

Figure 4.37 illustrates the pressure drop response after the fourth dust feed for 28 A and B for SAE coarse and fine dust respectively. It is evident that the pressure drop response is higher for SAE fine dust which indicates that fine particles tend to penetrate further through the filter medium compared to the coarse particles of the SAE coarse dust. Fine dust particles settling into the depth of filtration medium causes the fibre diameter to increase and consequently changes to the depth of the filter as well as the porosity and as results increasing the drag force in the filter matrix. Since the drag force is directly proportional to the pressure drop, an increase in the latter is expected.

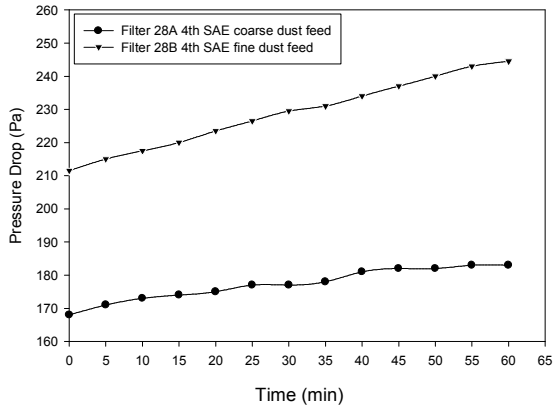

Figure 4.37: Pressure drop response for filters Group 28A and B after the fourth dust feed.

Similar observation and comment can be made for filters 34A and B as shown in Figure 4.38, however, the difference in the pressure drop response are smaller. This is attributed the fact that the pleats are closer to each in the 34 pleats/100 mm density compared to the 28 pleats/100 mm. It can be concluded that solid particles depositing within the fibrous structure change the geometry of the porous matrix which leads to substantial variations in the pressure drop and filtration efficiency.

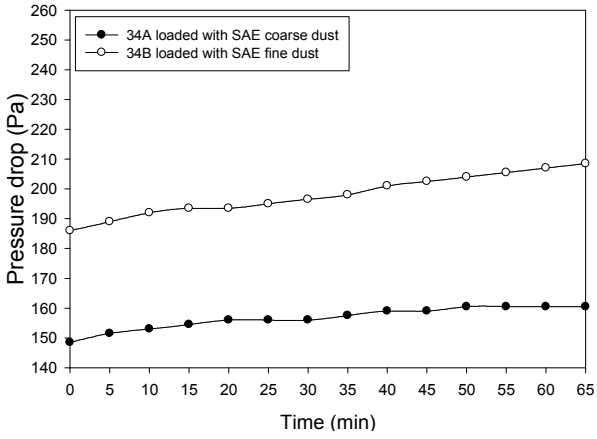

Figure 4.38: Pressure drop response for filters Group 34 A and B after the fourth dust feed.

Figure 4.39 shows pressure drop response versus mass deposited per surface area for Filters of group A which indicated that the higher the pleating density the lower the pressure drop (this does not consider the losses of the surface area during operation). Filter 28A exhibits the highest pressure drop response when compared with other

densities. On the other hand, the response of the 34A show the least response in pressure drop due to higher surface area provided. Figure 4.40 shows pressure drop response versus mass deposited per surface area for Filters group B using fine dust, it can be seen that the differences in the pressure drop with varying pleating density is smaller than the coarse dust in group A filters. This is due to the fact that finer particles are more penetrating and are capable of occupying interstitial spaces inside the filter medium which is responsible for the rise in the pressure drop of the filter.

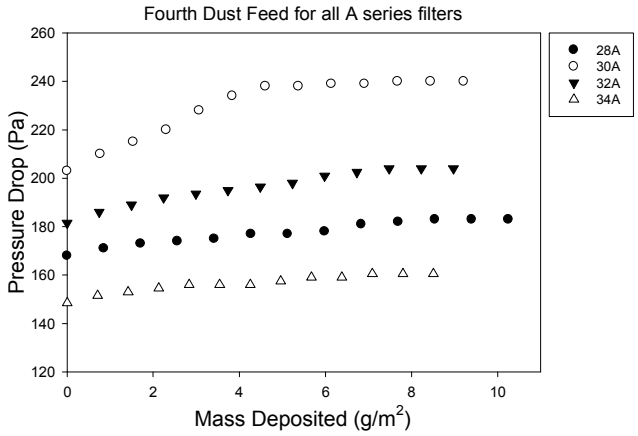

Figure 4.39: Pressure drop response versus mass deposited per surface area for filter group A using SAE coarse dust.

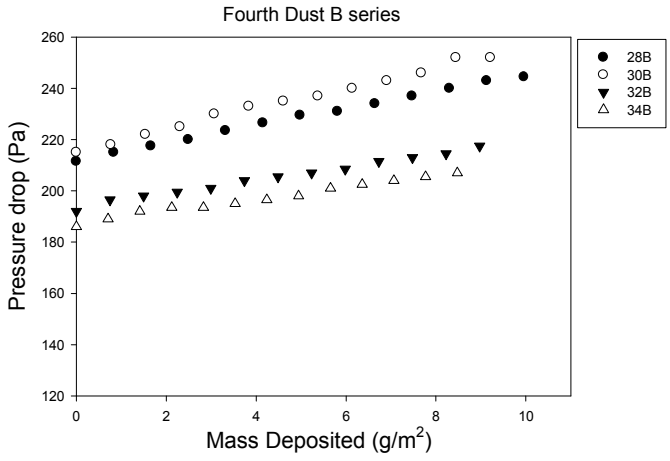

Figure 4.40: Pressure drop response versus mass deposited per surface area for Filters group B using SAE fine dust.

4.3.3.2 Dust Loaded Pressure Drop Prediction

Several authors have attempted to predict the pressure drop response of dust loaded filters. Equation 2.22 which will be modified to predict the pressure drop response of a full scale pleated filter in a V-shaped cartridge and is presented below:

$$\Delta P - \Delta P_o = [H]\frac{UM}{A_s} \tag{4.2}$$

where H is the slope which will be computed by means of linear regression technique. Figures 4.41 and 4.42 illustrate that the pressure drop predicted by Equation (4.2) for filters 28B and 34B loaded with SAE. The experimental pressure drop loaded with SAE fine dust is in good agreement with Equation (4.2). The slopes are listed in Table 4.12 which shows that as the pleating density and dust loading increase, the slope in Equation (4.2) increases. This signifies that the pressure drop is increasing not only due to the dust loading, but also to the increase of the pleating density. While Equation (4.2) presents a reasonable tool to predict the dust loaded pressure drop, the variations in slope due to pleating density and dust loading suggests that a constant slope chosen based on the average may not give an good indication of the predictive pressure drop. The rest of the pressure drop difference predictions for all the filters tested in this study are listed in Appendix M.

	Slope in Equation 4.2			
Filter	1st Dust Feed	2nd Dust Feed	3rd Dust Feed	4th Dust Feed
28A	83	104	126	127
30A	61	79	138	187
32A	78	79	67	96
34A	54	32	33	39
28B	83	103	126	108
30B	78	90	117	154
32B	82	81	110	90
34B	73	83	93	79

Table 4.12: The slopes of each pleating density and dust loading according to Equation (4.2).

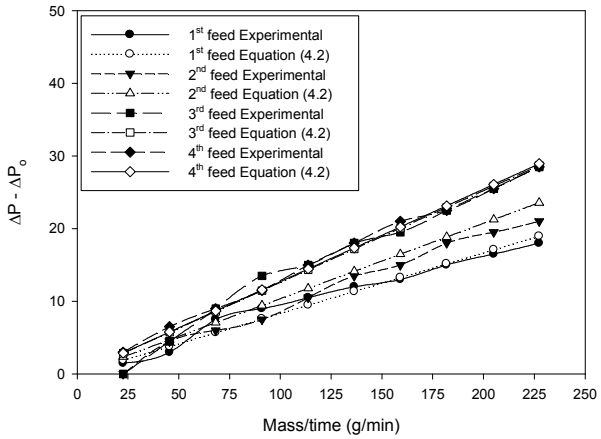

Figure 4.41: Comparison between experimental pressure drop and that predicted by Equation (4.2) for Filter 28B loaded with SAE fine dust.

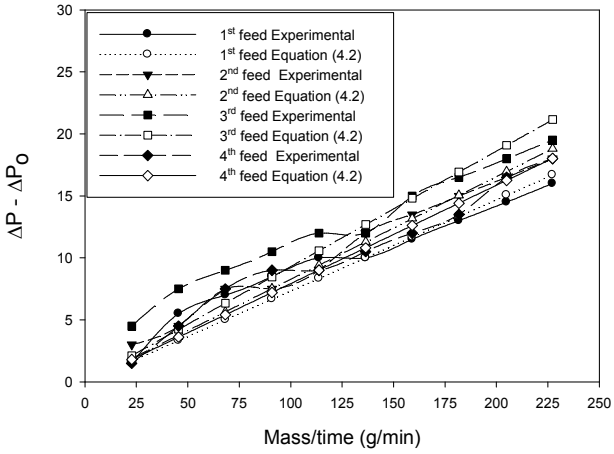

Figure 4.42: Comparison between experimental pressure drop and that predicted by Equation 4.2 for Filter 34B loaded with SAE fine dust.

4.4 Interpretation of Initial Capture Efficiency

Several authors have considered interpreting the overall efficiency of filters and encountered several difficulties. Some of these difficulties are considering the interference of neighbouring fibres, fibre orientation, and inhomogeneity on the flow field of the filtration medium which causes the air flow to deviate from the ideal flow patterns predicted theoretically.

This study introduces and deals with another important practical aspect of filter design that causes a difficulty to the researcher which is the HEPA class pleated media panels constructed in a V-shaped filter cartridge. No engineering model exists that deals with such filters even at the initial stage of no dust loading. The analysis of this study will lead to introduction of a modified model that would better predict the overall initial efficiency of pleated HEPA filters in a V-shape cartridge.

4.4.1 Models Applied to DEHS Efficiencies

Four efficiency models were taken from the models available in the literature and are listed in Table 4.13. Examining the efficiency models available in the literature, they mainly have the individual diffusion term added to the interception term, each multiplied by a constant.

	Diffusion Term	**Interception Term**	**Remarks**
Liu & Rubow [1990]	$1.6\left(\frac{1-\alpha}{Ku}\right)^{\frac{1}{3}} Pe^{\frac{-2}{3}} C_d$	$0.6\left(\frac{1-\alpha}{Ku}\right)^{\frac{1}{3}} \frac{R^2}{1+R} C_r$	$C_d = 1 + 0.388\, Kn_f \left(\frac{(1-\alpha)Pe}{Ku}\right)^{\frac{1}{3}}$ $C_r = 1 + 1.996\frac{Kn_f}{R}$
Lee and Liu [1982a]	$2.6\left(\frac{1-\alpha}{Ku}\right)^{\frac{1}{3}} Pe^{\frac{-2}{3}}$	$\left(\frac{1-\alpha}{Ku}\right)^{\frac{1}{3}} \frac{R^2}{1+R}$	
Lee and Liu [1982b]	$1.6\left(\frac{1-\alpha}{Ku}\right)^{\frac{1}{3}} Pe^{\frac{-2}{3}}$	$0.6\left(\frac{1-\alpha}{Ku}\right)^{\frac{1}{3}} \frac{R^2}{1+R}$	
Payet *et al* [1991]	$2.6\left(\frac{1-\alpha}{Ku}\right)^{\frac{1}{3}} Pe^{\frac{-2}{3}} C_d C_d'$	$0.6\left(\frac{1-\alpha}{Ku}\right)^{\frac{1}{3}} \frac{R^2}{1+R} C_r$	$C_r = \frac{1}{1+\eta_D}$ $C_d' = \frac{1}{1 + 1.6(\frac{1-\alpha}{Ku})^{1/3} Pe^{-\frac{2}{3}} C_d}$

Table 4.13: Efficiency models examined in this study.

The Lee and Liu [1982a] model as well as two other models are plotted and shown in Figure 4.43 against the experimental data to check if any of these models fit the trend. Although none of the models are in a precise agreement with experimental data, the Lee and Liu [1982a] model was chosen since the basic form of the terms in the equations for each model are similar, with the main differences being the coefficients in front of the

terms. These coefficients were originally obtained by fitting the model equations to the experimental data. Further, the Lee and Liu model [1982a,b] takes into account the flow interference effects of neighbouring fibres which provides better representation of the actual flow profile in the filter. For these reasons, the Lee and Liu terms of the equations have been used as a starting point for the analysis of this study.

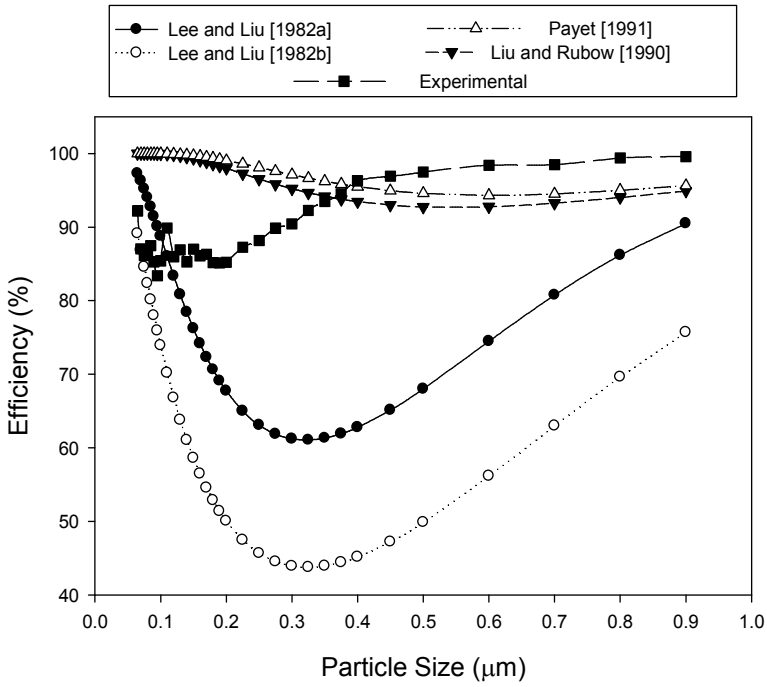

Figure 4.43: Comparison between the experimental efficiency data and the theoretical models examined.

4.4.2 Theoretical Efficiency Models

The simplest way to interpret the overall efficiency of the filter tested is to add the diffusion and interception mechanisms. This practice is based on the assumption that only one mechanism is dominant while the contribution of the other mechanism is not significant. Lee and Liu [1982a] suggested that this assumption is adequate based on the fact that as the particle size increases, the efficiency due to diffusion decreases the efficiency whilst the interception mechanism becomes increasingly prominent. They further assumed that the role of the impaction mechanism is not important and therefore they assumed that the overall efficiency to be:

$$\eta = 2.6\left(\frac{1-\alpha}{Ku}\right)^{\frac{1}{3}} Pe^{-\frac{2}{3}} + \left(\frac{1-\alpha}{Ku}\right)\left(\frac{R^2}{1+R}\right) \tag{4.3}$$

The overall efficiency model can then be rewritten as follows:

$$\eta = \beta_1 \left(\frac{1-\alpha}{Ku} \right)^{\frac{1}{3}} Pe^{-\frac{2}{3}} + \beta_2 \left(\frac{1-\alpha}{Ku} \right) \left(\frac{R^2}{1+R} \right) \tag{4.4}$$

where β_1 and β_2 are empirical constants to be derived from the experimental data. Following the method of the Friedlander [1958] and Spielman and Goren [1968], multiplying both sides of the Equation (4.4) by $Pe \frac{R}{\sqrt{1+R}}$ to become:

$$\eta Pe \frac{R}{\sqrt{1+R}} = \beta_1 \left(\left(\frac{1-\alpha}{Ku} \right)^{\frac{1}{3}} Pe^{\frac{1}{3}} \frac{R}{1+R} \right) + \beta_2 \left(\left(\frac{1-\alpha}{Ku} \right)^{\frac{1}{3}} Pe^{\frac{1}{3}} \frac{R^2}{1+R} \right)^3 \tag{4.5}$$

Defining $Y = Pe \frac{R}{\sqrt{1+R}}$ and $X = \left(\frac{1-\alpha}{Ku} \right)^{\frac{1}{3}} Pe^{\frac{1}{3}} \frac{R}{1+R}$, Equation (4.5) can then be rewritten in the form:

$$Y = \beta_1 X + \beta_2 X^3 \tag{4.6}$$

The significance of the empirical constants β_1 and β_2 represent the contribution of the diffusion and interception mechanisms in the filtration process respectively. β_1 and β_2 were obtained using the linear regression method based on the "Least Squares" model as implemented in “Excel Analysis” package from the experimental results. Since the whole exercise was to accurately model the region surrounding the MPPS with the ultimate objective of realizing better determination. The modified model resulting in Equation 4.6 was performed was fitted using the data in the range of interest, namely the region neighbouring the MPPS (0.065-0.375 µm). Table 4.14 lists the results for the filters A series and the β_1 and β_2 values for the corresponding flow rates. In addition, Figure 4.44 shows a good agreement between the efficiency experimental results and theoretical model of Lee & Liu for low flow rates of 500 and 1000 m^3/h. At higher flow rates such as 2000 through 3000 m^3/h, the model seems to overestimate the diffusion efficiency as the flow rates increases.

It essential to highlight that the Lee and Liu [1982a] model was developed for a flat filter of polyester fibre bed with an average diameter of about 11 µm, while the filters

examined in this study are polydispersed glass fibre pleated HEPA media with an average fibre mean diameter of 2.1 µm. clearly, the slip flow was not accounted for by Lee and Liu correlation which is important for fine fibres. Slip flow effects is particle size dependant and would lead to reduced diffusional deposition evident at higher flow rates in Figure 4.44. Further, the mean fibre diameter may not been necessarily accounted for the polydispersity of the entire filter fibres [Van Osedel *et al,* 1990]. Further, when a flat sheet of a filter media is considered, the surface area losses may be due to medium compression to great extent. On the other hand, when considering eight pleated panels, other underlying reasons behind the losses of surface in addition to the possible medium compression as discussed in 4.2.3.

The comparison in Figure 4.44 highlights the poor inclusion of Equation (4.6) for particles sizes below the MPPS. This effect is more pronounced as the flow rate increases which consequently signify that air velocity inside the media is higher and permeability reduction becomes more significant due to surface area losses. This would translate into lower air residence time inside the filtration media which may not be sufficient for a particle to be captured by fibre. If the penetrating particle scores the minimum efficiency, its particle size becomes of a critical importance since it would be the MPPS of this filter.. The higher the flow rate, the shorter the air residence time and Figure 4.44 shows that the deviation of particles smaller than MPPS is more pronounced as the flow rate increases. The Lee and Liu model [1982a] has either assumed that the air residence time remains unchanged with air velocity or longer than that of the experimental data. Experimentally, the air residence time decreases with the increase of air velocity and particles deviation from the Lee and Liu model [1982a] is more pronounced.

It is also important to note that Lee and Liu model [1982a] was later on modified by Liu and Rubow [1990] and Payet et al [1991] by including correction factors to account for the slip condition. The correction factors introduced by Liu and Rubow [1990] and Payet et al [1991] namely, C_d, $C_d^{'}$ and C_r include several parameters pertaining the filtration performance such as filter packing density, Peclet number, fibre Knusden number, interception parameter and diffusion efficiency. The influence of the variation of these

parameters is unknown at this point and it requires further investigation to highlight the contribution of each parameter. It is important to highlight that correction factors C_d and $C_d^{'}$ included the Peclet number which is function of air velocity. This inclusion signifies that the effect of face velocity has been accounted for by subsequent models of Lee and Liu [1982a], that is Liu and Rubow [1990] and Payet et al [1991].

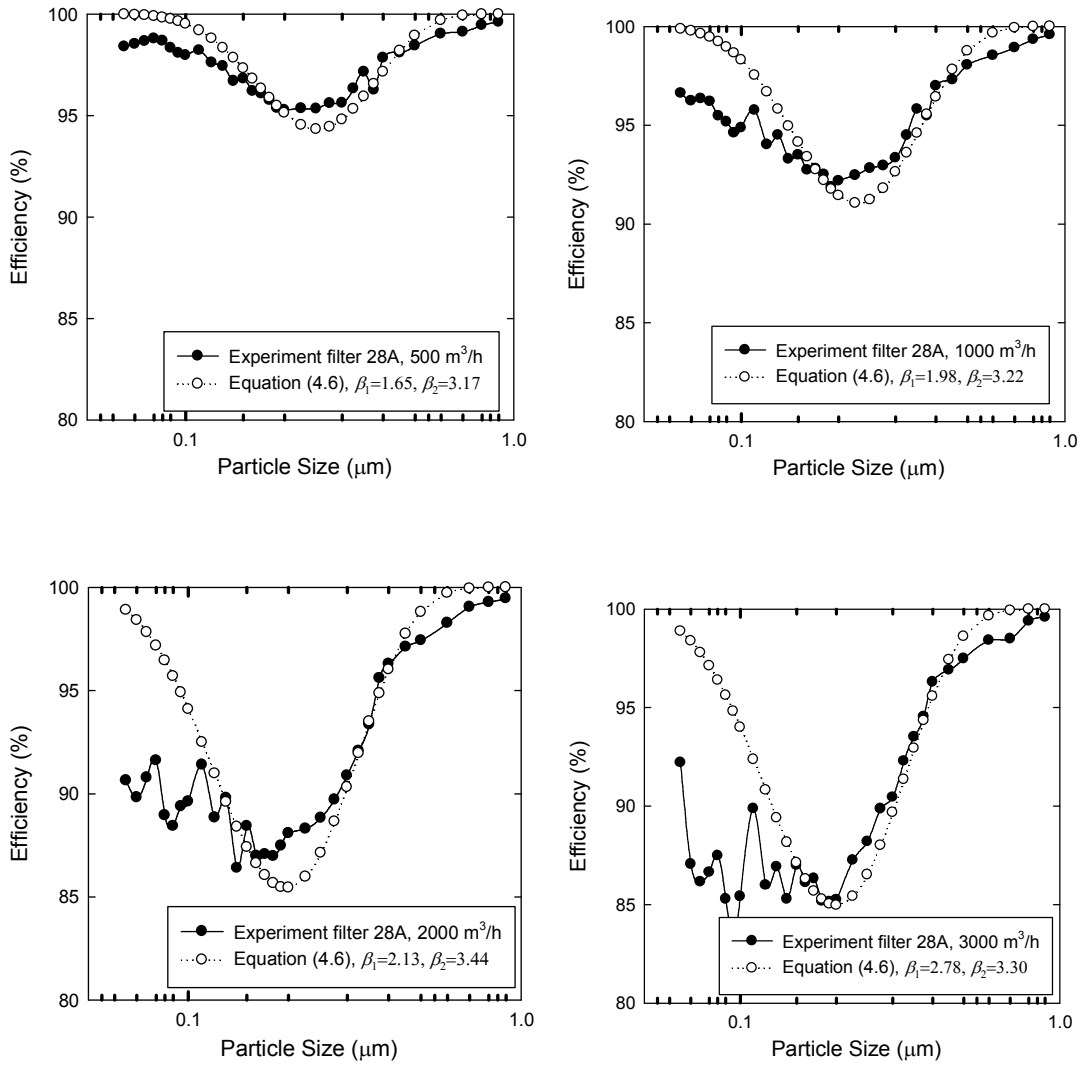

Figure 4.44: Initial efficiency comparison between experimental results and theoretical model of Lee & Liu [1982a] for filter flow rates of 500, 1000, 2000 and 3000 m^3/h.

Another possible explanation of the deviation in the sub MPPS region between Lee and Liu model [1982a] and experimental data could be due to the re-entrainment of fine

particle. Particles could have detached after they attached themselves to the fibre surface. However, a more pronounced effect to highlight is that as the flow rates and pleat density increase, the surface area losses increase which contribute further to the increase of air velocity inside the filtration media. Surface area losses signify less filtration media participating in the filtration process. Therefore, this translates to shorter air residence time which leads to lower likelihood for a particle to be captured by a fibre surface. Therefore, there are two reasons which contribute to the increase of air velocity inside the filter medium and can be summarized as follows:

1. Increasing the flow rate.
2. Increasing the surface area losses of the total pleated filter media as a consequence of increasing the flow rate due to reasons discussed in 4.2.3.
3. Increasing the pleat density which also exhibited a counterproductive effect in increasing surface area losses as shown in Appendix F.

The modified model resulting in Equation 4.6 was fitted using the experimental data in the range of interest (0.065-0.375 µm). Although the experimental results outside the MPPS range show large deviation from the fitted model particularly in the sub MPPS region, these values would only represent a practical problem if their fractional efficiency becomes minimum. The proposed modification shows better accuracy in describing the experimental data at lower flow rates, and poor inclusion of experimental data particularly for particle sizes lower than the MPPS at higher flow rates. The interception coefficient (β_1) for all tested filters varies little with flow rate and the number of pleats when analyzed using the Lee and Liu model [1982a] model. This is line with previous studies in the literature where it states that interception mechanism is relatively independent of the air velocity which was noticed in the range of the flow rates examined in this study. On the other hand, the diffusion contribution (β_2) to efficiency becomes more dominant as the flow rate increases. Equation (4.6) tends to overestimate the diffusional efficiency, and suggests that the equation form may not be correct for filtration onto larger scale pleated media or higher flow rates.

Flow rate (m^3/h)	28A Coefficients		30A Coefficients		32A Coefficients		34A Coefficients	
	Diffusion β_1	Interception β_2	Diffusion β_1	Interception β_2	Diffusion β_1	Interception β_2	Diffusion β_1	Interception β_2
500	1.65	3.16	1.59	3.29	1.55	3.44	1.79	2.72
1000	1.98	3.22	1.82	3.37	1.85	3.27	1.84	3.36
1500	1.91	3.45	1.88	3.19	1.96	3.34	2.22	3.06
2000	2.13	3.44	2.28	3.19	2.33	3.06	2.44	3.06
2500	2.43	3.37	2.29	3.40	2.61	3.31	2.33	3.38
3000	2.78	3.30	2.73	3.18	2.46	3.45	2.74	3.18
Flow rate (m^3/h)	28B Coefficients		30B Coefficients		32B Coefficients		34B Coefficients	
	Diffusion β_1	Interception β_2	Diffusion β_1	Interception β_2	Diffusion β_1	Interception β_2	Diffusion β_1	Interception β_2
500	1.70	3.90	1.61	3.77	1.70	3.70	1.57	4.00
1000	2.10	3.05	1.90	3.44	1.79	3.59	1.75	3.78
1500	2.29	3.25	2.08	3.40	2.13	3.47	2.10	3.62
2000	2.51	3.30	2.18	3.34	2.30	3.34	2.28	3.55
2500	2.56	3.35	2.20	3.25	2.36	3.30	2.34	3.20
3000	2.62	3.44	2.35	3.30	2.47	3.65	2.39	3.81

Table 4.13: Values of β_1 and β_2 for different pleating densities for Group A and B filters using [Lee and Liu Model 1982a].

4.4.3 Effect of Dust Type Loaded on Efficiencies for Different Pleating Densities

The fractional efficiencies were plotted versus particle size for filter 28A after each dust feed of 250 grams. All dust loading and efficiency measurements were conducted starting from 500 until 3500 m^3/h is reached with an increment of 500 m^3/h. The complete graphs illustrating the efficiency increase as dust loading increases for all filters are listed in Appendix L.

In this section, four parameters are being varied, amount of dust mass loaded, flow rate, dust type and pleating density. Figure 4.45 shows the entire variation in fractional efficiency as more dust challenges the filter and as the flow rate is increased. It is evident that the filter is more efficient as more dust is being fed at a given flow rate. However, the fractional efficiency drops as the flow rate increases. It can also be noticed that at a flow of 500 m^3/h all filters scored the highest efficiency.

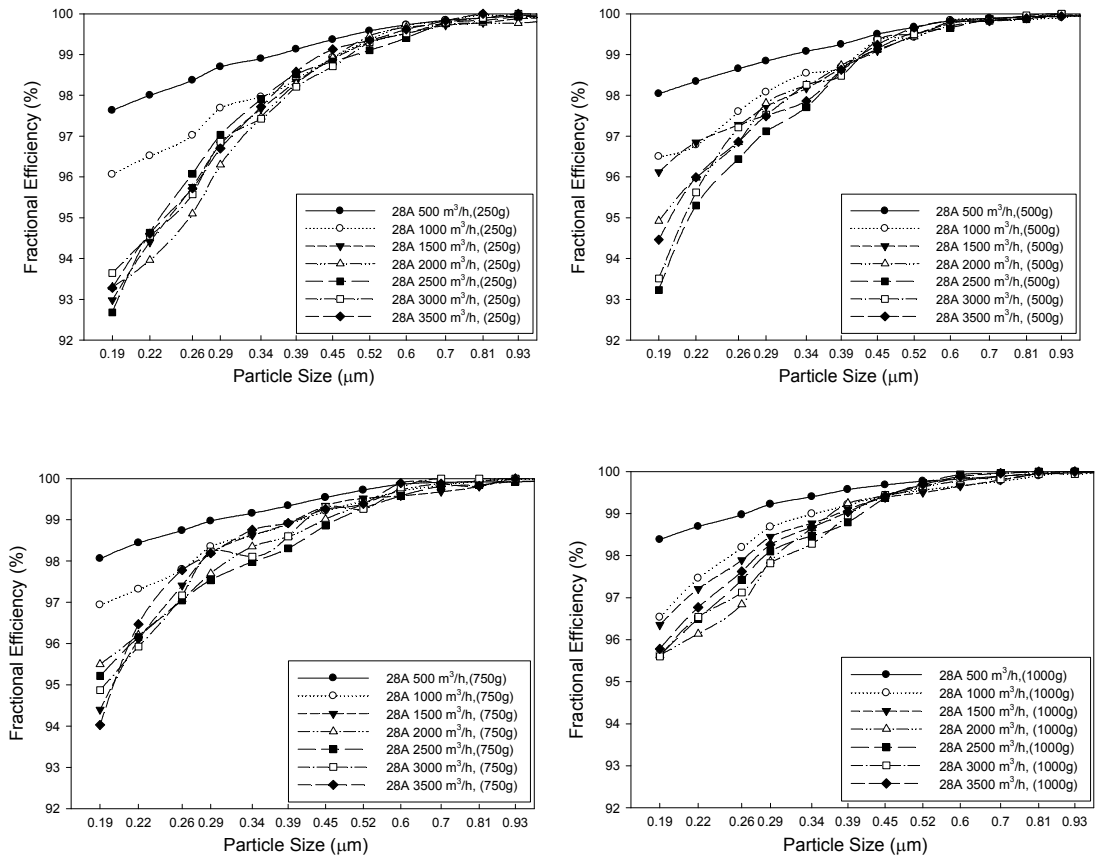

Figure 4.45: Dust-loaded efficiencies for pleating density of 28 pleats/100 mm at different flow rates and dust feeds.

All filters experience a substantial drop in efficiency as the flow rate increases beyond 500 m^3/h when compared with the efficiency drops between other flow rates starting for example at 1500 m^3/h until 3500 m^3/h. The efficiency drop between the 1000 m^3/h and the rest of the flow rates is not as substantial as the one between 500 m^3/h and the rest of the flow rates. Another important consideration is the relation between total surface area of the filter and its effective surface area during operation. Table 4.17 shows that at a flow rate of 500 m^3/h, the effective surface area equals the total surface which means the total area is participating in the filtration action. In fact, at higher than this 500 m^3/h, the permeability of the filter changes due to reasons mentioned in Section 4.2.3 and it begins to lose surface area and continue to do so as the flow rate increases. This signifies that as the flow rate increases from 500 m^3/h to higher flow rates, the drop in efficiency is more

pronounced as the air suddenly experiences higher resistance since it is exposed to less surface area of the filtration media. This effect increases substantially the face velocity on entire filter increases resulting in the efficiency drops shown in Figure 4.45 and the complete array of graphs in Appendix L. These results conform to previous studies of the face velocities on HEPA filters [Sinclair, 1976].

At a low flow rate such 500 m^3/h, the fractional efficiency comparison between filter Group A is shown in Figure 4.46 after 1000 g of AC coarse dust is fed. The comparison shows negligible differences in fractional efficiencies as the pleating density varies. This is reasoned to the fact that while higher pleat densities offer more surface area, in practice, the effective surface areas are not always equal to the total surface areas as shown in Table 4.17. For example, the effective surface area addition increases by 5% at a flow rate of 3500 m^3/h as the pleating density increases from 28 to 34 pleats per 100 mm in Group (A). Such 5% amounts to only one square metre addition in the total effective surface area while the actual addition in the total surface area was 4.9 m^2. Therefore, Figure 4.48 shows similar fractional efficiency measurements as the pleat density increases. While the pleat density did not have a major influence on the fractional efficiency, it important to realize the underlying reasons as far as the effective surface area not the total surface area.

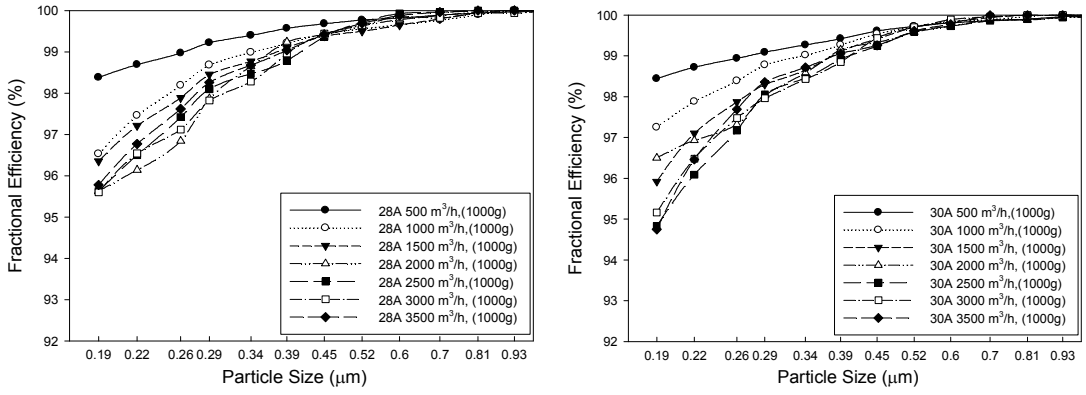

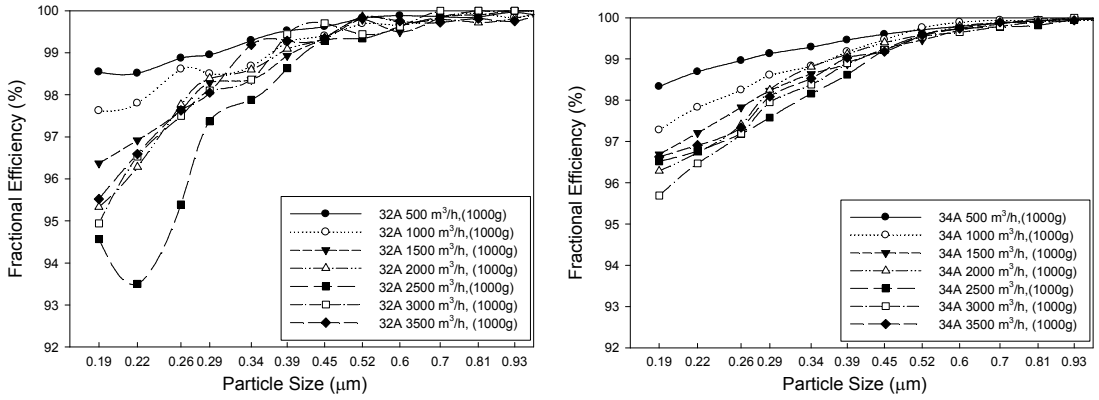

Figure 4.46: AC coarse dust-loaded efficiencies for different pleating densities at different flow rates after feeding 1000g.

Figure 4.47 illustrates the effect of mass loading on efficiency for different pleating densities after the fourth dust feed. Filter 34A recorded the highest losses in surface area as shown in Table 4.17 prior to dust loading. At a flow rate of 3500 m^3/h, which is the flow rate at all dust loaded pressure drops were measured, the same filter recorded a medium loss of 31.1% of the total surface area. This highlights the caution that should be exercised while selecting the optimal pleat density for a given filter design. Introducing or loading dust into a filter which exhibits initially high pressure drop response will add to the increase of air resistance.

Table 4.17 shows that although the surface area increased from filter 32A to 34A by 1.5 m^2, the effective surface was the same for both filters. The pressure drop readings for both filters are similar, even though the initial and dust loaded fractional efficiency of 34A are slightly higher. On the other hand, 34A, 32A and 30A scored efficiencies below the H10 requirement according to the DIN 1822 Standard, which means that the efficiency requirement is not satisfied although these filters provided higher surface area via a higher pleat density at particular flow rates. In fact, filter 28A has satisfied the efficiency requirement according to the DIN 1822 Standard, used the least surface area and consequently has the lowest loss of surface area. This is would make filter 28A, a pleated filter cartridge with a filter Class HEPA 10, a filter with good pleat count from effective surface standpoint even though it has the highest pressure drop response.

Further, 26 pleats per 100 mm was not considered in this study which could have had a higher or lower pressure drop relative to 28A. Clearly, the optimal pleat count may not necessarily exist and as far as this study is concerned there has not been a definite optimal pleat count that would have the least pressure drop and satisfies the efficiency requirement simultaneously.

Pleat Density	**28A**	**30A**	**32A**	**34A**
Total A_s [m^2]	**23.9**	**26.6**	**27.3**	**28.8**
Q (m^3/h)	A_{Eff}	A_{Eff}	A_{Eff}	A_{Eff}
500	23.9	26.6	27.3	28.8
1000	23.9	23.9	26.6	24.8
1500	22.9	22.9	24.5	23.9
2000	21.7	22.1	22.8	22.8
2500	20.6	20.9	21.6	22.2
3000	19.4	19.9	20.5	20.5
3500	18.6	19.0	19.5	19.6
4000	17.7	18.1	18.5	18.8
4500	16.9	17.2	17.7	17.8
5000	16.2	16.5	16.9	16.9

Table 4.17: Effective area vs. different flow rates for different pleating densities.

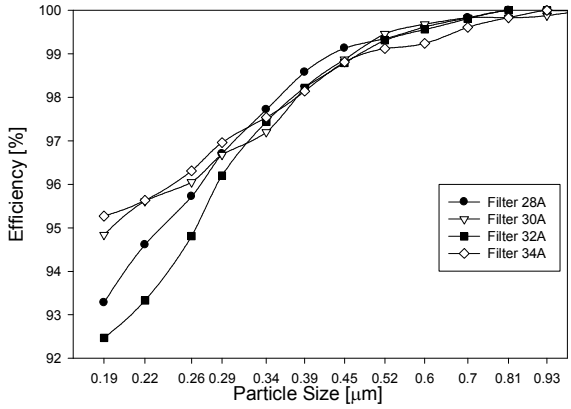

Figure 4.47: Efficiency after the fourth SAE coarse dust feed for different pleating density at 3500m^3/h.

To further investigate the fractional efficiency from a pleat density standpoint. A good example to highlight the role of effective surface area concept and its effect on fractional efficiency is to compare two filters with different pleating densities, but with the same effective surface area. Previously, this occurred for filters 32A and 34A at flow rate of

2000 m^3/h. Table 4.17 shows an addition of 1.5 m^2 total in surface area as the pleat densities increases from 32 to 34 pleats per 100mm and the effective surface area remained the same, namely, 22.8 m^2. The fractional efficiency measurements show very similar readings for filters 32A and 34A with the same effective surface area at all dust feeds as shown in Figure 4.48. On the other hand, the losses in surface area are greater as the flow rate increases compared to the pleat density increase. Therefore, it can be concluded that flow rates variations have greater influence on fractional efficiencies reduction when compared to pleat density variations.

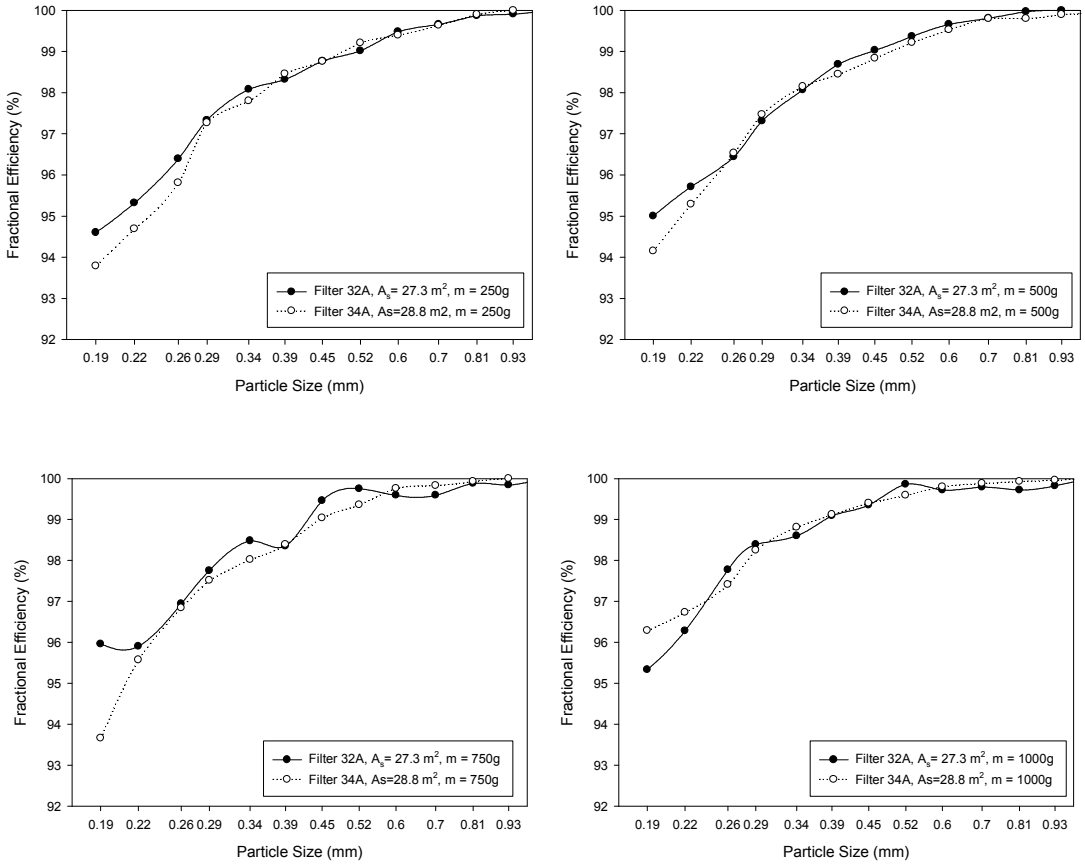

Figure 4.48: AC coarse dust-loaded efficiencies for 32A and 34A pleat density at 2000 m^3/h for different dust feeds for the same effective surface area.

Figure 4.51 shows the filter group B which was loaded with AC fine dust recorded higher efficiencies than filter group A which was loaded with AC coarse dust. It also recorded the highest efficiencies among the entire pleating densities and flow rates used. Fine

particle are more capable than coarse ones to penetrate into the depth of the filter and change the inner structure of the filtration medium by settling around the fibre and changing the filter matrix. Dust particle settling around the fibre enhances the probability of particle-fibre and particle to particle contact and which will be translate into an increase in efficiency. This is of course relative to the pore size and particle size. In other words, the particle size has to be fine enough to penetrate into the depth of the filter and settle inside the filter medium. It is important to note this efficiency increase is associated with an increase of the pressure drop as well. Coarse particles on the other hand, will settle on the surface of the filters and will have lower pressure drop rise and a lower efficiency as shown in Figure 4.49.

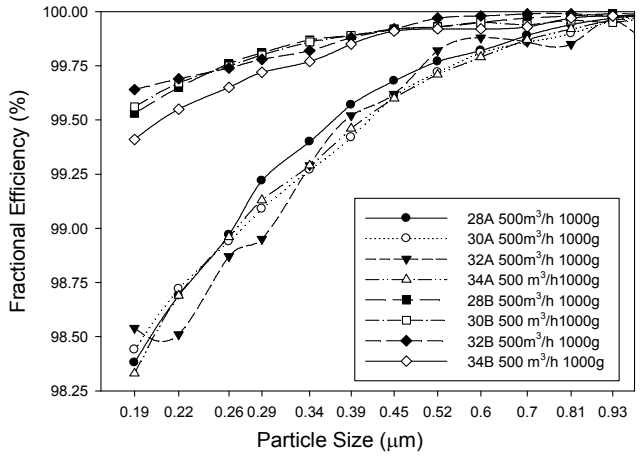

Figure 4.49: Dust-loaded efficiencies for Group A (AC coarse) and B (AC fine) at 500 m^3/h after 1000 g.

The fractional efficiency among filter Group A is compared after being loaded with AC coarse dust at the highest and lowest flow rates used, namely, 500 and 3500 m^3/h. Clearly, higher flow rates translate into higher face velocities and as a result the particle residence is shortened. Consequently, the probability of particle to collide with a fibre and leave the air stream to improve the efficiency is minimized. The fractional efficiency difference tends to increase as the flow increases and this is apparent at 3500 m^3/h as shown in Figure 4.50.

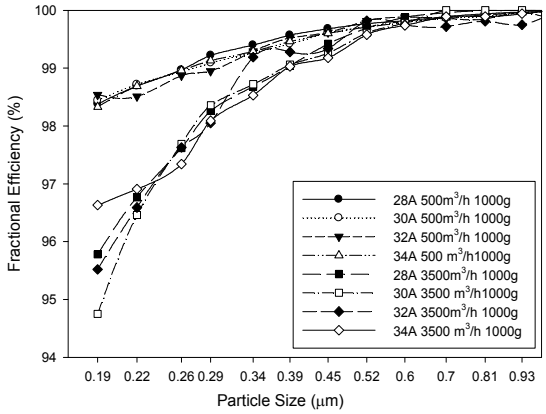

Figure 4.50: SAE coarse dust loaded efficiencies for different pleating densities at two different flow rates after 1000 g of dust are fed.

Figure 4.51 illustrates the increase of efficiency for each dust feed of SAE coarse dust as particle size and dust mass loading increases. Clearly, as more dust is loaded into the depth of the filtration medium, additional changes in the inner structure occur. Consequently, permeability decreases and as a results the pressure drop response increases. Furthermore, such an effect is associated with an increase in efficiency and the fourth dust feed records the highest in efficiency according to Figure 4.51.

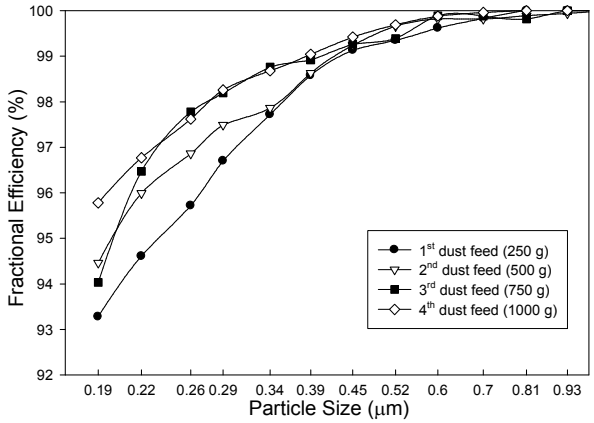

Figure 4.51: Efficiency after each SAE coarse dust feeding stages for Filter 28A at 3500 m^3/h.

The effect of dust type on the fractional efficiency is highlighted in Figure 4.52. It compares the efficiency experimental readings for filter 28A and B for SAE fine and coarse dust for each dust feed. The highest efficiency was recorded for fourth SAE fine

dust feed. This was also associated with the highest pressure drop readings amongst all dust feeding processes for both filters 28A and 28B.

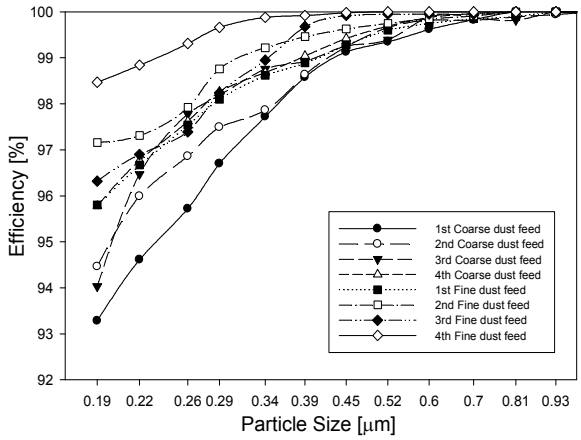

Figure 4.52: Efficiency after each SAE coarse and fine dust feeding stage for 28A and 28B pleat density.

4.5 The Effect of Pleat Orientation on the Filter's Performance

To study the effect on the filter performance, two filters of same filtration medium properties were manufactured with vertical and horizontal pleat orientations as shown in Figure 4.53. Initial pressure drop and fractional efficiency were measured without dust loading. Fractional efficiency was conducted using DEHS for six flow rates starting at 500 m^3/h until 3000 m^3/h is reached. Table 4.18 tabulates the pressure drop starting at 500 m^3/h until 6000 m^3/h in addition to the MPPS and its measured fractional efficiency.

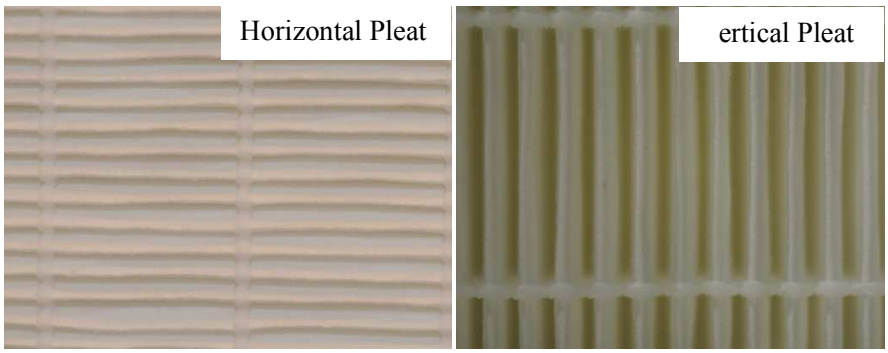

Figure 4.53: The vertical and horizontal pleat orientations examined in this study.

Filter	Horizontal Pleat, A_s =23.5 m^2					Vertical Pleat, A_s =24.4 m^2				
Flow Rate m^3/h	ΔP (Pa)	MPPS	Fractional Efficiency	Filter Class Achieved	δ(μm)	ΔP (Pa)	MPPS	Fractional Efficiency	Filter Class Achieved	δ(μm)
500	14	0.18	97.94	H11	13	12	0.17	97.89	H11	11
1000	30	0.18	95.33	H11	28	28	0.17	95.19	H11	26
1500	49	0.14	93.30	H10	45	46	0.17	92.25	H10	43
2000	69	0.16	91.22	H10	64	67	0.15	91.29	H10	62
2500	92	0.14	90.56	H10	85	89	0.12	89.95	H10	83
3000	117	0.14	89.38	H10	109	113	0.14	88.02	H10	105
3500	143				133	139				129
4000	172				160	166				154
4500	202				187	195				181
5000	236				219	227				211
5500	270				250	256				237
6000	306				284	295				274

Table 4.18: Pressure drop and MPPS measurements for horizontal and vertical pleats filters.

The filter cartridge with vertical pleats has a surface area of 24.4 m^2 whereas the horizontal pleat filter has 23.5 m^2. The addition of surface area is nearly one square metre which is due to losses after the addition of the bonding material which connects the pleated fibrous material to the plastic housing. The horizontal-pleat filter has more losses since the bonding material covers more pleats when compared to the vertical ones.

Observations:

1. From a pressure drop point of view, the vertical pleat filter has a slightly lower pressure drop as show in Figure 4.54. This is due to the vertical pleating which is thought to give more strength to the pleated media panel, and hence less deformation occurs at higher flow rates.
2. The MPPS shifts to a smaller particle size as the face velocity increases with both pleat orientations.
3. Fractional efficiency readings are very close for both pleat orientations at lower flow rates, but as the flow rate increases the horizontal pleating offers a pressure drop that becomes increasingly more than that of the vertical pleating.
4. The slightly lower pressure drop of the vertical pleats is probably more than offset by the greater fractional efficiency of the horizontal pleats, making the horizontal pleats a better practical option.

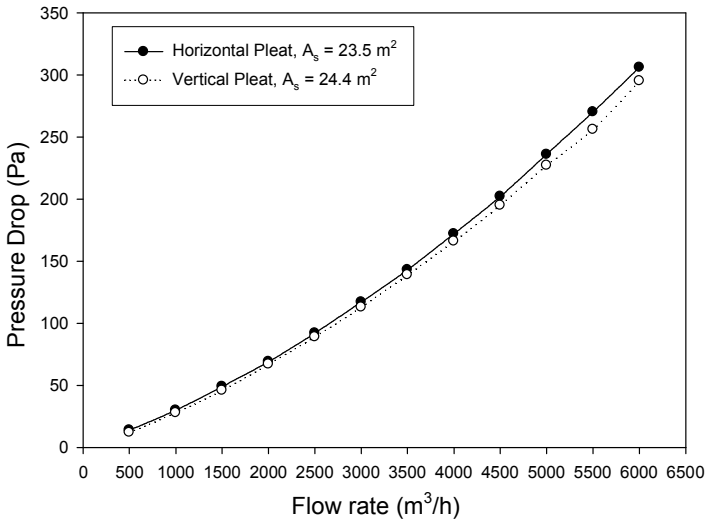

Figure 4.54: Initial pressure drop for vertical and horizontal pleat filters at different flow rates.

Figure 4.55 illustrates the pressure drop comparison between the flat sheet and horizontal and vertical pleats of the same medium. The flat sheet pressure drop response is linear while pressure drops for both pleating directions exhibit identical pattern. For lower flow rates, the pleated pressure drop curves initially starts with a linear response as shown in the simulated pressure drop responses. The simulation of the linear pressure drop was quantified from using Darcy's Law as the indicated in procedure in Section 3.8 and as discussed in Section 4.2.2. The comparison in Figure 4.55 shows that as the face velocity increases, the pressure drop departs linearity and losses in surface area are more pronounced.

In can also be shown that permeability reduction due to flat medium compression is not that significant in comparison with the flat sheet to the other factors such as pleat crowding, pleat deformation and pleated panel deformation. This concludes that surface area losses and their consequential permeability reductions are mainly due to pleat crowding, pleated panel deformation and pleat deformation. As illustrated in Figure 4.55 and Table 4.18, this examination was conducted at the same face velocities to ensure that all the pressure drop reading can be compared.

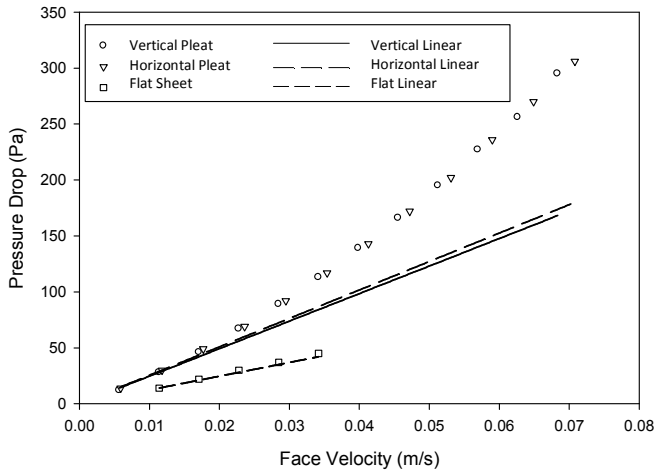

Figure 4.55: Comparison between simulated and experimental initial pressure drop for flat sheet, vertical and horizontal pleat filters at different face velocities.

Surface area losses are compared in Figure 4.56, the vertical pleat orientation cartridge experience higher losses when compared to the horizontal pleat orientation. However, there is one square metre difference between the surface area of filter cartridge with vertical pleats (24.4 m^2) and the horizontal pleats filter (23.5 m^2) which could be responsible for the small variation in pressure drop and consequently in the surface area losses.

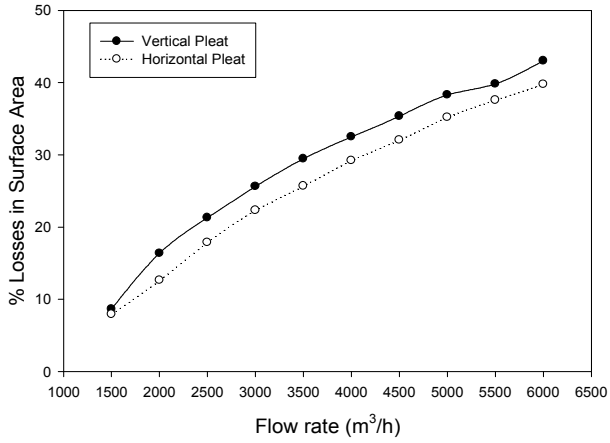

Figure 4.56: Surface area losses comparison between vertical and horizontal pleat filters at different flow rates.

In terms of efficiency, the vertical pleated filter seems to have lower efficiencies at lower and higher flow rates as shown in Figure 4.57. The horizontal pleated filter exhibits higher efficiency when compared to the vertical pleated filter. This effect is more pronounced is higher flow rates such 3000 m^3/h. It is evident that the vertical pleat orientation provides less efficiency readings and at low flow rates such as 500 and 1000 m^3/h flow, a H11 filter class was achieved for both pleat orientation. On the other hand, the MPPS shifts to smaller particle size as the face velocities increase as shown in Figure 4.58 and Table 4.18. Further, the pleat orientation did not have a distinct effect on the MPPS.

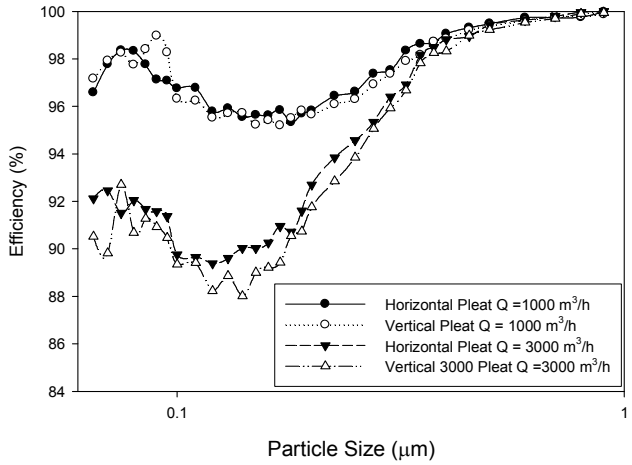

Figure 4.587: Initial fractional efficiency and MPPS comparison for vertical and horizontal pleat filters at different flow rates.

4.6 Summary and Conclusions

This chapter presented detailed analysis of the experimental investigation of the effect of face velocity, pleat density and orientation on the initial and dust loaded pressure drop and the fractional efficiency of full scale HEPA filters. The physical and chemical characterizations have revealed that ASHRAE dust is not representative of Kuwaiti atmospheric dust. The initial pressure drop analyses have shown that air filter permeability remains constant for low flow rates and decreases as the face velocity and the pleat density increase. Throughout this study, optimal pleat count which satisfies both initial and dust loaded pressure drop and efficiency requirements may not necessarily exist. This experimental work has also suggested that a valid comparison of the pleat

densities should be based on the effective surface area which participates in the filtration action and not the total surface area the pleat density provides. For a pleat through which fluid flow obeys Darcy equation, the losses of media surface area due to one or combination of the following reasons: pleat crowding, deflection of the entire pleated panel, pleat distortion at the corner of the pleat and/or filtration medium compression. All these effects reduce filter permeability and as a result raise the pressure drop of the filter.

As the particle size increases, the efficiency decreases until the MPPS is reached. Beyond the MPPS, the efficiency increases with increase of particle size. On the other hand, the filter efficiency decreases with the increase of the filter face velocity for particle sizes surrounding the MPPS region. At larger particle size beyond MPPS, the effect of face velocity on the efficiency becomes increasingly negligible. The MPPS shifts to a smaller particle size as the face velocity increases but increases slightly or remains constant as the pleating density increases. In general, the pleat density and orientation variations did not have a pronounced effect on the MPPS. As far as the dust loading is concerned, the effect of pleat density variations on the efficiency of dust loaded filters is negligible. The effect of increasing dust loading mass and flow rates is more pronounced on the filter efficiency. As more dust mass was fed into the filter, the pressure drop of the filter increased with higher response of SAE fine higher than the SAE coarse dust. The dust loaded pressure drop modified model (Equation 4.2) shows a good agreement with experimental results.

A modification of the Lee and Liu [1982a] model (Equations 4.6) was proposed and verified to show a good agreement with the experimental data. Equation (4.6) shows better accuracy in describing the experimental data at lower flow rates, and poor inclusion of experimental data particularly for particle sizes lower than the MPPS at higher flow rates. The interception coefficient for all tested filters varies little with flow rate and the number of pleats when analyzed using the Lee and Liu model [1982a] model. On the other hand, the diffusion contribution to efficiency becomes more dominant as the flow rate increases. Equation (4.6) tends to overestimate the diffusional efficiency, and

suggests that the equation form may not be correct for filtration onto larger scale pleated media.

The initial pressure drop response comparison between vertical and horizontal pleats filters has shown that the vertical pleat filter has slightly lower pressure drop. Comparison of the pressure drop responses for different pleating orientations and flat sheet medium have shown that the permeability reduction due to filter medium compression in the flat medium is negligible. Fractional efficiency readings are very close for both pleat orientations at lower flow rates, but as the flow rate increases the horizontal pleating offers a pressure drop that becomes increasingly more than that of the vertical pleating. The slightly lower pressure drop of the vertical pleats is probably more than offset by the greater fractional efficiency of the horizontal pleats, making the horizontal pleats a better practical option. However, future dust loaded experiments and variations of the temperature and relative humidity have their own influence on the selection of pleat orientation.

The work in this thesis has presented novel contribution to original knowledge in four aspects. The first aspect is the experimental investigation of a full scale HEPA filters and not just a flat sheet or a small panel filter. The second contribution is demonstrated when subjecting the HEPA filters to wide range of flow rates and the analysis of this selected range was able to reveal the pressure drop deviation from Darcy's law. The analysis of this deviation highlighted the filter surface area losses which led to permeability reduction as the flow rate increased. The third aspect of this work has shown that the pleat density which is thought to provide higher surface area when increased has in fact increased the surface area losses. The calculation of surface area losses have shown that increasing the pleat density had a counterproductive effect on the overall surface area, pressure drop and filter permeability. The analysis of the underlying reasons behind filter surface area losses and the consequential permeability reduction have facilitated the proposal of design modifications of full scale HEPA filters examined in this study are presented in Chapter five.

CHAPTER FIVE

CONCLUSIONS AND FUTURE RECOMMENDATIONS

Ten filters were manufactured and tested in this research. Eight filters were used to evaluate the performance by measuring initial and dust-loaded pressure drop and efficiencies respectively. Measurements were conducted for different flow rates while varying the pleating densities. The filters were split into three groups, A and B, to be dust loaded with AC course and AC fine synthetic dusts accordingly. The remaining two filters (Group C) were manufactured with the same pleating density but with different pleat orientation, and were tested for initial pressure drop and fractional efficiency. In these two filters no dust loading took place.

5.1 Optimal Pleat Count

It is evident that as the pleating density and flow rates increase, the permeability decreases as Figure 5.1 illustrates. The experimental results of this work have shown that the filter permeability decrease with the increase of pleating density is an agreement with a previous numerical study of Chen *et al* [1995]. It also shows that pressure drop response of the filter is directly proportional to air face velocity. The pressure drop response deviated from linearity nearly beyond 1000 m^3/h. In fact, assuming the optimal pleat count exists, the pleat densities chosen to be tested in this study particularly for the V-shaped HEPA filter cartridge may have not covered the optimal pleat count. Furthermore, the optimal pleat count should be considered based on the effective surface area which is the area participating in the filtration action and not the total area the pleat density provides. As this study have shown, the effective surface area is only equal to the total one at flow rate of 1000 m^3/h or lower. For higher flow rates, the optimal pleat count comparison can only be valid if based on the effective surface area. Therefore, additional analysis supported by experiments must be conducted before reaching conclusions solid enough to determine the optimal pleat count. Further investigation for flow rates lower than 1000 m^3/h may also reveal a different results for certain pleat densities and a particular filter cartridge design. It is

recommended that the pressure drop response to be measured for lower flow rates with smaller increment of 50 m^3/h until 1000 m^3/h is reached.

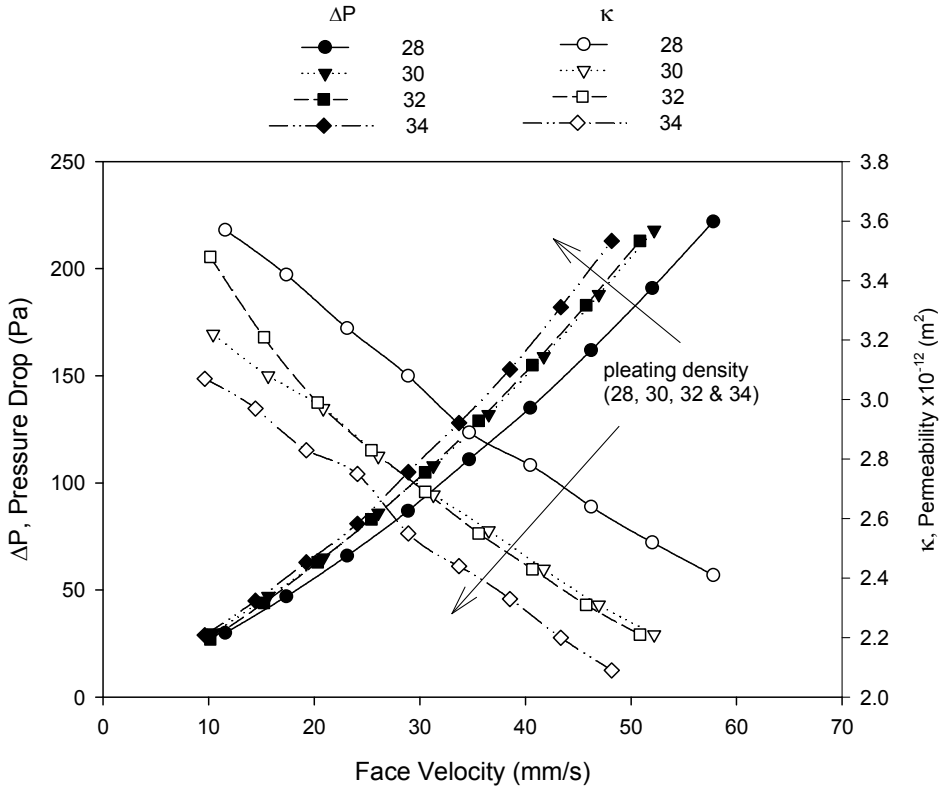

Figure 5.1: The effect of face velocity on the filter's permeability and pressure drop.

The permeability change is due to losses in surface area in the filtration medium or to compression of the medium. The Darcy model indicates a linear variation of pressure drop with flow rate and is only valid when there is no compression of the filtration medium. For a pleat there can be a loss of media surface due to pleat crowding and/or expansion of pleats. Media distortion at the crease of the pleat also influences the filter surface area losses; the effect is due to compression at the inner surface and expansion at the outer surface of the crease of the pleat. The higher the number of pleats, the more geometrical deformation is expected to take place. Therefore, additional permeability reduction is expected in higher pleating densities such with 32 and 34 pleats/100 mm. An additional deformation or buckling takes place in the overall pleated panel which would also lead to loss of surface area and reduction in permeability. This sort of buckling can also lead to fracture of the pleated panel during operation.

Introducing surface area is not the point; the point is introducing effective surface area that participates in the filtration action by allowing the air to access it. If this does not happen, the extra surface area will have a counter effect by reducing permeability and consequently raise the pressure drop. It is also important to consider that the pleating density may not be appropriate or excessive within the allocated space for the pleated filtration media for a particular filter cartridge design. This research has strongly emphasized that the long believed rule which suggests the higher the pleating density, the lower the pressure drop is not always true. This experimental work has shown that the higher the pleating density, the higher the number of pleats, so the more geometrical deformation that can be expected to take place. Therefore, additional permeability reduction is expected in higher pleating densities such as with 32 and 34 pleats/100 mm. An additional deformation or buckling is expected to take place in the overall pleated panel which would also lead to loss of surface area and a subsequent reduction in permeability. This sort of bulking could also lead to fracture of the pleated panel during operation.

Another aspect that affects the filter performance is concerned with the structural integrity of the plastic housing which is deforming under higher flow rates. This compromises the overall performance of the filtration process. The permeability reduction is evident for the reasons discussed and design improvements are required and will be presented in Sections 5.7 and 5.8.

5.2 Dust Appropriateness and Selection

In terms of appropriate synthetic dust to be used to represent the Kuwait atmospheric dust as an extreme case of a climate sustaining sand storms, this research has shown that ASHRAE dust is not representative of Kuwaiti atmospheric dust due to differences in physical and chemical characterization. SAE fine dust seems to be closer in that regard.

Physical characterisation of Kuwaiti atmospheric dust is mainly non spherical particles and is silica based. It also contains other contaminants such as pollen. The particle size distribution of Kuwaiti dust falls between the SAE fine and SAE coarse size distributions. Therefore, these synthetic dusts work as a lower and upper size distribution limits for the Kuwaiti atmospheric dust respectively. The pressure drop

response of SAE fine dust was higher of that of the SAE coarse particles. This confirms that the smaller particles are more penetrating than coarse particle for a given filtration medium which is in this case the H10 [DIN 1822, 1998] with fibre size range between 0.8-6µm. This is an agreement with previous studies by [Novick and Klassen, 1998; Snyder and Pring, 1955; Pich, 1966; Stenhouse *et al*, 1992; Japuntich, *et al*, 1994]

Dust concentrations during sand storms reach higher levels which may not be attained in laboratory settings. While the Kuwaiti dust was used as a benchmark for harsh climates where dust poses a major daily challenge to HVAC and gas turbine applications, the dust in this experimental work was loaded according to international standards [ASHRAE 52.2, 1999; DIN EN779, 2002] to ensure the global applicability of this experimental investigation.

5.3 Filtration Medium Used

The 94% porous filtration medium used in this study was glass fibre with an average fibre diameter of 2.1 µm, and a thickness of nearly 500 µm. The measurement of pore size distribution of different absolute filtration media shows that as the largest pore diameter decreases, the mean flow pore diameter decreases. Also the maximum pore size distribution increases for higher filter classes. Relating the pore size distribution to the overall efficiency, pressure drop response and pleating density to the filter classification would be an interesting topic to investigate in future work.

5.4 General Remarks

The MPPS shifts to smaller particle size as the filter face velocity increase for all pleating densities at a given surface area and filter medium. The MPPS increases slightly or remains constant as the pleating density increases. Filter class H10 efficiency requirement according to Standard DIN 1822 [1998] was achieved for flow rates 2000-2500 m^3/h for most filters. On the other hand, higher filter class H11 [DIN 1822, 1998] was achieved for flow rate of 500 m^3/h for filters with 28 pleat/100 mm density.

The minimum efficiency decreases with increasing the flow rate, the lowest readings for the efficiency takes place at the highest flow rate of 3000 m^3/h. Filter efficiency

decreases for particle sizes less than the MPPS at this face velocity. Beyond the MPPS, the efficiency increases as the particle size increases. The MPPS shifts to a smaller particle size as the face velocity increases for both pleat densities and orientations. Fractional efficiency readings are very close for both pleat orientations at lower flow rates, but as the flow rate increases the horizontal pleating offers a pressure drop that becomes increasingly more than that of the vertical pleating. The slightly lower pressure drop of the vertical pleats is probably more than offset by the greater fractional efficiency of the horizontal pleats, making the horizontal pleats a better practical option.

The pressure drop response comparison between vertical and horizontal pleated filters revealed that the vertical pleat filter has a slightly lower pressure drop. This is due to the vertical pleating which is thought to give more strength to the pleated media panel, and hence less deformation occurs at higher flow rates. However, it is premature to select a preferred pleat orientation at this stage until a complete testing of a similar nature of this study is done on both pleat orientation (including dustloading). Further, the vertical pleat cartridge had a one square metre additional surface area which may have shifted the pressure drop response to its favour. The addition of the casting material is always controlled as discussed in Section 4.1.4.1.

5.5 Proposed Engineering Model

Based on a Lee & Lui [1987] model, a modified engineering model of the experimental data was introduced to describe the initial fractional efficiency for pleated filters. Further refinement of the Lee and Lui model led to proposing a modified model with different coefficients that better fit the experimental data. The proposed modification shows better accuracy in describing the experimental data at lower flow rates, and poor inclusion of experimental data particularly for particle sizes lower than the MPPS at higher flow rates.

The interception coefficient (β_1) for all tested filters varies little with flow rate and the number of pleats when analyzed using the Lee and Liu model [1982a] model. This is line with previous studies in the literature where it states that interception mechanism is relatively independent of the air velocity which was noticed in the range of the flow rates examined in this study. On the other hand, the diffusion contribution (β_2) to

efficiency becomes more dominant as the flow rate increases. The modified model indicates a fluctuation in the diffusion contribution as the pleating density changes and it increases as the flow rate increases. Figure 5.2 illustrates the initial efficiency comparison between the experimental results and the theoretical model of Lee & Liu [1982a] with new diffusion and interception coefficients listed previously in Table 4.13.

The modified model resulting in Equation 4.6 was fitted using the experimental data in the range of interest (0.065-0.375 μm). The analysis of various pleating densities and flow rates have shown that Equation (4.6) tends to overestimate the diffusional efficiency, and suggests that the equation form may not be correct for filtration onto larger scale pleated media or higher flow rates. Therefore, it is recommended for future work that Liu and Rubow [1990] and Payet et al [1991] models to be used to fit the experimental data. This would be of a great interest since they involved correction factors such as C_d, $C_d^{'}$ and C_r which include several parameters that influence the filtration performance.

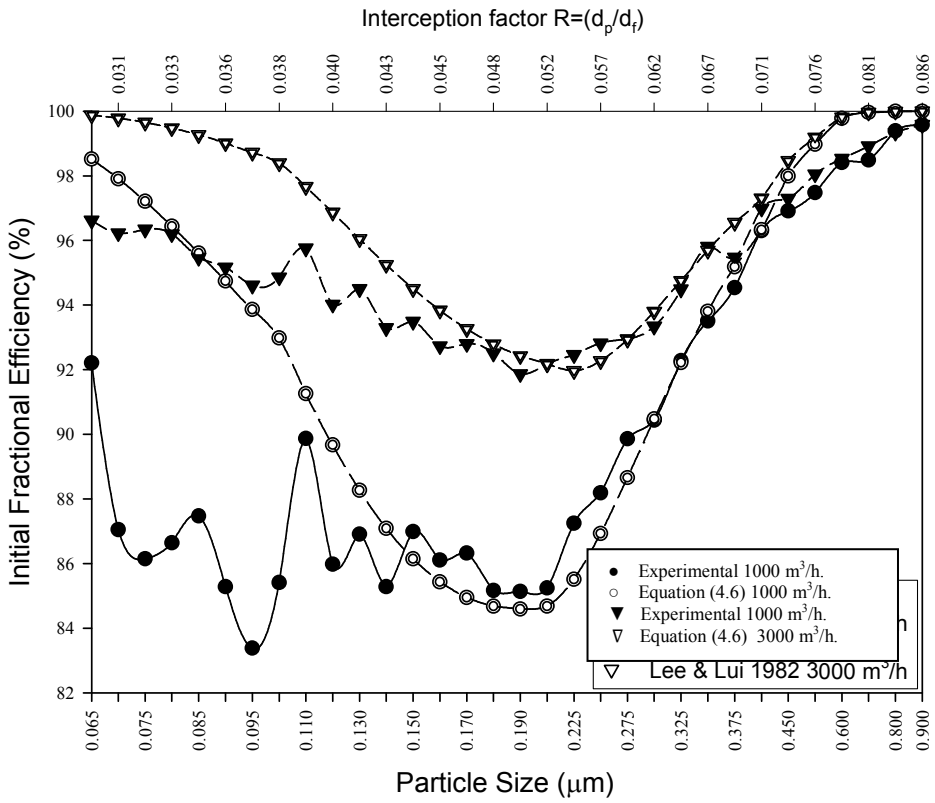

Figure 5.2: Initial efficiency comparison between experimental results and Equation (4.6).

5.6 Future Work

During the experimental work of this study, ten filters were manufactured and tested. Four pleating densities were introduced and two filters were manufactured with the same pleating density. The filter groups A and B were subjected to different dust-loading types of 1000 grams in four separate dust feeds. The pressure drop of the filter showed a linear response for initial pressure drop under 1500 m^3/h, and a non-linear one at higher face velocities. The dust cake formation stage was not reached in the dust loading tests. It is recommend in future work that the dust the feed be continued beyond the depth filtration stage. This will enable the investigation of dust cake formation; assessment of the dust cake porosity for synthetic or any atmospheric dusts would enable the certification of the clogging point, and analysis of the variation in pressure drop response. It will also facilitate the comparison of the dust cake formation stage for different dusts, for example, how does particle size distribution play a role in the dust cake formation.

5.6.1 *In-situ* Testing Method

To facilitate a real time filter performance assessment for the atmoshperic ambient conditions considering dust type, relative humidity and temperature, it is suggested that a mobile air filtration testing facility is designed, constructed and used. This facility will enable real time testing using actual atmospheric dust without having to accelerate testing in a laboratory setting. The mobility of the testing facility will help examine effect of dust type for different locations, which is important due to the widely varying dust types and atmospheric loadings (due to frequent periods of high winds). It will also be a useful tool to measure filter performance in industrial areas and assess dust concentration and dust types and other contaminants. The results of such experimental work will make filter selection more appropriate and suitable for each application such as in buildings in downtown or close to urban area.

Another means of obtaining more practical results is reproducing synthetic dust similar in physical and chemical characteristics to atmospheric dust of interest, and load it in a laboratory setting. This method has two major drawbacks; firstly, it is still an accelerated method of testing which means it would provide less accurate results compared to the *in-situ* method. Secondly, it is a costly process to reproduce the sufficient amounts of dust to complete a wide array of testing procedures which is

necessary to give equipment users confidence in their air filter systems. In addition, the particle size distribution, physical and chemical characteristics depend upon the geographical location and environmental conditions. Therefore, reproducing the atmospheric dust to include all variations of physical and chemical properties may be tedious task and increases the uncertainty in the results obtained. Furthermore, the *in-situ* method facilitated by virtue of a mobile laboratory will make assessment of pleated filter performance with a prefilter possible. Pleated filters are not, in practice, used without a prefilter, therefore they do not encounter the atmospheric dust in its full size distribution, and a prefilter is usually used to lower the dust concentration and alters the particle size distribution challenging the HEPA filter.

5.6.2 Filter Class Variation

This research could be expanded in the future by adding another design parameter which is the filtration medium class. Filter class H10 was used in this experimental work and repeating the same set of experiments but with introduction of another filter class paper such as H13 or H14 will enable the comparison of the effect of varying pleating density on filter pressure drop and efficiency. This will facilitate the comparison of efficiencies versus face velocities for two different filter classes while varying the pleating densities. It will also facilitate the study of the optimal pleat count relative to the filter class of the filtration medium selected.

5.6.3 Testing with New Design Alterations

It is also recommended that the same set of experiments is repeated maintaining the filter class H10 but with supporting the media by means of a grid to prevent the pleated medium from deforming and losing surface (which leads to great losses in permeability).

If the design alterations suggested in subsequent sections are implemented and a filter cartridge is manufactured, it is then recommended to repeat the same experimental work to verify the effect of the design improvements and its influence on the permeability reduction as well as the efficiency measurement.

5.7 Design Alteration

Several design alterations are suggested in the existing design of filter under study. These alterations aim to produce a more aerodynamic filter with enhanced efficiency. The design alterations are:

1. Provide a bigger opening frontal area of the filter whether by enlarging or expanding the opening face area of the filter or by lowering the number of openings. Clearly, the media surface area will also be lower which in turn requires testing the filter to verify if it will achieve the required filtration class. If not, then pleat depth can be increased to provide sufficient filter surface area to attain the efficiency requirement.

2. Reinforce the filtration medium by providing sufficient support to the back side of pleated medium panel. This would reduce the losses in surface area contributing to reduction in permeability in the overall air filter cartridge. Such support can be provided by means of a protection grid or a fleece. This also introduces a factor of safety for the filter cartridge and the most suitable operating conditions including maximum flow rates.

3. Optimize the hot melt spacing in order to expose more surface area to the air flow which in turn increases permeability without compromising the pleat reinforcement.

4. Investigate enhancing the efficiency by other means than increasing pleating density, such as providing more efficient media with lower pressure loss.

5. Use different pleating density for different efficiency.

6. Increasing the pleat depth as another means of the increasing the surface area. To ensure this is an effective means of extending the surface area, filters have to be manufactured with same surface area varying the pleating density and compare it with current results.

7. Replace the top plastic parts highlighted in Figure 5.3 of the filter with filtration medium to provide more surface area.

Figure 5.3: Top view of the pleated filter suggested to be replaced with pleated medium.

5.8 The Proposed Design.

In the filter design examined in this study with a schematic diagram shown in Figure 5.4, the air accesses eight pleated panels of filtration media through four openings which corresponds to a surface area ranging from 28 to 34 m^2. While this geometrical design provides high surface area, the total open area of the four openings is around 40% of the total frontal area. While this geometrical design provides room to install eight pleated panels of filtration medium, it results in a substantial reduction of frontal area which leads to evaluating the pressure drop just from a cartridge design stand point.

The proposed design which is illustrated in Figure 5.5 with two openings will provide larger openings and slower face velocity and thefore, increase the air residence time inside the filter. The reduction in the overall surface area when compared to four opening filter will be compensated by means of providing deeper pleats only if additional surface area is needed. However, this research has proven that not all the surface area in the four openings design has participated in the filtration action due to reasons discussed in Chapter 4.

Further investigation using the same procedure used in this research is required to verify if the surface area of the two-opening filter has achieved the desired efficiency. If so, then the surface area needs further optimization to ensure that an excessive number of pleats have not been used. If the desired efficiency is not achieved, the 28 mm pleat depth of the four-opening filter could be increased in the two-opening filter cartridge to provide the optimized surface area required.

All of design modifications suggested in this study might require further investigation prior to possible implementation in the industry. It is also important to highlight that these design alterations may have a influence on one another and therefore, further developmental preparation are highly recommended. The design modifications suggested in this study are currently under review by the EMW Filtertechnik.

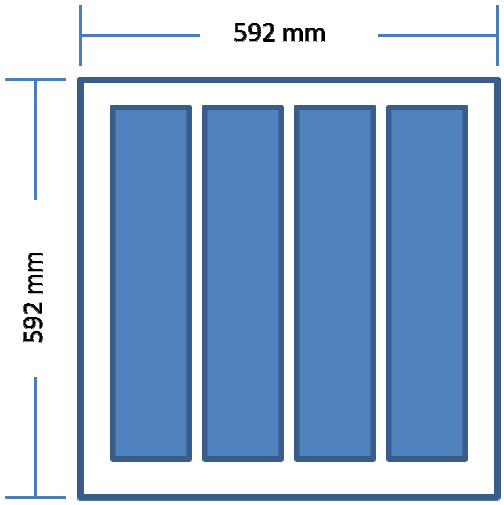

Figure 5.4 : Schematic diagram of front of the existing four opening filter cartridge.

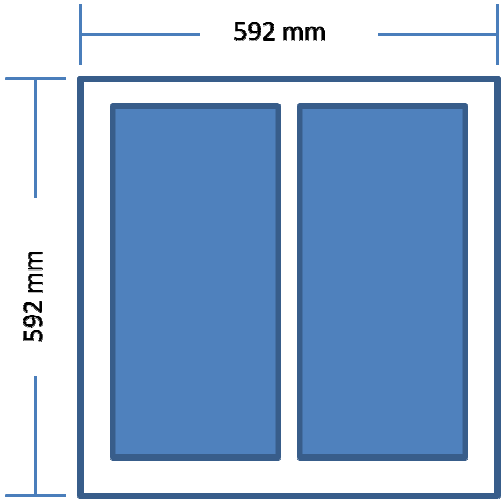

Figure 5.5: Front view of the proposed design of two opening filter cartridge.

5.9 Summary

This experimental work has provided an extensive study of the pleated absolute filters specifically HEPA filters. The study has highlighted the effect of face velocity, pleat density and orientation on the performance of the full scale HEPA filters used in industrial applications. It is evident that optimization is required and additional

investigations are of a paramount importance to enhance the design and therefore the overall performance of this class of filters. Design improvements may include aerodynamic cartridge design, more efficient filtration media and better pleating processes. All of these parameters will facilitate an enormous area of research and development of HEPA filters performance worldwide.

There are four main contributions of this experimental work. Firstly, it has investigated full scale HEPA filters constructed in V shape banks which are widely used in gas turbines and HVAC applications. Secondly, it examined and analyzed wide range of flow rates which revealed through the analysis of the experimental data the departure of the pressure drop response from linearity (Darcy's law). It was evident through this experimental work that as the flow rate increased the filter surface area losses became more significant which led to permeability reduction. A third contribution is the experimental discovery through which increasing the pleat density had a counterproductive effect on the overall surface area and pressure drop response. The fourth aspect is suggesting design modifications for possible reductions of filter surface and permeability. All design modifications are currently under review as they might need further investigation before a possible implementation in the future.

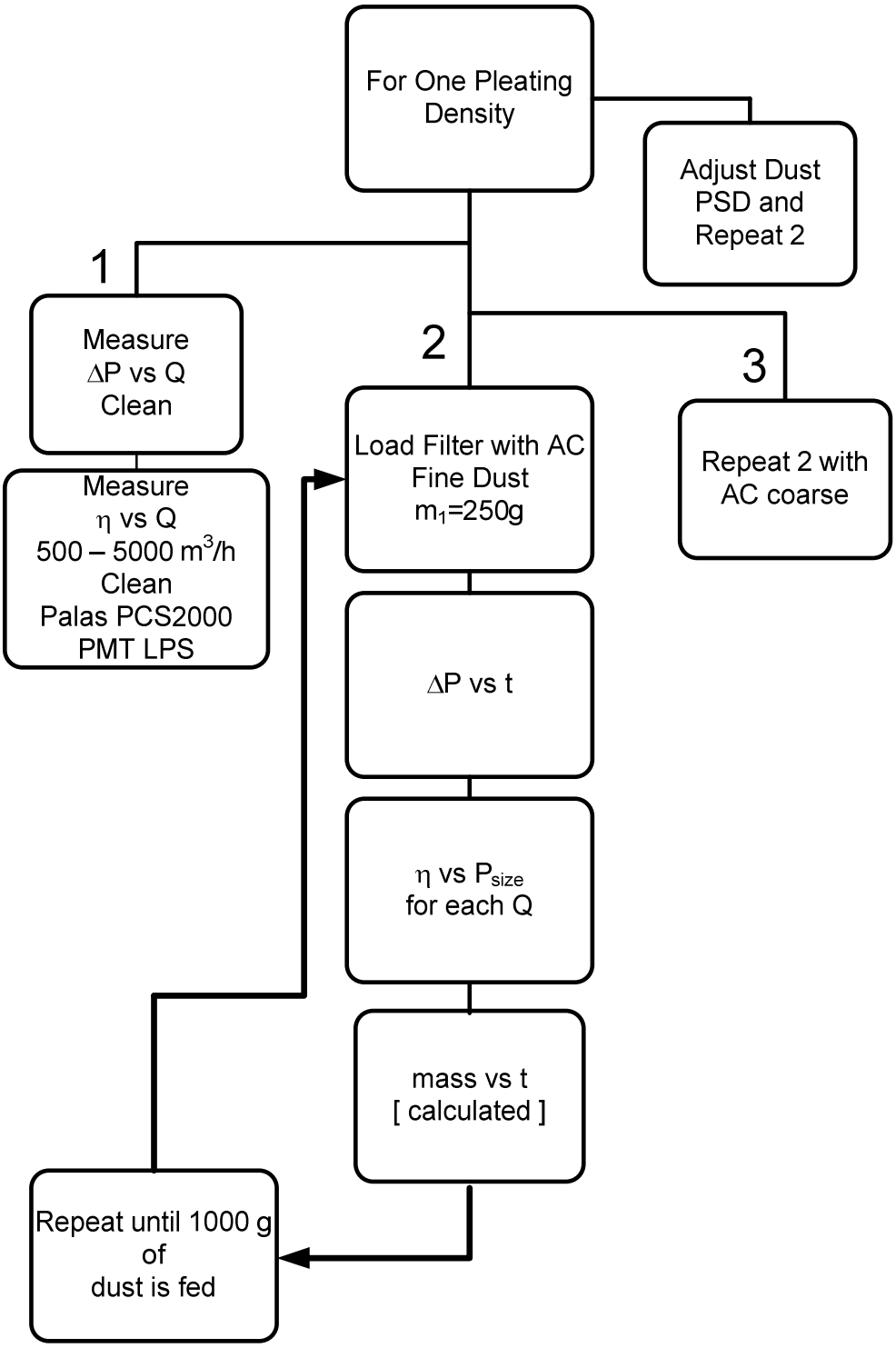
For One Pleating Density
Adjust Dust PSD and Repeat 2
1
Measure ΔP vs Q Clean
2
3
Load Filter with AC Fine Dust m1=250g
Repeat 2 with AC coarse
Measure η vs Q 500 – 5000 m3/h Clean Palas PCS2000 PMT LPS
ΔP vs t
η vs Psize for each Q
mass vs t [calculated]
Repeat until 1000 g of dust is fed

	Filter	ΔP_i	Initial Efficiency		Dust Feeding Stages							
	Filter	ΔP_i	η_i **Palas PCS2000**	η_i **PMT LPS**	ΔP_1	η_1	ΔP_2	η_2	ΔP_3	η_3	ΔP_4	η_4
AC coarse	28A	√	√	√	√	√	√	√	√	√	√	√
	30A	√	√	√	√	√	√	√	√	√	√	√
	32A	√	√	√	√	√	√	√	√	√	√	√
	34A	√	√	√	√	√	√	√	√	√	√	√
AC Fine	28B	√	√	√	√	√	√	√	√	√	√	√
	30B	√	√	√	√	√	√	√	√	√	√	√
	32B	√	√	√	√	√	√	√	√	√	√	√
	34B	√	√	√	√	√	√	√	√	√	√	√
Pleat Orientation	28H	√	√	√	-	-	-	-	-	-	-	-
	28V	√	√	√	-	-	-	-	-	-	-	-

ΔP_i= Initial pressure drop, no dust feeding

η_i = Initial Fractional efficiency

ΔP_1 = Pressure drop during the first dust feeding

ΔP_2 = Pressure drop during the second dust feeding

ΔP_3 = Pressure drop during the third dust feeding

ΔP_4 = Pressure drop during the fourth dust feeding

Palas PCS2000 particle counter [Size range: 0.19-14µm]

PMT LPS particle counter [Size range: 0.065 – 0.9 µm]

Appendix F *Initial efficiency comparison between experimental results and theoretical model of Lee & Liu [1982a] for different flow rates.*

Filter 28A

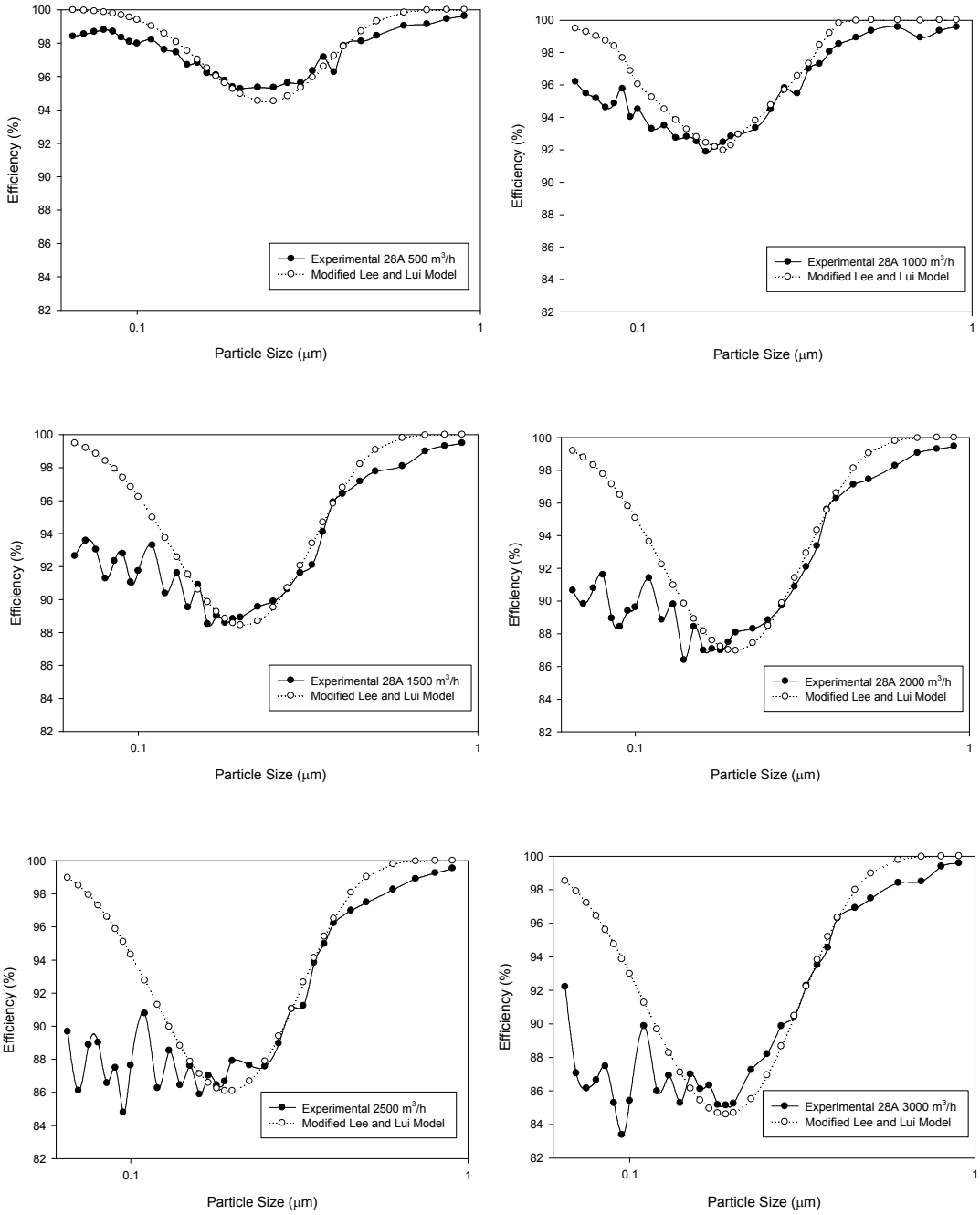

Figure F.1: Efficiency comparison between Equation (4.6) and experimental data for flow rates [filter 28A].

Filter 30A

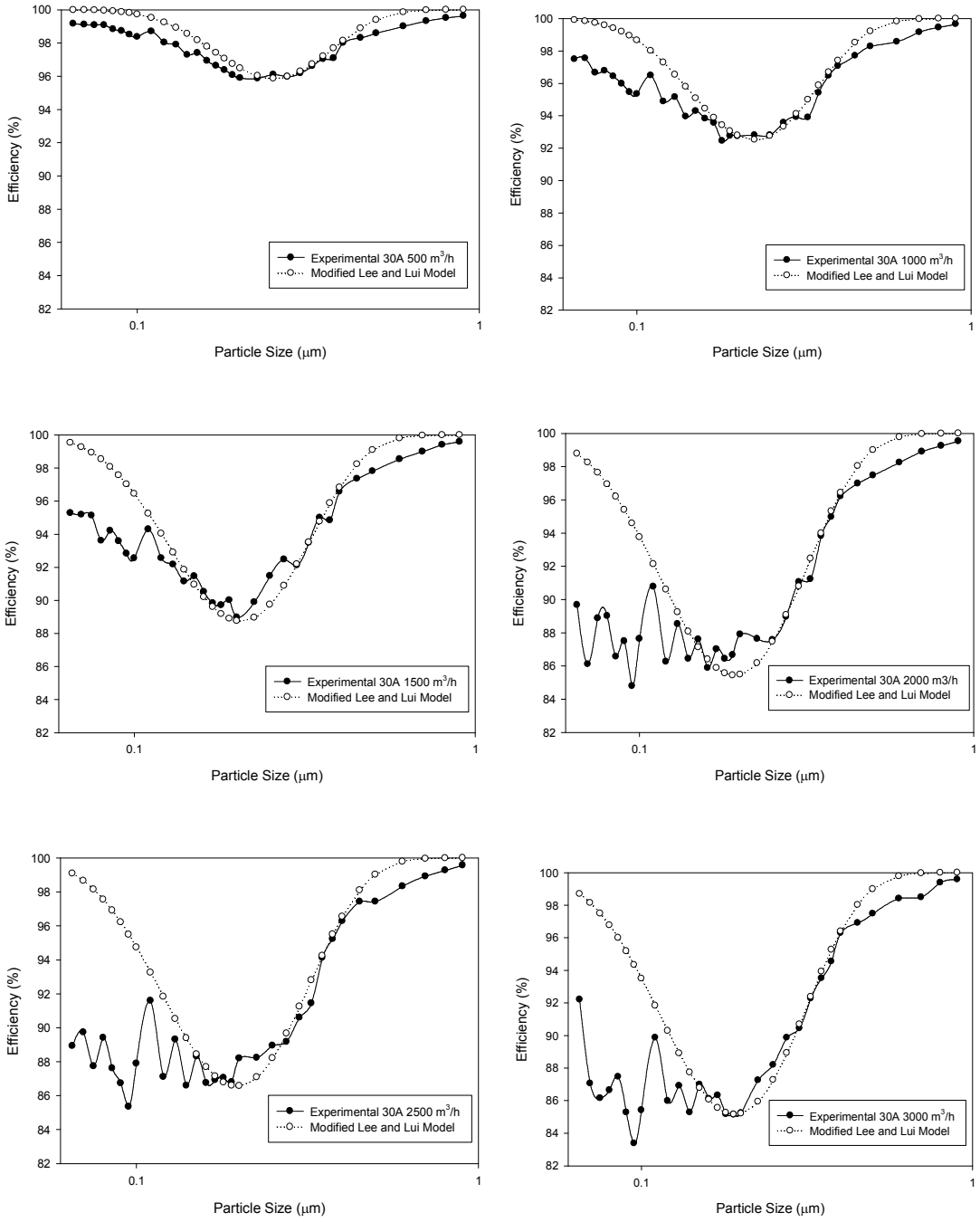

Figure F.2: Efficiency comparison between Equation (4.6) and experimental data for flow rates [filter 30A].

Filter 32A

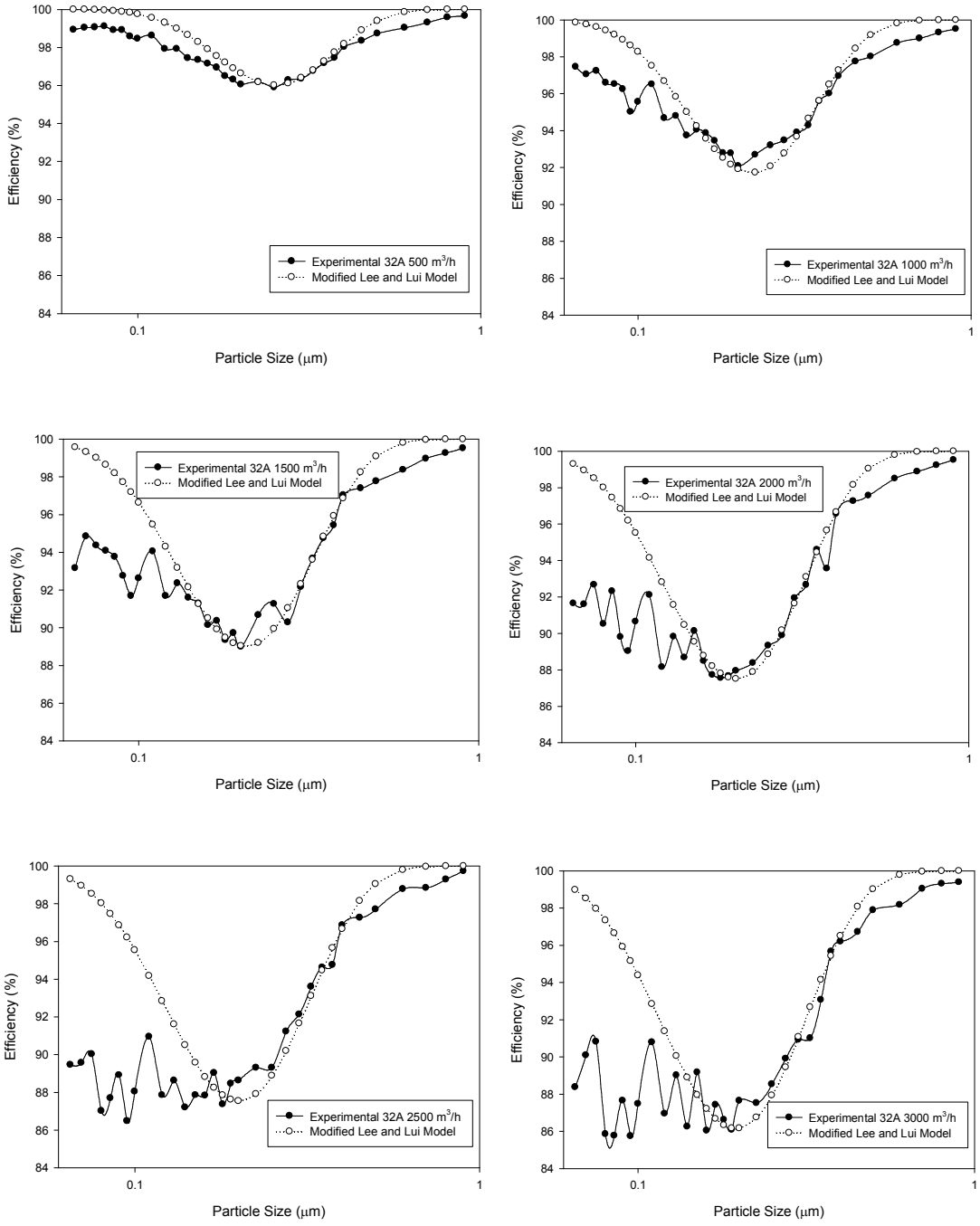

Figure F.3: Efficiency comparison between Equation (4.6) and experimental data for flow rates [filter 32A].

Filter 34A

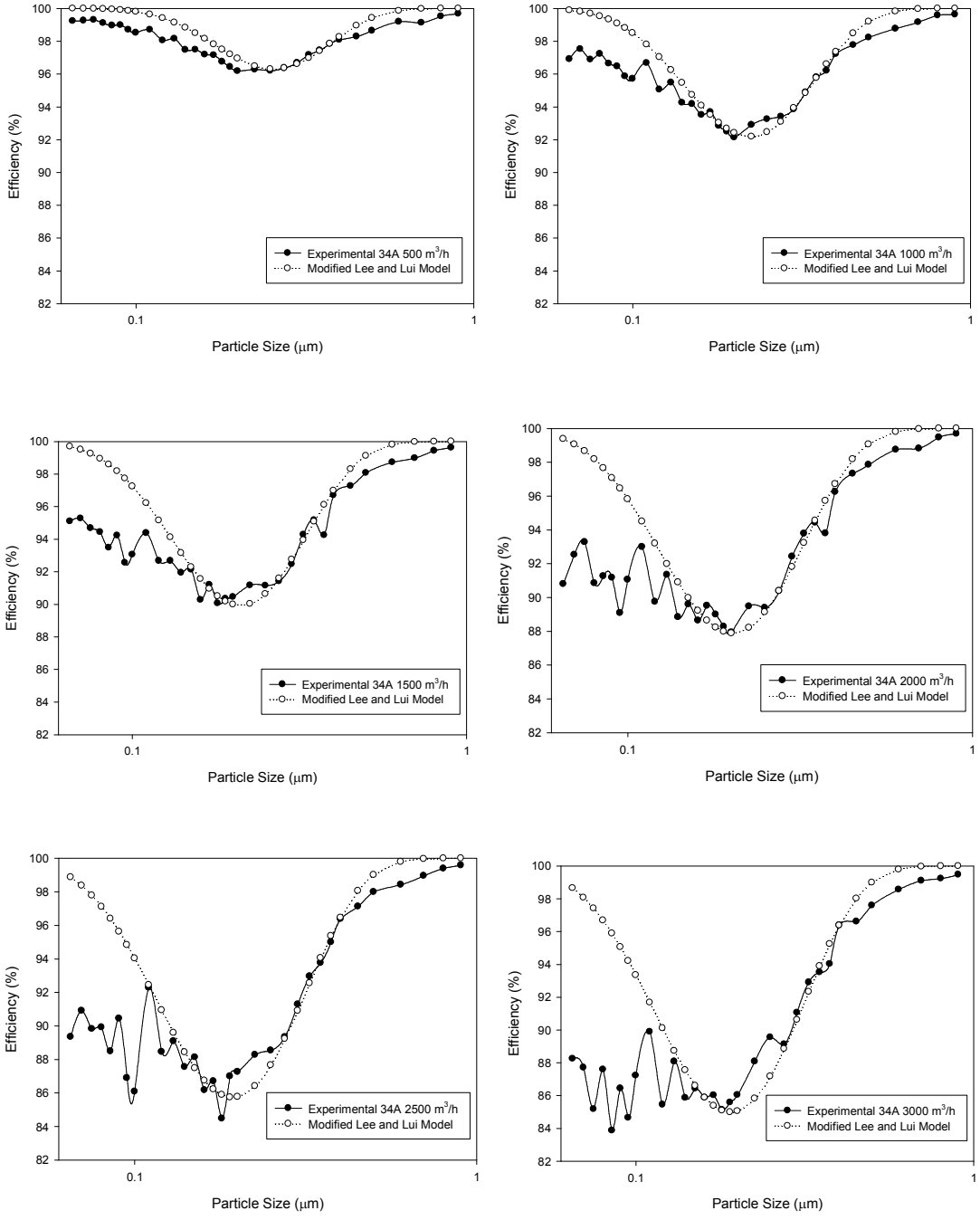

Figure F.4: Efficiency comparison between Equation (4.6) and experimental data for flow rates [filter 34A].

Filter 28B

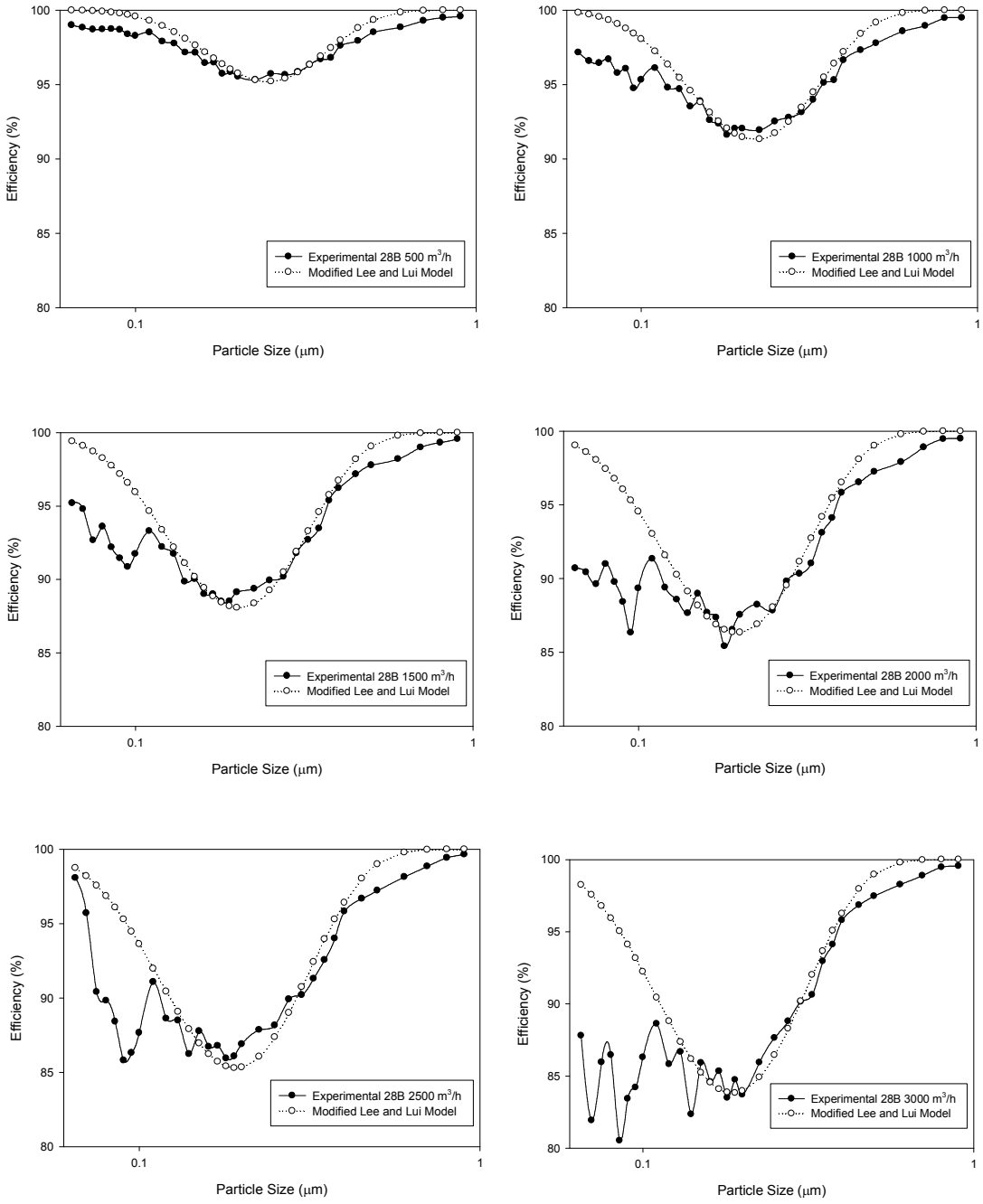

Figure F.5: Efficiency comparison between Equation (4.6) and experimental data for flow rates [filter 28B].

Filter 30B

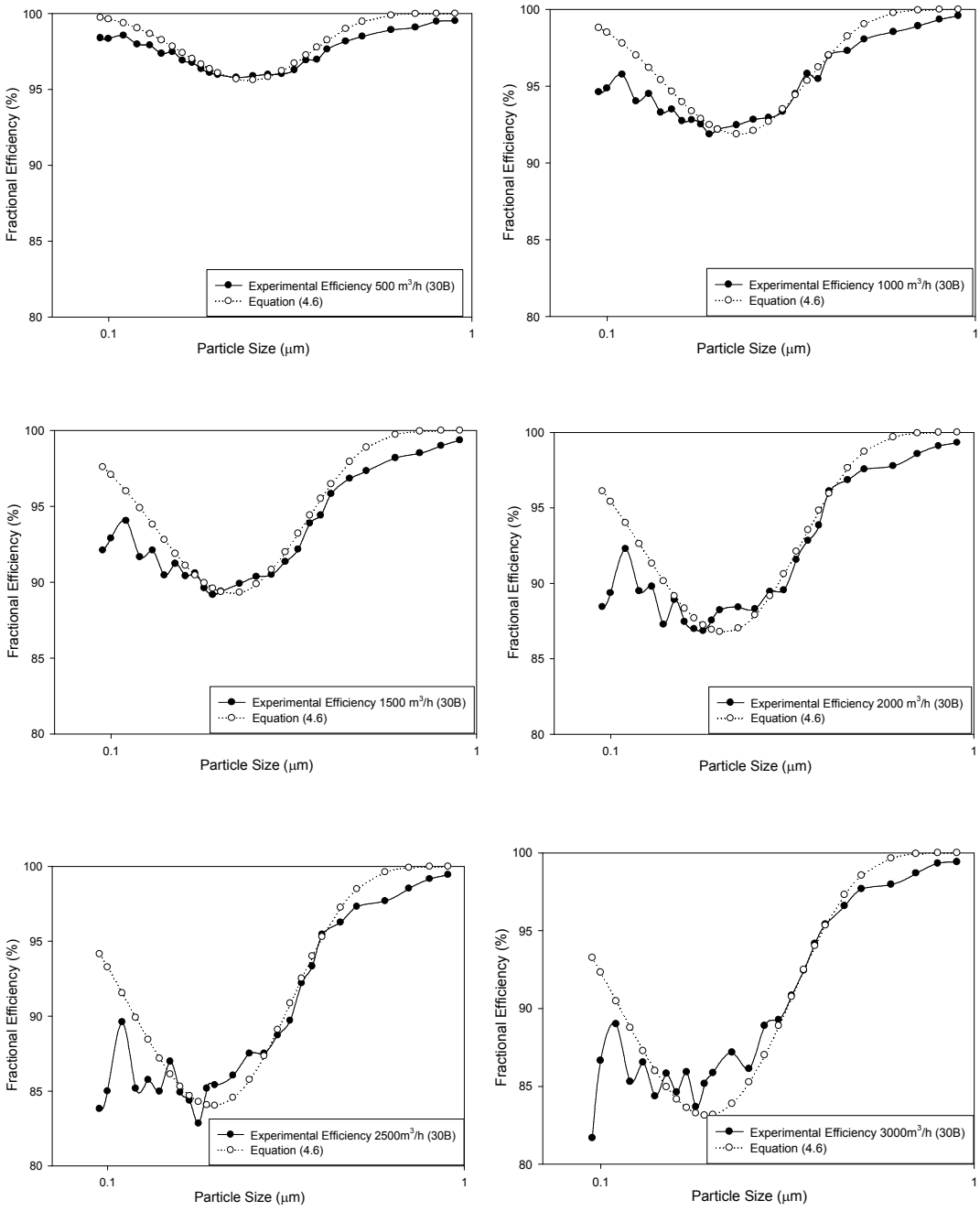

Figure F.6: Efficiency comparison between Equation (4.6) and experimental data for flow rates [filter 30B].

Filter 32B

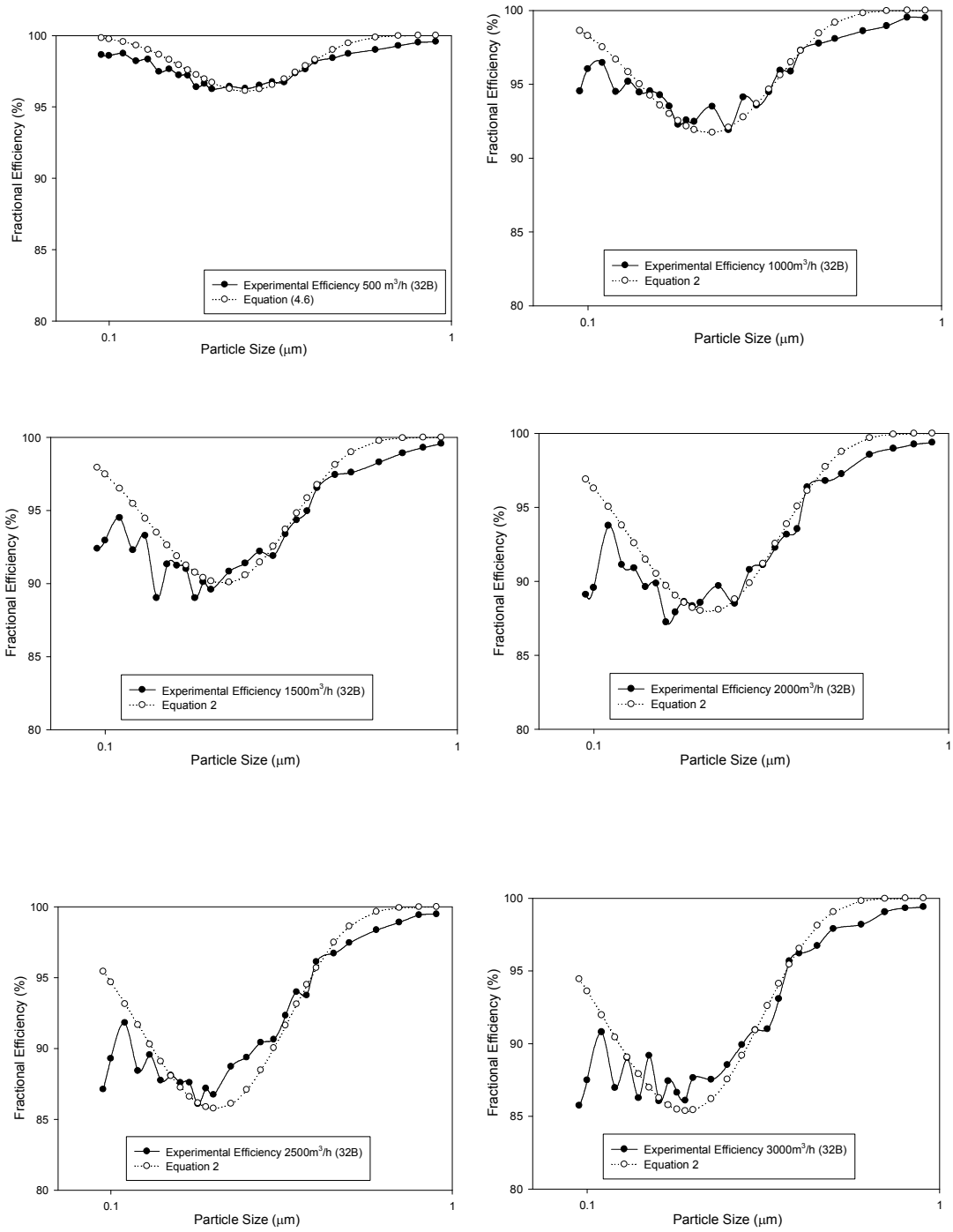

Figure F.7: Efficiency comparison between Equation (4.6) and experimental data for flow rates [filter 32B].

Filter 34B

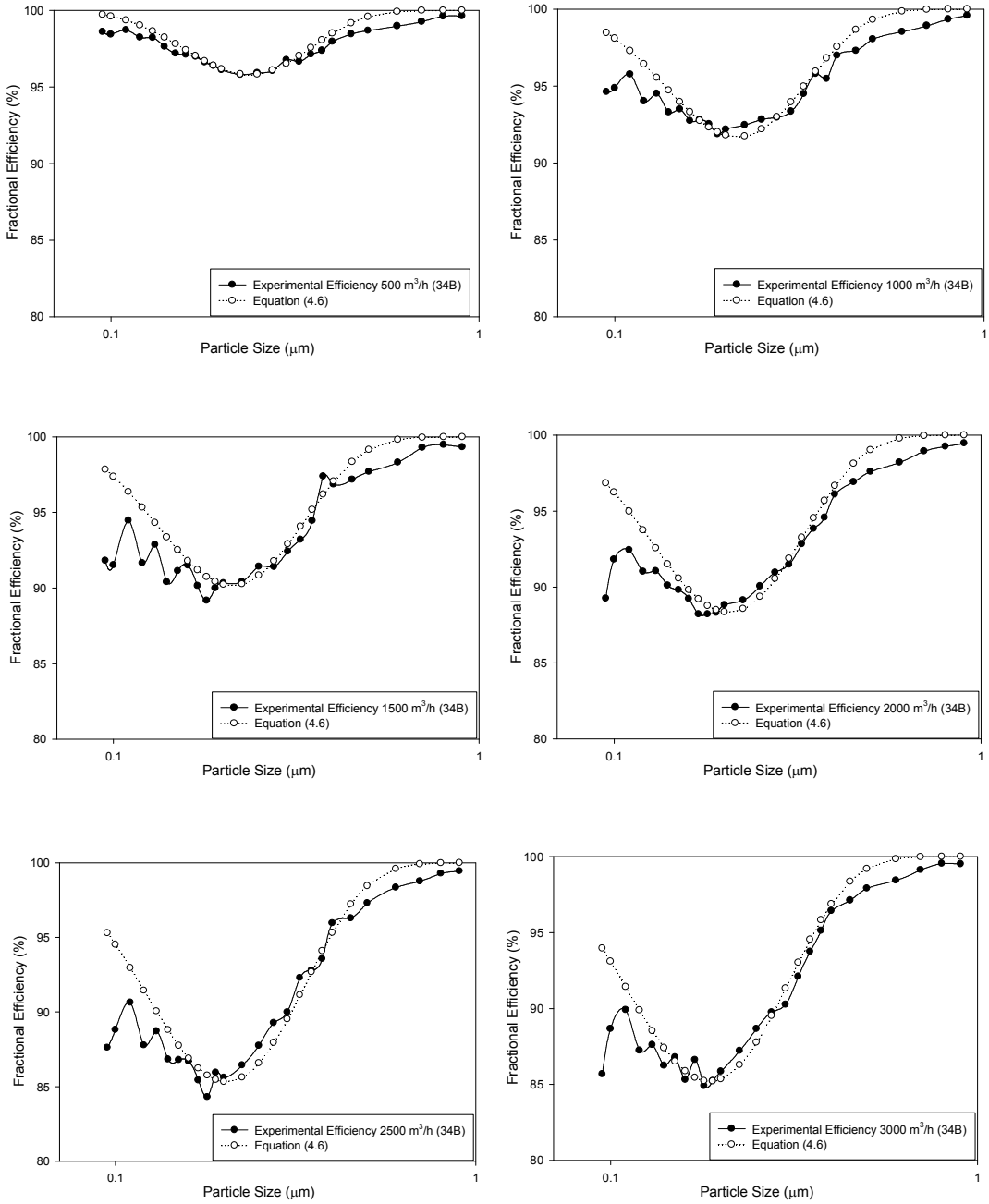

Figure F.8: Efficiency comparison between Equation (4.6) and experimental data for flow rates [filter 28B].

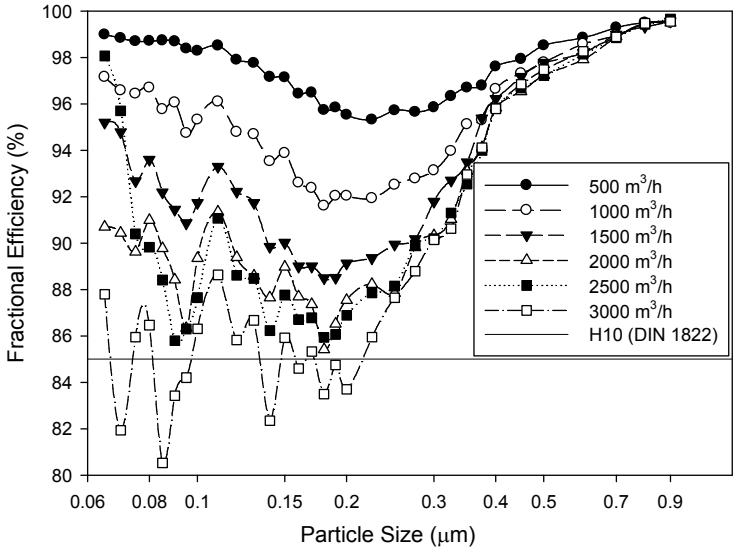

Figure G.1: Initial Efficiency according to DIN 1822 versus particle size for different flow rates [filter 28B].

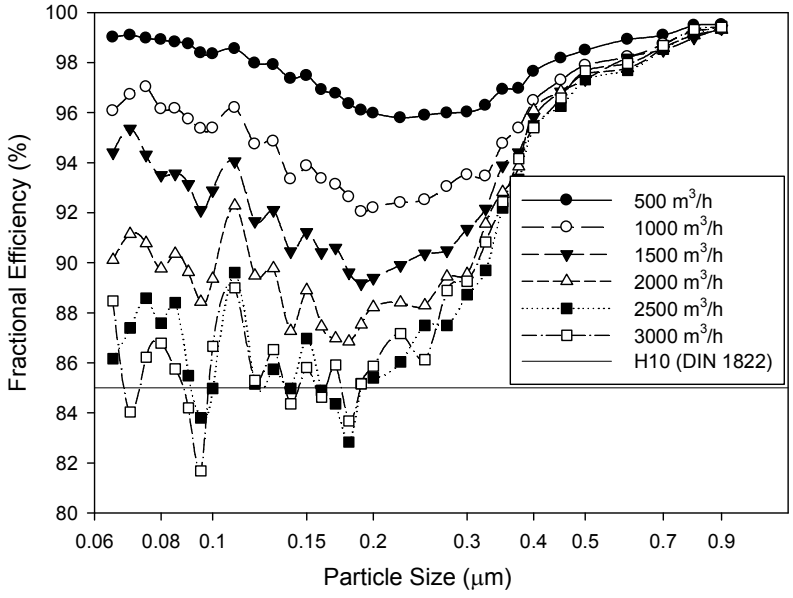

Figure G.2: Initial Efficiency according to DIN 1822 versus particle size for different flow rates [filter 30B]

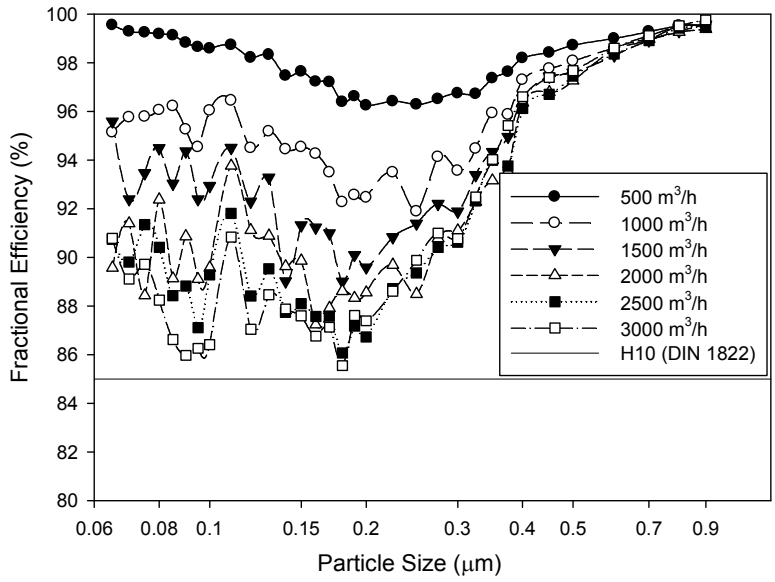

Figure G.3: Initial Efficiency according to DIN 1822 versus particle size for different flow rates

[filter 32B]

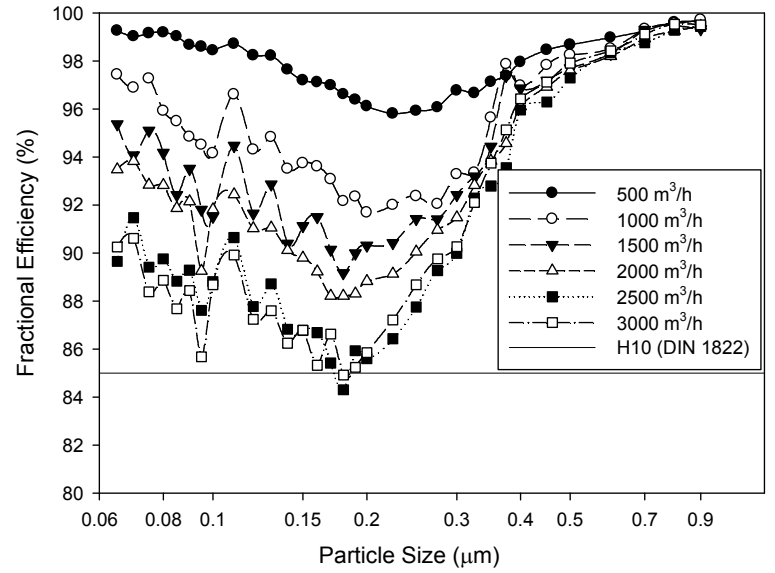

Figure G.4: Initial Efficiency according to DIN 1822 versus particle size for different flow rates

[filter 34B]

Filter	**Deflection δ (μm)**			
Q (m^3/h)	**28B**	**30B**	**32B**	**34B**
500	14.9	11.4	11.4	11.4
1000	26.3	26.3	25.5	25.5
1500	41.3	42.1	39.5	39.5
2000	58.0	58.0	55.3	55.3
2500	75.5	76.4	73.8	73.8
3000	94.8	97.5	94.0	94
3500	118.0	120.0	115.0	115.0
4000	141.0	145.0	139.0	140.0
4500	165.0	170.0	163.0	163.0
5000	191.0	199.0	190.0	191.0

Figure H.1: The comparison between the deflections of the experimental data of filter Group (B).

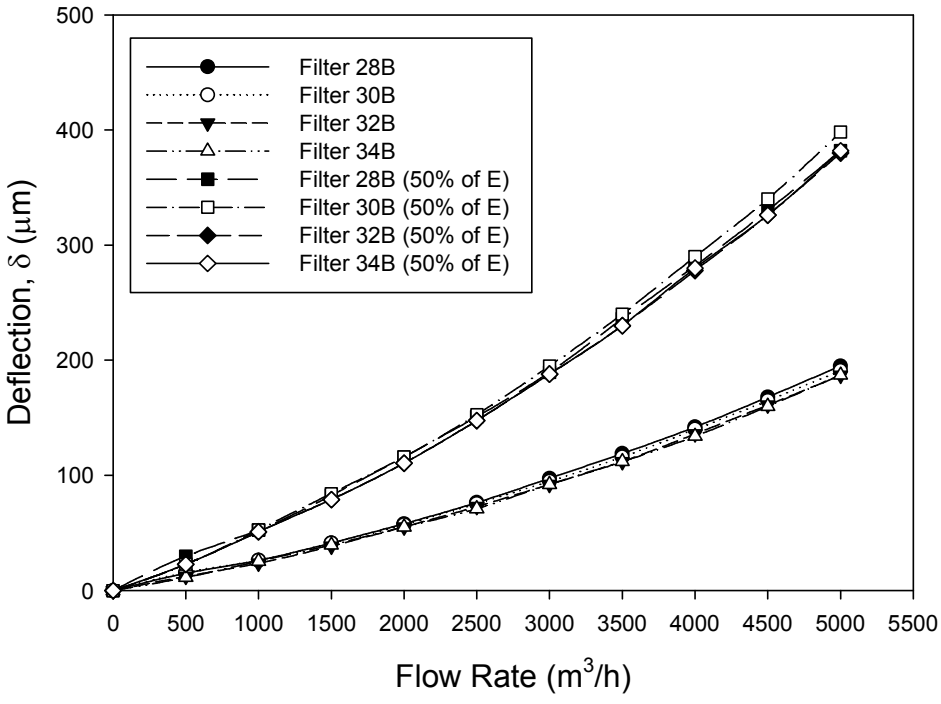

Figure H.2: Deflection comparison between using Equation 4.1 using 100% and 50% of the Young's modulus value for filter Group (B).

Appendix I *Pressure drop comparison between theoretical models and experimental data.*

Face Velocity (mm/s)	Happel [1959] (Pa)	Kuwabara [1959] (Pa)	Stechkina and Fuchs [1963] (Pa)	Davies [1952] (Pa)	Darcy [Davies, 1973] (Pa)	Experimental (Pa)
5.79	13	16	17	11	14	14
11.58	25	32	35	23	30	30
17.37	38	48	52	34	46	47
23.17	50	64	70	45	62	66
28.96	63	80	87	57	78	87
34.75	75	96	104	68	94	111
40.54	88	112	122	79	110	135
46.33	100	128	139	91	126	162
52.12	113	143	156	102	142	191
57.91	125	159	174	113	158	222

Table I.1: Pressure drop comparison between theoretical models and experimental data of Filter 28A.

Face Velocity (mm/s)	Happel [1959] (Pa)	Kuwabara [1959] (Pa)	Stechkina and Fuchs [1963] (Pa)	Davies [1952] (Pa)	Darcy [Davies, 1973] (Pa)	Experimental (Pa)
5.22	11	14	16	10	18	18
10.44	23	29	31	20	30	30
15.65	34	43	47	31	42	47
20.87	45	57	63	41	54	65
26.09	56	72	78	51	66	86
31.31	68	86	94	61	78	108
36.52	79	101	110	71	90	132
41.74	90	115	125	82	102	159
46.96	102	129	141	92	114	188
52.18	113	144	157	102	126	218

Table I.2: Pressure drop comparison between theoretical models and experimental data of Filter 30A.

Face Velocity (mm/s)	Happel [1959] (Pa)	Kuwabara [1959] (Pa)	Stechkina and Fuchs [1963] (Pa)	Davies [1952] (Pa)	Darcy [Davies, 1973] (Pa)	Experimental (Pa)
5.08	11	14	15	10	14	14
10.17	22	28	31	20	27	27
15.25	33	42	46	30	40	44
20.34	44	56	61	40	53	63
25.42	55	70	76	50	66	83
30.50	66	84	92	60	79	105
35.59	77	98	107	70	92	129
40.67	88	112	122	79	105	155
45.75	99	126	137	89	118	183
50.84	110	140	153	99	131	213

Table I.3: Pressure drop comparison between theoretical models and experimental data of Filter 32A.

Face Velocity (mm/s)	Happel [1959] (Pa)	Kuwabara [1959] (Pa)	Stechkina and Fuchs [1963] (Pa)	Davies [1952] (Pa)	Darcy [Davies, 1973] (Pa)	Experimental (Pa)
4.82	10	13	14	9	14	15
9.64	21	27	29	19	30	29
14.45	31	40	43	28	46	45
19.27	42	53	58	38	62	63
24.09	52	66	72	47	78	81
28.91	63	80	87	57	94	105
33.72	73	93	101	66	110	128
38.54	83	106	116	75	126	153
43.36	94	119	130	85	142	182
48.18	104	133	145	94	158	213

Table I.4: Pressure drop comparison between theoretical models and experimental data of Filter 34A.

Face Velocity (mm/s)	Happel [1959] (Pa)	Kuwabara [1959] (Pa)	Stechkina and Fuchs [1963] (Pa)	Davies [1952] (Pa)	Darcy [Davies, 1973] (Pa)	Experimental (Pa)
5.79	12	16	17	11		17
11.58	24	31	34	22		30
17.37	37	47	51	33		47
23.17	49	62	68	44		66
28.96	61	78	85	55		86
34.75	73	93	102	66		108
40.54	86	109	119	77		134
46.33	98	124	135	88		161
52.12	110	140	152	99		188
57.91	122	155	169	110		218

Table I.5: Pressure drop comparison between theoretical models and experimental data of Filter 28B.

Face Velocity (mm/s)	Happel [1959] (Pa)	Kuwabara [1959] (Pa)	Stechkina and Fuchs [1963] (Pa)	Davies [1952] (Pa)	Darcy [Davies, 1973] (Pa)	Experimental (Pa)
5.22	11	14	16	10		15
10.44	23	29	31	20		30
15.65	34	43	47	31		48
20.87	45	58	63	41		66
26.09	57	72	78	51		87
31.31	68	86	94	61		111
36.52	79	101	110	72		136.5
41.74	91	115	125	82		165
46.96	102	130	141	92		193.5
52.18	113	144	157	102		226.6

Table I.6: Pressure drop comparison between theoretical models and experimental data of Filter 30B.

Face Velocity (mm/s)	Happel [1959] (Pa)	Kuwabara [1959] (Pa)	Stechkina and Fuchs [1963] (Pa)	Davies [1952] (Pa)	Darcy [Davies, 1973] (Pa)	Experimental (Pa)
5.08	11	14	15	10		15
10.17	22	28	31	20		29
15.25	33	42	46	30		45
20.34	44	56	61	40		63
25.42	55	70	76	50		84
30.50	66	84	92	60		107
35.59	77	98	107	70		131
40.67	88	112	122	80		158
45.75	99	126	138	90		186
50.84	110	140	153	100		216

Table I.7: Pressure drop comparison between theoretical models and experimental data of Filter 32B.

Face Velocity (mm/s)	Happel [1959] (Pa)	Kuwabara [1959] (Pa)	Stechkina and Fuchs [1963] (Pa)	Davies [1952] (Pa)	Darcy [Davies, 1973] (Pa)	Experimental (Pa)
4.82	10	13	14	9		15
9.64	21	26	29	19		29
14.45	31	40	43	28		47
19.27	42	53	58	38		63
24.09	52	66	72	47		84
28.91	62	79	86	56		107
33.72	73	93	101	66		131
38.54	83	106	115	75		159
43.36	94	119	130	84		186
48.18	104	132	144	94		218

Table I.8: Pressure drop comparison between theoretical models and experimental data of Filter 34B

Given the grammage (weight per m^2) of the filter medium, the filter medium thickness and the true density of the glass fibre material

Define:

G = Medium grammage, g/m^2
h = Medium thickness, m
ρ_G = True density of the fibre material, kg/m^3

then

$$\frac{m^3 \text{of fibre}}{m^3 \text{of medium}} = \frac{G \times 10^{-3}}{\rho_G h}$$

and

$$\text{Porosity}, \varepsilon = \frac{m^3 \text{of medium - } m^3 \text{of fibre}}{m^3 \text{of medium}} = 1 - \frac{G \times 10^{-3}}{\rho_G h}$$

G = Medium grammage, 75 g/m^2
h = Medium thickness, 500 $x10^{-6}$m
ρ_G = True density of the fibre material, 2440 kg/m^3

$$\text{Porosity} = 1 - \left[\frac{\left(75 \times 10^{-3}\right)}{2440 \times 500 \times 10^{-6}} \right] = 94\%$$

Appendix L *Graphs for dust-loaded efficiencies using Palas Particle Counter PCS-2000*

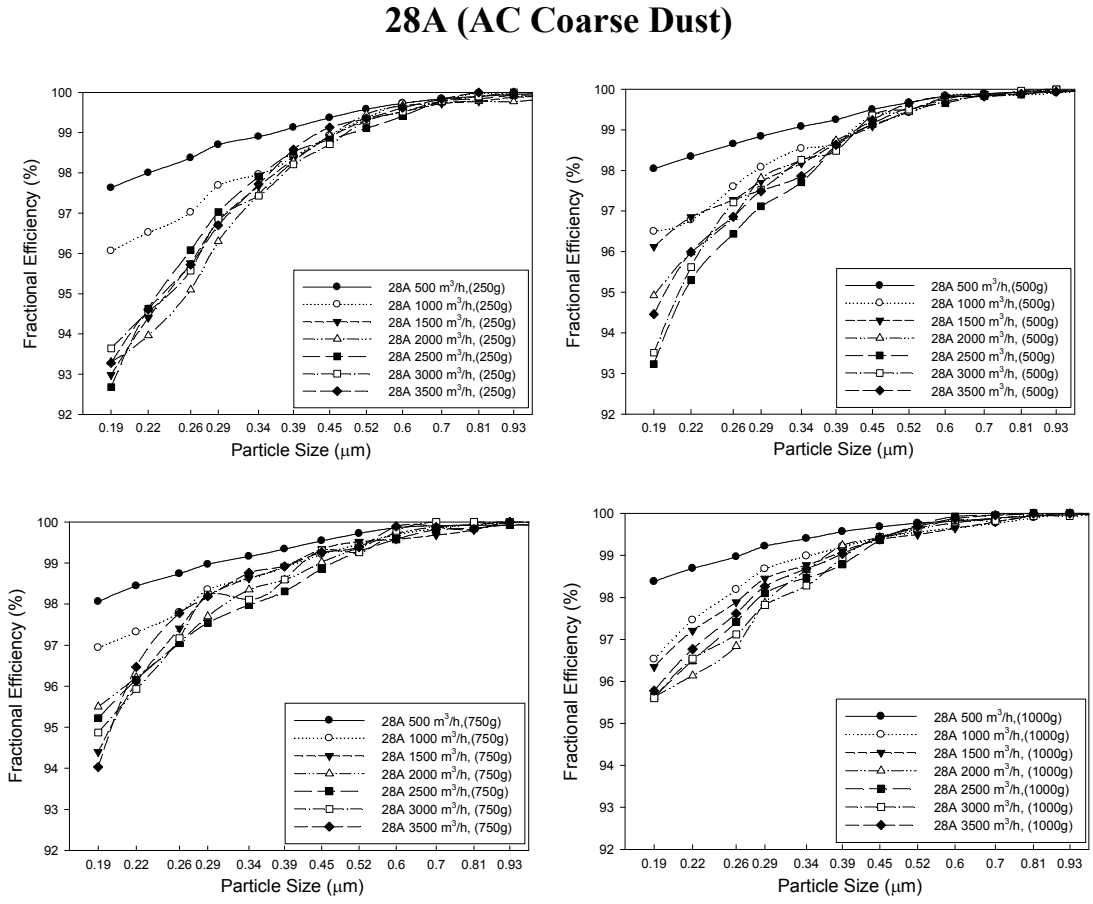

Figure L.1: Dust-loaded efficiencies for pleating density of 28 pleats/100 mm at different flow rates and dust feeds.

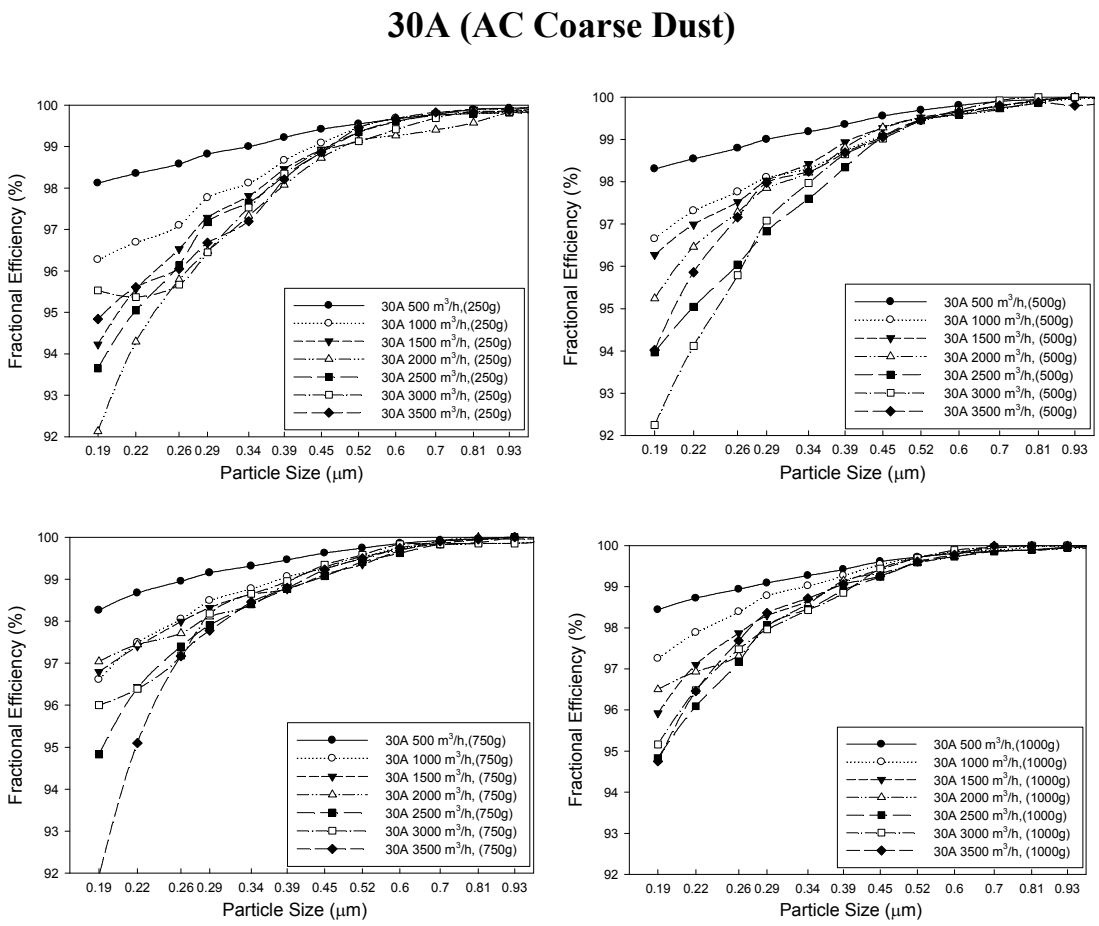

Figure L.2: Dust-loaded efficiencies for pleating density of 30 pleats/100 mm at different flow rates and dust feeds.

32A (AC Coarse Dust)

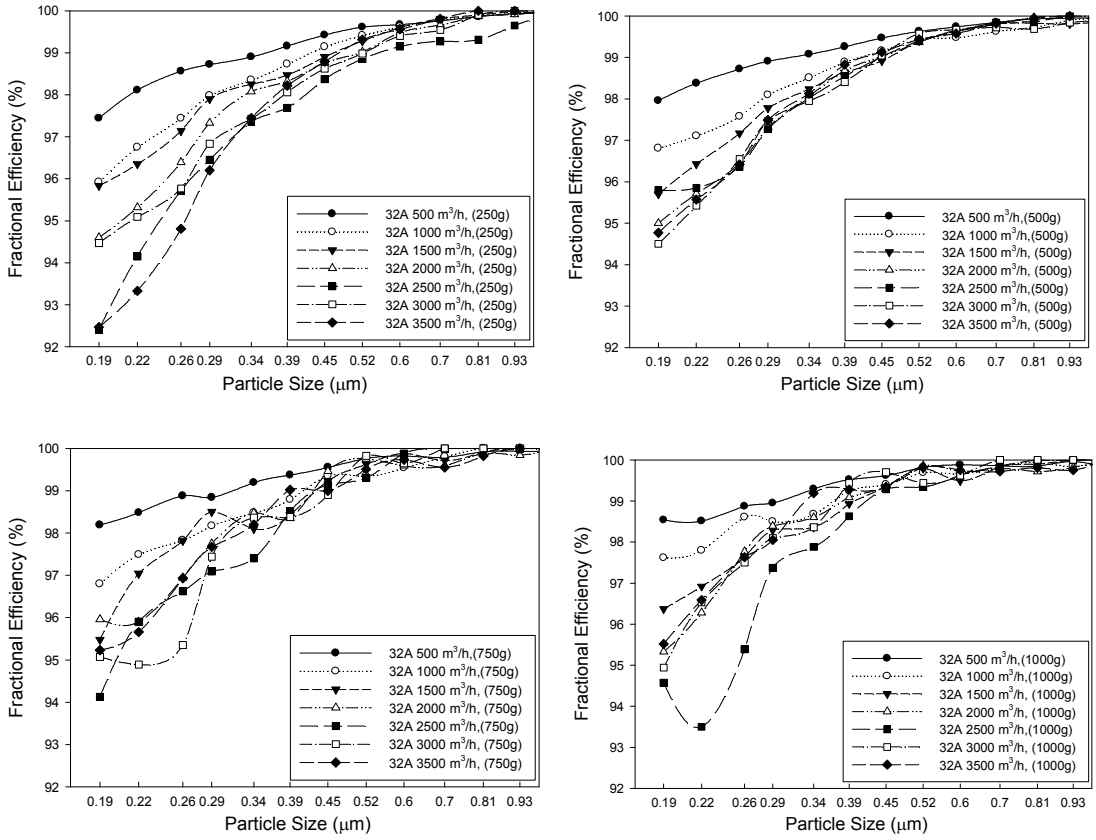

Figure L.3: Dust-loaded efficiencies for pleating density of 32 pleats/100 mm at different flow rates and dust feeds.

34A (AC Coarse Dust)

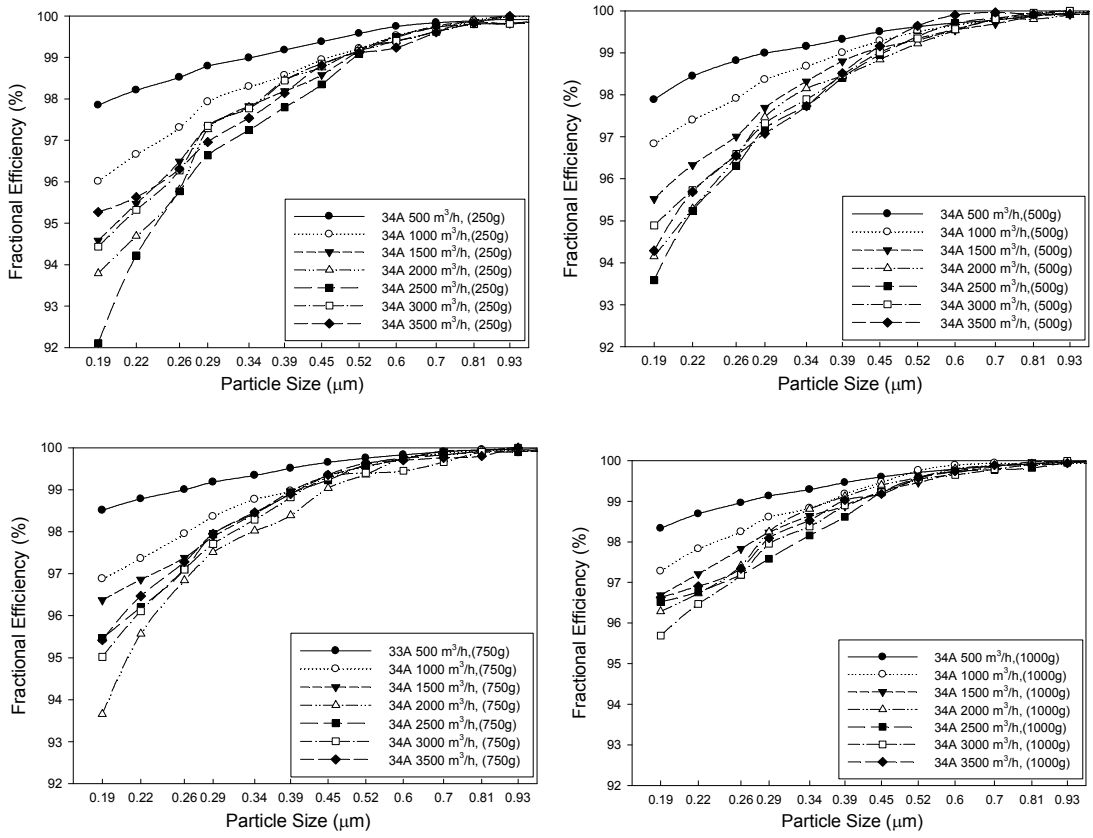

Figure L.4: Dust-loaded efficiencies for pleating density of 34 pleats/100 mm at different flow rates and dust feeds.

28B

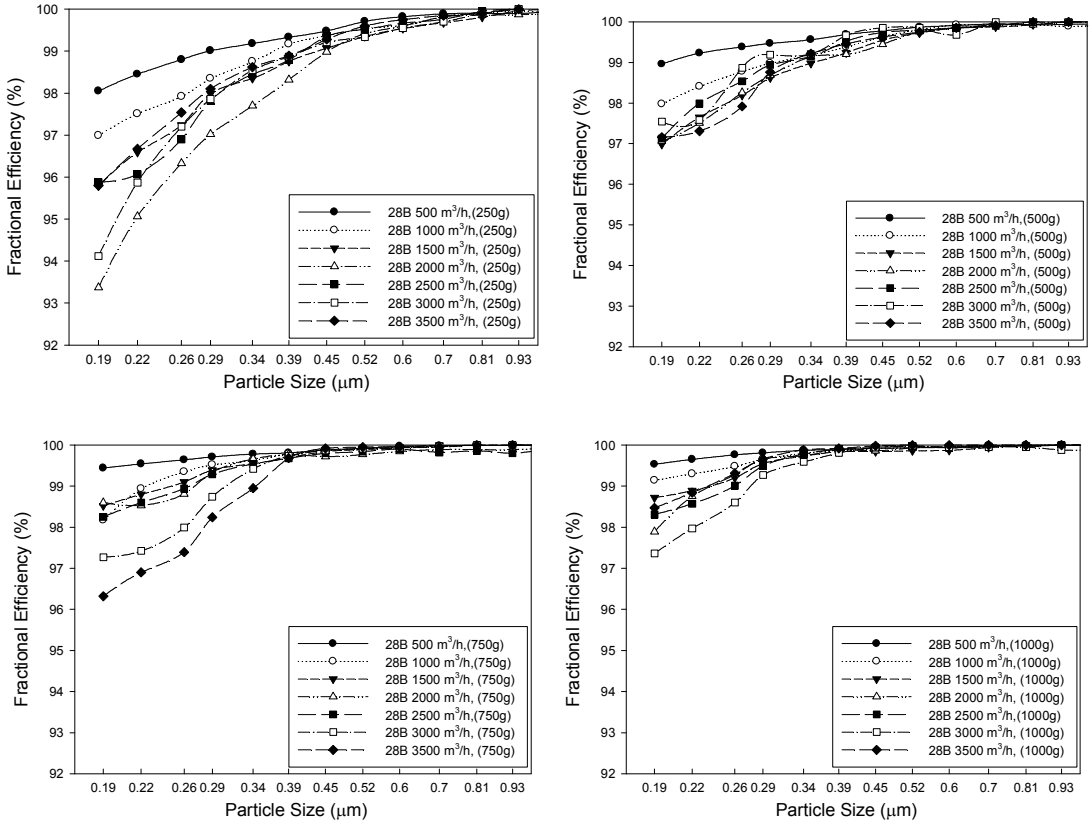

Figure L.5: Dust-loaded efficiencies for pleating density of 28 pleats/100 mm at different flow rates and dust feeds.

30B

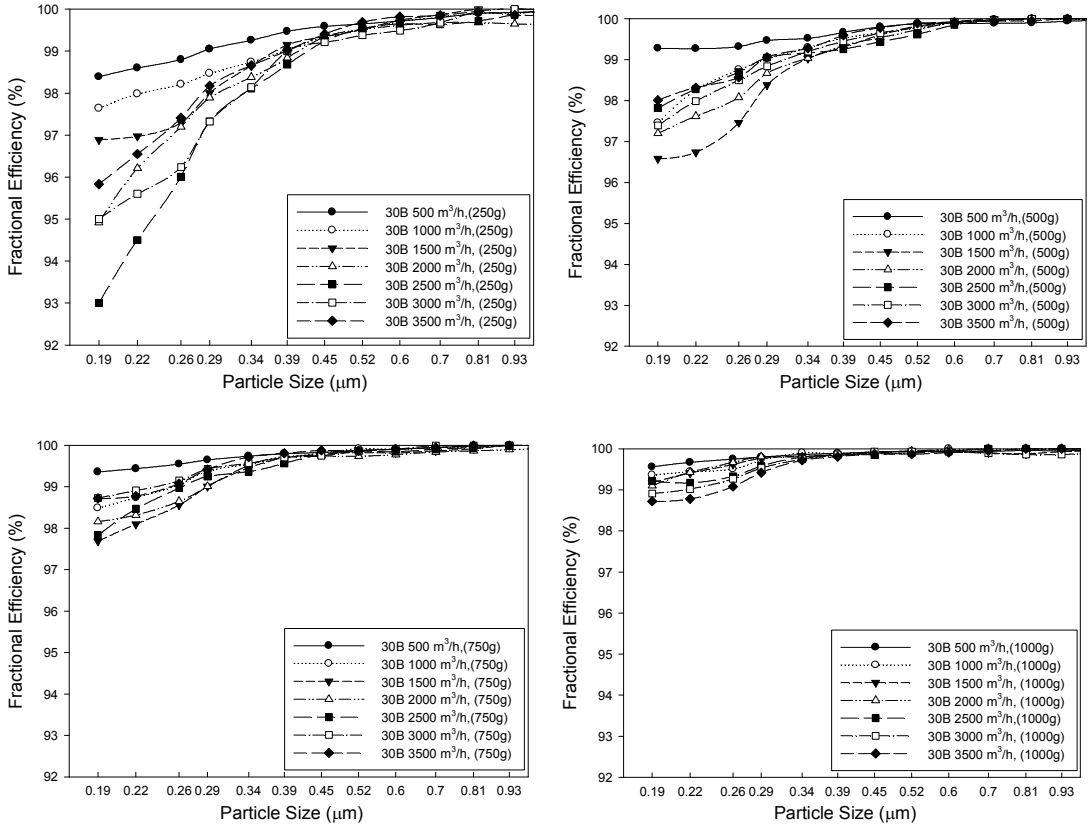

Figure L.6: Dust-loaded efficiencies for pleating density of 30 pleats/100 mm at different flow rates and dust feeds.

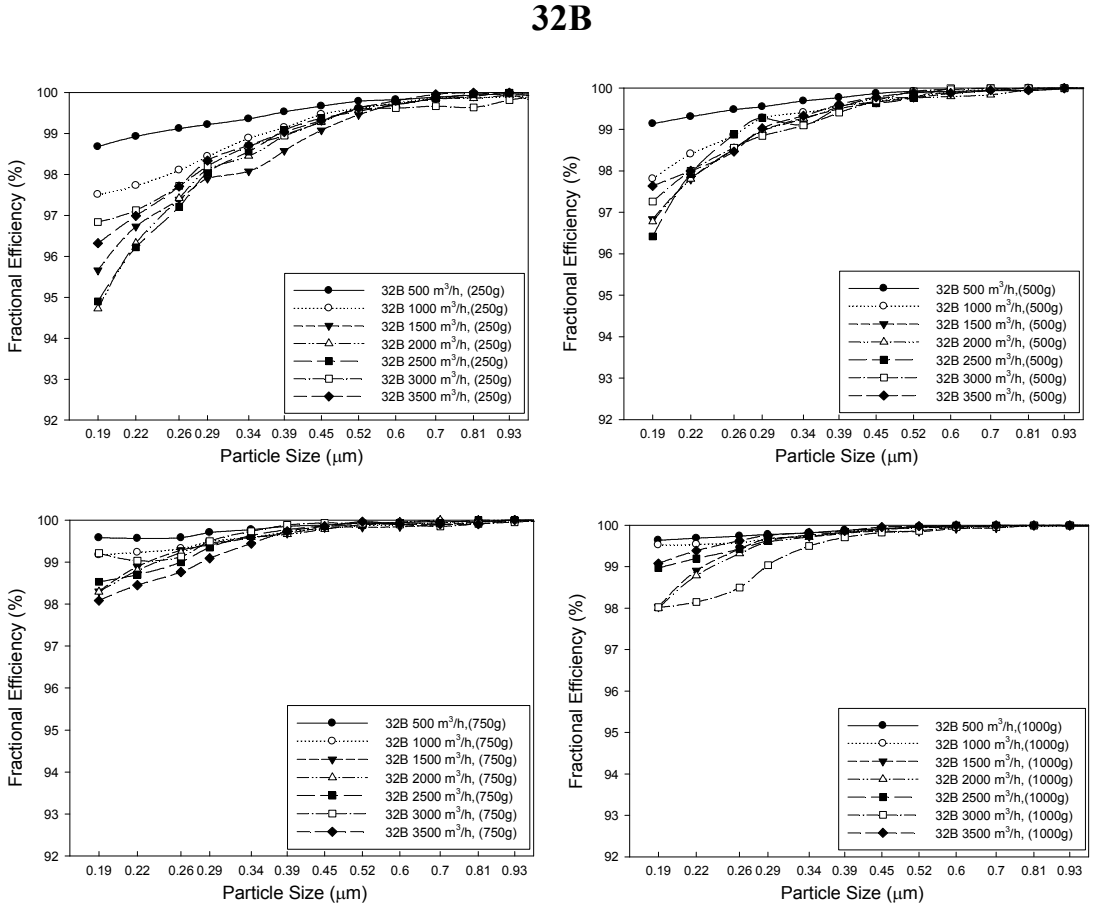

Figure L.7: Dust-loaded efficiencies for pleating density of 32 pleats/100 mm at different flow rates and dust feeds.

34B

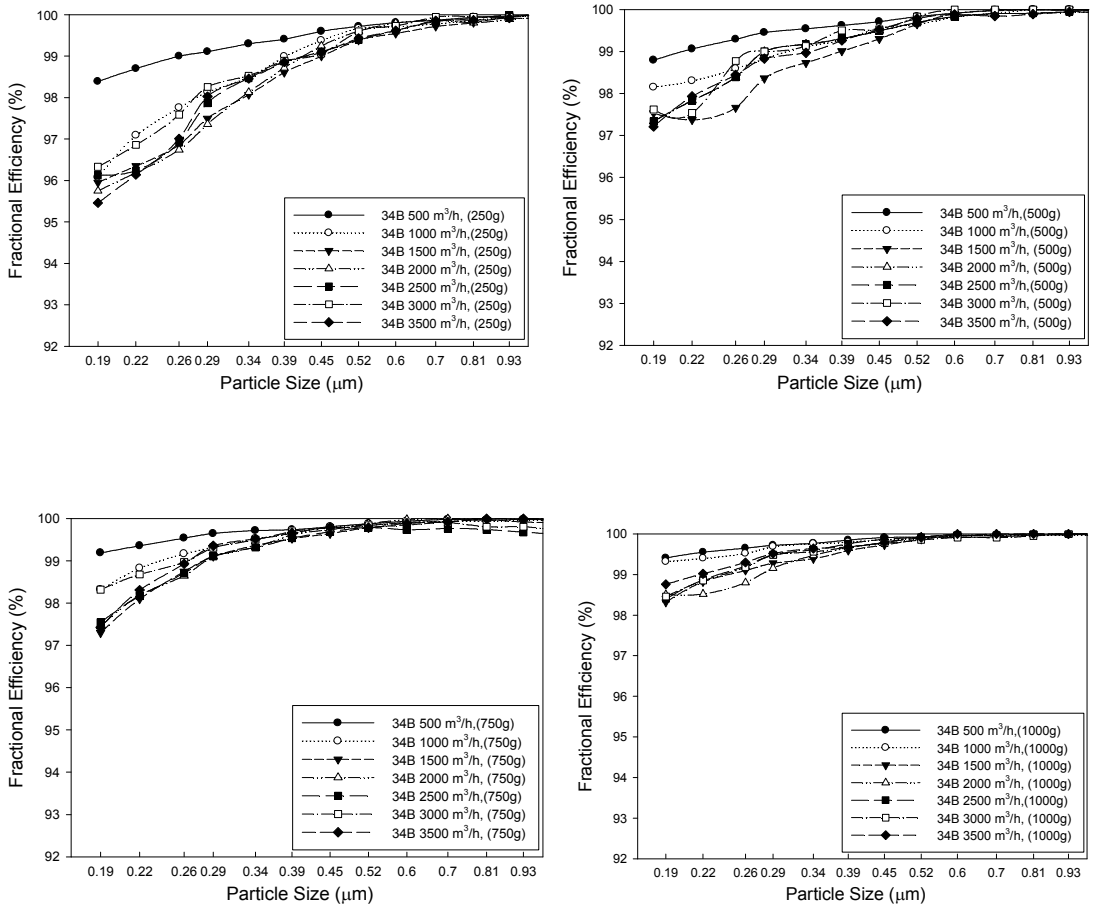

Figure L.8: Dust-loaded efficiencies for pleating density of 34 pleats/100 mm at different flow rates and dust feeds.

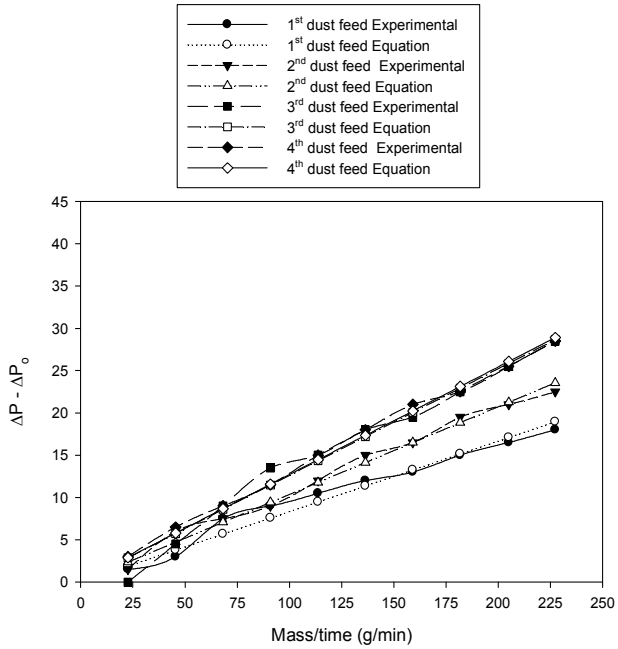

Figure M.1: Initial Efficiency for filter 28A with pleating density 28 pleats/100 mm at flow rate of 3500 m^3/h.

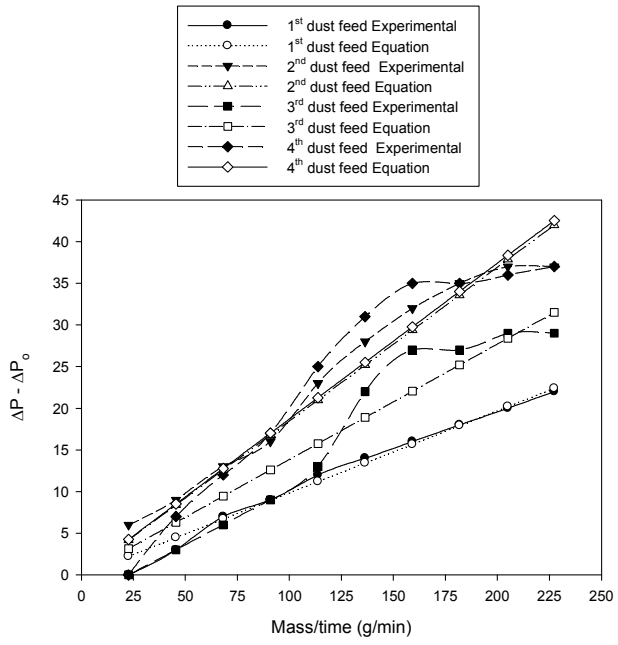

Figure M.2: Initial Efficiency for filter 30A pleating density 30 pleats/100 mm at flow rate of 3500 m^3/h

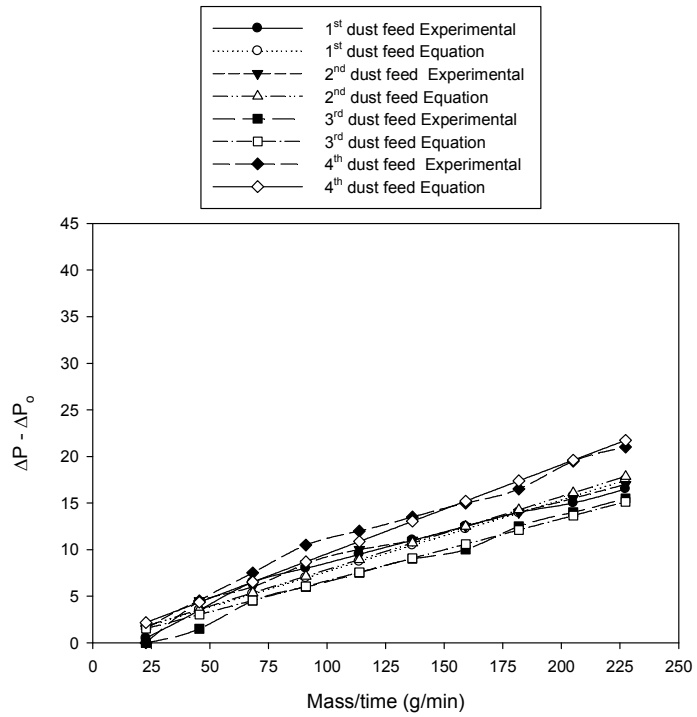

Figure M.3: Initial Efficiency for [filter 32A] pleating density 32pleats/100mm at flow rate of 3500 m^3/h.

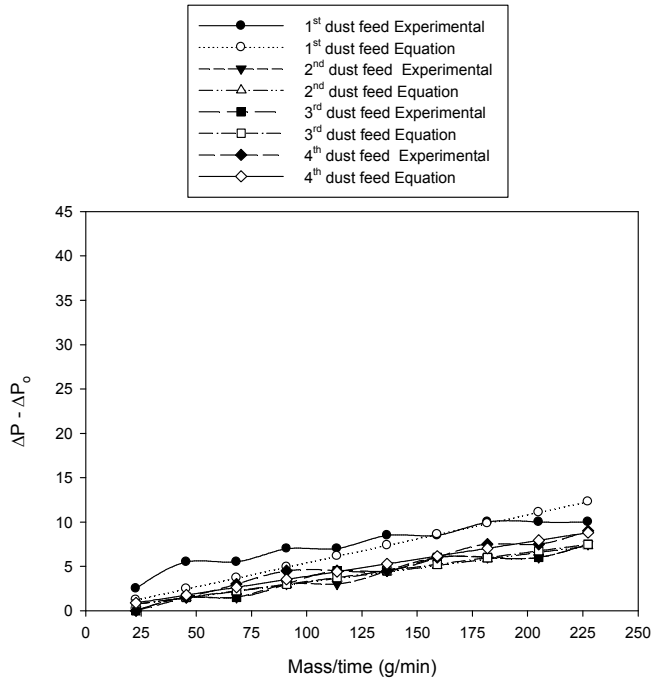

Figure M.4: Initial Efficiency for filter 34A with pleating density 34 pleats/100 mm at flow rate of 3500 m^3/h.

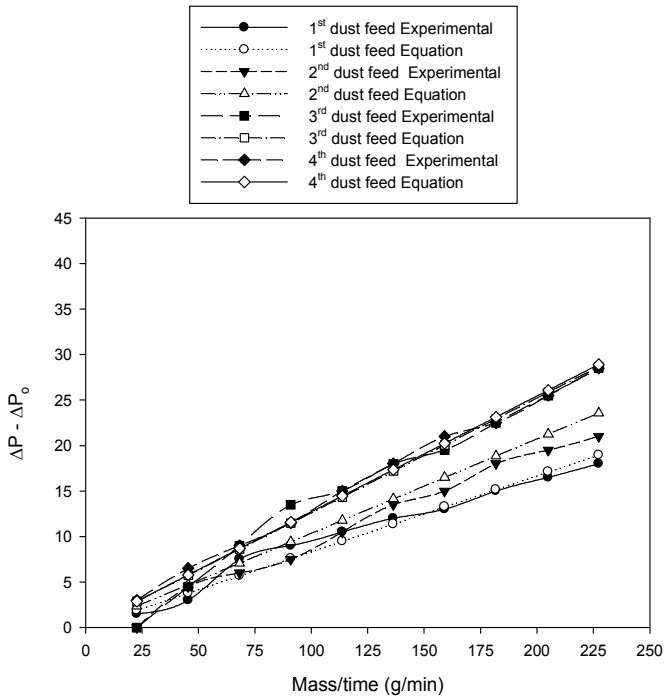

Figure M.5: Initial Efficiency for filter 28B pleating density 28 pleats/100 mm at flow rate of 3500 m^3/h.

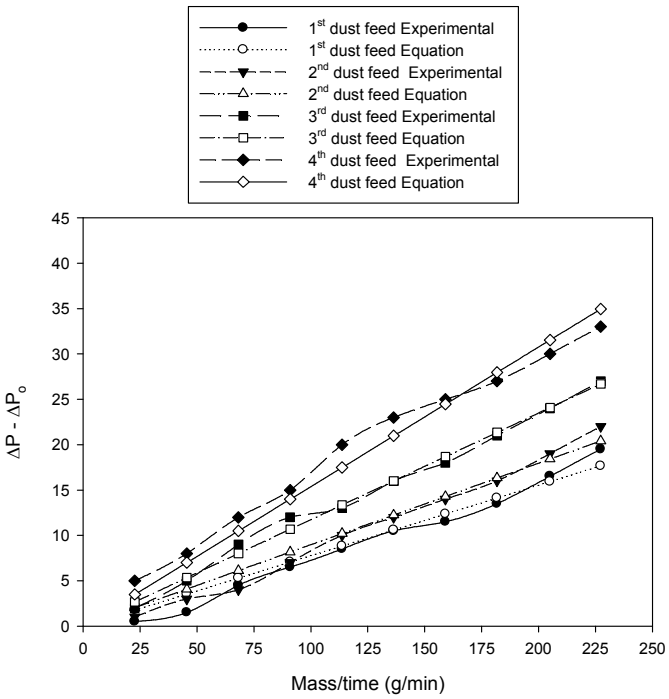

Figure M.6: Initial Efficiency for filter 30B pleating density 30 pleats/100 mm at flow rate of 3500 m^3/h.

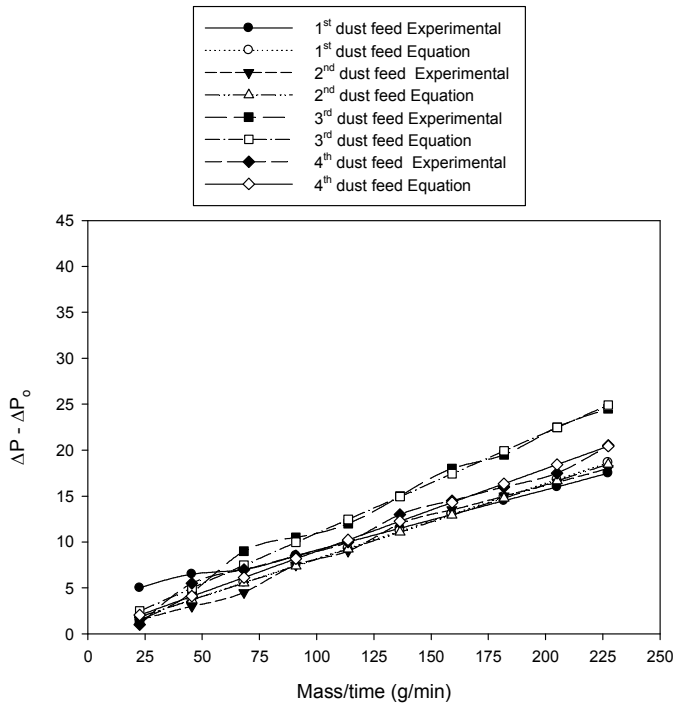

Figure M.7: Initial Efficiency for filter 32B pleating density 32 pleats/100 mm at flow rate of 3500 m^3/h.

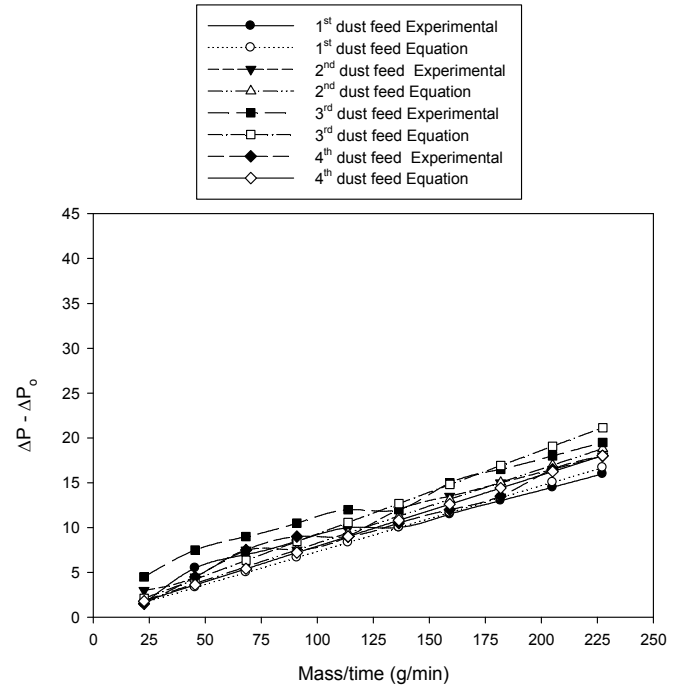

Figure M.8: Initial Efficiency for filter 34B with pleating density 34 pleats/100mm at flow rate of 3500 m^3/h.

Test	Width (mm)	Thickness (mm)	Load peak (N)	Stress peak (N/mm^2)	Strain break (%)	Elong@ break (mm)	Young's Modulus (N/mm^2)
1	25.5	0.3	17.6	2.3	1.0	1.0	271
2	24.9	0.3	16.7	2.3	1.2	1.2	231
3	24.9	0.3	14.4	1.8	1.2	1.2	241

Figure N.1: Modulus of elasticity measurement of three samples of the filtration media used in this study.

Test	Load Cell	Test Speed	Test Type	Pretension
1	5000 N	5 mm/min	Cross head movement	off

Figure N.2: Machine settings for the Testometric FS 150universal testing machine.

Appendix O

Publications

This study has produced three publications listed below:

1- Al-Attar I.S., Wakeman, R.J., Tarleton, E.S., and Husain A., 2009. The effect of pleat count and air velocity on the initial pressure drop and fractional efficiency of HEPA filters, *Filtration Journal*, **10** (3), 200-206.

2- Al-Attar I.S., Wakeman, R.J., Tarleton, E.S., and Husain A., 2010. Physical and chemical characterization of Kuwaiti atmospheric dust and synthetic dusts: Effects on the pressure drop and fractional efficiency of HEPA filters, *The 10th International Conference for Enhanced Building Operations,* Kuwait Institute of Scientific Research, KISR, Kuwait.

3- Al-Attar I.S., Wakeman, R.J., Tarleton, E.S., and Husain A., 2011. The effect of face velocity, pleat density and pleat Orientation on the most penetrating particle size, pressure prop and fractional efficiency of HEPA filters, *Filtech Europa* (II)**,** 318-329.

FILTRATION

ISSN 1479-0602

the international journal for filtration and separation



The FILTRATION Society

AFS

FILTRATION is the official journal of The Filtration Society and the American Filtration & Separations Society

INTRODUCTION

It is mandatory that water, after having been used and contaminated as in the case of municipal wastewater, has to be collected and purified as far as possible before it is discharged to the natural water cycle. The membrane process ultrafiltration has been shown to be a very reliable possibility to disinfect and purify the wastewater downstream of the biological treatment steps by separating all suspended solids and parts of the macromolecules. Thus, as well as the separation of bacteria and viruses, a certain reduction of COD, BOD_5 and phosphorus can also be achieved.

Ultrafiltration for the purification or disinfection of the secondary effluent from municipal wastewater treatment plants is becoming an important tool in global water management strategies. Similar to membrane bioreactor technology, where ultrafiltration is an integral part of the biological treatment plant itself, the post-treatment of effluents of conventional sewage treatment plants has reached acceptance as a reliable process step in wastewater treatment[1].

FAECAL CONTAMINATION OF BIOLOGICALLY TREATED MUNICIPAL WASTEWATER

The importance of this wastewater treatment step can be deduced from the fact that the effluent of municipal wastewater treatment plants (WWTP) still contains a large number of micro-organisms after biological treatment, including pathogenic agents such as bacteria, viruses and parasites. Their amount is reduced in the biological treatment process, for example, for *Escherichia coli*, used as one 'indicator organism' for faecal pollution, usually from 10^7 colony forming units per 100 millilitre (cfu/100 mL) to about 10^5 cfu/100 mL[2,3]. The majority of the pathogenic agents originate from the digestive tracts of humans and animals[4].

DEFINITION OF 'DISINFECTION OF WASTEWATER'

With wastewater disinfection the term disinfection is not employed in the strict medical sense as 'destruction or deactivation of all pathogenic micro-organisms', but rather as 'treatment of wastewater or sludge to reduce the activity of pathogenic agents below a certain laid down value'. The reduction can also be effected by retention. Sterilisation means the 'destruction or removal of all micro-organisms including their permanent forms' (which can be achieved by thermal or filtration methods). The terms decontamination and hygienisation are not specific and

---

THE EFFECT OF PLEAT COUNT AND AIR VELOCITY ON THE INITIAL PRESSURE DROP AND FRACTIONAL EFFICIENCY OF HEPA FILTERS

Iyad S. Al-Attar[1], Richard Wakeman[1,2] (richard.wakeman@lineone.net), SteveTarleton[1] and Adel Husain[3]

[1]Department of Chemical Engineering, Loughborough University, Loughborough, LE11 3TU, UK.
[2]Consultant Chemical Engineer, Clyst St Mary, Exeter, EX5 1DD, UK.
[3]Kuwait Institute for Scientific Research, Department of Building and Energy Technologies P.O. Box 24885, Safat, Kuwait, 305-343, Kuwait.

The importance of clean air to the well-being of people and industrial applications has highlighted the critical role of air filter performance. Accurate prediction of filter performance is important to estimate filter lifetime and reduce both energy and maintenance operating costs. To ensure appropriate filter selection for a specific application, the effects of pleat count and surface area on filter design and performance have been investigated. This paper examines the effects of air velocity on permeability during operation of HEPA pleated V-shaped filters, and the effect of pleat count on the initial pressure drop and fractional efficiency using DEHS testing according to DIN 1822. An empirical equation for predicting the efficiency of the filter is suggested.

INTRODUCTION

Air filters are expected to separate and retain particles on or within the internal structure of a filter medium to remove aerosol particles from air at different efficiencies with the least possible resistance. High Efficiency Particulate Air (HEPA) filters are made from fibrous media. They are widely used in applications such as operating theatres, the pharmaceutical industries, gas turbines, space stations, clean rooms, and semiconductor industries, amongst many others. HEPA filters are required to remove particles from a gas

stream with very high efficiencies at the least possible pressure drop. Removal efficiency and pressure drop are therefore the main filtration performance characteristics.

Although several authors have studied the performance of clean filters[1-3], the literature on the clean HEPA pleated filters is quite limited[4-6]. This paper investigates the effect of pleat count, surface area, and filter medium permeability on filter design and performance in terms of initial fractional efficiency and pressure drop.

FILTER PROPERTIES

The experimental work involved the testing of glass fibre pleated cartridges of HEPA Class H10 according to DIN 1822[7]. Eight filters were manufactured by EMW Filtertechnik with pleating densities varying from 28 to 34 pleats per 100 mm. Table 1 lists all the filters used for testing with their corresponding surface areas. The manufactured filters were divided into two groups, A and B. Both groups underwent similar testing procedures and were challenged with DEHS to give data for the initial fractional efficiency. Figure 1 shows the face dimensions of 592x592 mm with a depth of 400 mm. The filter cassette has a V-shape bank which contains eight pleated media panels.

The glass fibre media used in these filters is shown in Figure 2. Glass fibre filtration media was selected for all experiments in this work as it exhibits better resistance to high temperatures and has smaller fibre size compared to synthetic media. Glass fibre media are highly porous with a low resistance to air flow. The filter's performance is affected by several variables such as filter medium thickness, permeability, packing density, fibre diameter as well as the design of the filter module. Operating conditions such as filtration velocity and temperature also affect filter performance, in addition to the characteristics of the aerosol such as particle size distribution, particle shape and density. The properties of the media are listed in Table 2.

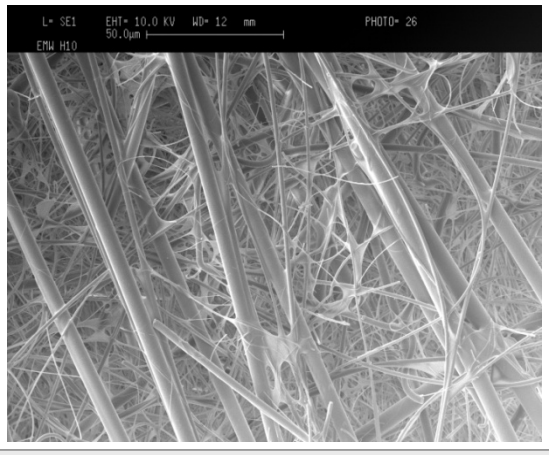

Figure 2: Image of the glass fibre HEPA filter medium (Class H10 according to DIN 1822).

Filter	Pleat density (pleats/100 mm)	Surface area (m^2)
28A	28	23.9
28B	28	24.6
30A	30	26.6
30B	30	26.6
32A	32	27.3
32B	32	27.3
34A	34	28.8
34B	34	28.9

Table 1: The filters tested and their surface areas.

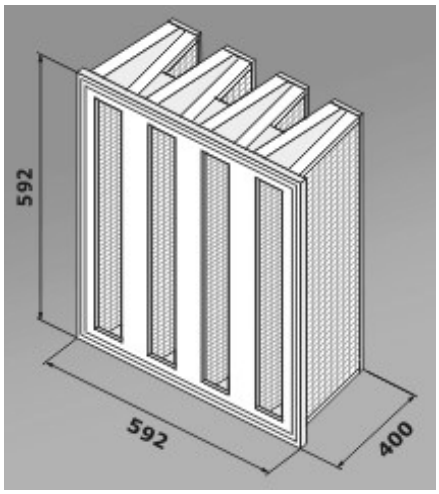

Figure 1: Pleated filter with V shape design (EMW Filtertechnik).

PLEATED MODULE PROPERTIES

Pleating the filter medium provides larger surface area in a given space, which increases particle loading capacity per unit area when compared with a flat sheet medium. Pleated medium panels are more stable than

Fibre diameter range (µm)	0.5-8.5
Average fibre diameter (µm)	2.1
Media thickness (µm)	500
Packing density (µm)	0.06
Porosity (%)	94
Fibre cross-section	circular

Table 2: Properties of the HEPA (H10) filter medium.

a flat sheet of the same medium, which is inclined to deform and eventually rupture. Another major advantage of increasing the surface area is to decrease the air approach velocity to the medium, which translates into an increase in the aerosol's residence time inside the medium. This increases the probability of particle-fibre contact and leads to an enhancement of diffusional capture efficiency. However, an excessive number of pleats or overpleating in a given area within a cartridge may also lead to failure by rupturing the filter medium. Consequently, the pleating density has to be optimized in order to provide the desired efficiency at the least possible pressure drop. Four different pleating densities were chosen for that purpose in this work.

Previous studies have highlighted the optimal pleat count. Chen *et al.*[5] developed a numerical finite element model to optimize the design of the pleats of filter materials with different permeabilities. Their results show that for a given pleat height, the optimal pleat density increases as the filter media permeability decreases. Currently, filter manufacturers have the same pleat density for all filter classes. This may signify ineffective use of the media since less pleat density is needed with lower filter classes. On the other hand, optimal pleat density also has to be considered from an efficiency point of view. For example, a pleat count might be optimal from a pressure drop standpoint, but it may not be able to achieve the desired efficiency. Therefore, optimal pleat density should be addressed in conjunction with efficiency.

CLEAN GAS PERMEATION

The passage of the clean gas through a filter enabled the pressure drop and efficiency to be measured. There is no dust loading at this stage of the testing. The Reynolds number was used to verify the flow regime in the testing tunnel and through the filter medium. The Reynolds numbers for the filter medium (using the fibre diameter) at the flow rates of 500 and 5000 m^3/h were 0.00122 and 0.0122, respectively. Therefore, the flow inside the filter medium was laminar. The Reynolds numbers in the rectangular feed duct to the filter (with a hydraulic diameter of 610 mm) at flow rates of 500 and 5000 m^3/h were 14,476 and 144,760 respectively, indicating that the flow inside the duct was turbulent.

The flow inside the filter medium can be interpreted using Darcy's Law to enable calculation of the permeability, k:

$$k = \frac{\mu V h}{\Delta p} \qquad (1)$$

where μ is the air viscosity, V the approach velocity of the air, h the filter medium thickness and Δp the pressure drop across the medium. The initial pressure

Filter	28A (23.9 m^2)			30A (26.6 m^2)			32A (27.3 m^2)			34A (28.8 m^2)		
Q (m^3/h)	Δp (Pa)	V_f (mm/s)	k x10^{-12} (m^2)	Δp (Pa)	V_f (mm/s)	k x10^{-12} (m^2)	Δp (Pa)	V_f (mm/s)	k x10^{-12} (m^2)	Δp (Pa)	V_f (mm/s)	k x10^{-12} (m^2)
500	14	5.78	3.82	18	5.22	2.68	14	50.84	3.36	15	4.82	2.97
1000	30	11.57	3.57	30	10.44	3.22	27	10.17	3.48	29	9.64	3.07
1500	47	17.36	3.42	47	15.65	3.08	44	15.25	3.21	45	14.45	2.97
2000	66	23.12	3.24	65	20.86	2.97	63	20.34	2.99	63	19.27	2.83
2500	87	28.90	3.08	86	26.08	2.81	83	25.42	2.83	81	24.09	2.75
3000	111	34.68	2.89	108	31.30	2.68	105	30.50	2.69	105	28.91	2.55
3500	135	40.46	2.78	132	36.52	2.56	129	35.59	2.55	128	33.72	2.44
4000	162	46.24	2.64	159	41.74	2.43	155	40.67	2.43	153	38.54	2.33
4500	191	52.02	2.52	188	46.96	2.31	183	45.75	2.31	182	43.36	2.20
5000	222	57.80	2.41	218	52.20	2.21	213	50.84	2.21	213	48.18	2.09
Filter	28B (24.6 m^2)			30B (26.6 m^2)			32B (27.3 m^2)			34B (28.9 m^2)		
Q (m^3/h)	Δp (Pa)	V_f (mm/s)	k x10^{-12} (m^2)	Δp (Pa)	V_f (mm/s)	k x10^{-12} (m^2)	Δp (Pa)	V_f (mm/s)	k x10^{-12} (m^2)	Δp (Pa)	V_f (mm/s)	k x10^{-12} (m^2)
500	17	5.64	3.07	15	5.23	3.22	15	5.09	3.14	15	4.80	2.96
1000	30	11.29	3.48	30	10.46	3.22	29	10.19	3.25	29	9.61	3.06
1500	47	16.94	3.33	48	15.69	3.02	45	15.29	3.14	47	14.41	2.84
2000	66	22.58	3.17	66	20.92	2.93	63	20.38	2.99	63	19.21	2.82
2500	86	28.23	3.04	87	26.15	2.81	84	25.48	2.81	84	24.01	2.64
3000	108	33.88	2.90	111	31.38	2.61	107	30.57	2.64	107	28.82	2.49
3500	134	39.52	2.73	136.5	36.61	2.47	131	35.67	2.52	131	33.62	2.37
4000	161	45.17	2.60	165	41.83	2.35	158	40.76	2.39	159	38.42	2.24
4500	188	50.81	2.50	193.5	47.06	2.24	186	45.86	2.28	186	43.22	2.15
5000	218	56.46	2.40	226.6	52.29	2.13	216	50.95	2.18	218	48.03	2.04

Table 3: Initial pressure drop, face velocity and permeability for different pleating densities.

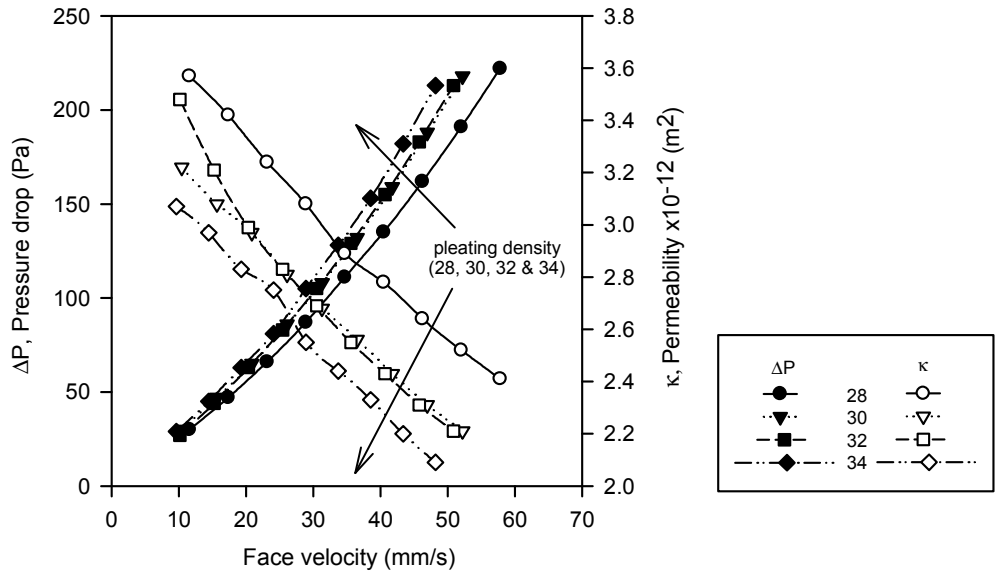

Figure 3: Initial pressure drop and permeability versus face velocities for Group A filters for different pleating densities.

drop was measured and this is shown in Table 3 at different flow rates ranging from 500 to 5000 m^3/h at increments of 500 m^3/h, together with the corresponding permeability values. A sample of the data is plotted in Figure 3 to show the non-linear variation of pressure drop with flow rate, and the typical variation of permeability with approach velocity is also shown in Figure 3.

Table 3 lists the permeabilities for all corresponding pressure drops and face velocities. It can be seen that as the flow rate (and face velocity) increases, the permeability decreases (Figure 3). As the pleat density increases, permeability is reduced. For both filter groups A and B, permeability remained the same as the pleating density increased from 30 to 32 pleats/100 mm. Figure 4 shows that filters 30B and 32B have the same permeability for different face velocities. Filter 30A exhibited higher pressure drop response than 28A and 28B with surface areas 23.9 and 24.6 m^2, and consequently its permeability was reduced. As the pleating density increased from 26.6 to 27.3 m^2 for filters 30B to 32B, the latter exhibited lower pressure drop and higher permeability.

The permeability change is due to losses in surface area in the filtration medium or to compression of the medium. The Darcy model indicates a linear variation

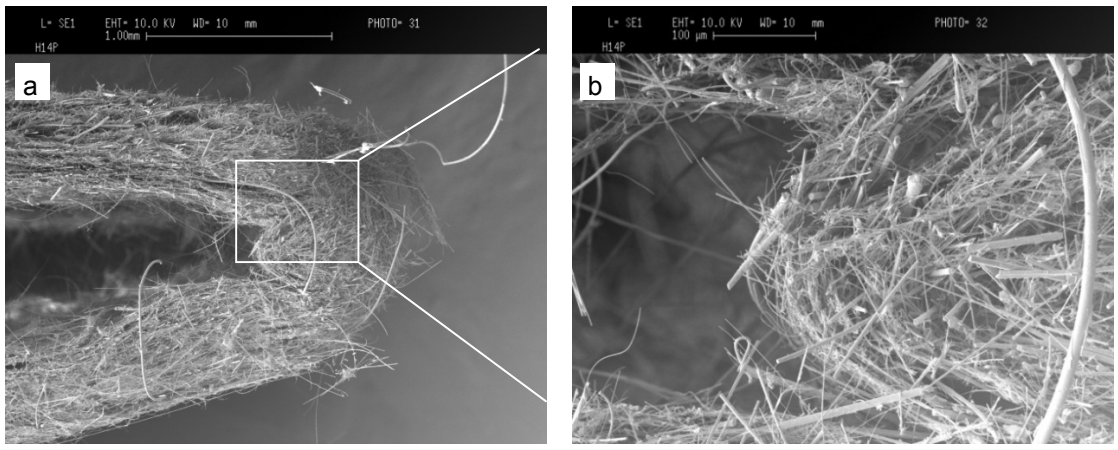

Figure 4: Views showing the crease in a mini-pleat: (a) Compression at the inner bend of a single pleat of the glass fibre media used, and (b) an enlarged view of the compressed zone of the pleat.

of pressure drop with flow rate and is only valid when there is no compression of the filtration medium. For a pleat there can be a loss of media surface due to pleat crowding and/or expansion of pleats. Media distortion at the crease of the pleat also influences the filter surface area losses; the effect of compression at the inner surface and expansion at the outer surface of the crease is shown in Figure 4.

The higher the number of pleats, so the more geometrical deformation that can be expected to take place. Therefore, additional permeability reduction is expected in higher pleating densities such as with 32 and 34 pleats/100 mm. An additional deformation or buckling is expected to take place in the overall pleated panel which would also lead to loss of surface area and a subsequent reduction in permeability. This sort of bulking could also lead to fracture of the pleated panel during operation.

INITIAL EFFICIENCY MEASUREMENT USING DEHS

The initial efficiencies were measured for all filters and flow rates using a PMT LPS particle counter capable of measurements over the size range 0.065 to 0.9 µm. The filters were challenged with DEHS aerosol in accordance with the DIN 1822 standard. In these experiments the flow rates were varied from 500 to 3000 m^3/h in increments of 500 m^3/h. Such measurements are of critical importance in determining the MPPS (Most Penetrating Particle Size) for each flow rate, and hence to enable the definition of the filter class. By way of example, Figure 5 illustrates the initial efficiency measurements for filter 28B which is typical of the results obtained.

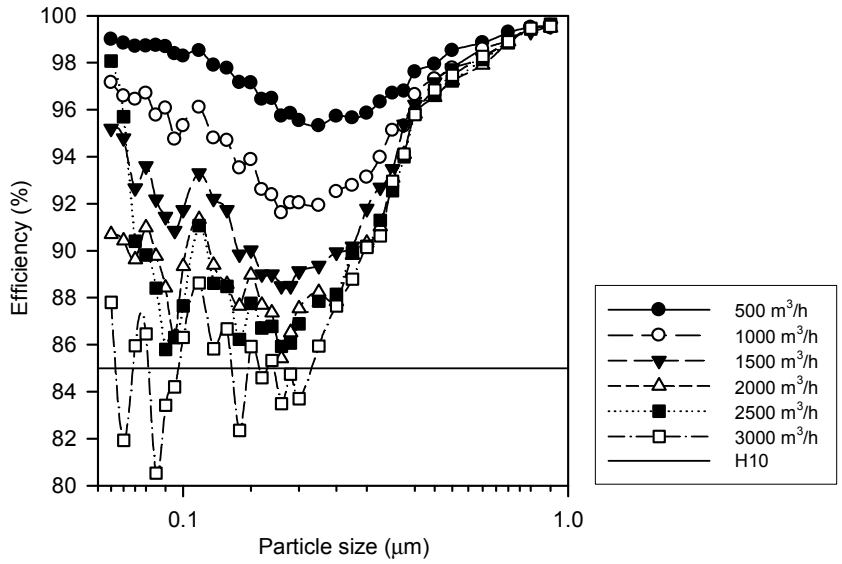

Figure 5: Initial efficiency (DIN 1822) vs. particle size for different flow rates (filter 28B).

	Diffusion term	Interception term	Remarks
Lee and Liu[8]	$E_D = 2.6\left(\frac{1-\alpha}{Ku}\right)^{1/3} Pe^{-2/3}$	$E_R = \left(\frac{1-\alpha}{Ku}\right)^{1/3} \frac{R^2}{1+R}$	
Liu and Rubow[9]	$E_D = 1.6\left(\frac{1-\alpha}{Ku}\right)^{1/3} Pe^{-2/3} C_d$	$E_R = 0.6\left(\frac{1-\alpha}{Ku}\right)^{1/3} \frac{R^2}{1+R} C_r$	$C_d = 1+0.388Ku\left[\left(\frac{1-\alpha}{Ku}\right)Pe\right]^{1/3}$ $C_r = 1+\frac{1.996Ku}{K}$
Payet *et al.*[10]	$E_D = 1.6\left(\frac{1-\alpha}{Ku}\right)^{1/3} Pe^{-2/3} C_d C_d'$	$E_R = 0.6\left(\frac{1-\alpha}{Ku}\right)^{1/3} \frac{R^2}{1+R} C_r$	$C_r = \frac{1}{1+E_D}$

Table 4: Efficiency models examined in this study.

Flow rate (m^3/h)	Filter 28A		Filter 30A		Filter 32A		Filter 34A	
	β_1	β_2	β_1	β_2	β_1	β_2	β_1	β_2
500	1.65	3.17	1.59	3.29	1.55	3.44	1.79	2.72
1000	1.98	3.22	1.82	3.37	1.85	3.27	1.81	3.36
1500	1.91	3.46	1.88	3.19	1.96	3.34	2.22	3.05
2000	2.13	3.44	2.28	3.19	2.33	3.06	2.44	3.06
2500	2.43	3.37	2.29	3.42	2.61	3.31	2.32	3.38
3000	2.78	3.30	2.73	3.18	2.46	3.45	2.74	3.18

Table 5: The values β_1 and β_2 obtained for the different flow rates with Group A filters.

MODELS APPLIED TO DEHS EFFICIENCY MEASUREMENTS

The efficiency models listed in Table 4 were fitted to the experimental data. It was found that the Lee and Lui[8] model showed the same trends as the experimental data and it was therefore chosen for further study as a possible engineering model to describe the initial efficiency of the pleated HEPA filters.

The Lee and Liu model for separation efficiency was rewritten as:

$$\eta = \beta_1 \left(\frac{1-\alpha}{Ku} \right)^{1/3} Pe^{-2/3} + \beta_2 \left(\frac{1-\alpha}{Ku} \right)^{1/3} \frac{R^2}{1+R} \qquad (2)$$

where β_1 and β_2 are constants to be derived from the experimental data, α is the fibre packing fraction, Ku the Kuwabara number, Pe the Peclet number and R is the ratio of the particle to fibre diameters. Table 5 collates the β_1 and β_2 values for filter Group A at the various flow rates. In addition, Figure 6 shows the agreement between the efficiency experimental results and equation (2) for flow rates ranging from 500 to 3000 m^3/h. It can be concluded that interception for all tested filters varies little with flow rate and the number of pleats. On the other hand, the diffusion contribution to efficiency becomes more dominant as the flow rate increases. Equation (2) tends to overestimate the diffusional efficiency, and suggests that the equation form may not be correct for filtration onto larger scale pleated media.

CONCLUSIONS

From the work presented in this paper the following conclusions can be drawn:

- Air filter permeability decreases with the increase of pleating density which is in agreement with a previous numerical study[5].
- The MPPS particle size decreases with the increase of filter face velocity for all pleating densities with a given surface area and filter medium. The MPPS increases slightly or remains constant as the pleating density increases.
- Filter Class H10 efficiency requirements according to Standard DIN 1822 were achieved for flow rates of 2000 to 2500 m^3/h for most filters. On the other hand, a higher filter class (H11) was achieved for a flow rate of 500 m^3/h for filters with 28 pleats/100 mm density.
- Higher mobility particles lower the diffusion collection efficiency of the filter.
- Efficiency decreases with increasing filter face velocity for particle sizes less than the MPPS at this face velocity. Beyond the MPPS, increasing the filter face velocity also increases the efficiency of filter. The minimum efficiency decreases with increasing flow rate, with the lowest efficiency occurring at the highest flow rate of 3000 m^3/h.
- The interception coefficient for all tested filters varies little with flow rate and the number of pleats. On the other hand, the coefficient applying to the diffusion contribution in the efficiency becomes greater as the flow rate increases.

REFERENCES

1. Davies C.N., 1973, *Air Filtration*, Academic Press, New York.
2. Brown R.C., 1993, *Air filtration: An integrated approach to the theory and application of fibrous filters*, Pergamon Press, Oxford.
3. Letourneau P., Mulcey Ph. and Vendel J., 1990, Aerosol penetration inside HEPA filtration media, *Proc. 21st DOE/NRC Nuclear Air Cleaner Conference*, pp.799-811, San Diego.
4. Wakeman R.J., Hanspal N.S., Waghode A.N. and Nassehi V., 2005, Analysis of pleat crowding and medium compression in pleated cartridge filters, *Trans IChemE*, **83**(A10),1246-1255.
5. Chen D.R., Pui D.H. and Liu B.Y.H., 1995, Optimization of pleated filter designs using a finite-element numerical model, *Aerosol Science and Technology*, **23**, 579-590.
6. Fabbro L.D., Laborde J.C., Merlin P. and Ricciardi L., 2002, Air flows and pressure drop modelling for

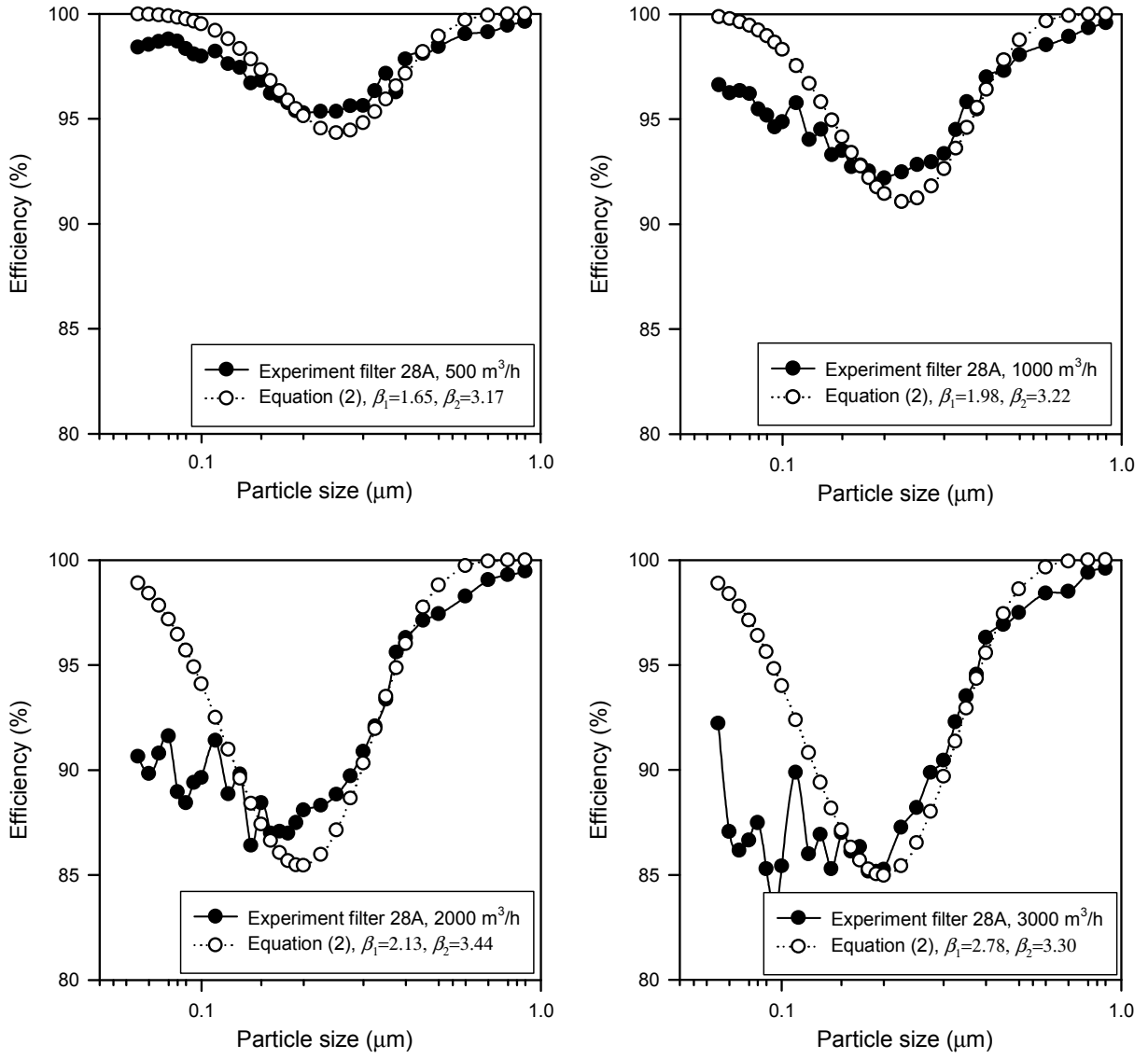

Figure 6: Initial efficiency comparison between experimental results and the theoretical model of Lee and Liu[8].

different pleated industrial filters, *Filtration & Separation*, **39**(1), 34-40.

7. DIN 1822-1, 1998, High efficiency air filters (HEPA and ULPA) - Part 1: Classification, performance testing, marking.
8. Lee K.W. and Liu B.Y.H., 1982, Theoretical study of aerosol filtration by fibrous filters, *Aerosol Science and Technology*, **1**(2), 147-161.
9. Liu B.Y.H. and Rubow K.L., 1986, Air filtration by fibrous media in *Fluid Filtration: Gas*, **1**, ASTM STP 975, Raber R.R. (Ed.), *American Society for Testing and Materials*, Philadelphia. 1-12.
10. Payet S., Boulaud D., Madelaine G. and Renoux A., 1992, Penetration and pressure drop of HEPA filter after loading with submicron liquid particles, *J. Aerosol Sci.,* **23**, 723-735.

PHYSICAL AND CHEMICAL CHARACTERIZATION OF KUWAITI ATMOSPHERIC DUST AND SYNTHETIC DUSTS: EFFECTS ON THE PRESSURE DROP AND FRACTIONAL EFFICIENCY OF HEPA FILTERS

I.S. Al-Attar[1], R.J. Wakeman[1,2], E.S.Tarleton[1] and A.Husain[3]
[1]Department of Chemical Engineering, Loughborough University, LE11 3TU, UK.
[2]Consultant Chemical Engineer, Clyst St Mary, Exeter, EX5 1DD, UK.
[3]Kuwait Institute for Scientific Research, Department of Building and Energy Technologies P.O. Box 24885, Safat, Kuwait, 305-343, Kuwait.

ABSTRACT
The importance of clean air to the indoor air quality affecting the well-being of human occupants and rising energy consumption has highlighted the critical role of air filter performance. Actual performance of air filters installed in air handling units in Kuwait tends to deviate from the performance predicted by laboratory results. Therefore, accurate filter performance prediction is important to estimate filter lifetime, and to reduce energy and maintenance operating costs. To ensure appropriate filter selection for a specific application, particulate contaminants existing in the Kuwaiti atmospheric dust were identified and characterized both physically and chemically and compared to the synthetic dust used in laboratories. This paper compares the physical and chemical characterization Kuwaiti atmospheric dust with the available commercial synthetic dusts. It also tests full scale HEPA pleated V-shaped filters used in Heating Ventilation and Air Conditioning (HVAC) and gas turbine applications to study the effect of different synthetic dust types and their particle size distributions on the pressure drop and fractional efficiency using DEHS testing according to DIN 1822.

KEYWORDS
Air Filters, Fractional Efficiency, Gas Cleaning, Glass Fibre, HEPA filter, Permeability, Pressure Drop.

1 Filtration of Air

The process of air filtration is a complex process which is influenced by several factors pertaining to the dust physical and chemical characteristics. To better understand and evaluate the filtration process and influential parameters affecting the filtration performance of air filters, an in-depth analysis of the dust must be conducted.

Although several authors have studied the performance of clean filters [1-3] and other authors considered dust loaded filters [4-5], the literature was limited to the study of flat filters. Studies have considered loading samples of filters with monodispersed [6] and polydispersed [7] aerosols. Literature on the HEPA pleated filter is limited [8-10]. Other authors studied the effect of particle size on the pressure rise [11-15] of filters but did not consider a full scale HEPA filter constructed in a V-shape cartridge with variable pleating density. This paper investigates the effect of synthetic polydispersed dust type and pleat density on filter design and performance in terms of fractional efficiency and pressure drop.

2. Filter Properties

The experimental work involved the testing of glass fibre pleated cartridges of HEPA Class H10 according to DIN 1822 [16]. Eight filters were manufactured by EMW Filtertechnik with pleating densities varying from 28 to 34 pleats per 100 mm. Table 1 lists all filters used for testing with their corresponding surface areas. The manufactured filters were divided into two groups, A and B. Both groups underwent similar testing procedures and were challenged with DEHS to give data for the initial fractional efficiency. Figure 1 shows the face dimensions of 592 x 592 mm with a depth of 400 mm. The filter cassette has a V-shape bank which contains eight pleated media panels.

Table 1: The filters tested and their surface areas.

FILTER	PLEAT DENSITY (Pleats/100 mm)	SURFACE AREA (m^2)
28A	28	23.9
28B	28	24.6
30A	30	26.6
30B	30	26.6
32A	32	27.3
32B	32	27.3
34A	34	28.8
34B	34	28.9

Table 2: Properties of the filter medium.

HEPA (H10) FILTER MEDIUM	
Fibre Diameter Range	0.5-8.5 µm
Average fibre diameter	2.1 µm
Media Thickness	500 µm
Packing Density	0.06 µm
Porosity	94%
Fibre Shape	Circular

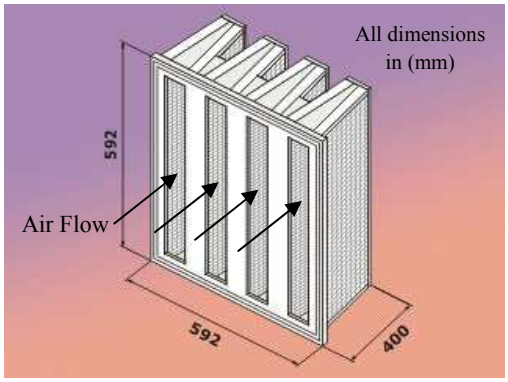

Figure 1: Pleated filter with the V shape design (EMW Filtertechnik).

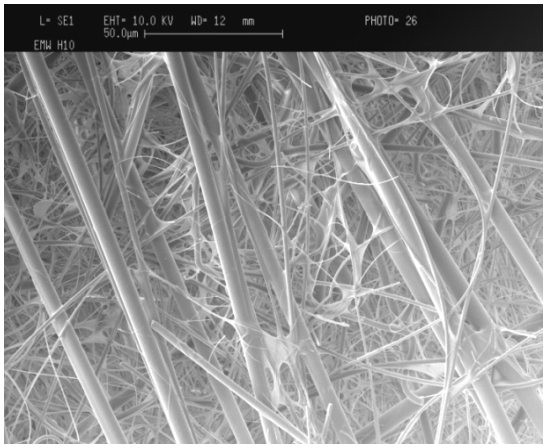

Figure 2: Image of the glass fibre HEPA filter medium (Class H10 according to DIN 1822).

The glass fibre media used in these filters is shown in Figure 2. Glass fibre filtration media was selected for all experiments in this work as it exhibits better resistance to high temperatures and has smaller fibre size compared to synthetic media. Glass fibre media are highly porous with a low resistance to air flow. Filter performance is affected by several variables such as filter medium thickness, permeability, packing density, fibre diameter as well as the design of the filter module. Operating conditions such as filtration velocity and temperature also affect the filter performance, in addition to the characteristics of the aerosol such as particle size distribution, particle shape and density. The properties of the media are listed in Table 2.

1.1 Dust Characterization

Kuwaiti and synthetic dusts were characterized physically and chemically to better learn about their behaviour in the filtration process. The physical and chemical characteristics of Synthetic dust were examined to choose one that represents the Kuwaiti atmospheric dust.

1.1.1 Chemical Characterization – EDAX

The three synthetic dusts; ASHRAE, SAE Fine and SAE Coarse were analyzed using *Energy Dispersive Analysis X-ray* (EDAX) to determine the chemical composition. The analysis shows that the Kuwaiti atmospheric dust is mainly silica and also contains aluminium, calcium, iron and some traces of potassium and magnetism. On the other hand, ASHRAE and SAE coarse dust contains carbon and they also consist of mainly silica. SAE fine dust contains aluminium, calcium and traces of potassium. From such chemical analysis, the ASHRAE dust seems to be the closest to the Kuwaiti dust from silica-content standpoint. However, analysis of the ASHRAE dust does not show any presence of aluminium, calcium and traces of potassium which are Pfound in the Kuwaiti dust. SAE fine and coarse on the other hand, contain aluminium, calcium and traces of potassium but have higher silica content than the Kuwaiti dust. In all Kuwaiti dust samples, the silica contents were higher than that of the ASHRAE content. Furthermore, ASHRAE dust contains cotton lint as shown in Figure 3 which is absent in the Kuwait dust.

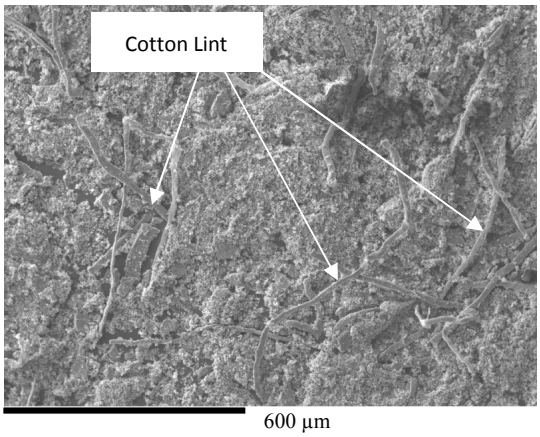

Figure 3: The existence of cotton lint in the ASHRAE dust.

While it is difficult to decide on the most representative dust using EDAX analysis, the SAE Fine dust seems to be the closest to the Kuwaiti atmospheric dust from a chemical composition stand point. Table 3 lists the chemical composition of samples of the Kuwait atmospheric dust, ASHRAE dust, SAE fine and SAE coarse dusts.

Table 3: The chemical composition of Kuwait atmospheric dust.

Element	Kuwait atmospheric	ASHRAE	SAE fine	SAE coarse
O	42.25	23.30	49.80	45.37
C	-	55.88	-	19.70
Mg	3.62	-	-	-
Al	7.75	-	4.31	-
Si	**29.18**	**20.82**	**38.80**	**34.93**
Ca	9.39	-	3.02	-
Fe	7.80	-	-	-
K	-	-	4.07	-
Totals	100.00			

1.1.2 Particle Size Distribution

While it is hard to obtain a commercially produced dust that fits the physical and chemical characterization of the Kuwaiti atmospheric dust, particle size analyses can give the particle size distribution of the Kuwaiti samples. Ten samples of Kuwaiti atmospheric dust were obtained from Kuwait Scientific Research Centre (KISR). The dust samples were then sized to obtain the particle size distribution using a Malvern MasterSizer. Each sample was inserted into an ultrasonic bath for one minute to ensure that the dust was dispersed. A 300RF lens was used which provides a size range between 0.05 and 880 μm. Since the Kuwaiti atmospheric dust was found from EDAX analysis to be mainly silica, a refractive index of 1.5 was used. The same refractive index was used for the synthetic dusts. Figure 4 shows the particle size distribution comparison between Kuwaiti atmospheric dust and the commercial synthetic dusts selected for the analysis.

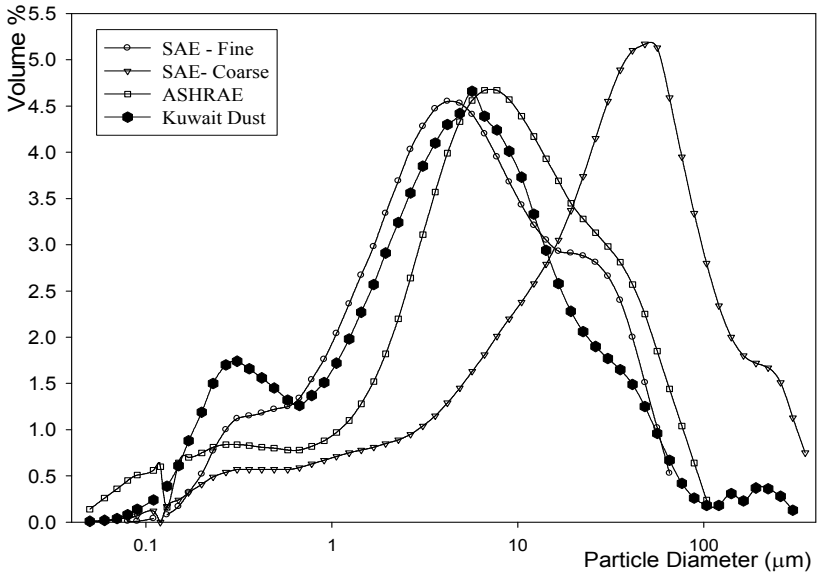

Figure 4: Particle Size distribution comparison between Kuwaiti Atmospheric Dust (sample 1) and commercially available dusts.

Sizing measurements revealed the dust size distribution of ASHRAE dust was dissimilar to the all of ten Kuwait dust samples as shown in Table 4. The size distribution of SAE coarse dust was also different from the Kuwaiti particle size distribution. This signified that each dust has different settling velocities, which increase rapidly with particle size and density. The particle size distribution of the SAE fine seems to be the closest to the Kuwaiti atmospheric dust. It can also be noticed that SAE coarse and fine dust can be considered as upper and lower limits in terms of size distribution to Kuwaiti atmospheric dust. Therefore, those two types were used for this study to conduct the comparison of the filter performance.

Table 4 lists the measured values of the mean diameters, volume mean diameters and surface area mean diameters of synthetic dusts in addition to the Kuwaiti one. The obtained specific surface area

mean diameter of ASHRAE and SAE coarse dust particles by Malvern MasterSizer are 1.84 µm and 1.75 µm respectively. Both measurements are lower than the surface area mean diameter of the Kuwait dust which has a range of 3.22 to 5.74 µm. The drag force is affected by the surface area of the particle which in turn means the drag force created by ASHRAE dust particle is lower than the Kuwait one. The mean surface area of SAE fine dust particles is 3.73 m^2/g which falls within the Kuwait atmospheric dust range of specific surface area mean diameter.

Table 4: Various experimental relevant diameters and properties of the Kuwaiti and Synthetic dusts under study.

	Mean Particle Size (µm)	**Volume Mean Diameter (µm)**	**Surface Area Mean Diameter (µm)**	**Specific Surface Area (m^2/g)**
KWT 1	5.03	14.14	1.34	4.47
KWT 2	5.11	25.85	1.21	4.94
KWT 3	4.94	27.63	1.04	5.74
KWT 4	8,54	35.52	1.31	4.58
KWT 5	6.94	21.44	1.54	3.54
KWT 6	13.24	31.09	1.69	3.22
KWT 7	6.43	34.20	1.16	4.71
KWT 8	6.26	18.15	1.35	4.43
KWT 9	6.36	26.86	1.45	4.13
KWT 10	7.32	26.86	1.53	3.93
ASHRAE	5.63 - 8.00	51.15	3.27	1.84
SAE Fine	10.24	36.23	1.61	3.73
SAE Coarse	33.18	57.18	3.41	1.75

1.1.3 Kuwaiti and Test Dusts

Prior to loading the filters under test with solid aerosol, it is imperative to characterize physically and chemically the commercially available dusts. Since most of the filters used in Kuwait are evaluated using ASHRAE dust, this dust was selected for this study in order to assess its appropriateness for filter performance via its similarities in physical and chemical characteristics to Kuwaiti atmospheric dust. The synthetic dusts selected were ASHRAE, SAE 726 coarse, and SAE 726 fine to include two different size distribution dusts.

ASHRAE synthetic dust is composed by weight of 72% standardized SAE 726 fine dust (Arizona Road Dust), 23% powdered carbon, and 5% cotton linters. Standardized air cleaner test dust is classified from dust gathered in a dessert area in Arizona. It is predominantly silica and has a mass mean diameter of approximately 7.7 µm, a geometric standard deviation of approximately 3.6, and density of approximately 2.7 g/cm^3.

The powdered carbon is carbon black in powder form, with ASTM D3765 CTAB surface of 27± 3 m^2/g, ASTM D2414 DBP adsorption of 0.68± 0.7 cm^2/g, and ASTM D3265 tint strength of 43 ± 4. The SAE 726 fine test dust is composed of mineral dust predominantly silica with other oxides present. It has a specific gravity 2.6 – 2.7 g/cm^3 [17]. On other hand, SAE 726 coarse dust is a naturally occurring mineral, which is predominantly SiO_2 with other oxides present. It has a mass mean diameter of approximately 7.7 µm, a geometric standard deviation of approximately 3.6, and density between 2.6 and 2.7 g/cm^3.

1.1.4 Reasons for Dust Selection

The particle shape of the Kuwaiti atmospheric dust along with ASHRAE Synthetic, SAE 726 coarse, and SAE 726 fine dusts was examined using a scanning electron microscope. Figures 5, 6 and 7 show that SAE coarse and fine dust as well the Kuwait atmospheric dust are mainly nonspherical particles. The drag force varies with the particle shape which in turn affects the aerodynamic behaviour. A spherical particle has higher velocity than an irregular particle with the same weight [18]. The aerodynamic behaviour of particles affects the filtration performance of air filters. Therefore, the angular velocity of irregular dust particles should be considered, and a modified equation of motion for spherical particles may be used to describe the non-spherical particle dynamics with more accuracy.

Clearly, the ASHRAE dust is not representative of Kuwaiti atmospheric dust as far as the particle shape is concerned. SAE 726 coarse, and SAE 726 fine dusts seem to be closer in this regard. However, particle shape similarity is not sufficient to select a representative dust since particle size

distribution and density measurements will also play a role in the verification process.

The true densities of all dusts were measured using a pycnometer. From a true density standpoint, all synthetic dusts have different densities when compared to the Kuwait atmospheric one. However, SAE 726 fine dust may be closer in terms of density than ASHRAE dust. The true densities of the dusts are listed in Table 5.

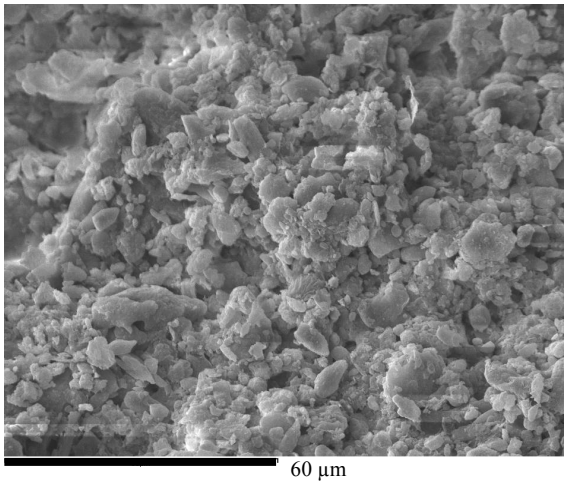

Figure 5: Scanning electron micrograph of Kuwait atmospheric dust.

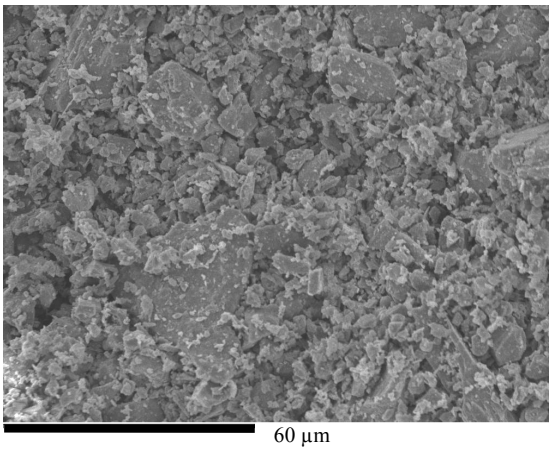

Figure 6: Scanning electron microscopic images of SAE fine dust.

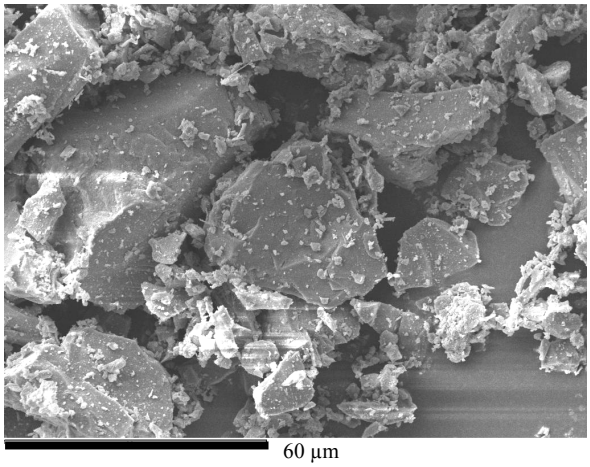

Figure 7: Scanning electron microscopic images of SAE coarse dust.

Table 5: True density measurement for Kuwaiti and Synthetic dust under study.

Dust	Mean Measured Density (g/cm^3)	Standard deviation of the three samples
ASHRAE 52/76	2.233	0.0416
SAE 726 Coarse	2.593	0.0611
SAE 726 Fine	2.613	0.0681
Kuwait Atmospheric	2.436	0.0737

For the scope of this experimental work, a series of filters (filter series A) was challenged by SAE fine while the series B filters were challenged by SAE coarse dust. Scanning electron microscope images of the same scale are shown of both dusts in Figures 6 and 7 for comparison purposes. It is evident that the SAE fine contains finer particle when compared to the SAE coarse dust. Dust particles of both dusts seem to have similar shape.

1.1.5 Particulate Matter in Kuwait Atmosphere

Several filter samples from different locations in Kuwait were examined using a scanning electron microscope to identify common air contaminants existing in the Kuwaiti atmosphere. Figure 8 shows SEM examination which revealed pollen grains deposition on the surface of the filter media. Pollen grains discharged by weeds, grasses and trees are capable of causing hay fever [19], and most are hygroscopic and therefore vary in mass with humidity [20]. A pollen count of 10 to 25 may make hay fever sufferers experience the first symptoms. The pollen grain found in the SEM examination of the filter media used in Kuwait ranged in size between 10 and 60 µm.

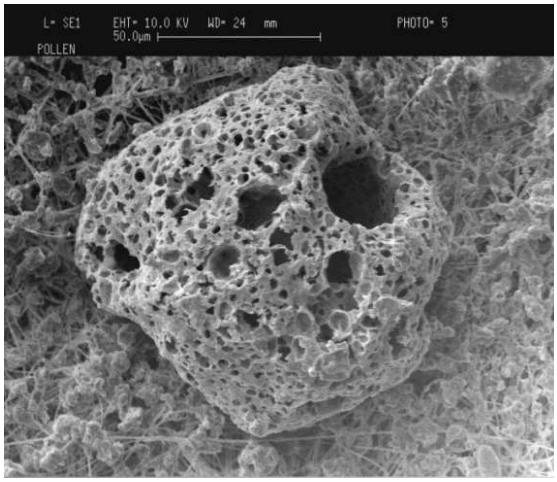

Figure 8: SEM examination of air filters used in air conditioning units in Kuwait.

2.2 Filter Efficiency Using Test Dusts

Description of initial filter behaviour constitutes a small part of the filter life time. While the study of clean filter performance is important, it does not predict the behaviour of the same filter during dust loading. When particle deposition begins to occur within the filtration medium, the filter's inner mechanical structure changes causing the overall efficiency and pressure drop to increase. Eventually, particles collect other particles leading to dendrite formation which would finally lead to dust cake formation. To better understand dust loaded filter performance, filter series A and B were loaded with SAE coarse and SAE fine dust respectively. Fractional efficiencies were measured after each dust feed every 500 m^3/h increment, stating at 500 m^3/h. On the other hand, the pressure drop responses were measured every five minutes at a single flow rate of 3500 m^3/h.

3 Effect of Pleating Density on Pressure Rise

A filter with 28 pleats per 100 mm was loaded with AC coarse dust. The 1000 g of dust was loaded in four increments each of 250 g. The pressure rise was always linear with time. The 1000 g was mainly deposited within the depth of the filter without a significant dust cake formation. Figure 9 shows the pressure drop response for different pleating densities for filter group A after each dust loading stage.

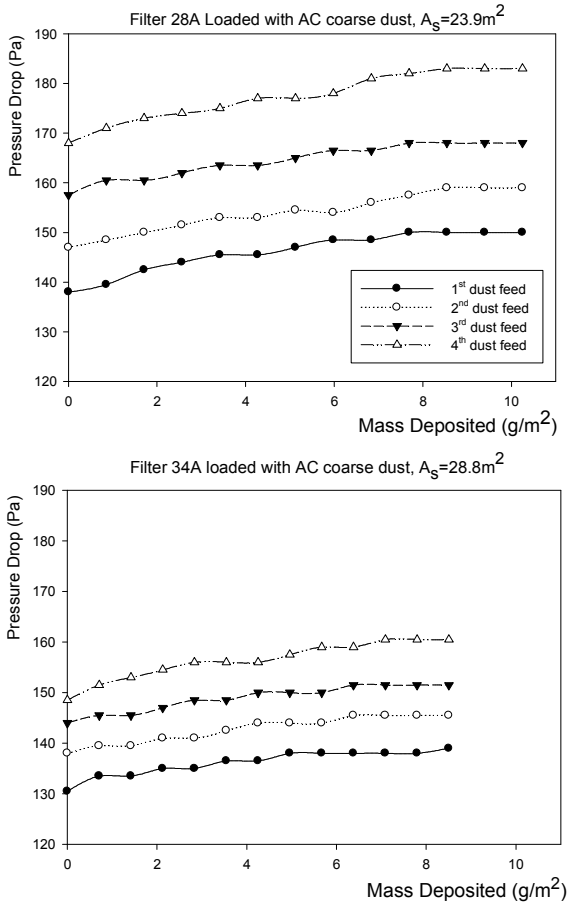

Figure 9: Behaviour of the time-dependent particle deposition in different pleating density filters (Group A) at a flow rate of 3500m^3/h.

As dust starts to be fed into the filter by means of a dust feeder, dust settlement into the depth of the filtration medium around the fibre and the rise in pressure drop is negligible. This is the so called the stationary filtration stage and it is represented by a linear response as shown in Figure 10. Filter 34A has the lowest pressure drop and a linear response which could be that the 1000 g of dust were not enough to make the filter depart from the stationary depth filtration to non-stationary filtration and finally to the dust cake formation. Furthermore, Filter 34A has the highest losses in the surface area and filter 38A has the least losses in the surface area. However, Filter 28A satisfies the efficiency requirement and its pressure drop response is acceptable and still a linear response. In other words, the 1000 g also did not form dust cake on the surface on the filter surface. This indicates that Filter 28A is more economical from cost point of view as well as from efficiency and pressure drop standpoints.

Figure 10(a) illustrates the pressure drop response after the fourth dust feed for 28 A and B for SAE coarse and fine dust respectively. It is evident that

the pressure drop response is higher for SAE fine dust which indicates that fine particles tend to penetrate further through the filter medium compared to the coarse particles of the SAE coarse dust. SAE fine dust particles settling into the depth of filtration medium causes the fibre diameter to increase and consequently changes to the depth of the filter as well as the porosity and as results increasing the drag force in the filter matrix. Since the drag force is directly proportional to the pressure drop, an increase in the latter is expected and was in fact, observed experimentally as shown in Figure 10(b). Similar observation and comment can be made for filters 30A and B as shown in Figure 10, however, the difference in the pressure drop response are smaller. This is reasoned to the fact the pleats are closer to each in the 30 pleats/100 mm density compared to the 28 pleats/100 mm.

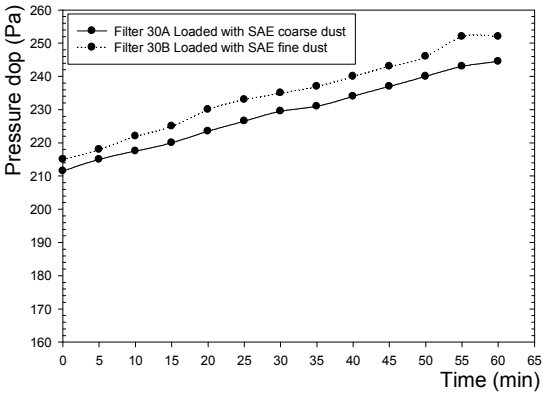

(a)

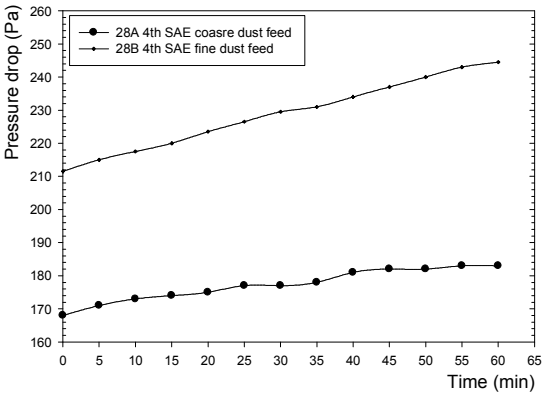

(b)

Figure 10: Pressure drop response for Filters (a) (30A) and (b) (28A) after the fourth dust feed.

Figure 11 shows pressure drop response versus mass deposited per surface area for filters of group A which indicated that the higher the pleating density the lower the pressure drop (this does not consider the losses of the surface area during operation). Filter 28A exhibits the highest pressure drop response when compared with other densities. On the other hand, the response of the 34A show the least response in pressure drop due to higher surface area provided. Figure 11 shows pressure drop response versus mass deposited per surface area for filter group B using fine dust; the differences in the pressure drop with varying pleating density is smaller than the coarse dust in group A filters. This is due to the fact that finer particles are more penetrating and are capable of occupy interstitial spaces inside the filter medium which is responsible for the rise in the pressure drop of the filter.

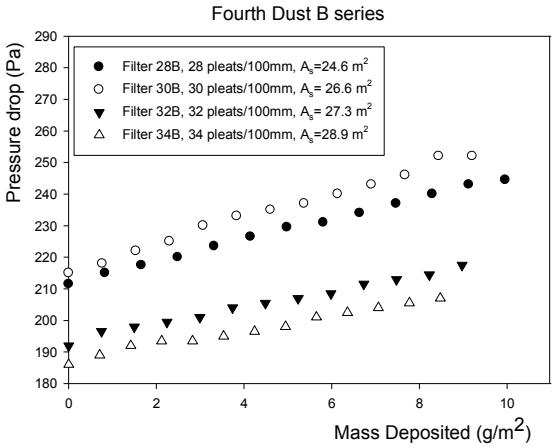

Figure 11: Pressure drop response versus mass deposited per surface area for filter group B using SAE fine dust.

The pressure drop response for the 34A and B filters are shown in Figure 12, which illustrates that the pressure drop response is smaller compared to the 28 pleats filters shown in the previous figure. It can be concluded that solid particles depositing within the fibrous structure change the geometry of the porous matrix which leads to substantial variations in the pressure drop and filtration efficiency.

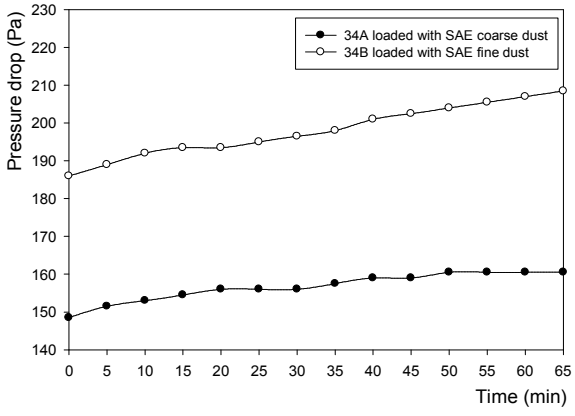

Figure 12: Pressure drop response for filters 34A and B after the fourth dust feed.

4 Effect of Mass of Coarse Dust Loaded on Filter Efficiency for Different Pleating Densities

The fractional efficiencies were plotted versus particle size for filter 28A after each dust feed of 250 g. All dust loading and efficiency measurements were measured at 3500 m^3/h. Figure 13 illustrates the increase of efficiency for each dust feed of SAE coarse dust as particle size and dust mass loading increases. Clearly, as more dust is loaded into the depth of the filtration medium, additional changes in the inner structure occur. Consequently, permeability decreases and as a results the pressure drop response increases. Furthermore, such effect is associated with an increase in efficiency and the fourth dust feed records the highest in efficiency according to Figure 13.

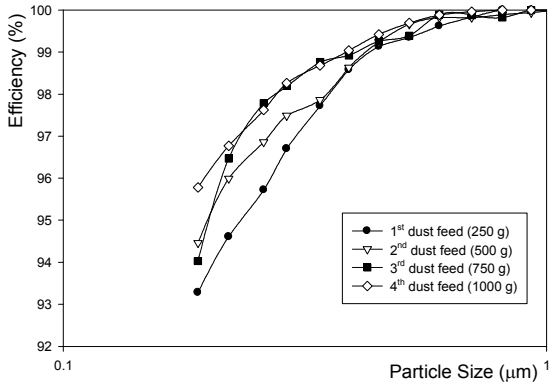

Figure 13: Efficiency after each SAE coarse dust feeding stages.

Figure 14 illustrates the effect of mass loading on efficiency for different pleating densities after the first dust feed. In addition, filter 32A recorded the lowest dust-loaded efficiency after the fourth feed. This excludes filter 32A from the competition for an optimal pleat count selection. Filter 34A recorded the highest dust loaded efficiency among other filters in its group, however, as the particle size increases; its efficiency recorded the lowest dust loaded efficiency. Furthermore, Filter 34A recorded earlier the highest losses in surface area prior to dust loading.

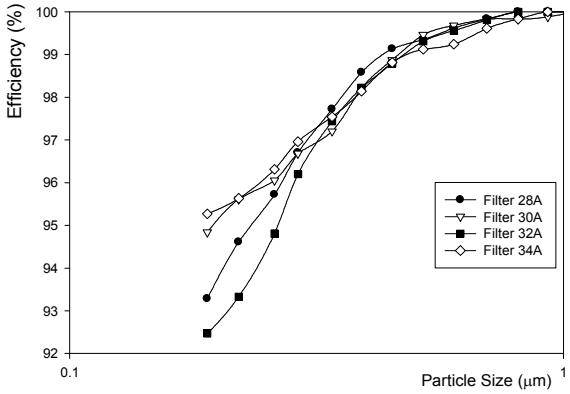

Figure 14: Efficiency after the fourth SAE coarse dust feeding stage for different pleating density.

5 Conclusions:

- ASHRAE dust is not representative dust of Kuwaiti atmospheric dust, due to differences in physical and chemical characteristics. SAE 726 fine dust is more representative of Kuwaiti dust.
- Kuwaiti atmospheric dust is mainly non spherical particles and is silica based. It also contains other contaminants such as pollen.
- The particle size distribution of Kuwaiti dust falls between the SAE fine and SAE coarse size distributions. Therefore, these synthetic dusts effectively act as lower and upper size distribution limits for the Kuwaiti atmospheric dust respectively.
- The pressure drop response of SAE fine dust was higher of that of the SAE coarse particles. This suggests that the smaller particles are more penetrating than coarse particle for a given filtration medium which is in this case the H10 [12] with fibre size range between 0.8-6 μm. This is in agreement with previous studies by [11-14]
- The MPPS (Most Penetrating Particle Size) decreases with the increase of filter face velocity for all pleating densities a given surface area and filter medium. The MPPS increases slightly or remains the same as the pleating density increases.
- Filter class H10 efficiency requirement according to Standard DIN 1822 was achieved for flow rates 2000-2500 m^3/h for most filters. On the other hand, higher filter class (H11) was achieved for a flow rate of 500 m^3/h for filters with 28 pleat/100 mm density.

6. References

1. Davies C.N., 1973, *Air Filtration*, New York, NY: Academic Press.
2. Brown R.C., 1993, *Air filtration: an integrated approach to the theory and application of fibrous filters*, Oxford, England: Pergamon Press.
3. Letourneau P., Mulcey, Ph., and Vendel J., 1990, Aerosol penetration inside HEPA filtration media. *Proc. 21st DOE/NRC Nuclear Air Cleaner Conference*, CONF-900813.
4. Lee K.W., Liu B.Y.H., 1982, Theoretical Study of Aerosol Filtration by Fibrous filters, *Aerosol Science and Technology*, **1**(2), 147-161.
5. Liu B.Y.H. and Rubow K.L., 1986, Air filtration by fibrous media, in "*Fluid Filtration: Gas"*, **1**, ASTM STP 975, (ed. R.R. Raber), *American Society for Testing and Materials*, Philadelphia, PA. 1-12.
6. Japuntich D.A., Stenhouse J.I.T., and Liu B.Y.H., 1994, Experimental results of solid monodisperse particle clogging of fibrous filters, *J. of Aerosol Sci*., **25**(2), 385-393
7. Thomas D., Penicot P., Contal P., Leclerc D. and Vendel J., 2001, Clogging of fibrous filters by solid aerosol particles: Experimental and modelling study, *Chemical Engineering Science*, **56**(11), 3549-3561.
8. Wakeman R.J., Hanspal N.S., Waghode A.N. and Nassehi V., 2005, Analysis of pleat crowding and medium compression in pleated cartridge filters, Trans IChemE, **83**(A10), 1246-1255.
9. Chen D.R., Pui D.H. and Liu B.Y.H., 1995, Optimization of pleated filter designs using a finite-element numerical model, *Aerosol Science and Technology*, **23**, 579-590.
10. Fabbro L D., Laborde J.C., Merlin P. and Ricciardi L., 2002, Air flows and pressure drop modelling for different pleated industrial filters, *Filtration & Separation,* **39**(1), 34-40.
11. Payet S., Boulaud D., Madelaine G. and Renoux A., 1992, Penetration and pressure drop of HEPA filter after loading with submicron liquid particles, *J. Aerosol Sci.,* **23**, 723-735.
12. Novick,V.J., Klaseen J.F., 1998, in *Advances in Aerosol Filtration*, by K.R. Spurny.
13. Snyder C.A., and Pring R.T., 1955. *Ind. Engineering Chemistry*, **47**, 960.
14. Pich J, 1966. Theory of aerosol filtration by fibrous filters and membrane, in *Aerosol Science*, Edited by C.N. Davies.
15. Stenhouse J.I.T., Japuntich D.A., and Liu B.Y.H., 1992, The behaviour of fibrous filters in the initial stages of filter loading, *J. of Aerosol Sci*., **23**, S1, 761-764.
16. EN 1822-5:2000 High Efficiency Air Filters (HEPA and ULPA) –Part 5 Determining the efficiency of filter element.
17. ANSI/ASHRAE 1999. ASHRAE Standard 52.2: Method of testing general ventilation air-cleaning devices for removal efficiency by particle size. American Society of Heating, Refrigerating, and Air-Conditioning Engineers, Inc., Atlanta, GA.
18. Dorman R.G., 1974, *Dust control and air cleaning*, Pergamon Press, Oxford.
19. Soloman W.R. and Mathews K.P., 1978, Aerobiology and inhalant allergens. *Allergy, principles and practices*, St. Louis, MO.
20. ASHRAE 2001. ASHRAE Handbook: Fundamentals. American Society of Heating, Refrigerating, and Air-Conditioning Engineers, Inc., Atlanta, GA.

THE EFFECT OF FACE VELOCITY, PLEAT DENSITY AND PLEAT ORIENTATION ON THE MOST PENETRATING PARTICLE SIZE, PRESSURE DROP AND FRACTIONAL EFFICIENCY OF HEPA FILTERS.

I.S. Al-Attar[1], R.J. Wakeman[1,2], E.S.Tarleton[1] and A. Husain[3]
[1]Department of Chemical Engineering, Loughborough University, LE11 3TU, UK.
[2]Consultant Chemical Engineer, West Hill, Ottery St Maryr, EX11 1UZ, UK.
[3]Kuwait Institute for Scientific Research, Department of Building and Energy Technologies P.O. Box 24885, Safat, Kuwait, 305-343, Kuwait.

ABSTRACT

The increasing need of clean air in critical industrial applications has highlighted the importance of the role of air filters in providing improved air quality. Actual performance of air filters installed in air handling units and in the intake of gas turbines tends to deviate from the performance predicted by laboratory results. Therefore, accurate filter performance prediction is important to estimate filter lifetime, and to reduce energy and maintenance operating costs. To ensure that the desired efficiency of a HEPA filter is attained, the effects of face velocity, pleat density and pleat orientation on the Most Penetrating Particle Size (MPPS) of pleated HEPA filters must be examined. This paper compares the effects of varying the face velocity, pleat orientation and the variation of pleat density on the MPPS of the HEPA filters. This paper also presents the initial pressure drop response and fractional efficiency curves using DEHS testing according to DIN 1822 for vertical and horizontal pleat orientation for HEPA filters. It also analyzes the underlying reasons causing surface area losses for different flow rates, pleat density and orientation as well as the effects on filter's permeability of HEPA filters. The tests conducted in this study used full scale HEPA pleated V-shaped filters used in Heating Ventilation and Air Conditioning (HVAC) and gas turbine applications.

KEYWORDS

Air Filters, Fractional Efficiency, Gas Cleaning, Glass Fibre, HEPA filter, Permeability, Pressure Drop.

1 Filtration of Air

The assessment of air filters performance is complex and influenced by several parameters such as face velocity, filter medium properties, filter design and dust types and their loading conditions. The performance characteristics under study in this paper are initial pressure drop and fractional efficiency. To make an appropriate filter selection for various applications, the influential parameters affecting the filtration performance must be evaluated.

Several authors have studied the performance of clean filters [1-5] and others have considered loading filters with monodisperse aerosols [6]. Most of these studies considered flat fibrous filter medium and the filtration performance was examined [7-8]. Other literature also covered the effect of particle and fibre charge on the filter performance [9-10]. Penetration of HEPA filters have also been studied [11-13] and several studies investigated the performance of loaded HEPA filters with solid particles [14-15], liquids particles [16-18] and a mixture of both [19-20]. The literature scope whether it is theoretical or experimental was limited to the study of flat filters

and small scale pleated panel HEPA filters and the filter properties were not always fully reported. Although some studies were done on pleated filtration media, the literature available on pleated HEPA filters is rather limited and is mainly based on numerical approaches used for performance analysis [23-32]. Unlike this study, the previous pleated filters studies have not considered a full scale HEPA filter constructed in a V-shape cartridge. This experimental work investigates the effect of face velocity, pleat density and pleat orientation on the initial pressure drop, fractional efficiency and associated MPPS of HEPA filters. Previous studies have considered the pleating density and highlighted the optimal pleat count [25-29].

2. Filter Properties

The experimental work involved the testing of full scale glass fibre pleated cartridges of HEPA Class H10 according to DIN 1822 [33]. Ten filters were manufactured by EMW Filtertechnik in Germany with pleating densities varying from 28 to 34 pleats per 100 mm. Table 1 lists all filters used for testing with their corresponding surface areas as well as their pleat orientation. The first eight manufactured filters were divided into two groups, A and B. Both groups underwent similar testing procedures and were challenged with DEHS to give data for the initial fractional efficiency. The remaining two filters, 28H and 28V represent 28 pleating density with horizontal and vertical pleat orientation respectively. Filter 28H and 28V were manufactured to investigate the effect of pleat orientation on the initial pressure drop and fractional efficiency. Figure 1 shows the face dimensions of 592 x 592 mm with a depth of 400 mm. The filter cassette has a V-shape bank which contains eight pleated media panels.

FILTER	PLEAT DENSITY (Pleats/100 mm)	SURFACE AREA (m^2)	PLEAT ORIENTATION
28A	28	23.9	horizontal
28B	28	24.6	horizontal
30A	30	26.6	horizontal
30B	30	26.6	horizontal
32A	32	27.3	horizontal
32B	32	27.3	horizontal
34A	34	28.8	horizontal
34B	34	28.9	horizontal
28H	28	23.5	Horizontal
28V	28	24.4	Vertical

Table 1: The filters tested and their surface areas.

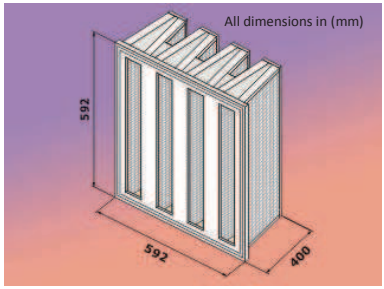

Figure 1: Pleated filter with the V shape design (EMW Filtertechnik).

The glass fibre media used in these filters is shown in Figure 2. Glass fibre filtration media was selected for all experiments in this work as it exhibits better resistance to high temperatures and has smaller fibre size compared to synthetic media. Glass fibre media are highly porous with a low resistance to air flow. Filter performance is affected by several variables such as filter medium thickness, permeability, packing density, fibre diameter as well as the design of the filter module. Operating conditions such as filtration velocity and temperature also affect the filter performance, in addition to the characteristics of the aerosol such as particle size distribution, particle shape and density. The filter properties of the media used in this study are listed in Table 2.

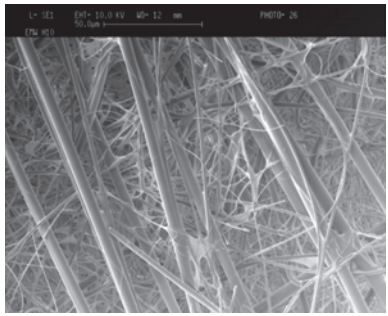

Figure 2: Image of the glass fibre HEPA filter medium (Class H10 according to DIN 1822).

HEPA (H10) FILTER MEDIUM	
Fibre Diameter Range	0.5-8.5 µm
Average fibre diameter	2.1 µm
Media Thickness	500 µm
Packing Density	0.06
Porosity	94%
Fibre Shape	Circular

Table 2: Properties of the filter medium.

3. Clean Gas Permeation

The passage of the clean gas through the filtration was enabled the pressure drop and efficiency to be measured, whilst challenging the filter with DEHS according to DIN 1822. There is no dust loading at this stage of the testing. The Reynolds number is used to verify the flow regime in the testing tunnel and through the filter medium. The Reynolds numbers for the filter medium (using the fibre diameter) at the flow rates of 500 and 5000 m^3/h are 0.00122 and 0.0122 respectively. Therefore, the flow inside the filter medium is laminar. The Reynolds numbers in the rectangular feed duct to the filter (with a hydraulic diameter of 610 mm) at flow rates of 500 and 5000 m^3/h are 14,476 and 144,760 respectively. Therefore, the flow inside the duct is turbulent.

The flow inside the filter medium can be interpreted using Darcy's Law to calculate the permeability, κ:

where μ is the air viscosity, V is the approach velocity of the air, h is the filter medium thickness, and ΔP is the pressure drop across the medium. The initial pressure drop was measured and is shown in Table 3 at different flow rates ranging from 500 to 5000 m^3/h at increments of 500 m^3/h, together with the corresponding permeability values.

Filter	28A, A_S = 23.9 m^2			30A, A_S = 26.6 m^2			32A, A_S = 27.3 m^2			34A, A_S = 28.8 m^2		
Q (m^3/h)	ΔP (Pa)	V_f (mm/s)	κ x10^{-12} (m^2)	ΔP (Pa)	V_f (mm/s)	κ x10^{-12} (m^2)	ΔP (Pa)	V_f (mm/s)	κ x10^{-12} (m^2)	ΔP (Pa)	V_f (mm/s)	κ x10^{-12} (m^2)
500	14	5.78	3.82	18	5.22	2.68	14	5.08	3.36	15	4.82	2.97
1000	30	11.57	3.57	30	10.44	3.22	27	10.17	3.48	29	9.64	3.07
1500	47	17.36	3.42	47	15.65	3.08	44	15.25	3.21	45	14.45	2.97
2000	66	23.12	3.24	65	20.86	2.97	63	20.34	2.99	63	19.27	2.83
2500	87	28.90	3.08	86	26.08	2.81	83	25.42	2.83	81	24.09	2.75
3000	111	34.68	2.89	108	31.30	2.68	105	30.50	2.69	105	28.91	2.55
3500	135	40.46	2.78	132	36.52	2.56	129	35.59	2.55	128	33.72	2.44
4000	162	46.24	2.64	159	41.74	2.43	155	40.67	2.43	153	38.54	2.33
4500	191	52.02	2.52	188	46.96	2.31	183	45.75	2.31	182	43.36	2.20
5000	222	57.80	2.41	218	52.20	2.21	213	50.84	2.21	213	48.18	2.09
Filter	28B, A_s = 24.6 m^2			30B, A_s = 26.6 m^2			32B, A_s = 27.3 m^2			34B, A_s = 28.9 m^2		
Q (m^3/h)	ΔP (Pa)	V_f (mm/s)	κ x10^{-12} (m^2)	ΔP (Pa)	V_f (mm/s)	κ x10^{-12} (m^2)	ΔP (Pa)	V_f (mm/s)	κ x10^{-12} (m^2)	ΔP (Pa)	V_f (mm/s)	κ x10^{-12} (m^2)
500	17	5.65	3.07	15	5.23	3.22	15	5.09	3.14	15	4.80	2.96
1000	30	11.29	3.48	30	10.46	3.22	29	10.19	3.25	29	9.61	3.06
1500	47	16.94	3.33	48	15.69	3.02	45	15.29	3.14	47	14.41	2.84
2000	66	22.59	3.17	66	20.92	2.93	63	20.38	2.99	63	19.21	2.82
2500	86	28.23	3.04	87	26.15	2.81	84	25.48	2.81	84	24.01	2.64
3000	108	33.88	2.90	111	31.38	2.61	107	30.57	2.64	107	28.82	2.49
3500	134	39.52	2.73	136.5	36.61	2.47	131	35.67	2.52	131	33.62	2.37
4000	161	45.17	2.60	165	41.83	2.35	158	40.76	2.39	159	38.42	2.24
4500	188	50.81	2.50	193.5	47.06	2.24	186	45.86	2.28	186	43.22	2.15
5000	218	56.46	2.40	226.6	52.30	2.13	216	50.95	2.18	218	48.03	2.04

Table 3: Initial pressure drop versus face velocities and permeabilities for different pleating densities.

5. Deviation from Darcy's Law

The Darcy pressure drop model will be examined to compare with the experimental work. The Darcy model gives a linear relationship between pressure drop response and flow rate, which also signifies that the permeability of the filtration medium does not change and the pressure drop should vary linearly with the filtration velocity. However, the experimental results exhibit a non-linear response which means the filter's permeability is changing as the flow rate varies, even though the flow inside the medium is laminar. Figure 3 shows that as the face velocity or pleating density increase, the permeability decreases. However, increasing filter's surface area decreases the face velocity and therefore, the pressure drop of the filter is expected to decrease. However, when the pleating density increases to extend the surface area, the pressure drop also increases. Therefore, there must be a competing effect that leads to the deviation from Darcy's Law.

A low pleat count, the face velocity is high and the pressure drop increases. On the other hand, over-pleating also causes an increase in pressure drop due to the increased viscous drag in the pleat spacing. It is evident from Figure 4 that while

higher pleating densities provide additional surface area, the losses of surface area also increase as the face velocity increases, which in turn means the air stream cannot access all of the surface area provided. The pressure drop rise from higher pleating density is related to the flow inside the pleat where the viscous and inertial forces play a role in raising the pressure drop. Therefore, this effect will be competing with increase of surface area provided by the higher pleating density. Figure 4 also shows that losses are similar in the 30 and 32 pleating densities. Examining Table 3, Filters 32A and 32B have lower pressure drop than 30A and 30B respectively. Filters with 32 pleats per 100 mm would be better from a pressure drop point of view and they have similar surface area losses compared to the 30 pleats per 100 mm filters. However, the comparison to determine the better pleat count is not complete until both filter's efficiency curves are examined both on the initial and dust loaded efficiency counts. This is simply to check that filter 30 has less surface area and has similar surface area losses when compared with 32 pleats per 100 filters. The area losses are not due entirely to one factor and there is no apparent optimal pleat density for a given rate. The data shows the area of the filter media is fully utilized at 500 m^3/h and underutilized at higher flow rates.

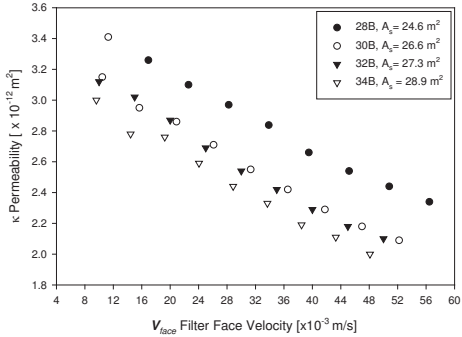

Figure 3: Permeability versus face velocities for filters of Group B.

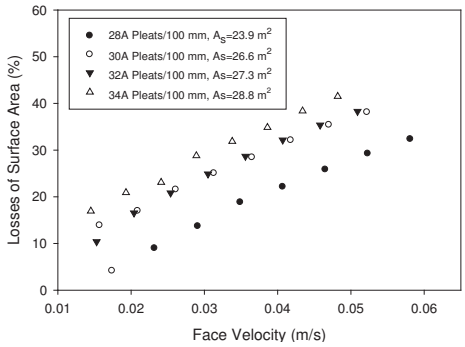

Figure 4: The losses of surface area of the different pleating densities filters at different face velocities.

For a pleat through which fluid flow obeys Darcy equation, the losses of media surface area due to one or combination of the following reasons:

- Pleat crowding, a geometric effect caused by excessive number of pleats in the pleated panel. The filtration medium surface area losses occur by having too many pleats next to each other. Clearly, as the pleat density increases, the surface area losses increase.

- Deflection of the entire pleated panel causing permeability reduction or by vicious or shear at the corner of the pleat would have more influence on the filter surface area losses. In the absence of the sufficient support on the back side of the pleated panels, the deflection is more pronounced.

- Pleat distortion at the corner of the pleat caused by delamination of the fibres layers from the filtration medium. Clearly, the higher the number of pleats, the greater this effect has on permeability reduction of the filtration medium. This effect also increases as face velocities increase.

- Filtration medium compression and therefore, the medium thickness will reduce resulting in higher pressure drop. It can also result from medium folding which leads to tension in the outer region of the pleated medium and compression at the inner region. Medium compression could also be due to the drag force exerted by flowing fluid on the surfaces of the particles or fibres forming the medium. Therefore, the medium compression increases as the shear stress acting on the fibre surfaces increases causing the pressure drop to rise.

Figure 5 illustrates the loss in the tested filters' surface areas versus their pleating densities. It can be seen that as the pleating density increases, the surface area losses increases. This indicates that the entire surface area is not utilized, and the higher the pleat density, the greater the losses in the surface area of the pleated filter.

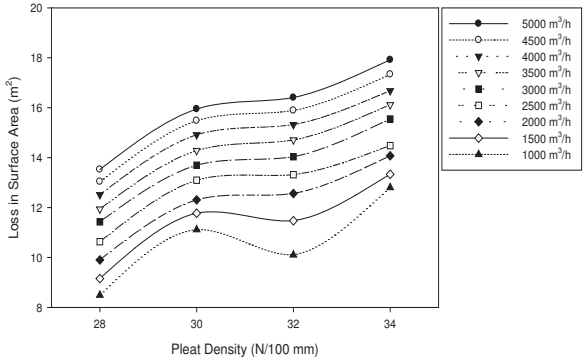

Figure 5: Losses of filter's surface area of Group B versus pleating density compared to Darcy equation.

Figure 5 also shows that higher pleating density has led to greater losses in the surface area of the filter. However, the focus of the design should be directed towards reduces surfaces area losses and not reducing the pleating density. Reducing surface area without verifying the efficiency requirement to be met would compromise the filter performance. It may also affect the mechanical/structural stability of the pleated panel. Surface area losses signify that the air flow does not get access to the total surface area, and as a result this part of the filtration medium does not participate in the filtration process and may have no substantial contribution to the enhancement of overall filter efficiency. This is an important aspect of the design of the filter because it would also reflect on the manufacturing cost. Introducing additional media that is not accessible by the air flow rate, but to the contrary, increases the resistance of the filter, defeats the intended purpose to the filtration process.

The effective surface areas are listed in Table 4 for different flow rates and pleating densities. At low flow rates such as 500 and 1000 m^3/h, the full surface area of the filter medium participates in the filtration process, and there are no losses in the filter medium and no permeability reduction. However, when the flow rate and pleating density increase further, the area losses begin to occur. The effective surface area decreases with increase of flow rate and pleating density. The surface area losses increase as pleating density increase suggests that the filter is over-pleated and may be possibly to obtain equally as good filtration using lower number of pleats. For a fixed pleating density and a given flow rate, there exist a minimum pressure drop that meets the efficiency requirement of the standards.

Pleat Density	**28A**	**30A**	**32A**	**34A**
Total A_s (m^2)	**23.9**	**26.6**	**27.3**	**28.8**
Q (m^3/h)	A_{Eff}	A_{Eff}	A_{Eff}	A_{Eff}
500	23.9	26.6	27.3	28.8
1000	23.9	23.9	26.6	24.8
1500	22.9	22.9	24.5	23.9
2000	21.7	22.1	22.8	22.8
2500	20.6	20.9	21.6	22.2
3000	19.4	19.9	20.5	20.5
3500	18.6	19.0	19.5	19.6
4000	17.7	18.1	18.5	18.8
4500	16.9	17.2	17.7	17.8
5000	16.2	16.5	16.9	16.9

Table 4: Effective area versus different flow rates for different pleating densities.

6. The Effect of Pleat Orientation on the Filter's Performance

Two filters of same filtration medium properties were manufactured in vertical and horizontal pleat orientation to study the effect on the filter's performance. Initial pressure drop and fractional efficiency were measured without dust loading. Table 5 tabulates the pressure drop starting at 500 m^3/h until 6000 m^3/h in addition to the MPPS and its measured fractional efficiency. Fractional efficiency was conducted using DEHS for six flow rates starting at 500 m^3/h until 3000 m^3/h is reached.

Filter	Horizontal Pleat, A_s =23.5 m^2				Vertical Pleat, A_s =24.4 m^2			
Flow Rate m^3/h	ΔP (Pa)	MPPS	Fractional Efficiency	Filter Class Achieved	ΔP (Pa)	MPPS	Fractional Efficiency	Filter Class Achieved
500	14	0.18	97.94	H11	12	0.17	97.89	H11
1000	30	0.18	95.33	H11	28	0.17	95.19	H11
1500	49	0.14	93.30	H10	46	0.17	92.25	H10
2000	69	0.16	91.22	H10	67	0.15	91.29	H10
2500	92	0.14	90.56	H10	89	0.12	89.95	H10
3000	117	0.14	89.38	H10	113	0.14	88.02	H10
3500	143				139			
4000	172				166			
4500	202				195			
5000	236				227			
5500	270				256			
6000	306				295			

Table 5: Pressure drop and MPPS measurements for horizontal and vertical pleats filters

Two filters of same filtration medium properties were manufactured in vertical and horizontal pleat orientation to study the effect on the filter's performance. Initial pressure drop and fractional efficiency were measured without dust loading. Fractional efficiency was conducted using DEHS for six flow rates starting from 500 to 3000 m^3/h. The filter cartridge with vertical pleats has a surface area of 24.4 m^2 whereas the horizontal pleat filter has 23.5 m^2. The addition of surface is nearly one square metre which is due to losses after the addition of the casting material which connects the pleated fibrous material to the plastic housing. The horizontal-pleat filter has more losses since the casting material covers more pleats when compared to the vertical ones.

7 Observations:

1. From a pressure drop point of view, the vertical pleat filter has slightly lower pressure drop as show in Figure 8. This is due to the vertical pleating which is thought to give more strength to the pleated media panel, and hence less deformation occurs at higher flow rates.
2. The MPPS shifts to a smaller particle size as the face velocity increases with both pleat orientations.
3. Fractional efficiency readings are very close for both pleat orientations at lower flow rates, but as the flow rate increases the horizontal pleating offers a pressure drop that becomes increasingly less than that of the vertical pleating.
4. The slightly lower pressure drop of the vertical pleats is probably more than offset by the greater fractional efficiency of the horizontal pleats and one squared meter difference in total surface area, making the horizontal pleats a better practical option.

Figure 6 illustrates the pressure drop comparison between the flat sheet and horizontal and vertical pleats of the same medium. The flat sheet pressure drop response is linear while pressure drops for both pleating directions exhibit identical pattern. Their pleated pressure drop curves initially starts with a linear response then as the face velocity increases it departs linearity and losses in surface area are more pronounced.

The comparison of simulated and experimental pressure drop responses is also shown in Figure 6. This examination was conducted at the same face velocities to ensure that all the pressure drop reading can be compared. In can also be shown that permeability reduction due to flat medium compression is not that significant in comparison with the flat sheet to the other factors such as pleat crowding, pleat deformation and pleated panel deformation. This concludes that surface area losses and their consequential permeability reductions are mainly due to pleat crowding, pleated panel deformation and pleat deformation.

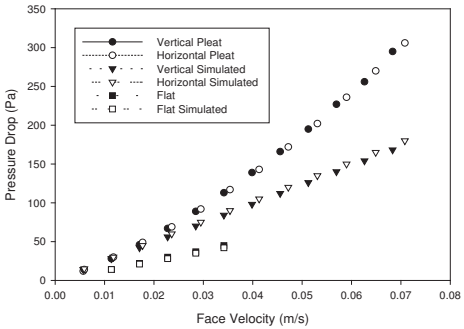

Figure 6: Comparison between simulated and experimental initial pressure drop for flat sheet, vertical and horizontal pleat filters at different face velocities.

Surface area losses are compared in Figure 7, the vertical pleat orientation cartridge experience higher losses when compared to the horizontal pleat orientation. Table 5 also tabulates the drop in fractional efficiency as the face velocity increases. It is evident that the vertical pleat orientation provides less efficiency readings and the HEPA H10 filter class is only attained for 500 and 1000 m^3/h flow rates for both pleat orientation. In terms of efficiency, Figure 8, the vertical pleated filter seems to have lower efficiencies at lower and higher flow rates although it has one square meter additional surface area. The horizontal pleated filter exhibits higher efficiency when compared to the vertical pleated filter. This effect is more pronounced is higher flow rates such 3000 m^3/h.

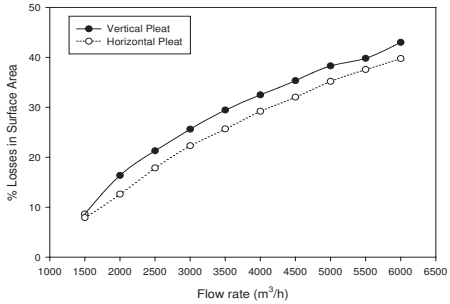

Figure 7: Surface area losses comparison between vertical and horizontal pleat filters at different flow rates.

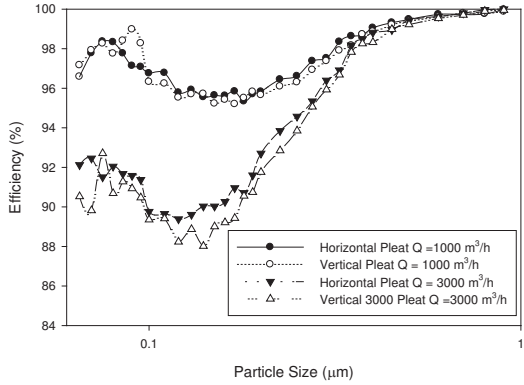

Figure 8: Initial efficiency for vertical and horizontal pleat orientation at different flow rates.

8. Conclusions:

This study has presented an experimental investigation of the effect of face velocity, pleat density and orientation on the pressure drop response and the initial fractional efficiency of full scale HEPA filters. The following are the conclusions of this study:

- The surface area losses increase as the pleating density and face velocity increase.
- Pleating density selection should be based on the corresponding effective filter's surface area it provides and the total surface area. Further, the pleating density selection should be made in junction with the requirement to achieve desired efficiency.
- An increase in pleating density and face velocity decreases filter medium permeability.
- At low flow rates such as 500 and 1000 m^3/h, the full surface area of the filter participate in the filtration process, and there are no losses in the filter medium and no permeability reduction.
- The fractional efficiency decreases as the face velocity increase for particle sizes lower than MPPS. While the fractional efficiency increases as the face velocity increases for particle sizes greater than the MPPS.
- Pressure drop response comparison between vertical and horizontal pleats filters has shown that the vertical pleat filter has slightly lower pressure drop.
- The MPPS shifts to a smaller particle size as the face velocity increases with both pleat orientations.
- Fractional efficiency readings are very close for both pleat orientations at lower flow rates, but as the flow rate increases the horizontal pleating offers a pressure drop that becomes increasingly less than that of the vertical pleating.
- The slightly lower pressure drop of the vertical pleats is probably more than offset by the greater fractional efficiency of the horizontal pleats, making the horizontal pleats a better practical option.

9. References

1. Davies C.N., 1973. Air Filtration, New York, NY: Academic Press.
2. Brown R.C. 1993. Air filtration: an integrated approach to the theory and application of fibrous filters, Oxford, England: Pergamon Press.
3. Happel J., 1959. Viscous flow relative to arrays of cylinders, *A.I.Ch. E.J.*, 5(2), 174-177.
4. Kuwabara S., 1959. The forces experienced by randomly distributed parallel circular cylinders or spheres in viscous flow at small Reynolds numbers, *J. of the Physical Society of Japan,* 14, , 527–532.
5. Stechkina I.B. and Fuchs N.A., 1963. "A note on the theory of fibrous filters" *Ann.Occup. Hyg*. 6, 27-30.
6. Brown R.C. and Wake D. 1999. Loading filters with monodisperse aerosols: macroscopic treatment, *J. of Aerosol Sci.*, (30)2, 227-234.
7. Lee K.W., Liu B.Y.H., 1982. Theoretical Study of Aerosol Filtration by Fibrous filters, *Aerosol Science and Technology*, 1(2), 147-161.
8. Liu B.Y.H. and Rubow K.L., 1986. Air filtration by fibrous media, in "*Fluid Filtration: Gas"*, 1, ASTM STP 975, (ed. R.R. Raber), *American Society for Testing and Materials*, Philadelphia. 1-12.
9. Brown R., Wake D., Thorpe A., Hemingway M. and Roff M., 1994. Theory and measurement of the capture of charged dust particles by electrets*, J. of Aerosol Sci.*, (25)1, 149-163.
10. Brown R.C. 1981. Capture of dust particles in filters by line dipole charged fibres*, J. Aerosol Sci.*, 12(4), 349-356.
11. Letourneau P., Mulcey, Ph. and Vendel J., 1990. Aerosol penetration inside HEPA filtration media, *Proc. 21st DOE/NRC Nuclear Air Cleaner Conference*, CONF-900813.
12. Vendel J., Mulcey Ph. and Letourneau P., 1992. Effects of the particle penetration inside the filter medium on the HEPA filter pressure, *22nd DOE/NRC Nuclear Air Cleaning conf.,* Denver, 128-142.
13. Sinclair D., 1976. Penetration of HEPA filters by submicron aerosols *J. of Aerosol Sci.*, (7)2, 175-179.
14. Novick V.J., Monson P.R. and Ellison P.E., 1992. The effect of solid particle mass loading on the pressure drop of HEPA filters, *J. of Aerosol Sci.,* 23(6), 657-665.
15. Payatakes A.C., 1977. Model of transient aerosol particle deposition in fibrous media with dendritic pattern, *A.I.Ch.E. J.*, 23, (2), 192.
16. Payatakes A.C. and Okuyama K., 1982. Effects of aerosol particle deposition on the dynamic behaviour of uniform or multilayer fibrous filters, *J. of Colloid and Interface Sci.,* 88(1), 55-78.
17. Frising T., Thomas D., Bémer D. and Contal P., 2005. Clogging of fibrous filters by liquid aerosol particles: Experimentaland phenomenological modelling study, *Chem Eng Sci.*, (60)10, 2751-2762.
18. Payet S., Boulaud D., Madelaine G. and Renoux A., 1992. Penetration and pressure drop of HEPA filter after loading with submicron liquid particles, *J. Aerosol Sci.,* 23, 723-735.
19. Penicot P., Thomas D., Contal P., Leclerc D. and Vendel J., 1999. Clogging of HEPA fibrous filters by solid and liquid aerosol particles: An experimental study, *Filtration & Separation,* 36(2), 59-64.

R E F E R E N C E S

Aguiar M.L. and Coury J.R., 1996. *Ind. Eng. Chem*. Res. 35, 3673.

Al-Sanad H.A., Ismael N.F. and Nayfeh A.J., 1993. "Geotechnical properties of dune sands in Kuwait", *Engineering Geology*, 34, (1-2), 45-52.

ANSI/ASHRAE [1992]. ASHRAE Standard 52.1: gravimetric and dust-spot procedures for testing air-cleaning devices used in general ventilation for removing particulate matter. Atlanta, GA: American Society of Heating, Refrigerating, and Air-Conditioning Engineers, Inc.

ANSI/ASHRAE [1999]. ASHRAE Standard 52.2: method of testing general ventilation air-cleaning devices for removal efficiency by particle size. Atlanta, GA: American Society of Heating, Refrigerating, and Air-Conditioning Engineers, Inc.

ASHRAE [2000]. ASHRAE handbook: HVAC systems and equipment. Atlanta, GA: American Society of Heating, Refrigerating, and Air-Conditioning Engineers, Inc.

ASHRAE [2001]. ASHRAE handbook: fundamentals. Atlanta, GA: American Society of Heating, Refrigerating, and Air-Conditioning Engineers, Inc.

Benmachou, K., Schmitz P. and Meireles M., 2003. "Dynamic clogging of pleated filter: experimental and theoretical approaches for simulation" Filtech Europa (2)**,** 51-57.

Bergman, W., Taylor, R. D., Miller, H. H., Biermann, A. H., Hebard, H. D., daRoza, R. A. and Lum, B. Y., 1979. "Enhanced filtration program at LLL-A progress report", *15th DOE Nuclear Air Cleaning Conference,* CONF-70822, 1058-1081.

Brown R.C. 1984. "A many-fibre model of airflow through a fibrous filter" *J. Aerosol Sci.*, **15**(5), 583-593.

Brown R.C. 1997. "Airflow pattern through granular filters and other simple three-dimensional filters" *Filtration & Separation*, **34** (2), 165-171.

Brown R.C. 1993a. "Air filtration: an integrated approach to the theory and application of fibrous filters", *Pergamum Press*, Oxford.

Brown R. C. 1993b. "Theory of airflow through filters modeled as arrays of parallel fibers" *Chemical Engineering Science*, **48**(20), 3535-3543.

Brown R.C., Wake D., Smith P.A. 1994a. "An electrically augmented filter made from conducting and dielectric fibres". *J. Electrostatics*, **33**(3), 393-412.

Brown R., Wake D., Thorpe A., Hemingway M., Roff M., 1994b. "Theory and measurement of the capture of charged dust particles by electrets". *J. Aerosol Sci*., **25**(1), 149-163.

Brown R. C. and Thorpe A., 2001. "Glass-fibre filters with bimodal fibre size distributions". *Powder Technology*, **118**(1-2), 3-9.

Brown R. C., Wake D. 1999. "Loading filters with monodisperse aerosols: macroscopic treatment". *J. Aerosol Sci.*, **30**(2), 227-234.

Carman P.C., 1956. "The flow of gases through porous media" *Academic Press*, New York.

Caesar T. and Schroth T., 2002. "The influence of pleat geometry on the pressure drop in deep-pleated cassette filters". *Filtration & Separation,* **39**(9), 48-52.

Chen D.R., Pui D.H., and Liu B.Y.H., 1995. "Optimization of pleated filter designs using a finite-element numerical model", *Aerosol Sci. and Tech*, 23, 579-590.

Chimack M.J. and Sellers D. 2000. "Using extended surface air filters in heating ventilation and air conditioning systems: reducing utility and maintenance costs while benefiting the environment". *American Council for an Energy-Efficient Economy,* Summer Study on Energy Efficiency in Buildings. http://www.aceee.org.

Cunningham E., 1910. "On the velocity of steady fall of spherical particles through fluid medium", *Proc. R. Soc*., A-83, 357-365.

Davies C.N. 1952. "The separation of airborne dust and mist particles", *Proc. Inst. Mech. Engng* 1B, 185-198.

Davies C. N. 1970. " The clogging of fibrous aerosol filters", *J. Aerosol Sci.,* **1**(1), 35-39.

Davies C.N., 1973. "Air Filtration", Academic Press, New York.

Davies C.N. 1983. "Filtration of aerosols", *J. Aerosol Sci.,* **14**(2), 147-161.

Dawson S.V. 1969. Ph.D. Thesis, Harvard Univ., Boston.

Devienne M., 1958. "Frottemente et Échanges Termiques dans les Gas Rarifiés", Gautheier-Villars, Paris.

DIN EN 1822-1, 1998. "High efficiency air filters (HEPA and ULPA)" - Part 1: Classification, performance testing, marking.

DIN EN 779, 2002. "Particulate air filters for general ventilation" : Determination of the filtration performance.

Dittler A., Gutmann B., Lichtenberger R., Weber H. and Kasper G., 1998. "Optical in situ measurement of dust cake thickness distributions on rigid filter media for gas cleaning", *Powder Technol.*, **99** (2), 177-184

Donovan R.P. 1985. "Fabric filtration for combustion sources, Fundamentals and basic technology" *Marcel Dekker Inc*., New York.

Dorman R. G. 1964. "Theory of fibrous filtration", in *High efficiency air filtration*", Ed. White P.A.F. and Smith S.E., Butter Worths, London.

Dorman R.G., 1974. "Dust control and air cleaning", *Pergamon Press*, Oxford.

Emi H., Kanaoka C. and Kuwabara Y., 1982. "The diffusion collection efficiency of fibers for aerosol over a wide range of Reynolds numbers", *J. Aerosol Sci*., **13**(5), 403-413.

EMW Filtertechnik, Diez, Germany. Website "www.emw.de".

Endo Y., Chen D. and Pui D., 1998. "Effects of particle polydispersity and shape factor during dust cake loading on air filters", *Powder Technology*, **98**(3), 241-249.

Fabbro L.D., Brun P., Laborde J.C., Lacan J., Renoux A. and Ricciardi L., 2000. "Study of the clogging of industrial pleated filters by solid particles", *J. Aerosol Sci*., **31**(S1), 210-211.

Fabbro L D., Laborde J.C., Merlin P., and Ricciardi L., 2002. "Air flows and pressure drop modelling for different pleated industrial filters", *Filtration & Separation,* **39**(1), 34-40.

Friedlander S.K. 1958. *Ind. Eng. Chem.*, 50, 1161.

Frising T., Gujisaite V., Thomas D., Callé S., Bémer D., Contal P., and Leclerc D., 2004. Filtration of solid and liquid aerosol mixtures: Pressure drop evolution and influence of solid/liquid ratio, *Filtration & Separation,* **41**(2), 37-39.

Fuchs N.A., 1964. "The mechanics of aerosols", Pergamon, Oxford.

Golan A. and Parekh B.S., 1985. "Hydrodynamic aspects of semi-dense pleat designs in pleated cartridges", *Filtration & Separation,* 10, 326–329.

Gupta A., Novick V.J., Biswas P. and Monson P.R., 1993. "Effect of humidity and particle hydgroscopicity on the mass loading capacity of high efficiency particulate air (HEPA) filters". *Aerosol Sci. and Tech*. **19**(1), 94-107.

Hanspal, N.S., Waghode, A.N., Nassehi, V. and Wakeman, R.J., 2005. "Numerical analysis of coupled Stokes/Darcy flows in industrial filtrations" *Transport in Porous Media*. **74** (1), 73–103

Happel J., 1959. "Viscous flow relative to arrays of cylinders", *A.I.Ch. E. J.*, **5**(2), 174-177.

Harrop J.A. and Stenhouse J.I.T., 1969. "The theoretical prediction of inertial impaction efficiencies in fibrous filters", *Chemical Engineering Science*, **24**(9), 1475-1481.

Hinds W.C., 1998. "Aerosol Technology", *Wiley*, New York.
Hollinger, W., 1998. "Fundamentals of the compression behavior of dust filter cakes", in K.R. Spurny (Ed.), *Advances in Aerosol Filtration,* pp349–360. *Lewis Publishers*, Chelsea.

Höflinger W., Stöcklmayer C., and Hackl A., 1994. "Model calculation of the compression behaviour of dust filter cakes", *Filtration & Separation,* **31**(8), 807-811.

Ilias, S. and Douglas, P.L., 1989. "Inertial impaction of aerosol particles on cylinders at intermediate and high Reynolds numbers", *Chemical Engineering Science*, **44**(1), 81-99.

Jacobson A.R. and Morris S.C., 1997. "The primary pollutant, viable particulates, their occurrences, sources and effects. In Air pollution*,* 3rd edition, Academic Press, New York.

Japuntich D.A., Stenhouse J.I.T., and Liu B.Y.H., 1994, "Experimental results of solid monodisperse particle clogging of fibrous filters", *J. Aerosol Sci*., **25**(2), 385-393.

Japuntich D.A., Stenhouse J.I.T., and Liu B. Y. H., 1997. "Effective pore diameter and monodisperse particle clogging of fibrous filters", *J. Aerosol Sci*., **28**(1), 147-158.

Jaroszczjk T., Fallon S.L. and B.A. Pardue, 2002. "Analysis of engine air cleaner efficiency for different size dust distributions", Fluid/Particle Separation, **14**(2). 75-88.

Jeon K. and Jung Y., 2004. "A simulation study on the compression behaviour of dust cakes", *Powder Technology*, **141**(1-2), 1-11.

Kanaoka C., and Hiragi S., 1990. "Pressure drop of air filter with dust load", *J. Aerosol Sci*., **21**(1), 127-137.

Karadimos A. and Ocone R., 2003. "The effect of the flow field recalculation on fibrous filter loading: A numerical simulation", *Powder Technology,* **137**(3), 109-119.

Kaufmann A., 1963. Die Faserstoffe für Atemschutzfilter, Z, VDI, 80, 593.

Kirsh A.A., Stechkina I.B. and Fuchs N.A., 1975. "Efficiency of aerosol filters made of ultrafine polydisperse fibres", *J. Aerosol Sci.,* **6**(2), 119-120.

Kirsch A. A., 1972. "The influence of an external electric field on the deposition of aerosol in fibrous filters", *J. of Aerosol Sci.,* 3, (1), 25-29.

Kirsch A.A. and Fuchs N.A., 1968. *Ann. Occup. Hyg*., 11, 299.

Kirsch A.A., Stechkina I. B. and Fuchs N.A., 1971. "Effect of gas slip on the pressure drop in a system of parallel cylinders at small Reynolds numbers", *J. Colloid and Interface Sci.,* **37**(2), 458-461.

Kirsch A.A., and Stechkina I.B., and Fuchs N.A., 1973. "Effect of gas slip on the pressure drop in fibrous filters", *J. Aerosol Sci.,* **4**(4), 287-293.

Kirsch A.A., Stechkina I. B. 1973 "Pressure drop and diffusional deposition of aerosol in polydisperse model filter" *J. Colloid and Interface Sci.*, **43**(1), 10-16.

Kirsch A.A., Stechkina I.B. and Fuchs N.A., 1974. "Gas flow in aerosol filters made of polydisperse ultrafine fibres", *J. Aerosol Sci.*, **5**(1), 39-45.

Kirsch A. A., and Stechkina I.B., 1977. " Inertial deposition of aerosol particles in model filters at low Reynolds numbers", *J. Aerosol Sci.*, **8**(5), 301-307.

Kirsch A.A., and Stechkina I.B., 1978. "The theory of aerosol filtration with fibrous filters", Chapter 4, *Fundamentals of Aerosol Science* (Ed. D. Shaw), Wiley.

Kirsch A.A., and Lahtin U. B., 1975. *J. Colloid interface Sci*., 52, 270.

Kuwabara, S., 1959. "The forces experienced by randomly distributed parallel circular cylinders or spheres in viscous flow at small Reynolds numbers", *J. Physical Society Japan,* 14, 527–532.

Kuwabara S., 1959. "The forces experienced by randomly distributed circular cylinders or spheres in viscous flow at small Reynolds numbers", *J. Phys.Soc.* Japan **14**(4), 527-532.

Langmuir I., 1942. "Report on smokes and filters", Sec. I, *U.S. Office of Science Research and Development*, No.865, Part IV, 394-436.

Lee K.W., 1986. "Particle collection mechanisms pertinent to granular bed filtration". *In Fluid Filtration: Gas*., 1 (Ed. R.R. Raber), American Society for Testing and Materials, Philadelphia, ASTM STP 975, 46-59.

Lee K.W. and Mukund R., 2001. "Filter collection", in "Aerosol Measurement: Principles, Techniques, and Applications" 2nd edition, Ed. P.A.Baron and K.Wileke, 197-228.

Lee K.W., and Liu B.Y.H., 1982a. "Experimental study of filtration by fibrous filters", *Aerosol Sci. Technol.,* **1**(1), 35-46.

Lee K.W., and Liu B.Y.H., 1982b. "Theoretical study of aerosol filtration in fibrous filters", *Aerosol Sci. Technol.,* **1**(2), 147-161.

Lee K.W., and Ramamurthi, M., 1993. "Filter collection," in Willeke, K. and Baron, P.A. (Eds.) *Aerosol Measurement: Principles, Techniques, and Applications,* Van Nostrand Reinhold, New York.

Leibold H. and Wilhelm J.G. 1991. "Investigations into the penetration and pressure drop of HEPA filter media during loading with submicron particle aerosols at high concentrations" *J. Aerosol Sci.*, **22** S(1), S773-S776.

Letourneau P., Mulcey, Ph. and Vendel J., 1990. "Aerosol penetration inside HEPA filtration media", *Proc. 21st DOE/NRC Nuclear Air Cleaner Conference*, CONF-900813.

Lisowski A., Jankowska E., Thorpe A. and Brown R.C., 2001. "Performance of textile fibre filter material measured with monodisperse and standard aerosols", *Powder Technology*, **118** (1-2), 149-159.

Liu B.Y.H., and Rubow K.L., 1986. "Air filtration by fibrous media". In "*Fluid Filtration: Gas"*, 1, ASTM STP 975, (Ed. R.R. Raber), *American Society for Testing and Materials*, Philadelphia. 1-12.

Liu B.Y.H., and Rubow K.L., 1990. "Efficiency, pressure drop and figure of merit of high efficiency fibrous and membrane filter media". *Proc. of 5th World Congress*, The Filtration Society, Nice.

Lücke, T. and Fissan, H., 1996. "The prediction of filtration performance of high efficiency gas filter element". *Chem. Eng. Sci*. **51**, 1199–1208.

Matteson M.J. and Orr C., 1987. "*Filtration, Principles and Practices*", Marcel Dekker, New York.

Ministry of Electricity and Water, 2000. "Statistical yearbook, Electrical energy, (25th ed.) State of Kuwait.

Morris K. and Allen R.W.K., 1996. "The influence of dust and gas properties on cake adhesion in fabric filters", *Filtration & Separation,* **33**(4), 339-343.

Mouret G., Thomas D., Chazelet S, Appert-Collin J. and Bemer D., 2009. "Penetration of nanoparticles through fibrous filters perforated with defined pinholes" *J. Aerosol Sci.*, **40**(9), 762-775.

NAFA, 2001. "Guide to air filtration", Washington, DC: National Air Filtration Association.

Neiva A.C. B. and Goldstein L. Jr., 2003. "A procedure for calculating pressure drop during the build-up of dust filter cakes", *Chemical Engineering and Processing,* **42**(6), 495-501.

Nguyen X. and Beeckmans J.M., 1975. "Single fibre capture efficiencies of aerosol particles in real and model filter in the interial-interceptive domain", *J. Aerosol Sci.,* **6**(3-4), 205-212.

Novick V. J., Monson P.R., and Ellison P. E., 1992. "The effect of solid particle mass loading on the pressure drop of HEPA filters", *J. Aerosol Sci.,* **23**(6), 657-665.

Novick,V. J. and Klaseen J.F., 1998, in "Advances in aerosol filtration" Ed. K.R. Spurny, Lewis, 337-347.

Ogorodnikov B.I., and Budyka A.K., 1993. "Pressure drop across fiber filter at RE>0.5 and inertial capture of particles", *J. Aerosol Sci.,* **24** (S1), S269-S270.

Payatakes A.C., and Gradoń L., 1980. "Dendritic deposition of aerosol particles in fibrous media by inertial impaction and interception", *Chem. Eng. Sci.,* **35**(5), 1083-1096.

Payatakes A.C. and Okuyama K., 1982. "Effects of aerosol particle deposition on the dynamic behaviour of uniform or multilayer fibrous filters", *J. Colloid and Interface Sci.,* **88**(1), 55-78.

Payatakes A.C. and Tien C., 1976. "Particle deposition in fibrous media with dendrite-like pattern: A preliminary model", *J. Aerosol Sci.,* **7**(2), 85-94.

Payatakes A.C., 1977. "Model of transient aerosol particle deposition in fibrous media with dendritic pattern", *A.I.Ch.E., J.,* **23**(2), 192.

Payet S., 1991. " Filtration stationnaire et dynamique des arosols liquides submicroniques". *Thése de l'universitéParis XII*, 150 p.; rapport CEA-R-5589.

Payet S., Boulaud D., Madelaine G., and Renoux A., 1992. "Penetration and pressure drop of HEPA filter after loading with submicron liquid particles", *J. Aerosol Sci.,* **23**(7), 723-735.

Penicot P., Thomas D., Contal P., Leclerc D. and Vendel J., 1999. "Clogging of HEPA fibrous filters by solid and liquid aerosol particles: An experimental study", *Filtration & Separation,* **36**(2), 59-64.

Pich J, 1966. "Theory of aerosol filtration by fibrous filters and membrane in aerosol science", in "*Aerosol Science"*, Ed. Davies C.N., Academic Press, London, 223-285.

Ptak T. and Jaroszczyk, T. 1990. "Theoretical-experimental aerosol filtration model for fibrous filters at intermediate Reynolds numbers". *Proc. 5th World Filtr. Congr.,* Nice, France, 566-572.

Pui D.Y.H. and Chen, D-R, 1996. "Optimization f pleated filter designs" *J. Aerosol Sci.*, **27**(4), 654-655.

Pui, D.Y.H., Chen D-R and Liu, B.Y.H., 1993. "Optimization of pleated filter design using a finite-element numerical method" *J. Aerosol Sci.*, **24**(S1), 39-40.

Raber R.R., 1982. "Pressure drop optimization and dust capacity estimation for a deep-pleated industrial air filter using small sample data". *In: Proceedings of World Filtration Congress III*, (52).

Ramarao B.V., Tien C. and Mohan S., 1994. "Calculation of single fiber efficiencies for interception and impaction with superposed Brownian motion", *J. Aerosol Sci.,* **25**(2), 295-313.

Rebai M., Prat M., Meireles M., Schmitz P. and Baclet R. 2010a. "A semi-analytical model for gas flow in pleated filters", *Chem Eng. Sci.* **65**(9)**,** 2835-2846.

Rebai M. Prat M., Meireles M., Schmitz P. and Baclet R. 2010b. " Clogging modeling in pleated filters for gas filtration" *Chem. Eng. Research and Design,* **88**(4)**,** 476-486.

Reist P.C 1984. "Introduction to Aerosol Science" MaCmillan Publishing Company, Inc, New York.

Schmidt E., and Löffler F., 1990. "Preparation of dust cakes for microscopic examination", *Powder Technology*, **60**(2), 173-177.

Schmidt E., and Pilz T. 1996. "Raw gas conditioning and other additional techniques for improving surface filter performance", *Filtration & Separation*, **33**(5), 409-415.

Schmidt E., 1997a. "Theoretical investigations into the compression of dust cakes deposited on filter media", *Filtration & Separation,* **34**(4), 365-368.

Schmidt E., 1997b. "Experimental Investigations into the compression of dust cakes deposited on filter media", *Filtration & Separation,* **32**(8), 789-793.

Scurrah K.L., 1999. "Filtration of Solid and liquid aerosol particles", *PhD thesis*, Loughborough University.

Statistics Department and Information Centre, Electrical Energy, 1998. "Statistical year book" *Ministry of Electricity and Water*, State of Kuwait.

Spielman, L., and Goren, S.L, 1968. "Model for predicting pressure drop and filtration efficiency in fibrous media" *Environ. Sci. Technol.*, **2**(4)**,** 279-287.

Stenhouse J.I.T., Japuntich D. A., and Liu B.Y.H., 1992. "The behaviour of fibrous filters in the initial stages of filter loading", *J. Aerosol Sci*., **23**(S1), 761-764.

Stechkina, I.B. and Fuchs, N.A. 1963. "A note on the theory of fibrous filters". *Ann. Occup. Hyg*. 6, 27-30.

Stechkina I.B. and Fuchs N. A., 1963. "A note on the theory of fibrous filters", *Ann. occup. Hyg.,* **6**(27), 27-30 .

Stechkina I. B., Kirsch A.A., and Fuchs N. A. 1969. *Ann. Occup. Hyg*. **12**(1) Kolloidn; . *Z.*31(121)*, Colloid J. USSR* (English Translation) 31-97.

Stöcklmayer C. and Höflinger W., 1998. Simulation of the filtration behaviour of dust filters, *Simulation Practice and Theory*, **6**(3), 281-296.

Snyder C.A., and Pring R.T., 1955. *Ind. Eng.Chem.*, **47**, 960.

Sinclair D., 1976. "Penetration of HEPA filters by submicron aerosols" *J. Aerosol Sci.*, **7**(2), 175-179.

Spurny K. R. 1999. "Analytical chemistry of aerosol" Lewis Publishers.

Tarleton E.S. and Wakeman R.J. 2008. "Dictionary of Filtration and Separation" Filtration Solutions, Filtration Solutions, Exeter.

Thomas D., Contal P., Renaudin V., Penicot P., Leclerc D. and Vendel J., 1999. "Modelling pressure drop in HEPA filters during dynamic filtration", *J. Aerosol Sci.,* **30**(2), 235-246.

Thomas D., Penicot P., Contal P., Leclerc D. and Vendel J., 2001. Clogging of fibrous filters by solid aerosol particles Experimental and modelling study, *Chem. Eng. Sci.*, **56**(11), 3549-3561.

Thorpe A. and Brown R. C., 1998. "Performance of textile and paper filters with bimodal fibre size distributions" *J. Aerosol Sci.*, 29(S2), S937-S938.

Ugural A.C. and Fenster S.K. 2003 "Advanced strength and applied elasticity" Fourth Edition, New Jersey Prentice Hall Inc.

Van Osdell D.W., Liu B.Y.H., Rubow K.L. and Pui D.Y.H., 1990. "Experimental study of submirometer and ultrafine particle penetration and pressure drop for high efficiency filters", *Aerosol Sci. and Technol.* **12**(4), 911-925.

Vaughan N. P. and Brown R.C.1992. "Measurement of filter structure" *J. Aerosol Sci.*, **23**(S1), 741-744.

Vendel J., Mulcey P. and Letourneau, P., 1990. "Aerosol penetration inside HEPA filtration media". *Proc. 21st DOE/NRC nuclear air cleaning conference*, *CONF*-920823, San Diego, 799-808.

Vendel J., Letourneau, P. and Renaudin, V., 1992a. "Effects of the particle penetration inside the filter medium on the HEPA filter pressure drop". *Proc. 22nd DOE/NRC Nuclear Air Cleaning Conference*, *Conf.*-920823, Denvers.

Vendel J., Mulcey Ph. and Letourneau P., 1992b. "Effects of the particle penetration inside the filter medium on the HEPA filter pressure", *Proc. 22nd DOE/NRC Nuclear Air Cleaning Conf.,* Denver, 128-142.

Wakeman R. J., 1986. "Progress in Filtration and Separation 4" (Ed. Wakeman R. J.), Elsevier, New York.

Wakeman R.J. and Tarleton E.S., 1999. "Filtration, Equipment Selection Modeling and Process Simulation", Elsevier Advanced Technology, Oxford.

Wakeman R.J. and Harris, P.R., 1993. "A methodology for modelling flow in pleated (star) filter cartridges", *Proc FILTECH Europa*, Karlsruhe, 335–343.

Wakeman R.J., Hanspal N.S., Waghode A.N. and Nassehi V., 2005. "Analysis of Pleat Crowding and Medium Compression in Pleated Cartridge Filters", *Chem. Eng. Research and Design,* **83**(A10), 1246–1255.

Walsh D.C., 1996. Recent advances in the understanding of fibrous filters under behaviour under solid particle load, *Filtration & Separation*, **33**(6), 501-506.

Walsh D.C. 1998. "Possibilities for the design of fibrous filter materials with enhanced dust holding capacity", *J. Aerosol Sci.*, **29**(S2), S939-S940.

Walsh D.C., 1995. "The behaviour of electrically active and prefilter fibrous filters under solid aerosol load", *PhD Thesis*, Loughborough University.

Walsh D.C., and Stenhouse J.I.T., 1997. "Clogging of an electrically active fibrous filter material: experimental results and two-dimensional simulations", *Powder Technol.,* **93**(1), 63-75.

Wang P.K., 1991. *Aerosol Sci. Technol*., **15**, 149-155.

Yeh H.C. and Liu B.Y.H., 1974a. "Aerosol filtration by fibrous filters – Part I. Theoretical", *J. Aerosol Sci.,* **5**(2), 191-204.

Yeh H.C. and Liu B.Y.H., 1974b. "Aerosol filtration by fibrous filters – Part II. Experimental", *J. Aerosol Sci.,* **5**(2), 205–217.

Yu H.H.S. and Goulding C.H., 1992. "Optimised ultra high efficiency filter for high-efficiency industrial combustion turbines, *ASME Gas Turbine and Aeroengine Congress and Exposition*, Cologne, Germany, Paper 92-GT-39.